APPLICATIONS

8th International Conference on Sandwich Structures
ICSS 8
A. J. M. Ferreira (Editor)

SKIN CONSOLIDATION IN VACUUM MOULDED THERMOPLASTIC COMPOSITE SANDWICH BEAMS

Richard Brooks, Palanivel P. Kulandaivel and Christopher D. Rudd

School of Mechanical, Materials and Manufacturing Engineering
University of Nottingham
University Park, Nottingham NG7 2RD, UK
e-mail: richard.brooks@nottingham.ac.uk

Keywords: Sandwich beams; thermoplastic composite skins; vacuum moulding; void content; processing variables; interlaminar shear strength

Summary. *This paper reports on work undertaken to measure the level of skin void content and hence consolidation in thermoplastic composite sandwich beams made by a non-isothermal vacuum moulding process. The effects of processing variables, such as skin preheat temperature and mould temperature on void content are established and the influence of different types of void, e.g. inter-tow, on the delamination properties of the skin are reported. Sandwich beam performance, in terms of peak load to failure under quasi-static and dynamic (impact) flexural loading, is measured. Processing conditions for optimising beam performance are established and discussed with respect to those necessary for maximising skin consolidation.*

1 INTRODUCTION

For thermoplastic composite (TPC) laminates, void content has been shown to have a significant effect on the ultimate laminate properties [1-3]. Furthermore, processing parameters can affect void content in the moulded part [4]. Several studies have reported on the manufacture of thermoplastic composite sandwich structures [5,6], all involving compression moulding. In these studies, processing conditions are shown to affect the properties of the structure significantly and skin consolidation has been a key factor affecting performance. The authors have reported on the development of a one-step vacuum moulding route for TPC sándwich structures with potential for cost-effective manufacture [7]. The process involves skin preheating before combining with the cold core under vacuum pressure. As this is a non-isothermal process, it is important to maintain temperature whilst pressure is applied to obtain good skin consolidation. At the same time, excessive crushing of the core must be avoided as this will affect the section modulus in the final structure and hence its performance under load. This paper focuses on the effect of processing conditions in the vacuum moulding process on the void content in the skin and on the ultimate performance of the structure under flexural conditions.

2 SPECIMEN MATERIALS AND MANUFACTURE

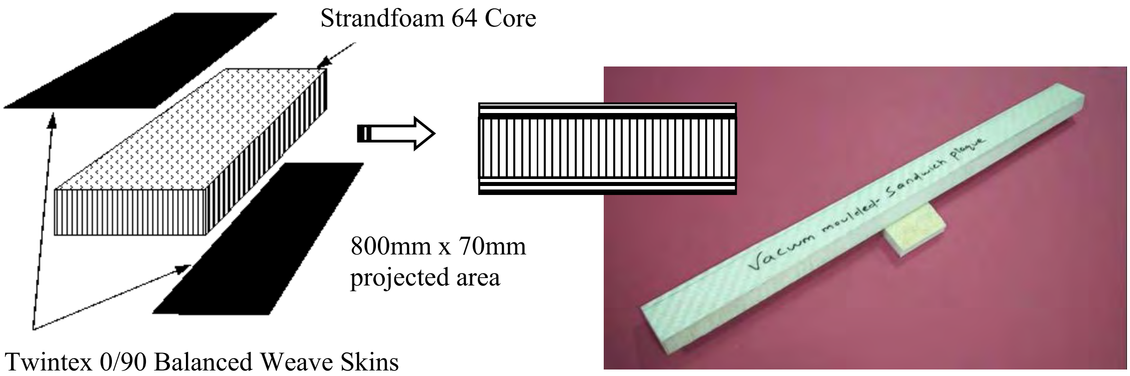

Figure 1 Vacuum moulded large sandwich beam (800mm x 70mm projected area)

Large TPC sandwich beams have been made from 60 wt% 0/90 weave commingled glass/polypropylene skins (Twintex®) and anisotropic polypropylene foam core (Strandfoam®), density 64 kgm^{-3}, as shown in Fig. 1. The beams have a projected area of 800 mm x 70 mm, a nominal core thickness of 25 mm (before moulding) and varying skin thicknesses of 1 mm, 2 mm or 3 mm. The 0° fibre direction in the Twintex® skins is oriented along the main beam axis and the core strand direction is oriented through the thickness, the latter to maximise crush properties of the beam. This thermoplastic structure lends itself to relatively rapid processing rates (~ 10 minute cycle time) and offers good recycling potential due to it being a single polymer system.

The beams have been manufactured by a one-shot vacuum molding process illustrated in Figures 2 (a) to 2(c). This process involves the stacking of Twintex® layers (two stacks, one for each skin) onto aluminium transfer plates and preheating in a hot air oven, for approximately 10 minutes, to a temperature in the range 180 °C to 220 °C. Heating time depends on the thickness of each stack. A hot air oven is used to ensure uniform heating across the surface and through the thickness of the stack. The two preheated Twintex® stacks, supported on the transfer plates, are then transferred rapidly to the vacuum table where they are combined with the cold foam core. Transfer and assembly time is typically in the range 25 to 35 seconds. The transfer plates maintain the temperature of the stacks during this process. The vacuum table lid (silicone membrane) is then closed on the whole assembly (including transfer plates) and the vacuum applied for a period in the range 5 to 15 minutes. The mould base temperature is also controlled within the range 30 °C to 80 °C. A schematic of the vacuum moulding setup is shown in Fig. 3.

After cooling, the moulded beam is trimmed along its edges and cut using a band saw into six equal coupon sandwich beams of projected area 250 mm x 30 mm and final thickness depending on processing conditions and chosen skin thickness.

(a) Heated stack (including transfer plates assembled on the vacuum table

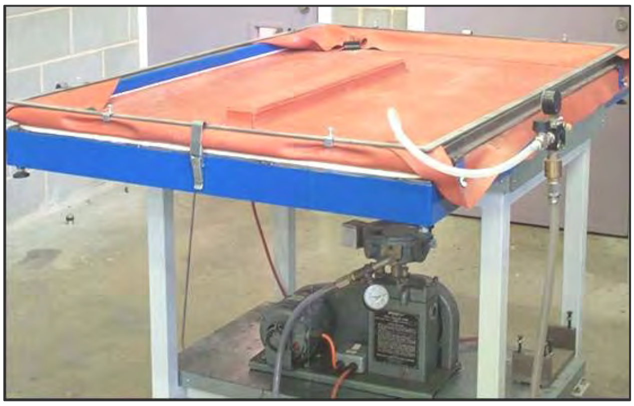

(b) Membrane closed and vacuum applied

(c) Moulded process complete

Figure 2 Stages in the vacuum moulding process

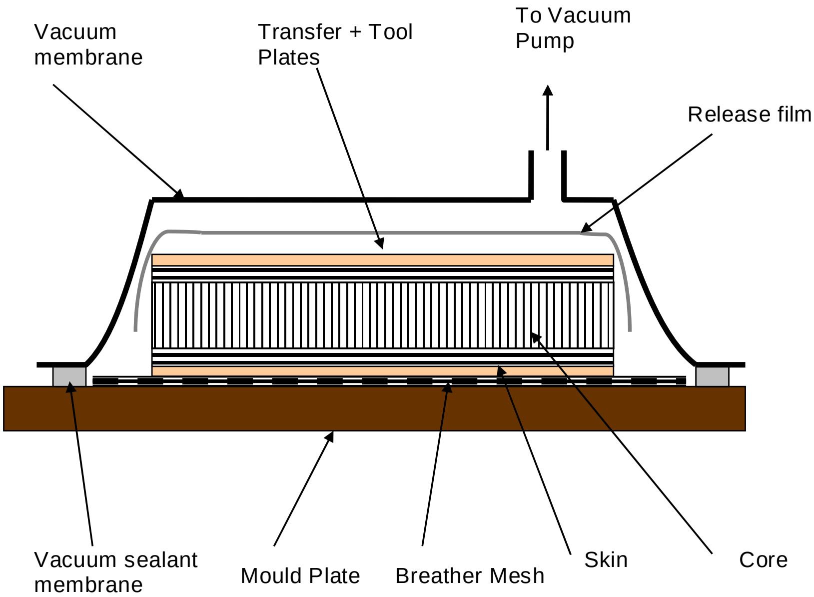

Figure 3 Schematic of the vacuum moulding setup

3 MEAUREMENT OF VOID CONTENT AND INTERLAMINAR SHEAR STRENGTH (ILSS) IN THE SKINS

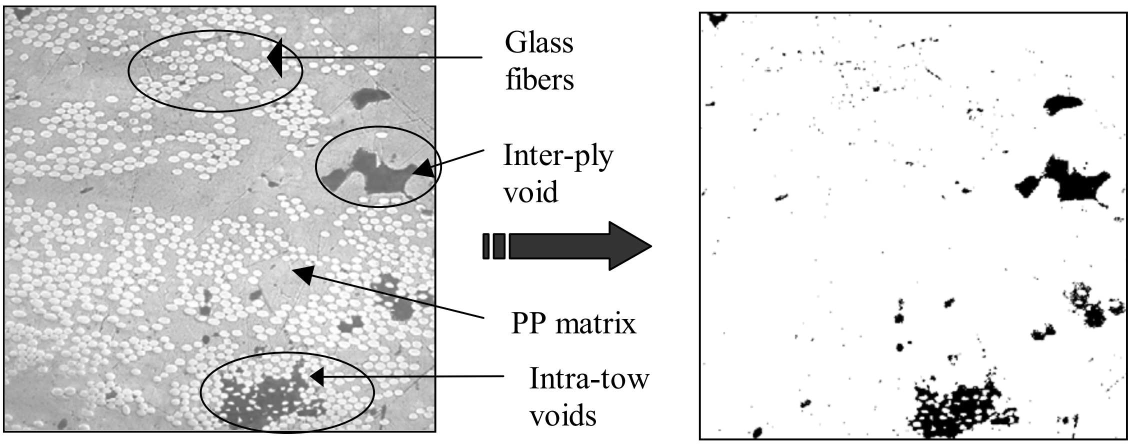

Figure 4 Conversion of a skin micrograph to a binary image

Micrographs of the moulded sandwich beam skins were taken using a Zeiss microscope and Aphelion™ image capture software. Aphelion™ has an adjustable image frame capable of a maximum resolution of 280,000 pixels (700*400). The captured micrographs were then analysed using the UTHSCSA Image Tool. This Software allows the identification of 256 grey levels (0=black, 255=white). A *thresholding* process can distinguish the objects on the

basis of their grey level or brightness and creates a binary image (see Fig. 4). The black and white pixels are then calculated and expressed as black% and white%. The black% corresponds to the void content in the micrograph. In this study 50x and 200x magnifications were used. In both cases the total number of pixels per image was 262,144. Each pixel in the image captured by 50x and 200x represents 4.1 μm and 1 μm resolution respectively. The 200x lens was used for only the initial part of the study but it was found that the voids could be classified and measured with good accuracy using a 50x lens. The advantage is that a larger area and fewer images can be tested using this lens. To obtain a statistically reliable measure, 100 mm^2 of area was covered for the analysis of each specimen.
As shown in Fig. 4 both inter-ply and intra-tow voids are measured separately

In addition to void content, the interlaminar shear strength of the skins is measured using the *Short Beam Shear Method* to ASTM D 2344-76. Detached moulded skins are prepared by grinding away the bonded core and cutting to size. Short beams with a 5:1 span:thickness ratio are tested in 3-point bending at a loading rate of 1 mm/min. The results for 8 specimens (4 beams x 2 skins) are averaged for each processing condition. Due to limitations in test span, the 1 mm skins are not tested but ILSS values are obtained by linear extrapolation from the thicker skins in this case.

4 STATISTICAL INFLUENCE OF PROCESSING PARAMETERS ON CONSOLIDATION

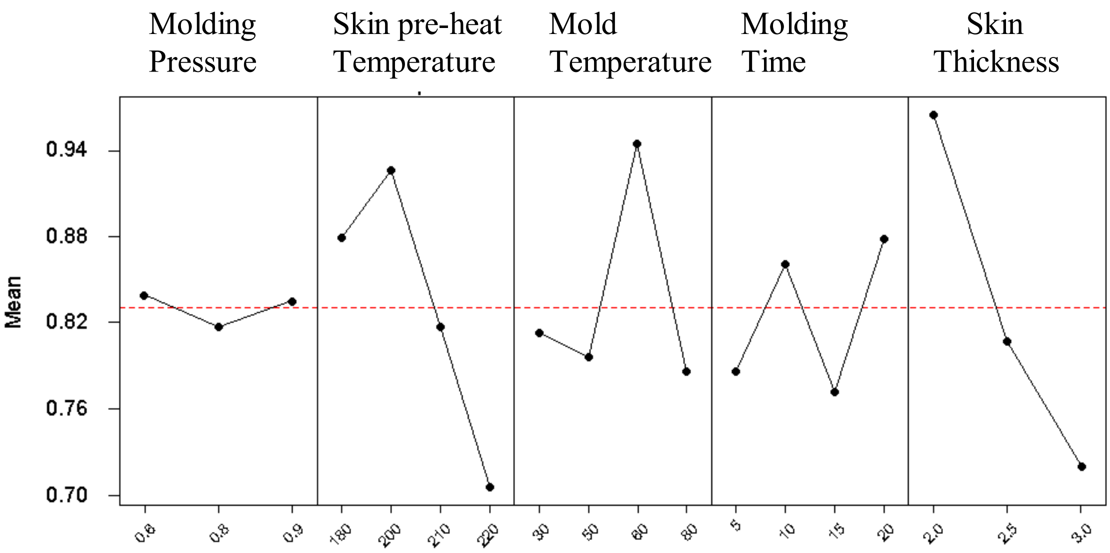

Figure 5 Statistical analysis of the effects of the processing conditions on skin consolidation

The influence of the four processing parameters: moulding pressure, skin pre-heat temperature, mould temperature and moulding time have been studied. In addition, a fifth parameter, skin thickness was also considered. The results of this study were statistically analysed and are presented in Fig. 5 as the mean of the average values of the two output variables, skin interlaminar shear strength (ILSS) and void %, combined and scaled in the range 0 to 1 (1 indicates low void% i.e. good consolidation and high ILSS). From the figure, it can be seen that skin pre-heat temperature, mould temperature and skin thickness are the most influential parameters. Consolidation quality increases with a reduction in skin thickness as might be expected. For both skin preheat temperature and mould temperature there are optimum values for good consolidation (200°C and 60°C respectively).

4 IMPORTANCE OF SKIN PREHEAT TEMPERATURE

Skin preheat temperature appears to be the most influential parameter and for that reason its effects on void content are presented in more detail in Figure 6. The total void% is low for intermediate preheat temperatures – typically 200°C. At high preheat temperatures (and prolonged heating times) the polymer can degrade as a result of Thermo Oxidative Induction (TOI) [3]. The TOI time is lower for higher preheat temperatures. At lower preheat temperatures the polymer viscosity is high resulting in poor flow and impregnation and hence consolidation. Although it would be possible to improve consolidation by higher moulding pressures and moulding times, this is not an option for non-isothermal vacuum moulding.

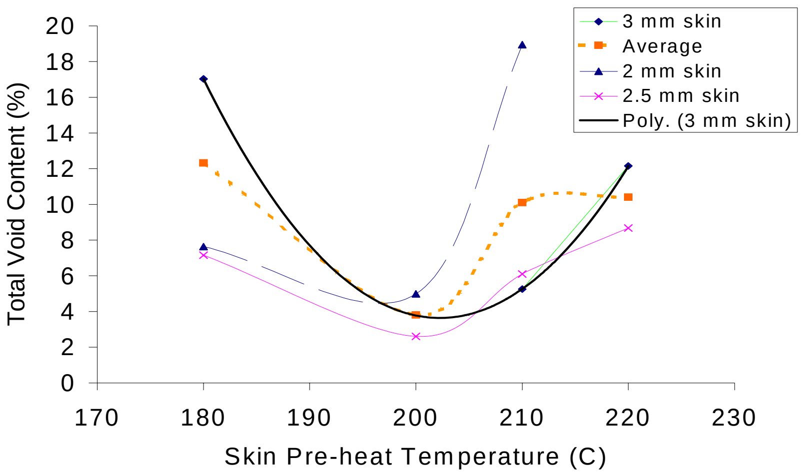

Figure 6 Effect of the skin pre-heat temperature on the total void content %

4 VOID CONTENT AND ILSS

The measured total void content includes micro-voids, intra-tow and inter-ply voids. Filtering of the binary image on the void size basis was undertaken to separate out these individual voids (see Fig. 7) and consider only inter-ply voids to see if a relationship exists between void content and ILSS.

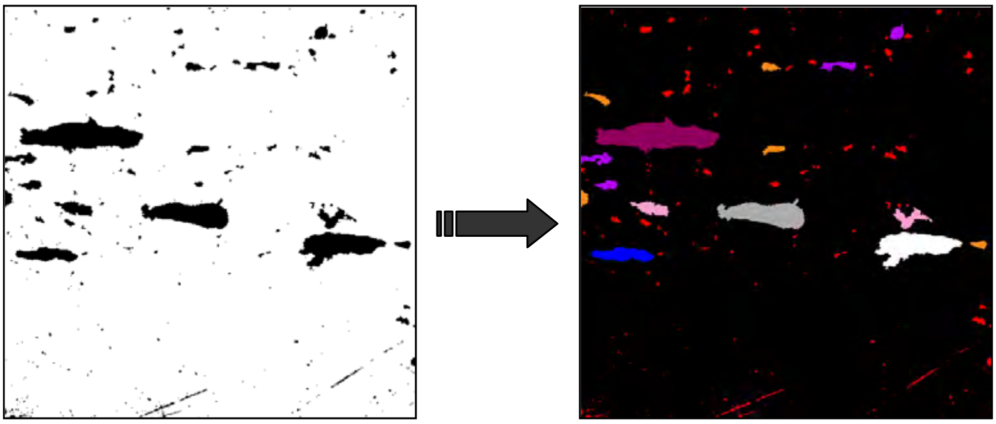

Figure 7 Segregation of the voids based on size

Interlaminar shear strength (ILSS) has been chosen as an appropriate measure of skin integrity contributing to beam performance, and, as such, has been measured and is plotted against both the total void content and the inter-ply void content in Fig. 8 for various processing conditions.

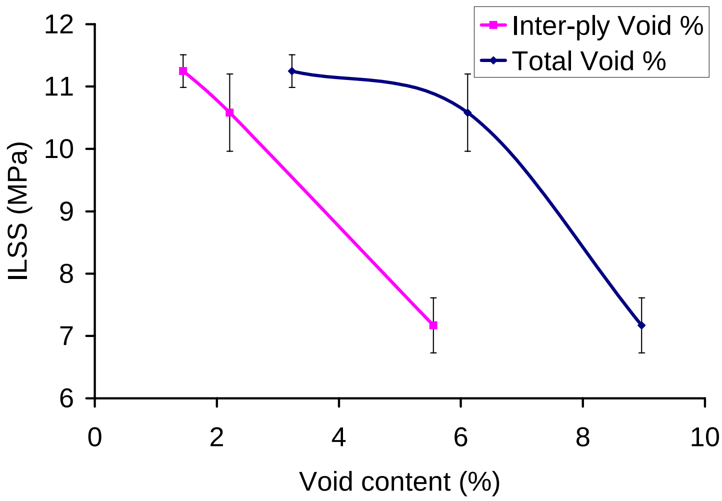

Figure 8 Skin interlaminar shear strength (ILSS) versus void content %
[Error bars signify 95% confidence limit]

It is evident that there is clear linear correlation between ILSS and inter-ply void content over the full range of void content. Total void content has less effect except at high levels of void content (> 6%) but this can be attributed to the presence of inter-ply voids in the total void count. Thus, it can be concluded that inter-ply voids affect the skin ILSS directly. This is a consequence of the influence of these relatively large voids on the delamination properties of the skin. Skin ILSS is clearly an important measure of the quality of consolidation in the skin and its potential contribution to the overall sandwich beam performance. Fig. 8 also indicates that inter-ply void content levels of less than 2% are required to ensure maximum ILSS performance.

5 SANDWICH BEAM PERFORMANCE

Beam performance has been assessed under both quasi-static and dynamic bending conditions. Relatively short span to thickness beams (~ 7:1 ratio) have been tested in 3-point bending to represent typical energy absorbing applications in the transport sector e.g. bumper beam structures.

5.1 Flexural peak load

Flexural peak load at failure is obtained quasi-statically for the coupon sandwich beams using a 3-point bending test setup to BS EN 2746:1998. The beams tested have a span of 200 mm and are loaded at a rate of 27 mm/min. For each skin thickness, a minimum of 4 coupon beams are taken from different large manufactured beams.

Dynamic (impact) testing of the coupon sandwich beams is also undertaken using a Rosand instrumented falling weight (IFW) machine. Again, a 3-point bending test setup is used with a 200 mm span. A constant impact mass of 7.213 kg and impact velocity of 6 ms^{-1} is maintained giving an impact energy of 130 Joules. In all cases this is sufficient to cause the beam to fail.

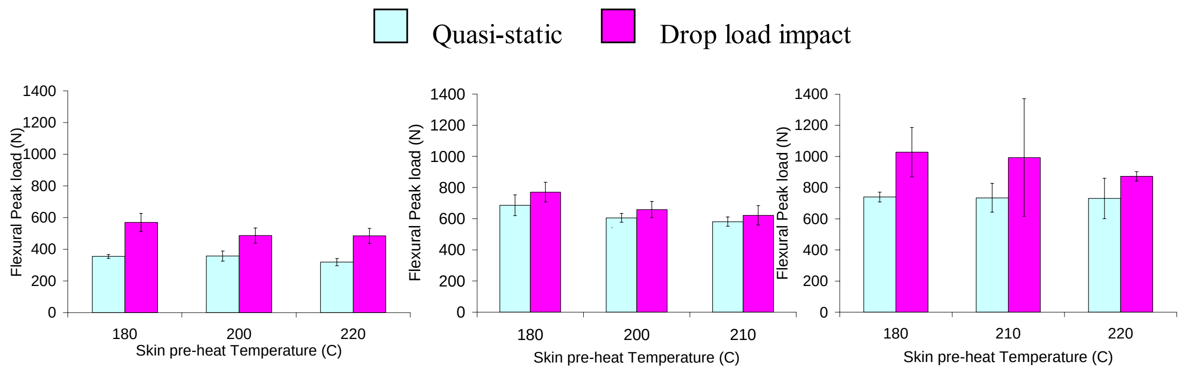

(a) 1 mm skin (b) 2 mm skin (c) 3 mm skin

Figure 9 Effect of the skin pre-heat temperature on the flexural peak load performance of vacuum moulded sandwich beams [error bars signify 95% confidence limit]

The flexural peak load, obtained under both quasi-static and dynamic loading, is plotted against the skin pre-heat temperature for a number of skin thicknesses (1, 2 and 3 mm) in Fig. 9. The quasi-static points on the graphs are mean values of 16 beams for each condition and the dynamic (drop load) points are for 4 beams. For both loading conditions and all skin thicknesses the peak load is a maximum for a skin pre-heat temperature of 180°C i.e. the lowest temperature. This is primarily a consequence of the reduction in core crush during beam manufacture, greater final beam thickness and hence structural efficiency. The reduced skin consolidation expected at this lower preheat temperature appears to have minimal influence on the overall beam performance.

As expected, a thicker skin also results in a higher peak load. Dynamic peak load is, in all cases, higher than quasi-static, most likely a consequence of the rate dependence of the beam materials.

5.2 Failure modes under impact

Several different modes of failure are observed during impact testing as illustrated in Fig. 10 for impact at 6 m/s. The impact failure mode changes with skin thickness. For the 1 mm skin, core shear failure is preceded by very localized skin indentation and core crush. For the 3 mm skin, the beam bends globally with minimal local deformation, again before shear failure of the core. For the 2 mm skin an intermediate condition occurs where the deformation is a combination of local and global bending before shear failure in the core. In all cases, ultimate failure is by core shear crack growth and subsequent debonding at the interface, a consequence of the relatively short span to depth ratios for these beams. An interesting observation is the location of the core shear crack, which occurs closer to the outer supports for a thicker skin.

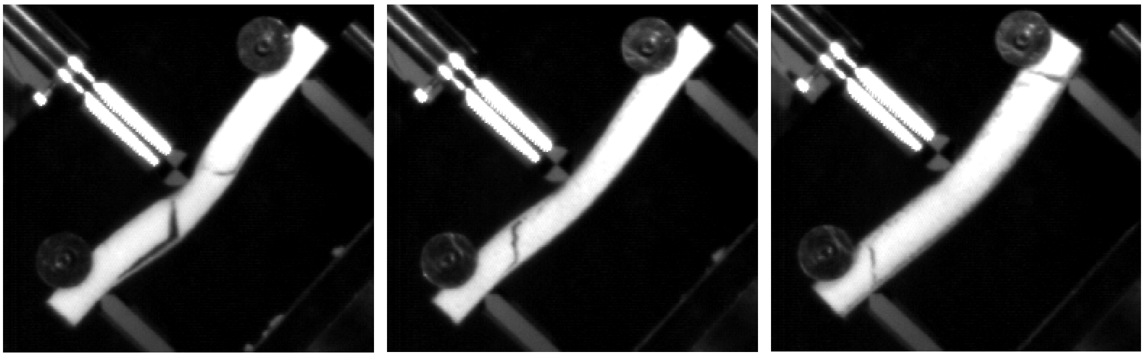

(a) 1 mm skin (b) 2 mm skin (c) 3 mm skin

Figure 10 Failure modes of the sandwich beams under 6 m/s falling weight impact

All of the above results are for beams where the skin and core are well bonded during manufacture. However, under some conditions of manufacture, poor interface bonding can lead to premature interface failure resulting in significantly lower beam performance. Fig.11 illustrates some conditions under which this can occur. Firstly, overheating of the skin can result in polymer degradation and consequent poor consolidation and interface bonding (see Fig. 11(a)). Secondly, insufficient core melting during manufacture can also result in a weak interface (see Fig. 11(b)). This latter condition was achieved by compression moulding (not vacuum moulding) a controlled interface thickness.

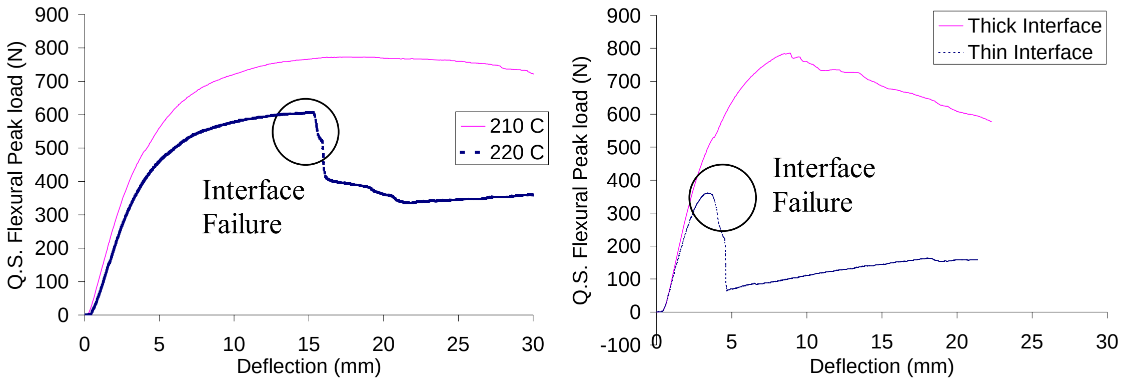

(a) Skin-core interface failure in 2.5 mm skin sandwich beams processed under vacuum at 210°C and 220°C skin preheat Temperature

(b) Skin-core interface failure in 2 mm skin sandwich beams processed under compression moulding at 180°C skin preheat temperature, at crush depths of 2mm (thick) and 0.5 mm (thin)

Figure 11 Effect of the skin-core interface on the sandwich beam performance

9 DISCUSSION AND CONCLUSIONS

The work presented in this paper has shown that a non-isothermal vacuum moulding process can be used for producing TPC sandwich beams with structural integrity. It is important, however, to maintain temperature of the skins during processing by using transfer plates during both transfer of material from the oven to the vacuum table and moulding itself. Detailed measurements of void content in the skins has shown that skin preheat temperature and skin thickness are the most influential parameters affecting void content with mould temperature also having an effect. As expected, minimum void content and hence optimum consolidation is obtained with the thinnest skin while there is also an optimum preheat temperature for minimizing void content: 200 °C for these PP based TPC structures. A closer look at the types of voids in the skins has revealed a direct relationship between interlaminar shear strength (ILSS) and inter-ply voids. Thus, whereas void content measurement can be used as a direct measure of skin consolidation quality, skin ILSS is an equally valid measurement which can be obtained with less effort. An inter-laminar void content of the order of 2% or less will maximize ILSS.

For the relatively thick section beams tested in this work, failure is generally by core shear and maximum peak load is obtained by minimizing the preheat temperature (180 °C). This reduces the amount of core crush during moulding and hence retains a greater section modulus for the moulded beam. However, as discussed above, lower preheat temperatures are not optimum for skin consolidation, so there is clearly a compromise depending on application. For these thick section beams, skin consolidation is clearly less important for performance. Thinner section beams, i.e. greater span to thickness ratios, are more likely to fail in the skins and in this case, skin consolidation will be an important factor. The paper has also shown that beam performance in bending is, not surprisingly, affected by the quality of the interface bond between skin and core. Poor bonding can result, for instance, from overheating of the skins or from too low a level of core melting being achieved during moulding. The latter could be a result of too low a level of skin preheat temperature. 180 °C appears to be the minimum preheat temperature for these PP based TPC structures.

REFERENCES

[1] K. J Bowles, S.Frimpong, "Void effects on the interlaminar shear strength of unidirectional Graphite-Fibre-Reinforced composites", *Journal of Composite Materials,* **26,** 1487-1509 (1992).

[2] A.P.Mouritz, "Ultrasonic and interlaminar properties of highly porous composites" *Journal of Composite Materials,* **34,** 218-239 (2000).

[3] M.D.Wakeman, T.A.Cain, C.D.Rudd, R.Brooks, A.C.Long, "Compression moulding of glass and polypropylene composites for optimised macro and micro-mechanical properties – 1. Commingled glass and polypropylene", *Composites Science and Technology* **58,** 1879-1898, (1998).

[4] J.Bernhardsson and R.Shishoo, "Effect of processing parameters on consolidation quality of GF/PP commingled yarn based composites", *Journal of composite materials,* **13,** 292-313, (2000).

[5] Passaro, A., Corvaglia, P., Manni, O, "Processing-properties relationship of sandwich panels with polypropylene core and polypropylene matrix composite skins", *Polymer Composites*, 25, 307-318 (2004)

[6] Mouritz, A, Thomson, R.S., "Compression, flexure and shear properties of a sandwich containing defects", *Composite Structures*, 44, 263-278 (1999)

[7] Brooks, R.,Kulandaivel, P., Rudd, C.D., "Vacuum moulding of thermoplastic composite sándwich beams", *25th SAMPE Europe Conference*, Paris, France (2004)

ACKNOWLEDGEMENTS

The authors would like to acknowledge the support of OCV Reinforcements and Dow Automotive for supply of materials. This work has been funded by the UK Engineering and Physical Sciences Research Council (EPSRC) through the Nottingham Innovative Manufacturing Research Centre (NIMRC).

8th International Conference on Sandwich Structures
ICSS 8
A. J. M. Ferreira (Editor)
© FEUP, Porto, 2008

DEVELOPMENT OF A CONTINUOUS PROCESS FOR THE PRODUCTION OF LIGHTWEIGHT PANELBOARDS

Jan Luedtke [a,*], Johannes Welling [b], Heiko Thoemen [a] and Marius C. Barbu [a]

[a] University of Hamburg
Department of Wood Science
Mechanical Wood Technology
Leuschnerstr. 91, 21031 Hamburg, Germany
www.uni-hamburg.de
*Corresponding author: j.luedtke@holz.uni-hamburg.de

[b] Johann Heinrich von Thünen Institute (vTI)
Institute of Wood Technology and Wood Biology
Leuschnerstr. 91, 21031 Hamburg, Germany
www.vti.bund.de

Key words: Sandwich panel, foam core, continuous production, wood-based facing, one-stage process

Summary. *Driven by the need to reduce the input of resources and to improve the ergonomically aspects of knockdown furniture, the use of lightweight materials has increased enormously over the past years. Yet, another motivation has been added by the steadily increasing costs for raw materials and energy. Different strategies for the production of wood-based lightweight panels are established: For example, the weight of conventional wood-based panels may be reduced by modifying the process parameters or applying adjusted gluing-systems. Another effective way to save weight while maintaining the mechanical properties is the use of sandwich panels. Production of sandwich panels can be done by batch-processing where prefabricated layers are agglutinated, or in situ by continuous processing where the foam core is injected between two prefinished facings. As both ways of assembly lack the possibility of an integrated production of sandwiches with wood based faces, the authors developed an one-stage process. In this innovative process the formation of the surface layers takes place directly before the expansion of the core layer. A three-layered mat, comprising wood particles for the surface layers and expandable material for the core, is formed and then processed in a hot-press. Here, the resin treated surface layers are compacted and cured at a first stage. The thermo-active core is inactive until the core temperature in the middle layer exceeds 90 °C. Once this temperature has been reached the core material starts to react and an internal pressure builds up. The press is opened to a predefined distance to allow the expansion of the core. As this process can be realized with only slight modifications on existing production lines for wood-based panels, a fast implementation of this new technology appears to be feasible. This integrated process has been developed with the objective of both a batch-wise and a continuous production.*

1 BACKGROUND

The wood-based panel industry has shown a steady growth over the last decades. The most relevant products for the furniture industry in Europe are particleboard (PB) and medium density fibreboard (MDF). These products denoted a production volume of 37m m^3 (PB) and 13m m^3 (MDF) in 2006.

The furniture industry processed 53 % of the particleboard and 25 % of the MDF production [1]. With densities around 650 kg/m^3 and 800 kg/m^3, respectively, these types of panels cause high product weights. Especially the fast-growing market for knockdown furniture, where every second Euro for furniture is already spent, calls for pieces of furniture with a low weight [2]. This is reasonable as the costumer picks the packed up pieces of furniture from the storage rack by himself. Thus, the packages have to meet dimensions that match the ergonomic desires, especially in matters of weight. Heavy pieces of furniture have to be split into more than one package. A maximum weight of 25 kg per unit seems adequate [3]. However, decreasing the mass of furniture not only reduces the number of packages. In addition, handling can be simplified when the product is assembled. This reduces the risk of damages and extends the service life of the product [4].

Besides the enhanced ergonomic properties, the desire to reduce the input of resources and to substitute raw materials with lower-priced alternatives are driving forces for developing lightweight panels. Yet another motivation for weight reduction has been added by the steadily increasing costs for energy. The amount of transported goods is often not limited by the volume itself but by the weight. It represents a strong economical factor when more goods per volume can be transported, even though the lightweight alternative seems to be more expensive at first sight. However, classical wood-based panels show a strong price increase and the gap between these panels and lightweight panels made from artificial foams has become much smaller [5]. On the medium-term up to 30 % of the produced wood-based panels can be substituted by light-weight panels [4].

2 OBJECTIVE

Wood based panels can be lightened by different techniques. Either by using lighter raw materials, i.e. less dense wood, by applying adjusted gluing-systems or by modifying the process parameters, the weight of wood-based panels can be reduced. Beside these techniques, it is possible to form a structurally intelligent material by sandwich layering. Placing structurally important and, in most cases, dense parts on the surfaces and less dense parts in the core represents an effective way to save weight while obtaining the mechanical properties.

Many such materials, in particular foam core panels, also provide a good absorption potential for acoustic energy and a high isolation rate for thermal energy [6]. However, sandwich panels do not only hold advantages over conventional boards. The poorly conceived production techniques, a problematic quality control and difficulties with connecting single components of sandwich panels are examples of the downsides of the material [7, 8]. Moreover, the use of a light core is often linked with problems concerning the connectivity and particularly the edge processing. In many cases, e.g. honeycomb boards, the light core consists of a big-celled structure, which strongly constrains edge processing like coating or post forming. This shows that weight saving does not necessarily represent an advantage. The logical consequence is a core layer made from a light and stiff material that completely fills out the core, thereby allowing the processing in nearly every form and direction [9].

The benefit of low weight is often neutralized by the high costs for sandwich materials, as the production is more laborious. Naturally, this is a problem for most composite materials, as different materials have to be combined. At the same time, this opens up an area where improvements can increase the efficiency of production on a grand scale.

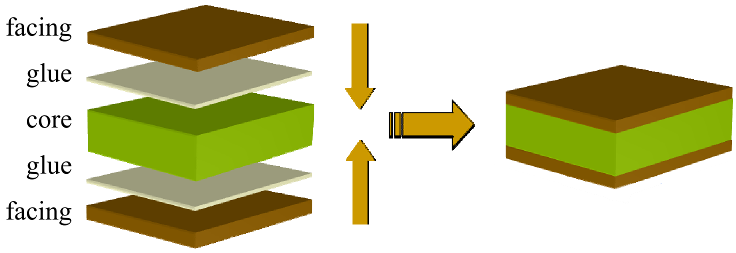

Fig. 1 Principle of a batch-wise foam core panel production

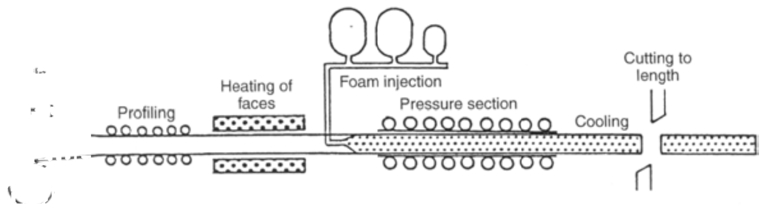

Fig. 2 Principle of a continuous foam core panel production [7]

The production of sandwich panels can be done by batch processing where prefabricated layers are agglutinated (Fig. 1). In such a **discontinuous** production, the prefabricated facings, like thin particleboard, MDF-panels or veneer sheets, are glued to one or more core layers [10]. This represents a general problem when using wood-based surface materials as they are produced in fixed lengths [7] and because of their stiffness not suited to be rolled up. The discontinuous production can therefore be broken down into three separate processes: production of the facings, production of the core layer and the formation of a bonding between these layers [11].

Accordingly, **continuous** processes are used to produce sandwich panels when the facings can be fed in continuously from coils, like foils or papers (Fig. 2). The foam core layer is injected *in situ* between the surfaces. The layered structure runs through a double-belt press where the foam core expands isochoric as the press platens define the final volume. After the core has built a self-supporting matrix and the structure is stable enough to be further processed, the panel can be formatted. The continuous production of sandwich panels means a reduction to two process steps as no more additional bonding is necessary.

Both ways of assembly lack the possibility of an integrated production of sandwich panels with wood-based facings. The objective of this research results from the urgent need to develop a process that combines the advantages of the discontinuous (three-stage) and the continuous (two-stage) production processes. It shall provide a method that allows the production of sandwich panels with wood-based facings in a single-stage process. In the new process, the independent process steps (production of facings, formation of lightweight core) need to be combined in order to increase the effectiveness of the lightweight panel production.

3 PROCESS AND PRODUCT DESCRIPTION

During this research an innovative one-stage process for the production of lightweight panels was developed. The process is similar to existing wood-based panel processes. The processes for the production of particleboard and MDF are well established in the wood-based panel industry.

Basic principle is the scattering of a three-layered mat, comprising wood particles and expandable core material, which is then processed in a hot-press forming a lightweight sandwich panel. This can be done by either a continuous or a discontinuous process.

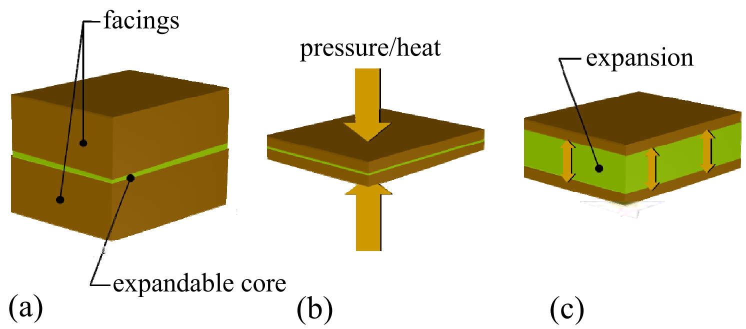

Fig. 3 Principle of the one-stage process, (a) formation of layers, (b) compaction of facings, (c) expansion of core

In a first step, a mat is formed comprising three layers. Two facings enclose the expandable core material by scattering three layers consecutively (Fig. 3a). The wood particles in the surface layers are typically resinated with a urea-formaldehyde resin content of 9-11 %. The dry core material can be scattered in a similar way to wood particles. It consists of a thermo-active polymer, which is able to expand its volume by 40 times upon heating. The temperature needed for the expansion corresponds to the resin curing temperature to ensure the hardening of all components at a certain temperature.

The formed mat is fed into a hot-press where firstly the surfaces are compacted. Under a high initial pressure and a high temperature, the resin cures and the surfaces harden (Fig. 3b). This generates high densities in the surfaces. At this stage, the not yet expanded core material behaves neutral and inactive, and presents a separation layer between the surface layers. By conductive and convective transfer processes, the heat reaches the center of the mat [12]. The reaction of the polymer starts by exceeding its activation temperature of about 90 °C. This causes a pressure, which is built up by the polymer. Simultaneously the press opens to a predefined distance (final panel thickness) to give the core material room to expand (Fig. 3c). Thereafter the press is kept isochoric in this position until the temperature of the polymer foam falls below its active temperature. Preferably, this is done by a press that is capable of being cooled down actively. Because no more pressure is built up inside the foam, the expansion stops. Since the core polymer not only represents the lightweight core material, but also the bonding between the facings and the core, no additional gluing is needed to connect these layers.

As mentioned, the process is realisable in continuous as well as in discontinuous presses. Fig. 3 shows the basic principle of the one-stage process. The corresponding continuous process in a double-belt hot-press is illustrated in Fig. 4. The three-layered mat is compacted during the initial pressing zone in the continuous hot-press. After the facings are hardened, the core material expands with the synchronized opening of the press platens. Running through the cooling zone of the press, the now expanded sandwich panel stabilizes and is ready to be further processed after leaving the press.

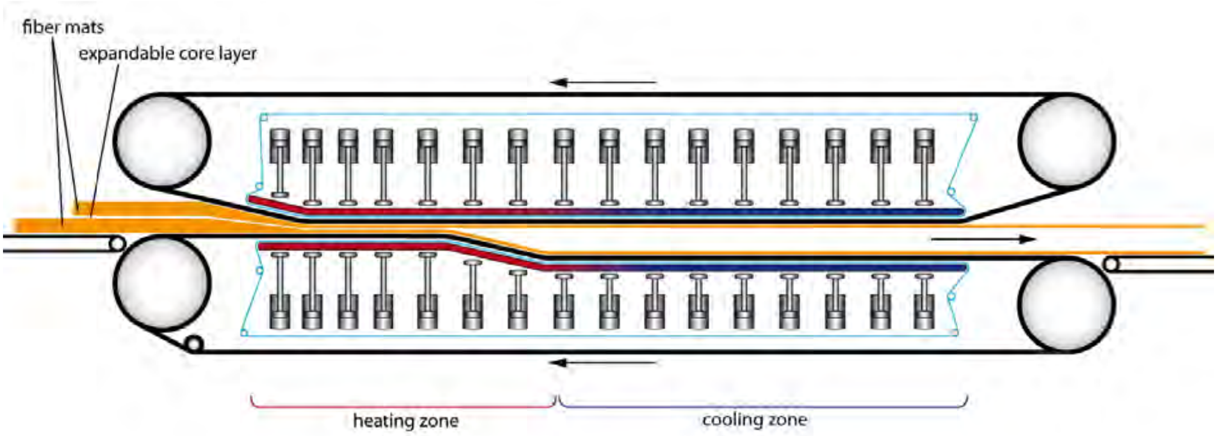

Fig. 4 Continuous production of foam core panels with wood based facings

As the process is similar to those for established wood-based panel processes, e.g. particleboards, only slight modifications of the equipment are needed for an industrial implementation of this technology.

4 RESULTS

The panels produced during the lab-trials revealed a high quality with respect to mechanical properties and further processing options. They showed that it is possible to vary the product parameters in a wide range. The overall density can be adjusted from 200 kg/m³ to 600 kg/m³. This is possible since the thickness of the facings can be as low as 0,5 mm while there is no technical upper limit. The same applies for the thickness of the core. Moreover, the density of the core can range between 100 kg/m³ and 400 kg/m³ by composing the expandable polymer with a mixture of denser materials, like wood particles. A typical density profile is shown in Fig. 5. The profile of the 24 mm thick panel is strongly symmetrical. The highly compacted facings, here with densities up to 1000 kg/m³, correspond to the aspired

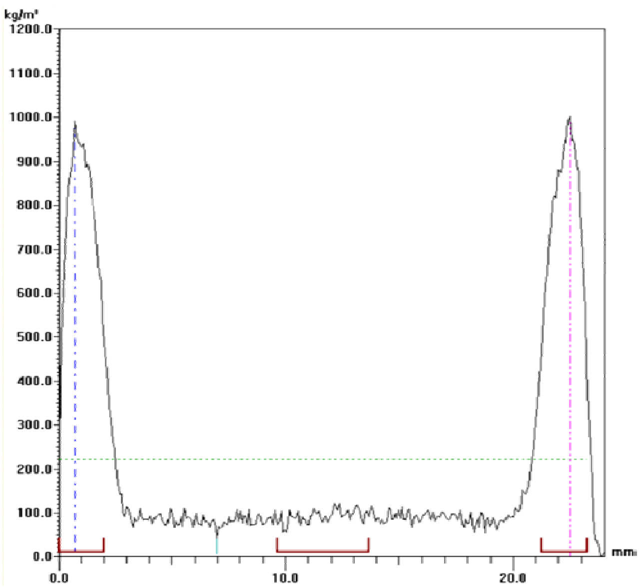

Fig. 5 Density profile of a typical lightweight panel produced using the one-stage process

structural specification. The core reveals a uniform density about 100 kg/m³ and does not show significant peaks that could possibly present a flaw. The mean density of the panel is around 220 kg/m³, which classifies the panel as lightweight, following the classification of Poppensieker and Thoemen [3].

The developed panel and its production process aim at partially substituting particleboard and MDF. Thus, the panels have to meet the demands of specific applications where the classical wood-based panels are predominant nowadays. Especially the furniture industry, as mentioned above, is a main customer for wood-based panels. As the production of the new panel is not sensitive to shape modifications, also three-dimensionally shaped boards with foam core are easily possible and offer a promising perspective [13].

5 CONCLUSIONS

The woodworking industry, especially the knockdown furniture industry, has a strong demand for panels, which meet current and prospective requirements in terms of mobility, ergonomics and economy. Lightweight panels offer an ideal answer in this regard. According to the numbers mentioned above [1], large volumes of lightweight panels will be necessary to substitute a significant part of classical boards. This can only be handled by production processes that are capable of mass-producing lightweight panels.

Foam core panels are not a new invention in this area. However, the production of foam core panels with wood-based facings takes place in separate sub-processes currently, which does not allow a continuous production. This leads to a cost-intensive production that is limited to panel dimensions predetermined by the size of the facing panels. The presented one-stage process demonstrates a method of resolution, which improves the efficiency of the industrial production, thereby increasing the output volume of lightweight panels with wood-based facings significantly.

The panels offer mechanical properties that are, with respect to the weight, comparable to classical wood-based panels. Still the panels are not depending on a frame construction like the established honeycomb boards, neither for structural reasons nor for processing purposes. In accordance with the wide range of product characteristics, like densities, dimensions and shapes, the developed panels and the process for their production could mean a promising innovation for the wood-based panel and the furniture industry.

6 REFERENCES

[1] EPF. *European Panel Federation, Annual Report 2006/2007*. Brussels: (2007).

[2] Knauf M., Frühwald A. Trendanalyse Zukunft Holz - Delphistudie zur Entwicklung der deutschen Holzindustrie. Zentrum Holzwirtschaft, Universität Hamburg; (2004).

[3] Poppensieker J. *Wabenplatten für den Möbelbau* [Diploma Thesis] University of Hamburg; (2005).

[4] Eierle B. *Leichtbau in der Möbelkonstruktion oder: "Billy hat Übergewicht"*. Landshuter Leichtbau-Colloquium; Landshut. (2005).

[5] Michanickl A. *Development of a New Light Wood-Based Panel*. 5th European Wood-Based Panel Symposium 2006; Hannover. (2006).

[6] Gibson L.J., Ashby M.F. *Cellular solids: Structure and Properties*. 2nd ed. Cambridge; New York: Cambridge University Press (1997).

[7] Davies J.M. *Lightweight sandwich construction*. Oxford: Blackwell Science (2001).

[8] Branner K. *Capacity and Lifetime of Foam Core Sandwich Structures* [Ph.D. Thesis] Lyngby: Technical University of Denmark; (1995).

[9] Rakutt D. *Entwicklung neuer Polymerschäume und Fertigungsverfahren zur Herstellung von Sandwichstrukturen: Abschlussbericht für das BMBF-Forschungsprojekt im Rahmen des Programms: Neue Materialien für Schlüsseltechnologien des 21. Jahrhunderts - MaTech.* Laupheim. (2003).

[10] Karlsson K., Åström T. "Manufacturing and applications of structural sandwich components" *Composites*. Part A:15. (1995).

[11] Luedtke J. *Entwicklung eines kontinuierlichen Verfahrens zur Herstellung von Leichtbauplatten* [Diploma Thesis] University of Hamburg; (2007).

[12] Bolton A.J., Humphrey P.E., Kavvouras P.K. "The Hot Pressing of Dry-formed Wood-based Composites. Pt.3: Predicted vapour pressure and temperature variation with time, compared with experimental data for laboratory boards" *Holzforschung*. 43 (4):265-74. (1989).

[13] Fruehwald A., Barbu M.C., Luedtke J. *Multifunctional boards to meet consumer demands*. Cosmu 2007 - 9th Habitat International Congress; Valencia. (2007).

8th International Conference on Sandwich Structures
ICSS 8
A. J. M. Ferreira (Editor)

MODIFIED OCTET TRUSS CELLULAR METALS FABRICATED BY EXPANDING METAL PROCESS

Jai-Hwang Joo* and Ki-Ju Kang†

* Automobile Research Center
Chonnam National University
300 Youngbong-dong, Buk-gu, Gwangju, 500-757, South Korea
e-mail: jjh3646@chonnam.ac.kr, web page: http:// altair.chonnam.ac.kr/~kjkang/

† Department of Mechanical Engineering
Chonnam National University
300 Youngbong-dong, Buk-gu, Gwangju, 500-757, South Korea
e-mail: kjkang@chonnam.ac.kr, web page: http://altair.chonnam.ac.kr/~kjkang/

Key words: Periodic cellular metal, Sandwich plates, Expanding metal process.

Summary. *A new idea is introduced for fabricating sandwich plates with tetrahedral truss cores through metal expanding and folding process and then brazing with solid face sheets. The compressive, shear and three-points bending responses of sandwich panels with the tetrahedral truss cores made of a wrought steel SS41 have been investigated. Good agreement is observed between the measured and predicted peak strengths. The failure mechanism maps are constructed based on the energy balance approach with the non-dimensional parameters: three geometric variables, material parameter, load index, and weight index. The structural failure characteristics of sandwich plates are discussed and an optimal design is derived. The validity is proved when compared with the results of experiments.*

1 INTRODUCTION

Recently, many studies have been performed on the mechanical, thermal properties and the fabrication process of truss PCMs (periodic cellular metals). Main features of the truss PCMs are that they consist of uniform trusses and that they have open cell structures. The former gives the higher specific strength and stiffness than other cellular metals, and the latter gives potential for multifunctional applications such as a heat exchanger. Pyramid, octet, and Kagome truss are typical examples composing the PCMs.

A number of techniques for fabricating truss PCMs have been reported. They are investment casting [1], stacking-up of wire meshes [1], folding of perforated sheet [2, 3], folding of expanded metal [4, 5, 6], tri-axial weaving of wires [7, 8, 9], 3-dimensional assembly of helical wires [10, 11], and so on. Among them, the techniques which are not only currently available for mass-production but also used to fabricate single-layered truss PCMs are folding of perforated sheet [2, 3] and folding of expanded metal [4, 5].

Fig.1 shows the technique ‘folding of perforated sheet’. A metal sheet is punched to be a net with hexagonal meshes, and then it is folded into a shape of triangular wave to be an octet truss PCM. Material loss due to the perforation is a shortcoming. Fig. 2 shows the other technique ‘folding of expanded metal’. A pyramidal truss PCM is fabricated by a conventional metal expanding process and then folding. Compared with the rests, a great advantage of these two techniques is that they are based on the well established, classical sheet forming process. Therefore, least investment is expected, which means low production cost.

In this work, a new technique for fabricating a truss PCM is intorduced. Combining the two techniques mentioned above, an octet-like truss PCM is fabricated by folding expanded metals. This is named ‘M-octet’ after ‘modified octet’. Its strengths under compression and shear load estimated by elementary mechanics are compared with experimental results and those of other competing cellular metals. When employed as a core in a sandwich panel, the load capacity subjected to bending load are estimated by energy based approach for various failure modes. Failure mechanism maps are constructed with the non-dimensional parameters: three geometric variables, material parameter (yield strain), load index and weight index. The predicted failure loads for three designs of geometries are compared with the values measured through experiments.

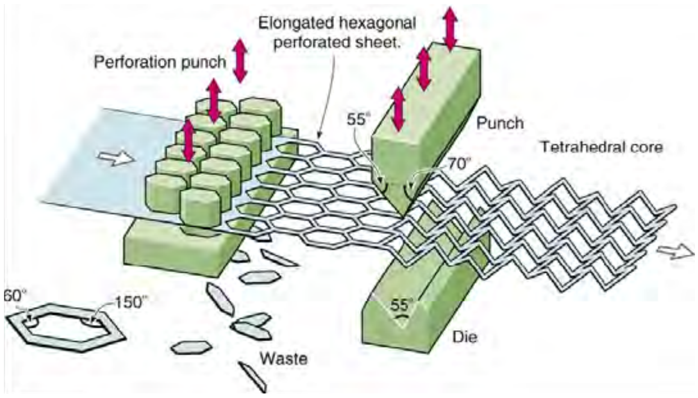

Figure 1 : Schematic of the manufacturing process of the tetrahedral truss PCM involving perforation and folding [2]

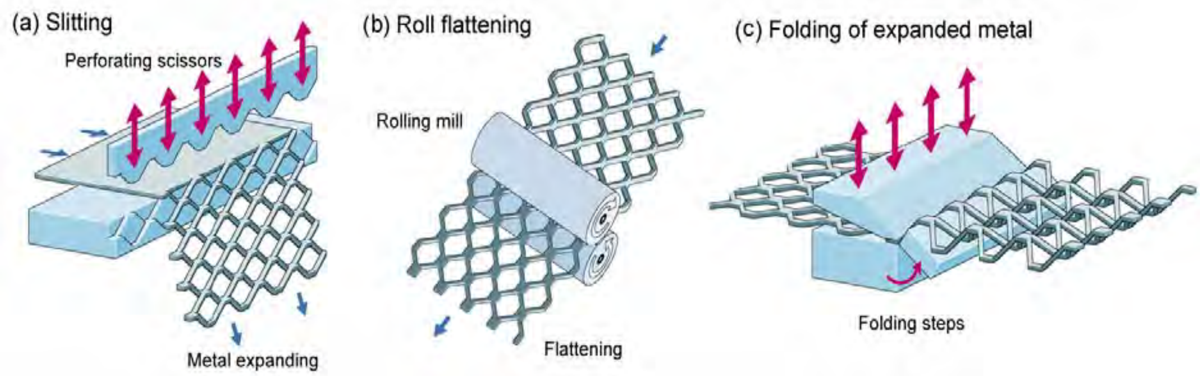

Figure 2 : Schematic of the manufacturing process of the pyramidal truss PCM [1, 5]

2 FABRICATION PROCESS

Fig. 3(a) shows a conventioanl expanded metal process. By a single stroke of pressing, shearing and expanding are carried out simultaneously. And together with incremental feed of a metal sheet and alternative shift of the cutter, a metal net with regular diamond meshes is fabricated. Then, rolling is followed to flatten the net. M-octet is fabricated by a slightly modified cutter. Namely, the width of top and bottom edges of the cutter shown in Fig. 3(a), *b*, get increased so as to have a size equivalent to that of the slanting edges, *c*. Figs. 3(b) and 3(c) show configurations of the modified cutter and the metal net with hexagonal meshes which are fabricated by the modified expanded metal process. After flattened through rolling, the metal net is alternatively folded along the dashed lines, as shown in Fig. 3(c), into a trigonal wave shape to form the M-octet truss PCM. Figs. 4(a) and 4(b) indicate the finally formed M-octet truss PCM and its unit cell, where the angles, α and β are fixed as 60° in this work. Because one of the struts composing the tetrahedron-like structure is twice as wide as the others, its length, l^*, is designed to be related to that of the other two, l as $l^* = 0.823\, l$, in order that the axial stresses acting in all the struts may be equalized under a compressive load, Q. However, the axial stresses are unequalized under a shear load, R, applied in the direction ϕ = 0° as shown in Fig. 4(b). On the contrary, if the struts is designed as $l^* = l$, in order that the axial stresses acting in all the struts may be equalized under a shear load applied in the direction ϕ = 0°.

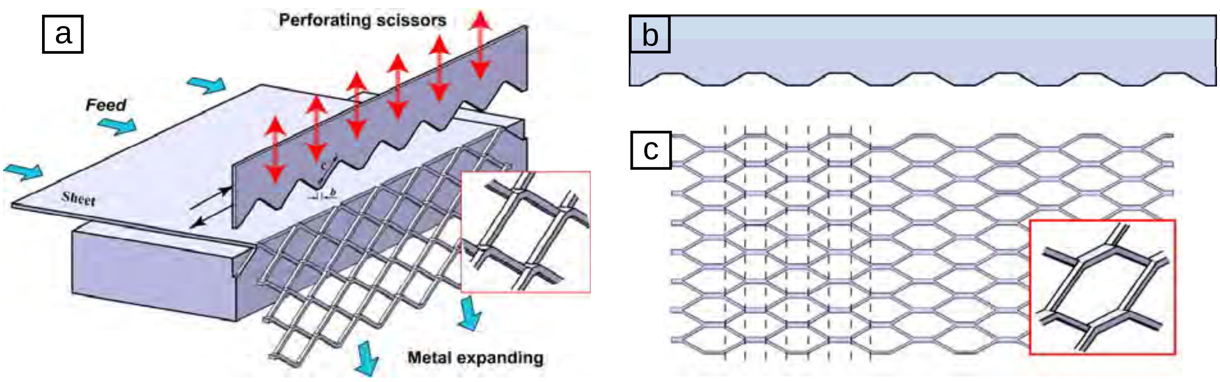

Figure 3 : Schematic of (a) a conventional expanded metal process and configurations of (b) the modified cutter and (c) metal net with hexagonal meshes have been fabricated by the modified expanded metal process.

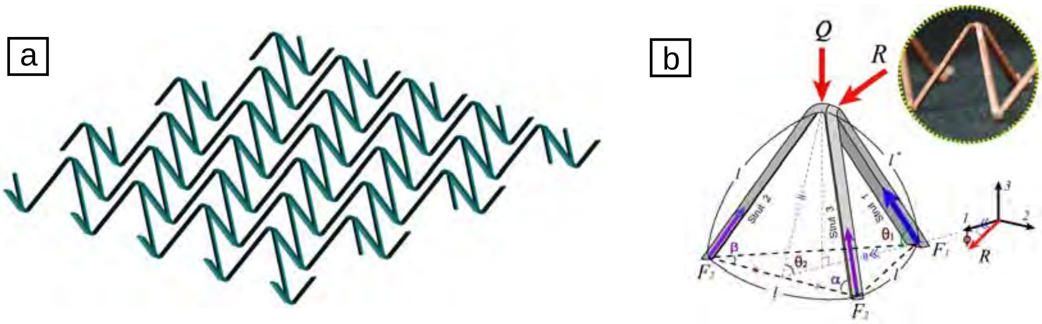

Figure 4 : Configurations of (a) M-octet truss PCM and (b) a unit cell of M-octet truss

3. ANALYTIC SOLUTION AND OPTIMIZATION

3.1 Analytic solutions

The sandwich panels may collapse by the local elastic or plastic buckling of the constituent struts. In order to estimate mechanical properties of a sandwich panels with the M-octet truss core, the equations based on the elementary mechanics of materials are derived as follows. It is assumed that the M-octet truss was composed with ideal struts connected with the ball joints and the force is transmitted to the struts only in the longitudinal (axial) direction. No bending moment is transmitted. First, regarding the core as a homogeneous material, the equivalent normal yield stress, σ_y^c, and the equivalent shear yield stresses, τ_y^c, of the core are given as follows:

$$\left.\sigma_y^c\right|_{elastic} = \frac{\sin(\theta_1+\theta_2)}{\cos\theta_1}\frac{\pi^2 E_c t_c t_f^3}{6l^4}, \tag{1a}$$

$$\left.\sigma_y^c\right|_{plastic} = \frac{\sin(\theta_1+\theta_2)}{\cos\theta_1}\frac{2t_c t_f}{l^2}\sigma_o , \tag{1b}$$

$$\left.\tau_y^c\right|_{elastic} = 1.73\frac{\pi^2 E_c t_c t_f^3}{6\sqrt{3}l^4}, \tag{2a}$$

$$\left.\tau_y^c\right|_{plastic} = 1.73\frac{2t_c t_f}{\sqrt{3}l^2}\sigma_o \tag{2b}$$

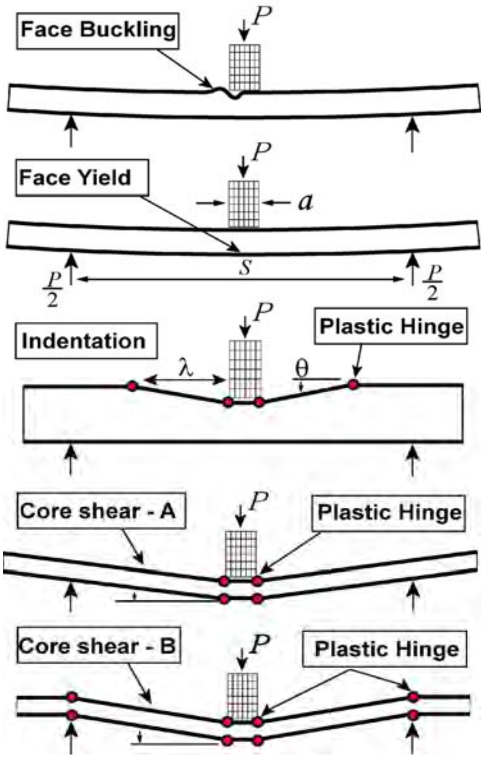

Figure 5 : Failure mechanisms of a sandwich panels with low density core [12]

If lengths of the struts are related by $l^* = 0.823\, l$, θ_1= 61.635° and θ_2= 56.73°. And if $l^* = l$, θ_1= 54.735° and θ_2= 70.53°. In the equations, σ_o and E_c are yield stress and Young's modulus of raw material. And t_c and t_f are the thickness of truss core and thickness of the face sheet, respectively.

The relative density of cores, ρ_{rel}, is expressed by

$$\rho_{rel} = \frac{4}{3}\left(\frac{2}{\sin\theta_2}+\frac{\sqrt{3}}{\sin\theta_1}\right)\left(\frac{t_c}{l}\right)^2 . \tag{3}$$

A sandwich panel with a low density core has five different failure modes under a bending load [12], as illustrated in Fig. 5. They are face sheet elastic wrinkling, face sheet yielding or plastic buckling, indentation, core shear in mode-A, and core shear in mode-B. For estimating the failure loads for each mode, except for face sheet wrinkling and yielding or plastic buckling, two different approaches are available, i.e., the force balance based approach [13] and the energy balance based approach [12]. The former does not consider either indentation or the difference between the core shear in mode-A and the core shear in mode-B.

Therefore, the energy balance based approach is adopted in this work. With the equivalent yield stresses of the core given in Eqs. (1) and (2), the critical loads for the failure modes are expressed as follows; For face sheet wrinkling (elastic), and yielding or plastic buckling, the load, P_f, is

$$P_f = \frac{4Bt_f(H_C + t_f)}{S-a}\sigma_y^f \tag{4a}$$

$$\sigma_y^f = \left(1+r^2\right)^2 \frac{\pi^2 E_f}{12(1-\nu_f{}^2)}\frac{t_f^2}{(l\sin\beta)^2}$$

$$\sigma_y^f = \sigma_o \, .$$

For indentation,

$$P_I = 2Bt_f\sqrt{\sigma_y^c\sigma_y^f} + Ba\sigma_y^c \; . \tag{4b}$$

For core shear modes A and B,

$$P_A = \frac{2Bt_f^2}{S}\sigma_y^f + 2BH_c\left(1+\frac{2D}{S}\right)\tau_y^c, \tag{4c}$$

$$P_B = \frac{4Bt_f^2}{S}\sigma_y^f + 2BH_c\tau_y^c, \tag{4d}$$

respectively. These equations are from Ashby et al. [12]. But, considering the finite width of the lower two contact blocks, a, the critical load for core shear in mode-B is slightly modified. In the equations, E_f and ν_f are the Young's modulus and Poisson's ratio of the face sheet, respectively. H_c is the core height, S is the span between the two supporting points, t_f is the face sheet thickness, and D is the overhang. Because there are two kinds of the equivalent yield stresses of the core, σ_y^c and there are two kinds of τ_y^c for a given orientation, as expressed in Eqs. (1) and (2), depending on the two kinds of strut failure, each of the last three failure modes has two modes, elastic and plastic. Therefore, there are eight failure modes in total.

3.2 Optimization of sandwich panels with M-octet truss cores

In order to derive optimal design of the sandwich panel with the M-octet truss core, and to evaluate it compared with other sandwich panels, the optimization procedure is similar to what Wicks and Hutchison [13] has taken is used. First, six dimensionless geometric design variables are defined as

$$\vec{x} \equiv \left(x_1, x_2, x_3, x_4, x_5, x_6\right) = \left(\frac{t_f}{\ell}, \frac{H_c}{\ell}, \frac{t_c}{\ell}, \frac{a}{\ell}, \frac{D}{\ell}, \frac{B}{\ell}\right), \tag{5}$$

where ℓ is the ratio of the maximum moment, M, to the maximum transverse force, V, $\ell = M/V$. Then, the equations for the critical load for the eight failure modes are converted to the dimensionless forms shown in Table 1, where abbreviations of the failure modes are added. In these constraints, there is one dimensionless material parameter, σ_o/E, and only one dimensionless load parameter, $\Pi = V/\sqrt{EM}$. Among the six variables, the 4th, 5th and 6th ones

	Elastic buckling	Yielding or plastic buckling
Face sheet buckling or yielding	$\left(\frac{V^2}{EM}\right)\left[x_1(x_1+x_2)\left(1+\frac{1}{\sin^2\theta_2}\frac{x_2^2}{x_6^2}\right)^2\frac{\pi^2}{16(1-\nu^2)}\frac{x_1^2}{x_2^2}\right]^{-1}\le 1$ **FE**	$\left(\frac{V^2}{EM}\right)\left(\frac{E}{\sigma_o}\right)\frac{1}{x_1(x_1+x_2)}\le 1$ **FP**
Indentation	$\left(\frac{V^2}{EM}\right)\left[\frac{\sqrt{6}\pi}{8}\left(\frac{\sigma_o}{E}\right)^{1/2}\sqrt{\frac{\sin(\theta_1+\theta_2)}{\cos\theta_2}\sin^2\theta_2\frac{x_1\cdot x_3^2}{x_2^2}}+\frac{3\pi^2}{64}\frac{\sin(\theta_1+\theta_2)}{\cos\theta_2}\sin^4\theta_2\frac{x_4\cdot x_3^4}{x_2^4}\right]^{-1}\le 1$ **IE**	$\left(\frac{V^2}{EM}\right)\left(\frac{E}{\sigma_o}\right)\left[\sqrt{\frac{\sin(\theta_1+\theta_2)}{\cos\theta_2}}\frac{\sqrt{6}}{2}\frac{x_1\cdot x_3}{x_2}+\frac{3}{8}\frac{\sin(\theta_1+\theta_2)}{\cos\theta_2}\sin^2\theta\frac{x_4\cdot x_3^2}{x_2^2}\right]^{-1}\le 1$ **IP**
Core shear -mode A	$\left(\frac{V^2}{EM}\right)\left[\left(\frac{\sigma_o}{E}\right)\frac{x_1^2}{2+x_4}+\frac{3\pi^2}{32}\sin^4\theta_2\frac{x_3^4}{x_2^3}\left(1+\frac{2x_5}{2+x_4}\right)\right]^{-1}\le 1$ **AE**	$\left(\frac{V^2}{EM}\right)\left(\frac{E}{\sigma_o}\right)\left[\frac{x_1^2}{2+x_4}+\frac{3}{2}\sin^2\theta_2\frac{x_3^2}{x_2}\left(1+\frac{2x_5}{2+x_4}\right)\right]^{-1}\le 1$ **AP**
Core shear - mode B	$\left(\frac{V^2}{EM}\right)\left[\left(\frac{\sigma_o}{E}\right)\frac{2x_1^2}{2+x_4}+\frac{3\pi^2}{32}\sin^4\theta_2\frac{x_3^4}{x_2^3}\right]^{-1}\le 1$ **BE**	$\left(\frac{V^2}{EM}\right)\left(\frac{E}{\sigma_o}\right)\left[\frac{2x_1^2}{2+x_4}+\frac{3}{2}\sin^2\theta_2\frac{x_3^2}{x_2}\right]^{-1}\le 1$ **BP**

Table 1 : Dimensionless forms of constraints due to several failure modes and abbreviations of the failure modes

regarding the contact block width, overhang and face-sheet width, respectively, are set fixed in this works. For a given set of the remaining three variables, i.e., $(x_1,x_2,x_3)=\left(\frac{t_f}{\ell},\frac{H_c}{\ell},\frac{t_c}{\ell}\right)$, the dimensionless weight defined as $\Psi=\frac{W}{\rho\ell}=2x_1+\left(\frac{2}{\cos\theta_1}+\frac{\sqrt{3}}{\sin\theta_1}\right)\sin^2\theta_2\frac{x_3^2}{x_2}$ and the dimensionless loads for the eight failure modes, Π, are calculated for design optimization. In Lim and Kang's article [15], three different optimizations were presented for a truss cored sandwich panel. They were to seek design parameters to give a minimum weight for a given load, to give a maximum load for a given weight, and to give a maximum load per weight for a given core height. For example, the dimensionless failure load per weight, Π^2/Ψ, was to be maximized for a given H_c under the eight constraints. Fig. 6 is

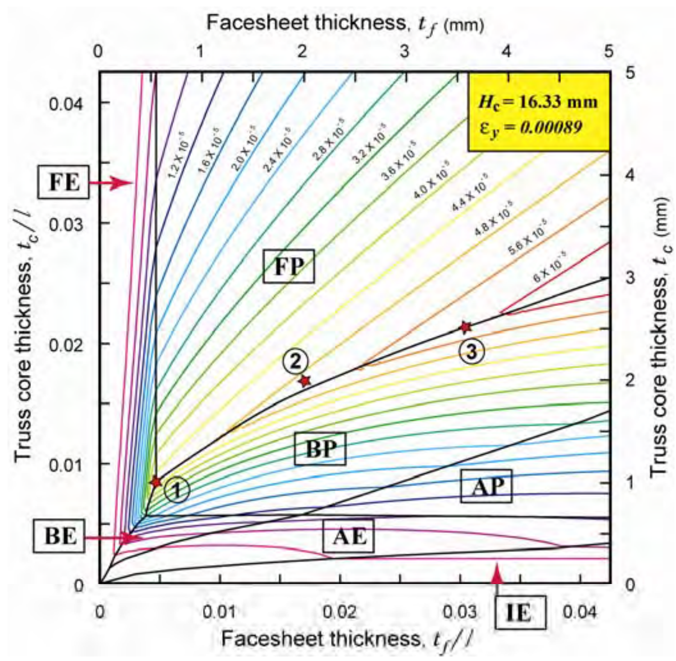

Figure 6 : Failure maps illustrated as functions of t_c and t_f for H_c=16.33mm. The domain boundaries and the contours of failure load per weight, Π^2/Ψ

a failure map plotted as functions of t_c and t_f for a given core height, H_c=16.33mm and for a given material ε_y=0.00089 of the specimens used for the experiments which will be presented in the next chapter.

4 EXPERIMENTS

4.1 Specimen design

For case studies, three kinds of specimens were designed as shown in Table 2. Those were named Design-1, 2 and 3. All the designs had the similar overall sizes, i.e., the total length, L (= S+2D) =374mm, the width, B =70mm, the core height, H_c=16.33mm. Also, all the designs were supposed to be loaded by one an identical three-point-bend jig with the span, S =265mm, the contact block width, a =30mm and the overhang, D =54.5mm. These three designs are indicated on the failure map of Fig. 6. Design-1 is located on the triple point among the face sheet buckling (FE) domain, face sheet yielding (FP) domain, and core shear-mode B plastic (BP) domain, while Design-2 and -3 are located on the boundary between face sheet yielding (FP) domain and core shear-mode B plastic (BP) domain. Design-3 has the thickest truss struts and face sheets.

Design No.	Face sheet thickness, t_f	Core height, H_c	Truss core thickness, t_c	Total length, L	Width, B
1	0.55	16.33	1.0	374	70
2	2.0		2.0		
3	3.6		2.5		

Table 2 : Dimensions of three designs of three-point bend specimen (unit: mm)

4.2 Specimen preparation

Both the cores and face sheets were fabricated from sheets of a low carbon steel JIS SS41. Because developing the fabrication process including shearing and expanding machine will be another technical challenge, a simplified approach was taken to fabricate the specimen cores, temporarily. The M-octet truss sandwich panels are fabricated as follows: First, the cut of unique pattern was introduced on the sheet by using YAG laser. The sheet was expanded width-wise to be the metal mesh similar to that shown in Fig. 3(c). Then, the mesh was bent along the lines connecting the longer ends of the hexagon shapes as mentioned above. Finally, the core was bonded with the upper and lower face sheets by brazing with copper filler metal (Paste: CTK-C699, CHEM-TECH Korea Co.) which was carried out at 1120°C in de-oxidation atmosphere of H_2-N_2 mixture.

4.3 Experiments and the results

An electro-hydraulic test machine, SATEC TC-55, was used to measure the material properties of the raw material and to evaluate mechanical performance of the M-octet sandwich specimens. Tensile specimens of dog-bone geometry with the 2mm × 1mm cross sectional area were cut from the as-received low carbon steel JIS SS41 sheets and were subjected to the same heat cycle as that brazed to prepare the M-octet cored sandwich specimens. It was tested under 0.005mm/sec displacement control with an extensometer of 25mm gage length, attached on the surface. The engineering stress versus strain response of the as-received and as-brazed SS41 are shown in Fig. 7. The curve indicates a distinctive yield point and followed by a short load drop and then reincrease. The specimen metal behaves in a typical elastic-plastic manner with a Young's modulus E=196 GPa, a yield strength and ultimate tensile strength were 174.6 MPa and 420 MPa, respectively.

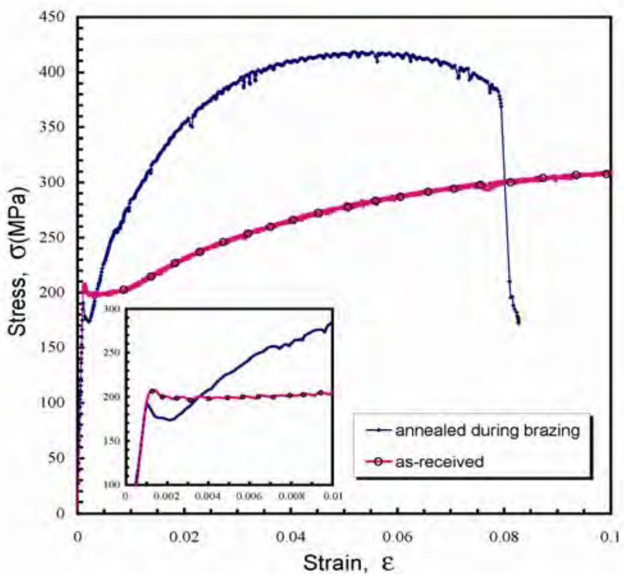

Figure 7 : Stress-strain curves of the as-received and annealed SS41 during brazing

Initially, two types of tests were conducted on the M-octet sandwich plate: (a) out-of-plane compression, and (b) shear in the direction ϕ= 0°. The sandwich core is regarded as a homogenous material and its stress versus strain behavior is measured. The optical images in Fig. 8 reveal buckled truss cores in the sandwich panels during compression and shear tests. The compressive and shear response of M-octet specimens are shown in Fig. 9. The solid lines denote the equivalent yield stress estimated by Eqs. (1b) and (2b). A little overestimation is observed. Therefore, it is concluded that the equations provide fairly good estimations of the equivalent yield stress of the M-octet truss cored sandwich panels.

Fig. 10 shows the performances of M-octet truss PCM as a function of relative density for competing sandwich panel core topologies. The normalized strength of the M-octet truss is slightly lower than that of the square honeycomb, but it is similar to that of pyramidal truss structures. In addition, the elastic modulus of the M-octet truss is similar or slightly higher to that of ideal octet truss under compression and shear load.

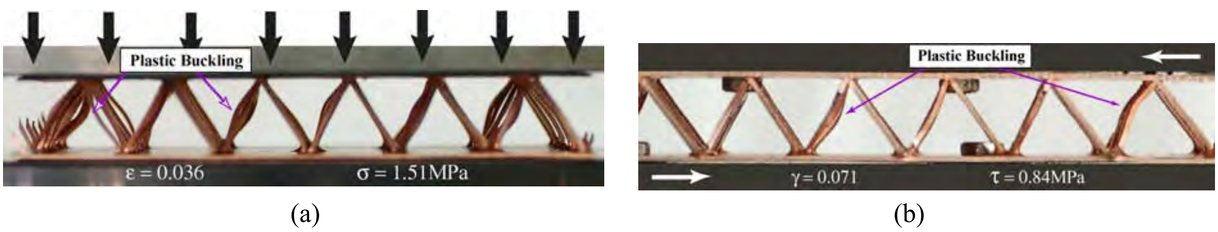

Figure 8 : Optical images showing buckled M-octet truss core in the sandwich panels : (a) out-of-plane compression, and (b) shear in the direction ϕ= 0°

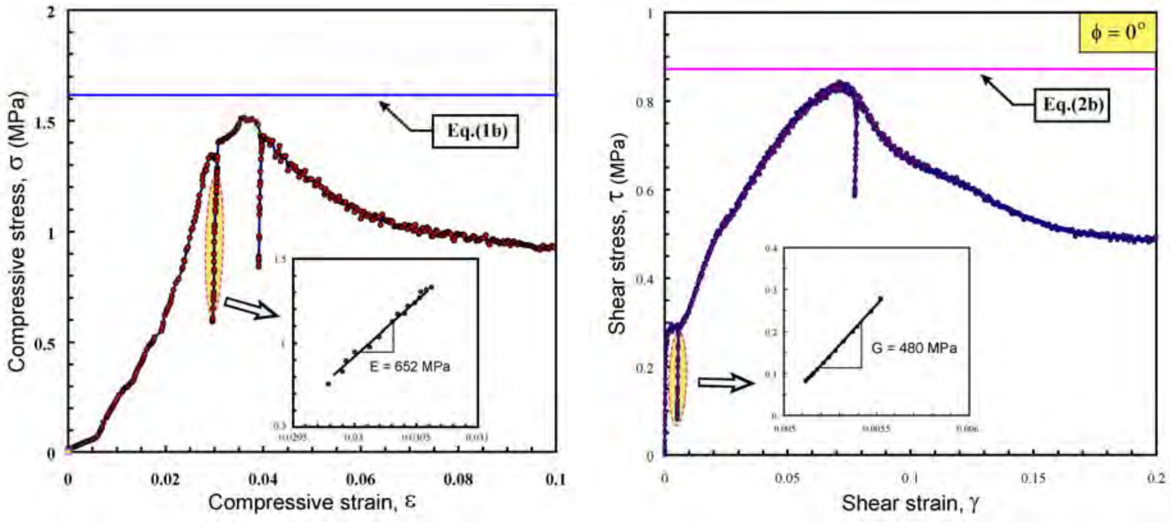

(a) (b)

Figure 9 : Compressive and shear response of M-octet truss PCM measured by the experiment in comparison with that estimated by Eq.(1b) and Eq.(2b). (a) out-of-plane compression, and (b) shear in the direction $\phi = 0°$

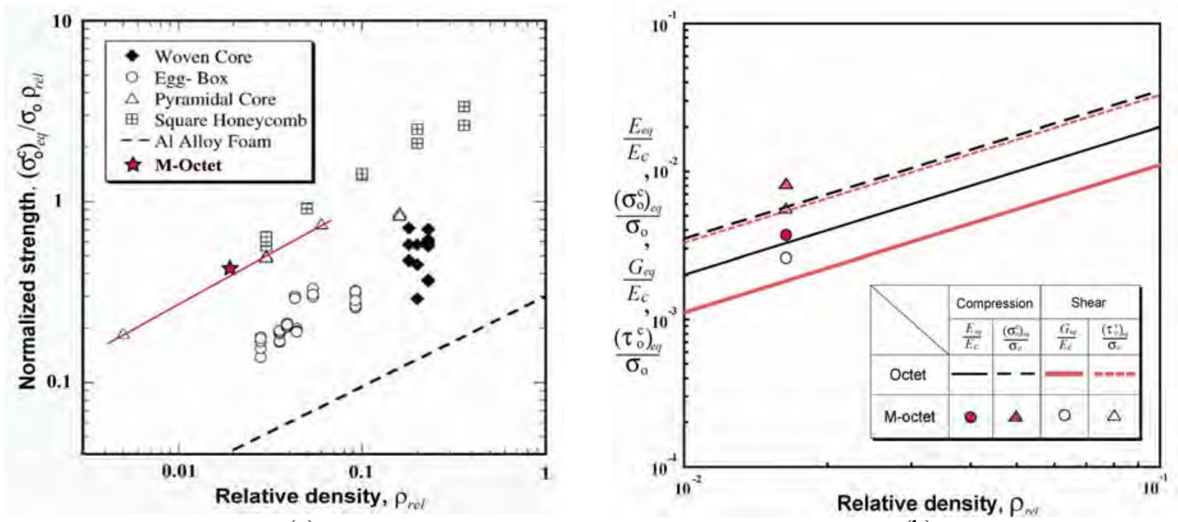

(a) (b)

Figure 10 : Performances of M-octet truss PCM as a function of relative density for competing sandwich panel core topologies [15, 3] : (a) normalized core strength (b) elastic modulus

Three-points bend tests were conducted with the sandwich specimens of the three designs. Instead of typical roller supports, roller-and-concave-block assembly was used to suppress the local indentation at the upper face sheet. Displacement was controlled at 0.005 mm/sec. The specimen deformation happening during the tests was monitored by a digital CCD camera. Fig. 11 shows the deformed shapes of specimens of Design-1 to 3 after the tests. Design-1 specimen was obviously failed by buckling of the upper face sheet, and Design-2 specimen was failed by yielding of the lower face sheet, while Design-3 specimen was failed by the core shear-mode B.

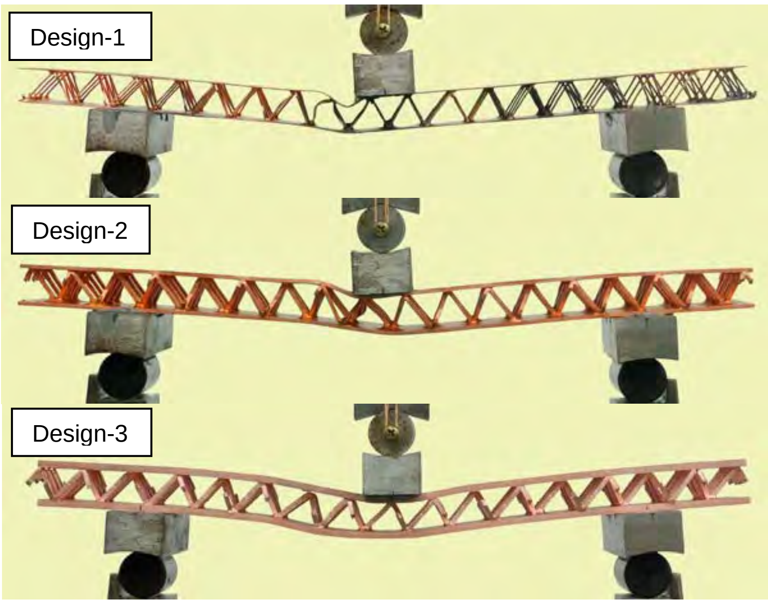

Figure 11 : Deformed shapes of Design-1, 2, 3 specimens after the three-point bend tests

Fig. 12 shows the measured load-displacement curves together with those estimated by Eqs. 4(a) to 4(d). Design-1 specimen reached earliest the peak load and the load level droped in a short period of time. In the curve of Design-2 specimen, even after the initial yield point, the load level increased steadily for a while, and then decreased slowly. On the contrary, in the curve of Design-3 specimen, the load level increased steadily for the longest time after the initial yield point, and then it partially and rapidly droped three times. According to the images monitored by the CCD camera, each sudden partial drop in the load level reflects breakaway of a strut from the face sheets. The difference among the load-displacement curves can be interpreted from a view point of nature of the deformations occurred in the three specimens. In Design-1 specimen, the failure occured due to the elastic buckling of the face sheet, In Design-2 specimen, the failure occured by plastic yielding of the lower face sheet and partailly yielding of core members, and in Design-3 specimen, however, it occured by plastic yielding of the core members accompanied with plastic hinges in the face sheets.

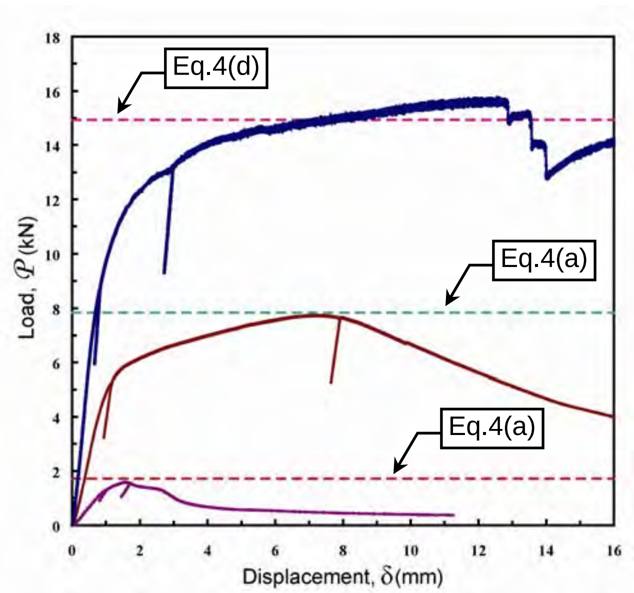

Figure 12 : Load-displacement curves measured during the three-point bend tests of Design-1, 2, 3 specimens compared with those estimated by Eqs. 4(a) to 4(d)

Table 3 listed the measured weight and critical load capacities of the three specimens in comparison with those estimated equations described in the section 3.1. In all the designs, the estimated critical loads agreed fairly well with the measured ones, which demonstrates accuracy of the approaches taken in this work, even though the equations are based on elementary mechanics of materials. The significant differences were observed among the critical load capacities of the three designs, but the load-per-weight and stiffness-per-weight ratios are not very different from each others. One might say that all the designs have similar performances. However, there is an obvious difference in the performance quality among the designs. That is, Designs-1 are substantially inferior to Design-2 and 3 in terms of the energy absorption and deformation stability after the peak point.

Specimen Name	Measured				Estimated				Error $\left(=\frac{B-A}{A}\times 100\right)$
	Weight (kg)	(A) P_{max} (kN)	P_{max} /Weight (kN/kg)	Stiffness /Weight (kN/mm kg)	(B) P_{max} (kN)	$\frac{\Pi^2}{\Psi}$	P_{max} /Weight (kN/kg)	Stiffness /Weight (kN/mm kg)	
Design-1	0.28	1.59	5.68	9.47	1.72	4.5×10^{-5}	7.34	7.75	8.2%
Design-2	0.96	7.75	8.07	9.61	7.84	5.3×10^{-5}	8.85	9.58	1.2%
Design-3	1.70	15.75	9.26	10.16	14.86	5.9×10^{-5}	9.80	10.56	-5.6%

Table 3 : Measured and estimated performance of the M-octet truss cored sandwich panels under bending load; weight and critical load capacities

5 CONCLUSIONS

In this work, a new technique for fabricating a truss PCM has been described. Namely, combining the two previous techniques, an octet-like truss PCM named 'M-octet' is fabricated by folding expanded metals. Its strengths under compression and shear load estimated by elementary mechanics were compared with experimental results and those of other competing cellular metals. When employed as a core in a sandwich panel, the load capacity subjected to bending load were estimated by energy based approach for various failure modes. For a given core height, a failure map was constructed with the non-dimensional parameters: three geometric variables, material parameter (yield strain), load index and weight index. By using the map, three designs were chosen for maximum load per weight ratio. The predicted failure loads for three designs of geometries were compared with the values measured through the experiments which were performed with sandwich specimens with the tetrahedral truss cores made of a wrought steel SS41. As the results, the following conclusions have been drawn:

i) The measured equivalent normal yield stress and shear yield stress were 7% lower than the estimated ones by the analytic solutions, which is regarded as a fairly good agreement.

ii) In the three-points bend tests, for Design-1 and 2, the critical loads and the corresponding failure modes are in good agreement with the estimated ones. But, for Design-3, the failure happened by breakaway of struts from the face sheets. The peak point was delayed the most, which gives a main benefit in the performance quality, that is, in terms of the energy absorption and deformation stability after the peak point.

ACKNOWLEGEMENTS

This work was supported by National Research Lab. of the Korea Science & Engineering Foundation (KOSEF grant number R0A-2006-000-10249-0).

REFERENCES

[1] H. N. G. Wadley, N. A. Fleck and A. G. Evans, "Fabrication and Structural Performance of Periodic Cellular Metal Sandwich Structures," *Composite Science and Technology*, 63, 2331-2343 (2003).
[2] D. J. Sypeck and H. N. G. Wadley, "Cellular Metal Truss Core Sandwich Structures," *Proceedings of the 2nd International Conference on Cellular Metals and Metal Foaming Technology (MetFoam 2001)* edited by J. Banhart, M. F. Ashby, N. A. Fleck, 381-386 (2001).
[3] S. Chiras, D. R. Mumm, N. Wicks, A. G. Evans, J. W. Hutchinson, K. Dharamasena, H. N. G. Wadley and S. Fichter, "The Structural Performance of Near-optimized Truss Core Panels," *International Journal of Solids and Structures* , 39, 4093-4115 (2002).
[4] F. W. Zok, S. A. Waltner, Z. Wei, H. J. Rathbun, R. M. McMeeking and A. G. Evans, "A Protocol for Characterizing the Structural Performance of Metallic Sandwich Panels: Application to Pyramidal Truss Cores," *Int. J. of Solids and Structures*, 41, 6249-6271 (2004).
[5] G. W. Kooistra and H. N. G. Wadley, "Lattice Truss Structures from Expanded Metal Sheet," *Materials and Design*, 28, 507-514 (2007).
[6] C. H. Lim, J. H. Lim, J. G. Jung, J. D. Lim and K. J. Kang, "Mechanical Behavior of Sandwich Panels with Quasi-Kagome Truss Core Fabricated from Expanded Metals," *Trans. of the Korean Society of Mechanical Engineers A*, 30, 1078-1085 (2006).
[7] J. H. Lim, S. J. Nah, M. H. Koo and K. J. Kang, "Compressive and Bending Behavior of Sandwich Panels with Octet Truss Core Fabricated from Wires," *Trans. of the Korean Society of Mechanical Engineers A*, 29, 470~476 (2005).
[8] J. H. Lim and K. J. Kang, "Mechanical Behavior of Sandwich Panels with Tetrahedral and Kagome Truss Cores Fabricated from Wires," *Int. J. of Solids & Structures*, 43, 5228-5246 (2006).
[9] J. H. Lim and K. J. Kang, "Wire Formed Cellular Metals," *Materials Transactions*, 47, 2154~2160 (2006).
[10] K. J. Kang and Y. H. Lee, US Patent Pending Application 10/578,421 (2005).
[11] Y. H. Lee, B. K. Lee, I. Jeon and K. J. Kang, "Wire-woven Bulk Kagome (WBK) Truss Cores," *Acta Materialia*, 55, 6084-6094 (2007).
[12] M. F. Ashby, A. G. Evans, N. A. Fleck, , L. J. Gibson, J. W. Hutchison and H. N. G. Wadley, Metal Foams: A Design Guide, Butterworth Heinemann, 116-120 (2000).
[13] N. Wicks and J. W. Hutchinson, "Performance of Sandwich Plates with Truss Cores," *Mechanics of Materials*, 36, 739-751 (2004).
[14] M. Zupan, V. S. Deshpande, and N. A. Fleck, "The Out-of-Plane Compressive Behavior of Woven-core Sandwich Plates," *European Journal of Mechanics* A/Solids, 23, 411~421 (2004).
[15] C. H. Lim, I. Jeon, and K. J. Kang, "A New Type of Sandwich Panel with Periodic Cellular Metal Cores and its Mechanical Performances," submitted to *International J. of Solids & Structures* (2007).

8th International Conference on Sandwich Structures
ICSS 8
A. J. M. Ferreira (Editor)

FREE FORM SANDWICH SHELLS AS LOAD BEARING STRUCTURES FOR LIQUID ARCHITECTURE

A.C.J.M. Eekhout[†], P.A. van de Rotten[*]

[†] Professor, Faculty of Architecture
Delft University of Technology (TU Delft), Octatube International BV
Berlageweg 1, 2628 CR Delft, the Netherlands
E-mail: A.C.J.M.Eekhout@tudelft.nl, web page: http://www.bk.tudelft.nl

[*] PhD, Faculty of Architecture
Delft University of Technology (TU Delft)
Berlageweg 1, 2628 CR Delft, the Netherlands
E-mail: P.A.vandeRotten@tudelft.nl, web page: http://www.blob.tudelft.nl

Key words: Free Form Sandwich Shells, Technology Transfer, Liquid Design, Architecture, Load Bearing Structure

Summary: Well educated Architects are able to control the most difficult 'free form' configurations with the newest design software; however the available structural palette for the structural engineer is limited. It is an important objective to design relatively lightweight, stiff and strong structures with also other qualities; freedom of design for architect and engineer in configuration, rigidity against bending moments which develop due to the sculptural design, thermal and acoustic isolation, larger free spans, resistance to fatigue and damage and low maintenance. Composites, and especially fibre reinforced sandwiches, have all of these qualities potentially. In this paper the main attention is given to the 'free form' roofs of the Rabin Centre in Tel Aviv. The principle idea for this roof was put forward in discussion with engineers from Aeronautics. The production stage was assisted by the transfer of technology from yachting industry, although the architectural application mainly in its size, transport, shipment and assembly had to be developed for the building industry's level of technology and pricing.

1. INTRODUCTION

This paper focuses on the structural consequences of free form design and the chances for fibre reinforced composite shells in these liquid designs.

Quote Zaha Hadid (Architect):"*In a design environment that is dominated by new software that enables us to rethink form and space radically, there is an urgent need for 'hightech' materials, which match our computer-generated complex shapes and special conditions.*"

Architects are continuously searching for innovative construction methods and inspirational materials which cover the new types of free form architecture. Since the introduction of users friendly 3D software a large group of architects is able to control the most difficult configurations of buildings. This ‘free form’, ‘fluid’ or ‘liquid’ design demands a totally different view on structures than a structural engineer is used to. It is not possibly to convert a difficult 3D model into simple 2D systems. In order to come to more efficient structures for liquid architecture real 3D structural action is demanded. It creates structural possibilities which one will never find when the structure is simplified in to 2D models. However, the structural palette for real fluid free form 3D structures is limited.

2 THREE DIMENSIONAL STRUCTURES; ARCHITECT VS ENGINEER

In the 1960-ies thin shells of concrete and fibre reinforced plastics, followed the ideal spherical, conical, cylindrical or hyperboloidal forms. Results were mostly 50 mm thick concrete shells with only one central reinforcement layer of steel bars, working as load bearing structure and a physical barrier or skin. Many shells had a Hispanic origin: Eduardo Torroja, Spain, and Felix Candela, Mexico were the prominent pioneers. The shells were built in countries with high material and low labour costs. In Switzerland, Heinz Isler prolonged the life of shells by strongly reducing the problem of local labour with clever wooden formwork techniques up to the 1990s. These shells were designed in an open and direct collaboration between architect and engineer. Nevertheless the pioneers of the 1970s retired and the concrete shell fashion stopped.

Blob architecture emerged in the late 1990s (Guggenheim Museum Bilbao, Frank O. Gehry, 1998) changed these conditions, as the architect designs either directly in models or on the computer as if he is a sculptor. The dramatic 3D effect dominates architectural thinking. The structural designer has not an equal position, but is asked subsequently after the architect has found out a model or geometry which suits him out of visual design considerations. There are usually no direct feed-backs. The required forms are now fully arbitrary and have not an ideal geometry for a traditional shell, nor for a tensile structure. Due to the limited structural palette load bearing structures do not often match with the configurations of the buildings. This led to a smoothly shaped skin which covers the rude polygonal structure, without any direct spatial relation between the two, see Figure 1.

Figure 1 Structure behind the skin of the Guggenheim museum

Figure 2 I-web at the TU Delft 2006, with new roof

The I-web of Cas Oosterhuis is constructed with a spatial load bearing structure which does follow the shape. The complete structure was created and designed only from geometric considerations and engineered just after that stage with the computer and 3D engineering programs. The project was a pilot for the 'file to factory system', or as Greg Lynn calls; mass customization. For the structural concept beams of steel plates, in fact only a structural web was used no flanges, creating a spatial frame which led to not very efficient and very heavy structure, see

Figure 2, 8 times heavier than a single layered space frame which was studied by Eekhout at the start of the project.

What if the structural skin is placed on both sides of the steel plates? This sandwich system could be an efficient structure in free formed buildings because it can handle bending moments. However, it is not easy to create these kinds of free form load bearing structures with steel.

For roofs the dead load is a major part of the total loads. Decreasing the weight of structure is an economic solution. But also other qualities are demanded: freedom of design for architect and engineer, rigidity against bending moments due to the non structurally optimized sculptural design, resistance to fatigue and damage and low maintenance. Composites, and specially fibre reinforced sandwiches, have all of these qualities potentially. An exoskeleton, like that of an insect, could work like a skin or a suit of armour for the building. Besides, the skins can adapt their stiffness and strength over the surface. Until now 3D-curved fibre reinforced sandwich shells are a new and under-exposed area in the building industry. Innovation in engineering, prefabricated production and assembly and smart use of materials is essential to arrive at a successful result.

To arrive at this result it is necessary to transfer the knowledge of fibre reinforced sandwich structures from other composite industries, like aeroplane and maritime engineering, into the building industry. After the transfer an adaptive development has to take place on (building) load cases, component sizes, connections, overall smoothness over the seams, tolerances of dimensions, transport and structural performance. These will present the designer a totally different context at which a different 3D-shell approach is necessary.

3 HISTORICAL OVERVIEW

Composites are not new as concept or material in the building industry. In fact thousands years ago people already mixed clay and straw to create stiff and strong walls for their houses; prehistoric composites. In this paper the focus is on fibre reinforced resins. The development of materials and production methods did never go as fast as the last decades. This is summarized in the evolution of engineering materials with the time in the graphics of Ashby [1].

For the fibre reinforced plastic composites a few important developments are listed. In the 1930s epoxies and the first structural glass fibres for the commercial market were developed in America. Only after the development of polyester in the 1940s the first combinations of fibre reinforced plastics were made. In 1957 the first fibre reinforced composite sandwich house was built; ‘The Monsanto House of the Future’ in Disney World, a cooperation between the Monsanto chemical Company and the Massachusetts Institute of Technology (MIT). The ideas and knowledge to combine structure and skin came from the airplane and boat industry. It is known as the first free form structural fibre reinforced composite sandwich used in the building industry. Each wing forms a cantilever of 4,88m. The top and bottom are composed of two sandwiches forming a box beam. The skins of each sandwich are made of 6-9mm glass fibre reinforced polymers and the core of 60-100mm PUR foam [2]. However the production was still a very labour-intensive process with hand made moulds and lay up processes to produce the composites.

Figure 3 Monsanto House of the Future

In the 1960s carbon fibres came onto the market which made it possible to create much stiffer and therefore lighter structures. Only these carbon fibres are at least 10 times more expensive then glass fibres, depending on their strength and stiffness. Or these fibres will become economic depends on the limitation of the glass fibres and the developments in prices of the carbon fibres.

After developing several pilot projects during the 1950s, 1960s and 1970s of glass fibre reinforced polyester houses the development stopped not only due to the oil crisis. In the building industry many people are involved which all must be convinced of the new materials, while steel and reinforced concrete are familiar. But perhaps the largest advantage of the material is directly the largest obstacle; the freedom of creating your own composition and material. There is hardly any standardization for fibre reinforced structures. For each project the composite and their details are custom made for the unique situation. For this reason it is important to change the traditional way of thinking for load bearing structures for liquid architecture.

Since the seventies progress is booked in the fibre reinforced plastic composite industry. New combinations of fibre and resins are possible, and the bonding is improved. For the resins an important progress is booked on fire-resistance, smoke and toxic emissions. However, the most progression has been made during the 1990s in the production methods. With ‘vacuum injection’ and ‘resin transfer moulding’ methods it became possible to create relatively fast large accurate composite components. It is a labour-extensive process and the styrene emission is very low. While the fibre volume percentages are much higher compared with hand lay up. This offers possibilities to create lighter and less expensive load bearing structures. With carbon-epoxy the strength and stiffness of the composite sandwiches is higher, however the carbon fibres are due to the high energy production process still expensive. Moreover an essential problem of sandwich composite shells in architecture is the overall site of the shells, which is usually larger then the curing oven allows.

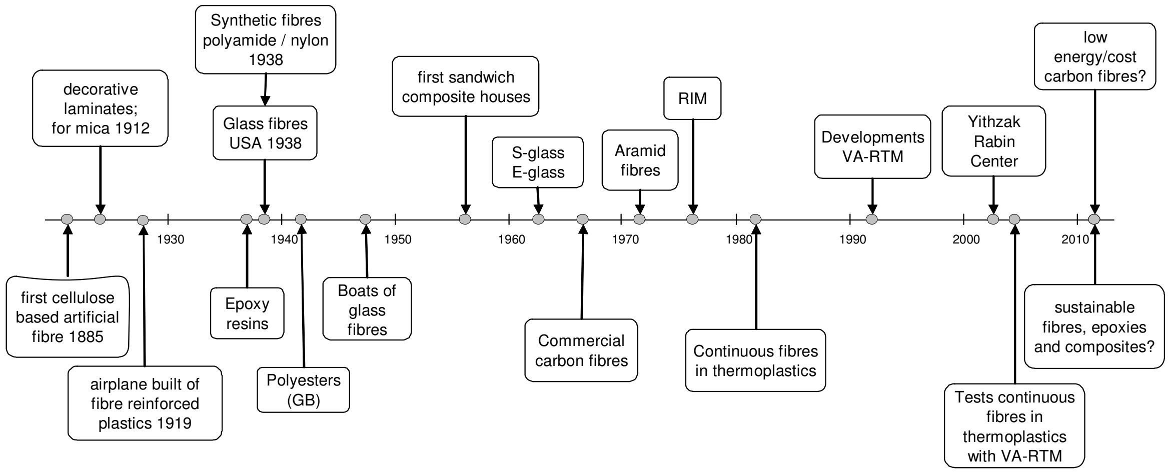

Figure 4 Time line; developments in the fibre reinforced plastic composites [3][4]

4 RABIN CENTER

4.1 The transfer of technology

In November 2002 Octatube received the tender drawings of the Yitzhak Rabin Center, Tel Aviv, designed by Moshe Safdie Architects. The drawings for the 3D roofs, resembling peace doves, were made by ARUP and analyzed as an arbitrary steel structure with a layer of concrete. The roof cladding was left open to the contractor, yet the architect had given the preference to a seamless solution. After a brainstorm session of the engineering department of Octatube the following idea was conceived: the roofs would be made as giant surfboards of foam with GRP skin, creating 5 different GRP sandwich roof wings with a maximum length of 30m and a maximum width of 15 to 20m. The principle idea was put forward in discussion with colleagues from Aeronautics. The process of design & engineering, made use of state-of-the-art design and engineering software, but relied even more on the abilities and imagination of the technical designer. The production stage was greatly assisted by the transfer of technology from yachting industry, although the architectural application, mainly in its size, transport, shipment and assembly had to be developed for the building industry’s level of technology and pricing.

Naturally assembly & erection was the third phase (after design & engineering and production & logistics), but its influence already played a big role during the concept, design, engineering and production.

The composite segments or components, produced in the Netherlands, had to be structurally connected on site to each other in order to hoist them in place. Each wing is subdivided in long curved segments of 3,5m width, divided at the place of the stringers, in order to reduce the number of seams that had to be finished on the building site. Since the curves of the roof proved to be quite large at certain points, some segments had to be subdivided in the length direction as well, because otherwise an economic and feasible transport would prove impossible.

From January 2005 onwards the production went into operation and the third year of experimental production and assembly started with experimental production of the components on the negative moulds milled by Nedcam from CAD/CAM files. The production technique used in this case had been taken from standard production techniques of producing sailing ship hulls. Experimental vacuum injected productions meant a clever step. However, the production proved to be very engineering intensive. Using vacuum-injection, glass fibre weaves were laid in the mould and impregnated with polyester resin. Since the resulting layer of GRP described the desired shape in the best possible way, this side of the mould became the upper layer of the roof. After this layer the fire-resistant polyurethane blocks were applied to the GRP roof layer. The foam blocks were subsequently covered with more glass fibre weaves and a foil for the next vacuum-injection. The integrated stringers, of 4-8mm thick glass fibre polyester resin, are positioned more or less perpendicular to the main span of the shells. They should eventually increase the stiffness of the shells, since bending and fatigue tests showed that the connection between foam and the polyester skin could delaminate rather quickly.

Figure 5 Inserts in order to make a connection between the roofs and the columns, transport and test-assembly

The connections between the individual segments can be divided in connections in the length and connections in the width of the segments. Both have a structural function. On the side of the segments a rabbet has been made of 220mm with and 15mm depth. In this rabbet a prefabricated reinforcement of 200mm with and 10mm depth, of high density glass fibre meshes that has been vacuum injected with resin, was placed. This reinforcement is glued and clamped by screws for curing purposes only.

After the final layer of finishing an UV resistant polyurethane top coating was applied. This layer more or less sacrifices itself by degrading under influence of UV light, leaving the structural parts intact. The lower side is protected with a fire retarding layer.

4.2 Tolerances

Due to the experimental character of the production process and the unfamiliarity with the consequences of vacuum deformation coupled with many one-off segments that had to be fitted together, it was decided to perform a test-assembly or pre-assemblage on the premises of Holland Composites in Lelystad of all the wings. The fitting took place on a positive steel frame. One of the conclusions was that the wings would be assembled inversely, so the downward curve would face upward for safety reasons. All the segments were produced on individual foam moulds and all had their own shrinkage and shrink-direction.

In general the segments proved to be somewhat smaller than intended. They had shrunk because of the vacuum injection, causing the seams to be 20-25mm, instead of the anticipated 12-15mm. When filling up the seams during assembly a bigger seam meant more fibre and more resin and thus causing a larger deadweight of the shell.

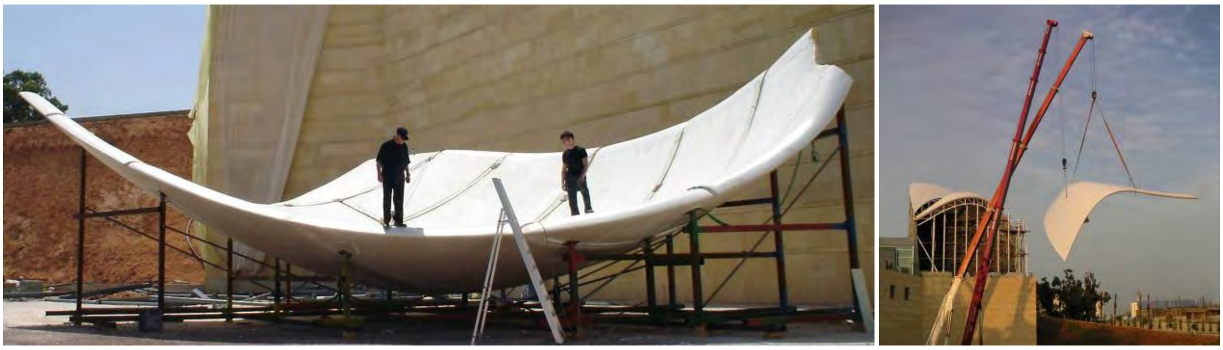

Figure 6 Preparation and hoisting

The shell was positioned on a steel flat truss sub-structure, which in its turn rests on a concrete wall with a much larger tolerance difference. The connection between the columns, concrete wall and the roof was a challenge. During the production at Holland Composites steel inserts were placed within the sandwich which were eventually bolted with the specially developed ball-and socket-connections on top of the columns.

Positioning directly from the crane onto the column heads, or wing-connectors with its adjustable shaft and connection plates, could only take place accurately by following the theoretical drawings. Until the end theoretical drawings remained the decisive factor. In all phases of engineering, production, assemblage up until the hoisting and positioning theoretical drawings were always present and compared, as this was the only assurance that at the end the wings would fit into position.

The concrete had the biggest tolerances, up to 100mm. The seams of the roof segment 12mm and the seams between the glass panels 10mm. And all these different tolerances have to be neutralized in their detail design. The geodetic supervision during the process of production and installation will always be important for a successful result.

Figure 7 Interior view of the building in April 2006

Figure 8 Finishing of the top layer of the roof by “airborne builders”

Due the lack of experience with free form composite sandwiches there is a large difference between the theory and practice in the building industry. For the Yitzhak Rabin Center the weight of the more than 800 m^2 shells in calculations was 41 kg/m^2 [5], but after production it approached the 70 kg/m^2 [6] including inserts, filling of the seams and coatings. The expectation is that with more experience and other detailing the final sandwich can approach this 40 kg/m^2. With CFRE lighter structures and larger spans should be available.

5 THE FUTURE

These blob shells are governed by bending moments due to their dictated unfavourable form and supports, rather than by normal forces and shear forces in the plane of the shell as the first generation of shells. The constructional solution of the new shells is in principle the one developed for the Rabin project: a double stressed skin sandwich construction in free form with a structural core. The next step in development is caused by the differences in loading behaviour between conventional structures in steel of concrete and glass fibre reinforced polyester shells. Blob shells, made of glass-fibre reinforced polyester are usually much more flexible, and cannot reach the stiffness and rigidity of conventional structures. For sailing yachts, often post-stressed by its masts and riggings, rigidity is a relative connotation. As long as the doors and cabinet doors in the yacht still close and open only a few sailors would mind the distortion in the hulls of their yachts. However, buildings components like windows and doors, often have glass components directly attached to the roof structure. These are influenced by the stiffness of the load bearing structure. Depending of the details, this requires the engineering attention.

Cantilevering blob-shells can be more flexible than a span in conventional structures. The cantilever of the tip of the largest wing at Rabin was analyzed as 100mm upwards and 210mm downwards. The total sandwich thickness was 310 mm. This fits in the general shell theory of Timoshenko, so that the shell still behaves as a shell. Alternatives in steel and in concrete were analyzed to show deformations of only 200, respectively 100 mm. The engineering line-of-thought was that as long as the movements of the roof under loading do not cause brittle fracture, delamination or other handicaps in the blob-shells internally and as long as the flexibility of the blob-shell does not lead to problems in the technical composition of the building around the blob-shells, larger movement would be acceptable. So no rules yet, but intelligent and responsible building technical engineering, characterizing the experimentation phase. The standardization and normalization phase will follow after 5 to 10 years only. But new projects involving blob-shells in future will show up with no doubt more strict requirements as to the anticipated deformations in GRP. We have to look into other materials as well. Epoxy and carbon-fibre is the alternative usually used in the production of high-tech sail yachts. The next generation will be blob-shells in carbon-fibre reinforced epoxy. This material is much more rigid, does hardly expand as the thermal expansion coefficient of carbon-fibre reinforced epoxy is very low, or even negative, compared with glass fibre polyesters. These advantages are accompanied by a much more strict production process including curing in a tempering oven, which limits the sizes of components. For transfer of technology from the yacht building industry, the costs play an important role. As the thresholds in the buildings industry are quite low and the price of carbon-fibre reinforced epoxy shells are high.

Figure 9 Drawings of the shape of the roof for the Mediatheque in Pau, designed by Zaha Hadid and interpreted by Octatube [7]

The famous London-based architect Zaha Hadid designed a ‘free form’ Mediatheque in Pau, France, near the Pyrenees, see Figure 9. Her first design images show the ‘Mediatheque’ in white, but the tender documents show a continuous black design with carbon-fibre as the basic material without seams. In the development of the tender design the proposal was to produce the segments of the carbon-fibre epoxy blob shell segments locally in a temporary factory shed, a re-assembled curing oven, next to the site. The tender price was 4 times that of the client’s budget for this extremely experimental project on a giant scale. The project champion, Pau’s mayor André Labarrère, died the day before the tender date. The project was cancelled. The Octatube design drawings indicate the design proposals in carbon-fibre epoxy blob shells.

6 CONCLUSIONS

From the experiences, acquired over the last years by architects who work in the relatively thriving sector of utility building, the current use of computer programs at architectural firms seems irreversible. The ease, with which architects conjure up complex shapes of buildings and their lay-outs on their computer and win design contests, is an indication of the total revolution of the spirit of the times. Structural designers have to anticipate answering architects with surprising structural designs for 'free form' designs. The shapes of free form buildings are of such complexity that all the familiar and forgotten know-how has to be recalled. Therefore, mobilise all sleeping, of the 1st pioneers knowledge, and all active knowledge on 3D structural technologies. The resulting design of this contribution shows that building technical design can lead to integrated and innovative structures.

Cladding is as important as the structure: therefore one should develop multi-material design solutions on both cladding and structural levels, where every material has its own function, and designed in an integrated way.

The results of this process have to be integrated into one technical artefact that satisfies all requirements and gives efficient answers or compromises in all of its life phases, be it conceptual design, material design, detail design, engineering, productions, assembly, installation, loading behaviour, functional use as a building, meaning of the artefact as a building, even as Architecture.

It may be true that the well-known restrictions in the volume prices of the building industry, as posed by the clients in the building industry, lead to traditional and well known technologies. Sometimes experiments are persistent, initiated by designers who are willing to wander though the entire experimental development processes and are able to solve all foreseen and unforeseen problems. In this case the interdisciplinary collaboration with Industrial Design Engineering, the Marine Industry and Aeronautics proved to be essential and enrichment in the field of Architecture.

Standardization in detailing, moulding processes and engineering is necessary to avoid many expensive tests for each individual project. The fibre reinforced sandwich shells will be developed on production, detail and global level. A balance between standardization and creating your own customized material must be found yet.

REFERENCES

[1] M. Ashby, *Materials Selection in Mechanical Design*, Elsevier Butterworth-Heinemann, Oxford, 2005, p5

[2] E. Genzel, P. Voigt, 2005, *Kunststoffbauten*, Teil 1 Die Pioniere, Poge Druck, Leipzig, 2005

[3] P.A. van de Rotten, *Consequences of Free Form Design, Chances for Fibre Reinforced Sandwich "Shells"*, IASS 2007, Conference Proceedings, 2007, p357-358

[4] P.K. Mallick, *Composites Engineering Handbook*, Marcel Dekker Inc., New York, 1997, p 1-166

[5] H.D. Uden, *Yitzhak Rabin Center, Composite roof Construction*, Engineering Report, Solico, 2005

[6] M. Eekhout, R.Visser, *Blob-shells: Composite Stressed Skin Roofs for Liquid Design Architecture*, Delft Science in Design, A Congress on Interdisciplinary Design, Conference proceedings, 2007, p43-70

[7] M. Eekhout, R. Visser, *Composites & the Renaissance of the Shell*, IASS 2007, Conference proceedings, 2007, p101-102

FRACTURE

8th International Conference on Sandwich Structures
ICSS 8
A. J. M. Ferreira (Editor)

DESIGN OF THE FACE/CORE INTERFACE FOR IMPROVED FRACTURE RESISTANCE

Christian Lundsgaard-Larsen*, Christian Berggreen* and Leif A. Carlsson†

*Department of Mechanical Engineering
Technical University of Denmark
2800 Kgs. Lyngby, Denmark
e-mail: cl@mek.dtu.dk and cbe@mek.dtu.dk, web page: http://www.mek.dtu.dk

†Department of Mechanical Engineering
Florida Atlantic University
Boca Raton, FL 33431, USA
e-mail: carlsson@fau.edu, web page: http://www.fau.edu

Key words: Sandwich structures, Damage tolerance, Cohesive law, Fiber bridging.

Summary. *This study investigates the face/core fracture behavior of sandwich specimens with different designs. The traditional interface with a quadraxial mat directly adhered to the foam core is compared to interfaces where an additional mat with randomly oriented fibers is inserted between core and face. The extra mat affects the crack propagation path in the sandwich specimen, and makes it more likely for the crack to propagate at or near the interface, instead of kinking into the laminate or core. Further, the extra mat acts as a source for fiber bridging, and hereby the fracture resistance is increased as bridging fibers shield the crack tip from the loading. Results show that the increase in fracture resistance due to fiber bridging is significant. Cohesive laws regarding cracking of sandwich interfaces are extracted.*

1 INTRODUCTION

1.1 Background and motivation

In sandwich structures face/core debonding is a common flaw that may form during production if there is a lack of resin adhesive. In service, impacts can damage the core and hereby generate a debond which might act as a starting crack propagating throughout large parts of the structure when exposed to moderate loading. This can reduce the load carrying capability drastically, and it is important to gain experience and develop tools for predicting the damage tolerance of sandwich structures. It is a goal to be able to assemble an optimal sandwich interface through knowledge of the individual fracture behavior of core, face and additional interface layers. With regards to damage tolerance one should be aware of the weakest link in the chain, since the crack tends to propagate where the resistance is the least. Hence, the interface region should be carefully tailored in accordance with the fracture properties of the face and core.

If the crack propagates at the face/core interface the fibers in the face laminate can form a bridging zone behind the crack tip. This can contribute significantly to the fracture resistance of the crack since the bridging fibers provide closing tractions between the separated crack surfaces [1]. In Figure 1 a photo from [2] illustrates the large scale fiber bridging that might develop in a sandwich structure.

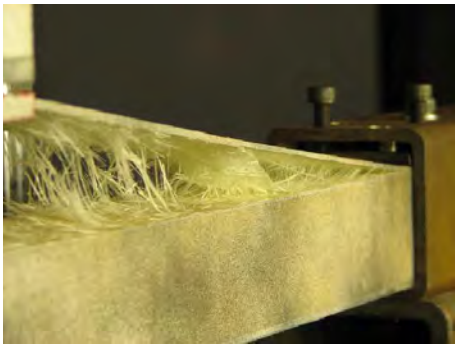

Figure 1: Large scale fiber bridging observed for cracking of a sandwich structure

1.2 Cohesive zone approach

In the case of large scale bridging tractions are being transferred between the separating surfaces in an area called the failure process zone. If the process zone is large compared to some relevant dimensions of the specimen e.g. the crack length, Linear Elastic Fracture Mechanics (LEFM) is not accurate and the effects caused by the large process zone should be taken into consideration. The Cohesive Zone Model (CZM) is widely used to simulate specimens where the process zone size has a significant influence on the fracture behavior. Consider a cracked sandwich specimen with a large process zone in Figure 2.

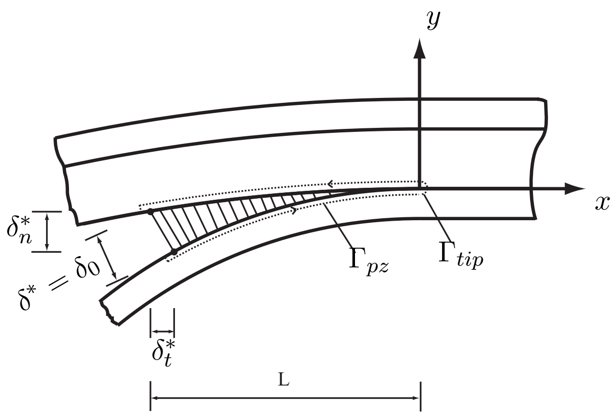

Figure 2: Process zone of a crack in a sandwich specimen subjected to mixed mode loading

The opening displacement of the pre-crack tip δ^* can be projected in normal and tangential opening displacement components, δ_n^* and δ_t^*, see Figure 2. A schematic graph of the fracture resistance, J_R, as function of pre-crack tip opening is sketched in Figure 3 (a). The fracture process can be separated in two different branches. Initially the pre-crack tip opens very little due to deformation or micro-cracking of the adhesive bonding layer at the interface and during this stage J_R increases rapidly. As the fracture resistance reaches a certain material specific value J_0, the interface separates and the crack tip opens more rapidly. With fibers bridging in between the separating crack faces J_R increases further, since fiber bridging in the process zone contributes to the crack growth resistance. Eventually J_R reaches a steady state plateau $J_{ss} = J_0 + J_{bridging}$ where J_0 and $J_{bridging}$ are contributions to the fracture resistance from the crack tip and fiber bridging respectively. The pre-crack tip opening $\delta^* = \delta_0$ as J_R reaches a plateau is considered a material property for a fixed normal/shear opening ratio δ_n^*/δ_t^*. Conversely, the length of the process zone at steady-state L is not a material property since it depends on the specimen geometry and loading [4].

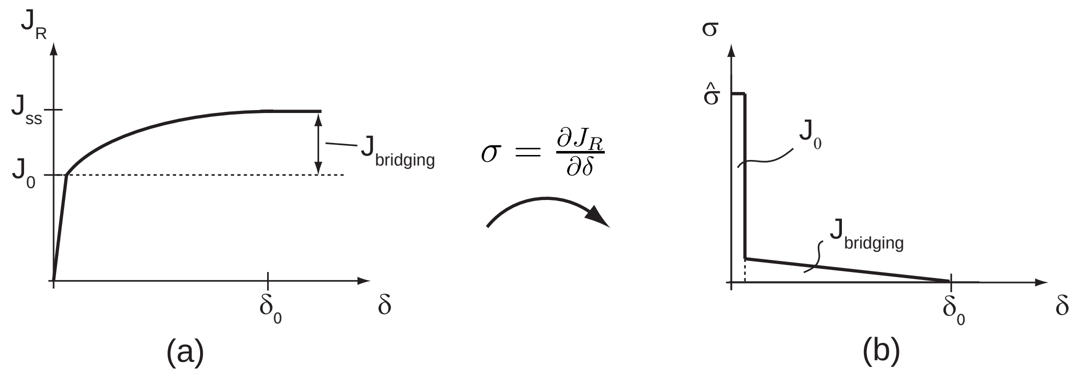

Figure 3: Schematic graph of J_R as function of pre-crack tip opening (a) and derived cohesive law (b).

The J integral as given by [5] can be derived for a multilayered sandwich specimen using laminate beam theory to describe the stress and strain distribution in the different layers. This will not be closer described here, but can be found in [3]. The cohesive law is derived from the J integral value by differentiating J_R with respect to the opening displacement of the pre-crack tip, see illustration in Figure 3 (b) and [3].

2 TAILORING THE SANDWICH INTERFACE

The objectives of this study are (1) devise a simple method to increase the fracture resistance of the interface due to fiber bridging and (2) design the interface so the crack does not kink into the adjacent core or laminate.

2.1 Crack kinking

When considering the propagation of an existing face/core debond, the crack can propagate in three basic ways; 1) propagate self similar in the face/core interface, 2) kink into the core, or 3) kink into the face, see the schematic in Figure 4.

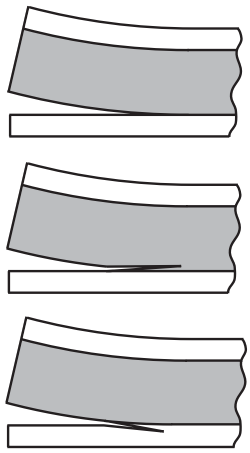

Figure 4: Schematic illustration of possible crack propagation paths in a sandwich specimen

The crack path is influenced by the stress state at the crack tip, e.g. described by the mode-mixity of the crack, and the resistance to crack propagation caused by the face, core and adhesive [7]. If the interface is weak and brittle compared to the core and face laminate, the crack may propagate in the interface regardless of the mode-mixity. If on the other hand the interface is very tough, the crack will propagate in the core or face laminate.

Under the assumption of LEFM it was proposed by [8] that the crack will kink out of the interface and into the core if

$$G/G^t_{max} < \Gamma(\Psi)/\Gamma_c \tag{1}$$

where G/G^t_{max} is the ratio between the energy release rate at the crack tip and maximized energy release rate with respect to the kink angle and $\Gamma(\Psi)/\Gamma_c$ is the ratio between interface fracture toughness and the mode I fracture toughness of the core.

As described above, the interface fracture toughness is given as a sum of energy dissipated at the crack tip and the process zone behind the crack tip, i.e. $J_{ss} = J_0 + J_{bridging}$. Regarding the kinking criteria in (1) it is assumed that the energy release rate of the interface $\Gamma(\Psi)$ is the energy dissipated at the crack tip, thus $\Gamma(\Psi) = J_0$, whereas the energy dissipated in the process zone will only have a minor influence on the crack path.

It is desired to reduce the tendency for crack kinking by minimizing the right hand term in (1), i.e. J_0 should be small. On the other hand it is desired to increase the energy dissipated as the crack grows in the interface, i.e. maximize $J_{ss} = J_0 + J_{bridging}$. It is therefore believed that an interface with small J_0 and large $J_{bridging}$ will satisfy the two criterions that the crack should stay in the interface and simultaneously posses a high resistance towards fracture.

2.2 Layer with randomly oriented fibers

In several applications a mat with randomly oriented fibers is inserted between the core and face. The purposes of this mat are (1) to increase the resin flow near the core during production and hereby avoid any dry areas and (2) obtain a more gradually changing stiffness from the compliant core to the stiff quadraxial face. Two different mat types are used for this purpose: Chopped Strand Mat (CSM) and Long Strand Mat (LSM), where the CSM consists of 4-6 cm long fibers bundled together and the LSM are very long fiber bundles. In both cases fibers are oriented randomly in the plane of the mat. In this study the CSM and LSM are used to intentionally create a relatively weak layer where the crack is likely to propagate. It is further believed that a mat with randomly oriented fibers is an effective source for fiber bridging, since fiber bundles are relatively easy being pulled out of the mat.

Fracture resistance curves for interfaces without and with CSM are schematically illustrated in Figure 5.

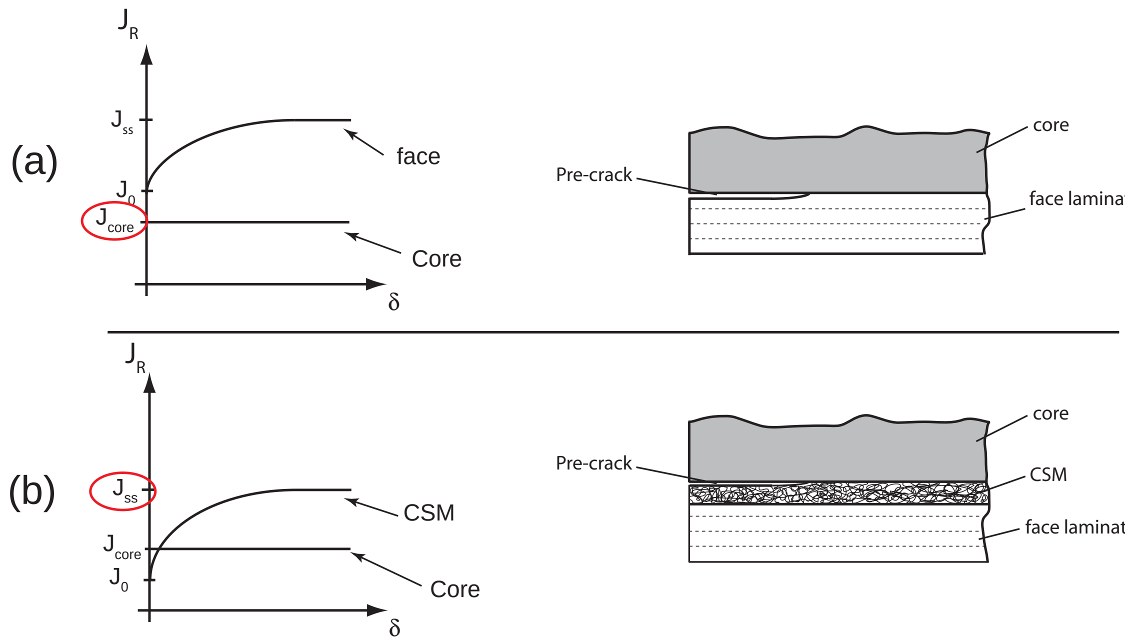

Figure 5: Possible fracture resistance curves for (a) interface without CSM and (b) interface with CSM. The red circle marks the steady state fracture toughness which is equal to the crack driving force necessary to propagate the crack when the process zone has evolved

As described previously the crack path is dictated by the local fracture toughness values at the interface and the core material along with the energy release rates for crack propagation in the interface and in the core material, see (1). For the interface without CSM, see Figure 5 (a), J_0 is larger than J_{core} and it is likely that the crack will propagate in the core, with the energy release rate equal to J_{core}. Regarding the other interface illustrated in Figure 5 (b) J_0 is smaller than J_{core} and it is likely that the crack will propagate in the CSM layer. This entails large scale fiber bridging and the total fracture resistance increases to $J_{ss} = J_0 + J_{bridging}$. It is therefore possible that the weaker CSM layer causes a more damage tolerant interface, and it is desired to investigate this further.

3 EXPERIMENTS

3.1 Test method

The Double Cantilever Beam loaded by Uneven Bending Moments (DCB-UBM) was previously used for fracture testing of monolithic composites [6]. The test-rig consists of a roller-wire system, that applies a pure bending moment to each of the two beams M_1 and M_2, and the ratio between moments is held fixed throughout one experiment. The ratio can be varied by changing the distance between rollers on each of the two arms, and the sign of the moment can be reversed by changing the mounting direction of the wire. A schematic illustration of the test-rig is shown on Figure 6.

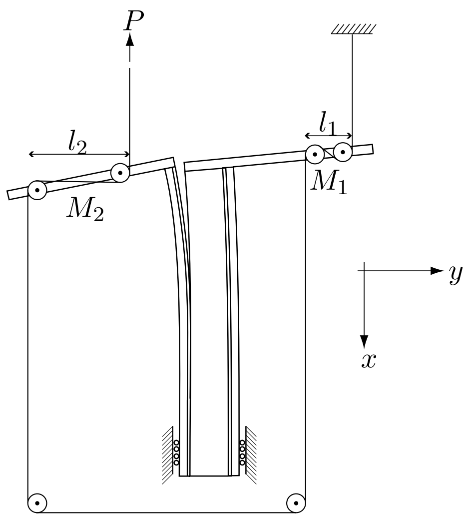

Figure 6: Schematic of the loading principle of a DCB-UBM sandwich specimen.

One important advantage of loading the specimen by moments (instead of edge forces) is that the J integral is independent of crack length, and depends only on geometry, elastic properties and applied moments [4].

3.2 Materials

Sandwich panels were manufactured using vacuum injection moulding with the glassfiber faces being approximately 3.5 mm thick with three different lay-ups.

1. [$DBLT_4$/Core/$DBLT_4$]
2. [$DBLT_4$/CSM/Core/$DBLT_4$]
3. [$DBLT_4$/LSM/Core/$DBLT_4$]

All specimen have four mats of quadraxial Devold Amt DBLT 850-E10-I. The mats with randomly oriented fibers are either Chopped Strand Mat (CSM) 450 g/m^2 or Long Strand Mat

(LSM) 450 g/m^2. All faces are assumed in-plane isotropic and the elastic properties of the individual layers are found in data sheets and calculated into overall elastic properties using classical laminate theory with an effective E-modulus of approximately 14 Gpa and a Poisson's ratio of 0.3.

The epoxy resin is Polylite® 413-575, which is specially suited for vacuum injection due to low viscosity. The 20 mm thick Divinycell H200 PVC foam core has a density of 200 kg/m^3 and is manufactured by DIAB. The core material is assumed linear elastic and isotropic and elastic properties are found in a manufacturer data sheet with an E-modulus and Poisson's ratio of 240 MPa and 0.32 respectively. The sandwich faces are relatively thin and the specimen will undergo large deflections during loading, which is prevented by adhering a 6 mm thick steel bar to each face. A description and analysis of the steel reinforced sandwich specimen is found in [3].

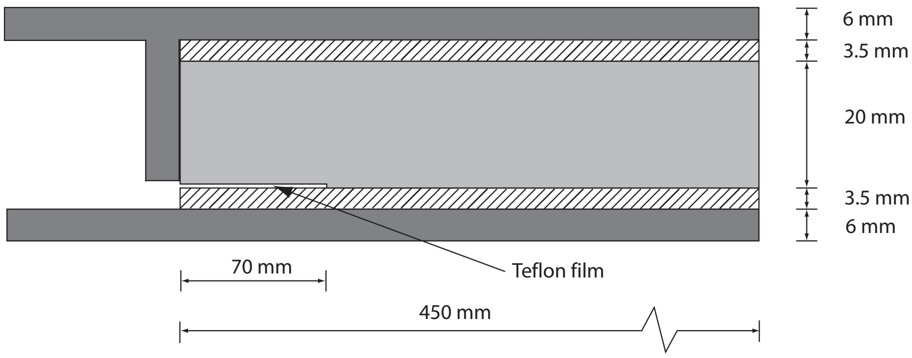

Figure 7: Sandwich specimen with pre-crack (dimensions in mm). The specimen is stiffened by 6 mm steel bars adhered to the faces.

4 RESULTS

The following describes and discusses some general results concerning the variation in fracture behavior for the different tested lay-up types. Examples of results for three different representative specimens are shown and further it is described how these results are processed. In this paper only a small selection of results are included.

4.1 Crack path

As described previously the crack propagation path is highly influenced by the moment ratio M_1/M_2 applied to the specimen since this affects the mode-mixity at the crack tip. The crack can either propagate in the interface or kink into the core or laminate, and the behavior depends on the lay-up. In Figure 8 an estimate of the results regarding crack kinking are given. The considered specimens are; no intermediate layer, CSM and LSM.

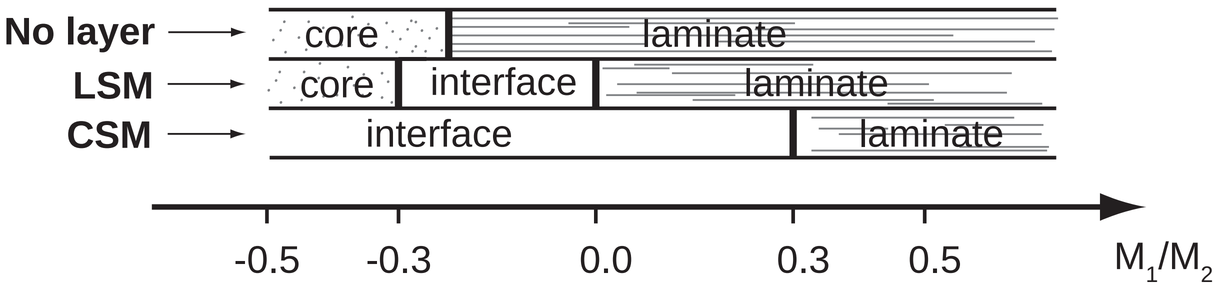

Figure 8: Crack path map for different lay-up configurations. The terms core, laminate and interface refers to where the crack propagates for a particular range of moment ratio M_1/M_2.

It is observed for specimens without any CSM or LSM layer that the crack will not propagate in the interface, but instead propagate either in the core or in the quadraxial laminate. It is assumed that the interface for this configuration is very tough compared to the adjacent materials, and that the crack therefore will not propagate here, cf. (1). For specimens with CSM or LSM laminate in the interface the crack will propagate in the interface for a certain range of applied moment ratio M_1/M_2. This range is considerably larger for the CSM layer compared to the LSM configuration.

4.2 Observations

The following describes visible observations from the experiments regarding fracture behavior of the different lay-ups. There is a considerable difference between the CSM and LSM configurations regarding large scale bridging developing in the interface, see Figure 9 (a) and (b). The LSM configuration shows heavy fiber bridging whereas the amount of fibers for the CSM configuration is relatively limited. Additional fracture tests were conducted in order to investigate the pure mode I fracture toughness of the core material. In this case the steel bars were adhered directly to the foam material and the specimen tested with a moment ratio of $M_1/M_2 = -1$ (i.e. pure mode I). The crack then propagates at the center of the core in steps of 3-4 cm, see Figure 9 (c)

(a) (b) (c)

Figure 9: Photos of DCB-UBM specimens with the crack propagating in a) CSM, b) LSM and c) the core. The observed fiber bridging is much heavier for specimens with LSM compared to CSM.

4.3 Fracture resistance

The fracture resistance J_R is measured by use of the J integral described previously. The fracture resistance is plotted as function of pre-crack tip opening δ^* and examples are given for cracking in the CSM and LSM configuration and for the core.

Consider the measured fracture resistance of the LSM interface as function of pre-crack tip opening in Figure 10. The J_R-curve increases initially rapidly until J_R = 810 J/m^2 where the pre-crack tip opens and the crack starts propagating. As the process zone evolves, the fracture toughness increases due to fiber bridging The crack propagates in small jumps of 2-3 cm thus the curve is not smooth but consists of several peaks which represents the crack driving force at the time of crack propagation i.e. the fracture resistance of the material. The local peak points are identified and extracted from the full data set.

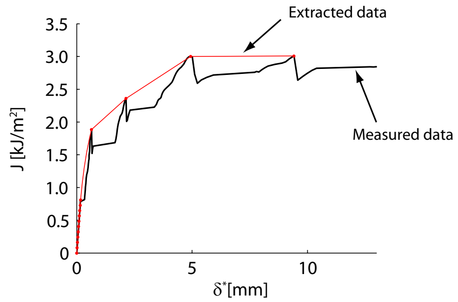

Figure 10: $J - \delta^*$ curve with measured data and extracted data for the LSM interface and $M_1/M_2 = 0$. J_0 is found to be approximately 800 J/m^2

The extracted data points are fitted with a piecewise second order differentiable spline using the least squares criteria, see Figure 11.

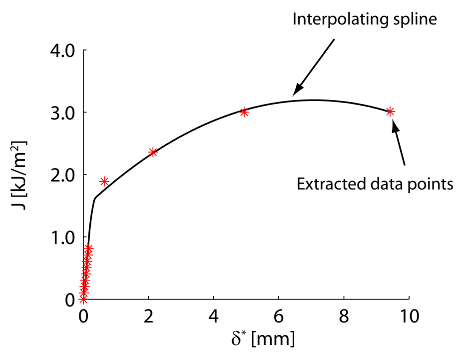

Figure 11: The extracted data are fitted with piecewise 2nd order polynomial splines

The above described data reduction is performed for all considered interface configurations. The results are presented in Figure 12.

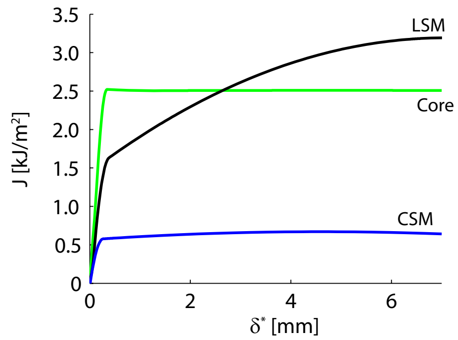

Figure 12: Selected results for the investigated configurations in the form of fitted polynomials. The fracture resistance of the LSM configuration increases during crack propagation, whereas the increase is considerably smaller for the CSM configuration.

As the crack starts propagating (curve deviates from linear) the CSM configuration show modest increase in fracture resistance due to scattered fiber bridging, whereas the LSM configuration show large increase due to a more dense fiber bridging. Results are given in Table 1.

Interface configuration	$J_0[kJ/m^2]$	$J_{ss}[kJ/m^2]$
CSM	0.469	0.640
LSM	0.810	3.02

Table 1: Fracture resistance J_0 and J_{ss} for the CSM and LSM configuration.

It is illustrated by the results given in Table 1 that fiber bridging may contribute significantly to the fracture resistance of the sandwich structure. The experimental results show that the increase in fracture toughness from J_0 to J_{ss} due to fiber bridging is approximately 50% for the CSM configuration and 400% for the LSM. For comparison, as the crack propagates in the core the fracture process zone is very small, and it can be assumed that all energy is dissipated near the crack tip (J_0 equals J_{ss}, see Figure 12). The fracture toughness of the core tested in pure mode I is 2.51 kJ/m^2.

4.4 Cohesive laws

The cohesive law is derived by differentiating J_R with respect to δ^*, as described in a previous section. Results are plotted in Figure 13.

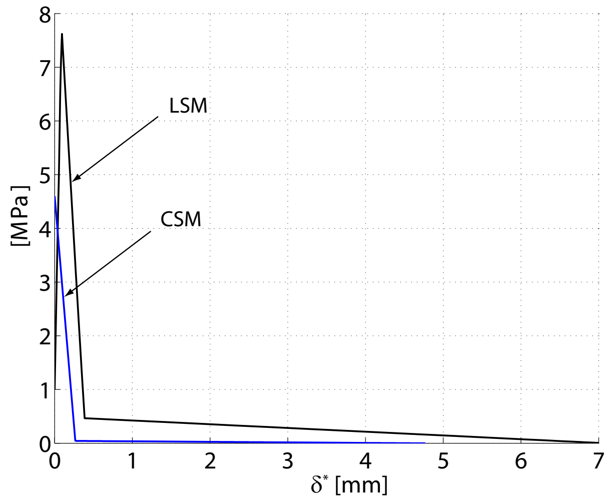

Figure 13: Derived cohesive laws for the CSM and LSM interface configuration.

The cohesive law for the LSM configuration consists of two branches: separation of the interface under large stress, and post-separation behavior, where bridging fibers transfer stresses between the separated faces. The stress at separation rises to a peak at 7.6 MPa. For $\delta^* = 0.3$ mm the interface has separated and stress has reduces to 0.4 MPa. The stress decreases slowly to 0 as the displacement increases to 7 mm. The curve for the CSM configuration shows that the interface separates at a stress of approximately 4.5 MPa and bridging is limited compared to the LSM.

5 CONCLUSION

The fracture behavior of a sandwich interface with two different randomly oriented mats (long and short fibers), is investigated and compared to a traditional sandwich interface without any extra mat. The additional mat acts as a source for fiber bridging which shields the crack tip for the applied load, and increases the fracture resistance with up to 400% of the energy dissipated at the crack tip. It is believed that this behavior might have a considerable potential regarding increasing the fracture toughness without risking that the crack either kinks into the core or load carrying laminates. Both scenarios will decrease the global load carrying capacity of the structure, and are therefore considered unwanted.

6 ACKNOWLEDGEMENTS

This work has been performed within the Network of Excellence on Marine Structures (MARSTRUCT) and has been partially funded by the European Union through the Growth Programme under contract TNE3-CT-2003-506141. The sponsoring of core materials from DIAB is highly appreciated.

REFERENCES

[1] B.F. Sørensen and T.K. Jacobsen. Delamination of fiber composites: determination of mixed-mode cohesive laws, Submitted, 2008.

[2] C. Lundsgaard-Larsen, C. Berggreen, K. Karlsen, C. Jenstrup and B. Hayman. Improving performance of polymer fiber reinforced sandwich X-joints in naval vessels - part II: Damage tolerance. *16th Int. Conf. on Comp. Mat*, Kyoto, Japan, 2007

[3] C. Lundsgaard-Larsen, B.F Sørensen, C. Berggreen and R.C Østergaard. A modified DCB sandwich specimen for measuring mixed mode cohseive laws. *Eng. Frac. Mech.*, In press, 2008.

[4] Z. Suo, G. Bao, B. Fan, Delamination R-curve phenomena due to damage. *J. Mech. Phys. Solids*, **40**, 1-16, 1992.

[5] J.R. Rice, A path independent integral and the approximate analysis of strain concentrations by notches and cracks. *J. Appl. Mech.* **14**, 379-86, 1968.

[6] B.F. Sørensen, K. Jørgensen, T.K. Jacobsen, R.C. Østergaard. DCB-specimen loaded with uneven bending moments, *Int. J. of Fract.* **141**, 163-76, 2006.

[7] C. Berggreen, B.C. Simonsen, K.K. Borum. Experimental and numerical study of interface crack propagation in foam-cored sandwich beams. *J. of Comp. Mat.*, **41**, 193-520, 2007.

[8] J.W. Hutchinson and Z. Suo, Mixed mode cracking in layered materials. *Adv. in App. Mech.*, **29**, 63-191, 1992.

8th International Conference on Sandwich Structures
ICSS 8
A. J. M. Ferreira (Editor)

CRACK PROPAGATION AT CORE JUNCTIONS IN SANDWICH PANELS

Anders Lyckegaard*, Johnny Jakobsen†, Jens H. Andreasen †, and Elena Bozhevolnaya†

*NKT Flexibles I/S, Priorparken 510,
2605 Brondby, Denmark e-mail: anders.lyckegaard@nktflexibles.com

†Department of Mechanical Engineering, Aalborg University
Pontoppidanstrde 101, 9220 Aalborg, Denmark

Key words: Sandwich structure, fracture mechanics, damage tolerance

Summary. *The crack propagation in a sandwich panel containing core junction is investigated. Experiments show that it is possible to change the crack path by changing the geometry of the core junction. The stress state in the vicinity of the crack tip at the core junction is investigated by eigenfunction analysis.*

1 INTRODUCTION

A typical sandwich structure is made from a number of different core materials. This is done to optimize the structure of lowest possible weight. Hence, a sandwich structure will often have a number of core junctions.

A common failure mode of sandwich structures is delamination of the interface between core material and one of the face sheets. Cracks are often initiated somewhere in the core material, and will propagate towards the interface and subseqently along the interface. Changing the direction of crack growth is a first step in introducing damage tolerance.

Cracks propagete along the interface quite easily, so it is desireable if the crack may be diverged away from interface some means. Core junctions may be designed to do this.

Just recently a new concept where face sheet peeling is stopped by embedding a special designed core component has been proposed by Jakobsen et al. [1, 2]. The idea of the concept is to force a face-core interface crack to propagate away from the face-core interface and follow a core-core interface instead. By the introduction of new core component into a sandwich structure a tri-material corner is created and stress singularities appears. The nature of the singularity and the corresponding eigenfunctions will govern the stress state in the vicinity of the tri-material corner are therefore important for the design of the core component.

In the present paper experimental results that demonstrate the effect of core junction design on the interface crack propagation is presented. Analysis of the stress singularities at the critical moment where the crack has reached the core junction is presented. The results of the analysis will be compared with the experimental results that give the actual crack path.

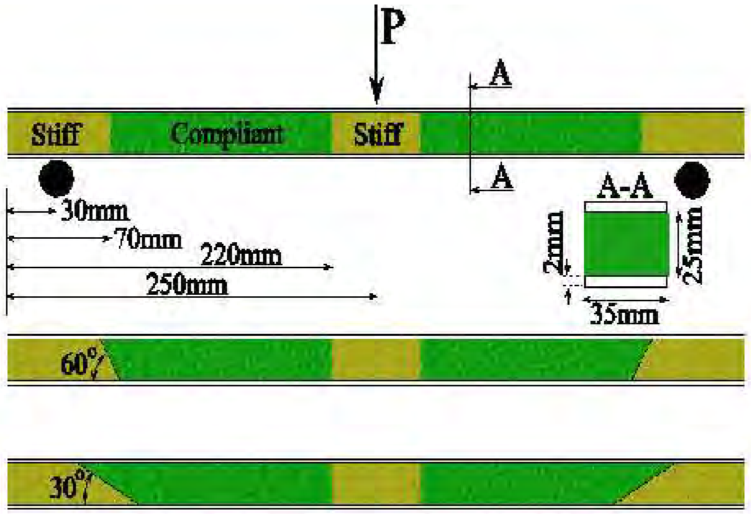

Figure 1: The geometry of the test specimens.

	E modulus [MPa]	Poissons ratio
Face sheets: GRFP $(0, 90)_4$	$E_{homogeneous}$ 25050	0.3
Stiff core: Divinycell H200	250 MPa	0.32
Compliant core: Divinycell H60	42 MPa	0.32

Table 1: The elastic material properties for the sandwich beam constituents are given in this table. However, it should be noted that the face sheet laminate may be simplified to a homogenous layer with the properties given in this table.

2 EXPERIMENTS

An experimental setup of three sandwich beam configurations subjected to a three point bending load condition illustrates partly the concept. The sandwich panels were loaded by three point bending, and had 5 sections of alternating core material.

For a crack approaching the tri-material corner (i.e. core junction) it is observed that for some geometrical configuration the interface crack is rerouted at the tri-material corner. This is illustrated in Fig. 3 and 2. While for other core junction geometries the crack propagate along the interface regardless of the core junction.

The sandwich beam specimens were made of PVC foam core materials H60 and H200 supplied by DIAB. The face sheets were made from GFRP by a resin infusion process and layed up in a alternating 0/90 configuration, see table 1 for details.

The configuration is a common sandwich configuration, and the modification to the core junction is quite modest. This could be made in using the standard tools that are used for producing these structures.

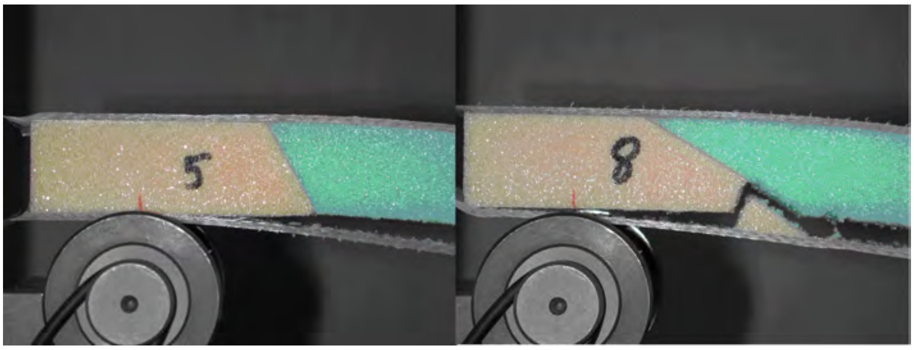

Figure 2: The crack paths for two cases. Left is the 60 degree case were the crack propagates along the face-core interface. Right is the case of 30 degrees were the crack propagate along the core-core interface before it kinks.

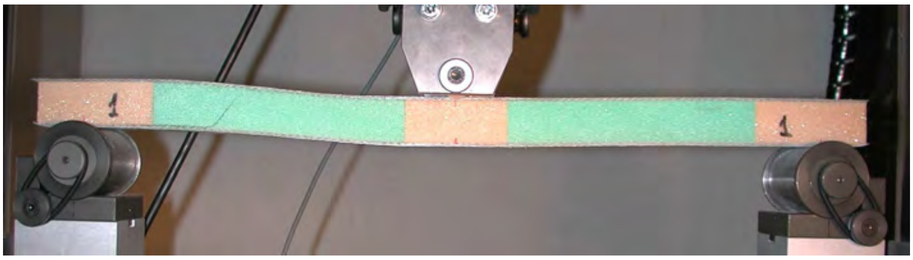

Figure 3: Shows the test setup used for the three point bending load condition.

Figure 4: A representative high speed image sequence of the failure process for a test specimen with 90 deg core junction angle.

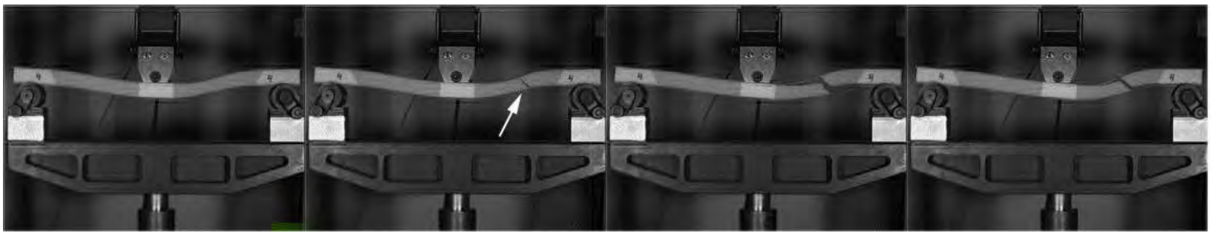

Figure 5: A representative high speed image sequence of the failure process for a test specimen with 60 deg core junction angle.

3 Experimental results

The failure initiated in the bulk of the compliant core and continued as delaminations along the upper and lower face-core interface. This was observed as a failure event for all three configurations. Representative failure initiation and progress of the three configurations may be seen in Fig 4, Fig 5, and Fig 6. The high speed images shown, in those figures, covers a period of time of only a few milliseconds. This very short period of time for the failure process is normal for sandwich beams loaded quasi statically and for this type of support condition.

4 DAMAGED PANEL STRESS STATE

The stress state in the vicinity of the crack tip is analysed subsequently. The geometry is locally defined by three radial lines that separate the three materials, i.e. the two core materials and the face sheet. All materials are assumed to be isotropic and linearly elastic.

Figure 6: A representative high speed image sequence of the failure process for a test specimen with 30 deg core junction angle.

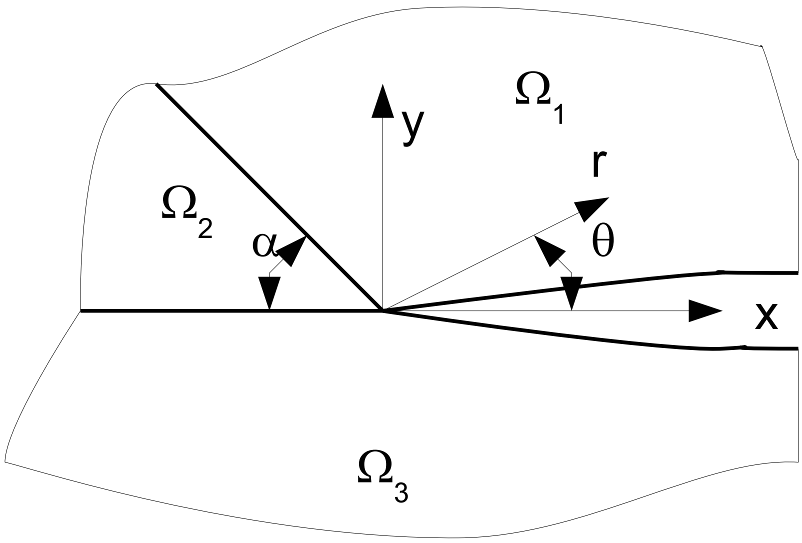

Figure 7: The local geometry at the tri-material-wedge.

The two core materials are assumed to be perfectly bonded, hence continuity of stresses and displacements may be assumed. Similarly for core 2 and the face sheet. The crack is on the other hand assumed to be stress free, see figure 7.

A solution that govern the stress state in the vicinity of the crack tip may be contructed using on a series expansion of the Mushelishvilii potentials, which was given by e.g. Pageau and Biggers [3].

$$\begin{aligned} \phi_k &= a_{1k} z^{\lambda} + a_{2k} z^{\overline{\lambda}} \\ \psi_k &= b_{1k} z^{\lambda} + b_{2k} z^{\overline{\lambda}} \end{aligned} \tag{1}$$

where $k = \{1, 2, 3\}$ refer to the material number. This problem yield a nonlinear eigenvalue problem which is defined as follows.

$$\mathbf{A}(\lambda)\mathbf{x} = \mathbf{0} \tag{2}$$

where $\mathbf{A}(\lambda)$ is a matrix with nonlinear functions of λ, and $\mathbf{x}$ is a vector of constants $a_{1k}, a_{2k}, \ldots$.

The eigenvalue problem defined above is solved numerically for the eigenvector pairs, which along with eq. 1, define eigenfunctions for the stress and deformation state.

Following Mushelishvilii the stresses in polar coordinates may be defined as:

$$\sigma_{rr} + i\sigma_{\theta\theta} = 2\left(\Phi(z) + \overline{\Phi(z)}\right) \tag{3}$$

$$\sigma_{\theta\theta} - \sigma_{rr} + 2i\sigma_{r\theta} = 2\left(\overline{z}\Phi'(z) + \Psi(z)\right)e^{2i\theta} \tag{4}$$

where Φ and Ψ are the derivatives of ϕ and ψ, respectively. Hence, if $\Re(\lambda) < 1$ the stresses will be singular. It may also be found that $\Re(\lambda) < 1/2$ then the strain energy density will be unbounded at the crack tip. Hence, solutions associate with $1/2 \leq \lambda \leq 1$ will be of primary interest, since these will lead to singular stresses that dominate the region near the crack tip.

The first three eigenvalues (λ) that were found for the current geometry and material properties are listed in table 2. The geometry defined in Fig. 7 is used for the analysis and the material properties defined in Table 1 were used for analysis along with plane strain assumptions.

Eigenvalue	30 deg	60 deg	90 deg
λ_1	0.58600+0.0745 I	0.63848	0.6420+0.07899I
λ_2	0.9971	0.67862	0.9998
λ_3	1.0	1.0	1.0

Table 2: The first three eigenvalues for the three cases.

For the case $\alpha = 30$ there is a strong first singularity, while the second eigenvalue yield only weakly singular behaviour. Hence, it may be assumed that the stress state close to the vertex is dominated completely by the first eigenfunction provided that it is active. Note also that the eigenvalue is complex, which define an oscilating behaviour of the stresses, i.e. $\sigma_{ij} \propto \cos(\omega \ln r)$. This define oscilating with increasing frequency as r approaches zero.

The eigenfunction define the distribution of circumferential displacements in a circle of radius 1 mm shown in figure 8. Here it is seen that the displacements are contineous across material boundaries as required and that there is a discontinuity at the crack $\theta = 0$. It may be seen that the crack is in an opening mode here.

The shear stresses $\sigma_{r\theta}$ may be seen in Fig. 9. These are zero at $\theta = 0$ by definition, and are quite high at the face-core interface $\theta = \pi$. The circumferential normal stresses $\sigma_{\theta\theta}$ are shown in Fig. 10. These are also zero at $\theta = 0$ and are nearly zero at the face core interface $\theta = \pi$. There is, however, a maximum close to $\theta = \pi/2$, and still significant tensile stresses at the core-core interface, $\theta = 5/6\pi$. The test results showed a crack that propagated along the core-core interface, which has significant shear stresses $\sigma_{r\theta}$ and tensile normal stresses $\sigma_{\theta\theta}$, but not the maximum of either one.

The situation $\alpha = 60^{\mathrm{deg}}$ showed two eigenvalues that had nearly the same singularity strength. The stress state at the vertex is thus expected to be dominated by a combination of the two first eigenfunctions.

The distribution of circumferential displaments corresponding to the first eigenfunction are shown in Fig. 11. The stress distributions are shown in Fig 12 and 13. Note that the shear stresses are quite high at the face-core interface $\alpha = \pi$, while the normal stress $\sigma_{\theta\theta}$ is compressive. The experiments showed crack growth along the face-core interface, hence it may be possible that the shear stresses are responsible for crack propagation. The second eigenfunction can also be important for this case, since it also has a strong singularity. This has not been investigated further in the present paper, however.

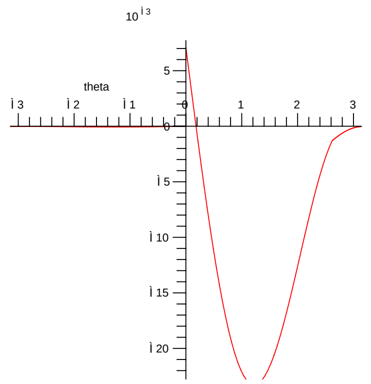

Figure 8: The circumferential displacement u_θ versus θ for the first eigenfunction for the case $\alpha = 30$. Here plotted along $r = 1\,mm$.

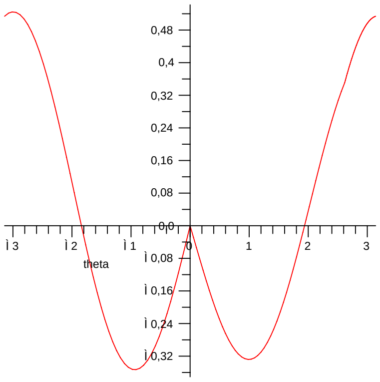

Figure 9: The circumferential displacement $\sigma_{r\theta}$ versus θ for the first eigenfunction for the case $\alpha = 30$. Here plotted along $r = 1\,mm$.

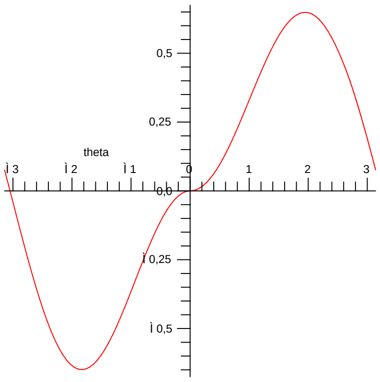

Figure 10: The circumferential displacement $\sigma_{\theta\theta}$ versus θ for the first eigenfunction for the case $\alpha = 30$. Here plotted along $r = 1\,mm$.

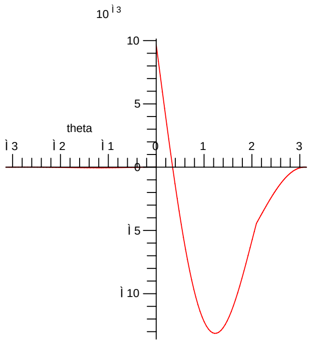

Figure 11: The circumferential displacement u_θ versus θ for the first eigenfunction for the case $\alpha = 60$. Here plotted along $r = 1\,mm$.

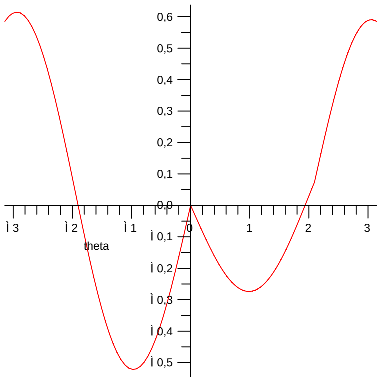

Figure 12: The circumferential displacement $\sigma_{r\theta}$ versus θ for the first eigenfunction for the case $\alpha = 60$. Here plotted along $r = 1\,mm$.

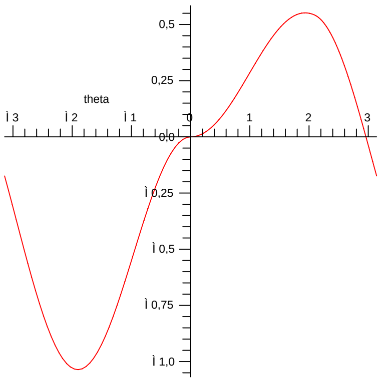

Figure 13: The circumferential displacement $\sigma_{\theta\theta}$ versus θ for the first eigenfunction for the case $\alpha = 60$. Here plotted along $r = 1\,mm$.

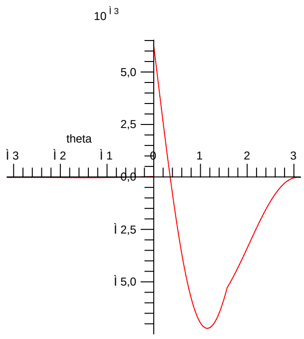

Figure 14: The circumferential displacement u_θ versus θ for the first eigenfunction for the case $\alpha = 90$. Here plotted along $r = 1\,mm$.

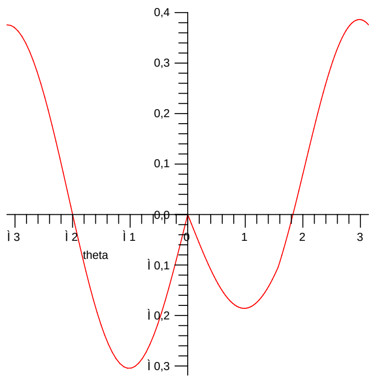

Figure 15: The circumferential displacement $\sigma_{r\theta}$ versus θ for the first eigenfunction for the case $\alpha = 90$. Here plotted along $r = 1\,mm$.

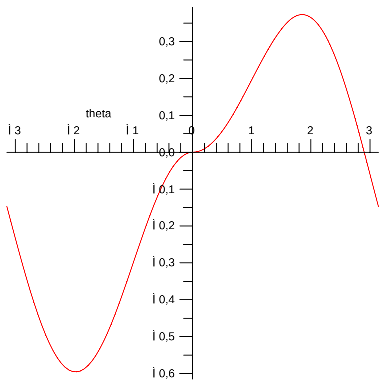

Figure 16: The circumferential displacement $\sigma_{\theta\theta}$ versus θ for the first eigenfunction for the case $\alpha = 90$. Here plotted along $r = 1\,mm$.

The case for $\alpha = 90$ has one strongly singular eigenvalue, while the second is only weakly singular. The first eigenfunction show a similar situation as the previous case. The displacement Fig. 14 show opening of the crack. The stresses corresponding are shown in Fig. 12 and 13. The experiment showed crack propagation along the face-core interface, and this correspond to the location where shear stresses are large, but normal stresses are sligtly compressive. Along the core-core interface there are some tensile stresses while shear stresses are nearly zero.

A final interesting fact is that all three cases has an eigenvalue of one. This eigenvalue correspond to the case of constant stresses. The eigenvalue analysis show, however, that the stress function potentials are zero in all cases. Hence, a state of constant stress cannot exist in the vicinity of the tri-material corner.

5 CONCLUSIONS

The present paper present experiments of three point bending of sandwich beams contaning two different cores. The experimental evidence showed that once the limit load was exceeded - a crack grew from the core and into the face core interface. The shape of the core-core interface could in some cases diverge the crack from the face-core interface to the core-core interface.

The situation of a crack propagated up to the tri-material corner formed by the two cores and the face sheet is analysed. It is assumed that the crack front has reached the tip of the tri-material corner. The eigen functions that dominate the stress state nearby is analysed, and comparision with the experimental results is done.

Presently, there is no criteria to determine the final crack propagation direction.

REFERENCES

[1] Jakobsen J., Bozhevolnaya E., Thomsen OT, Jakobsen L., Peel Stopper for Sandwich Components, *Patent Application 2006-521/01-0184*, Aalborg University, Denmark, 2006.

[2] Jakobsen J, Bozhevolnaya E, Thomsen OT., New peel stopper concept for sandwich structures. *Compos. Sci. Technol.*, (accepted for publication), 2007.

[3] Pageau, S S, Joseph, P F and Biggers, B, Jr , The order of stress singularities for bonded and disbonded three-material junctions, *Int. J. Solids Struct.*, **31**, 2979-2997, 1994.

8th International Conference on Sandwich Structures
ICSS 8
A. J. M. Ferreira (Editor)

A NUMERICAL INVESTIGATION OF FRACTURED SANDWICH COMPOSITES

E.E. Theotokoglou and I.I. Tourlomousis

Faculty of Applied Sciences, Dept. of Mechanics-Lab. of Strength Materials,
The National Technical University of Athens, Zographou Campus,
Theocaris Bld., GR-0157 73, Athens, Greece, Email:
stathis@central.ntua.gr;

Key words: Sandwich beam, Fracture mechanics, Flexural loading, Finite element method, Stress intensity factors.

Summary. *Finite element analyses have been carried out for fractured sandwich composites loaded in flexure. Core skin debonds parallel to the beam axis are considered at different distances from the upper skin interface. Static non-linear elastic two-dimensional finite element analyses of cracked sandwich beams are accounted for the evaluation of stress intensity factors at the crack tips.*

1 INTRODUCTION

In sandwich structures, low density foam core are receiving increasing attention. Mechanical properties of cellular foams have been summarized by Gibson and Ashby [1]. Ashby et al. [2] investigated the fracture mechanisms of linear elastic foam. Zenkert and Backlund [3] studied the mode-II and mixed-mode crack propagation of PVC cellular foam. Harte and Fleck [4] investigated failure modes in aluminium foam core sandwich panels loaded in cyclic flexure fatigue. Burchardt [5] numerically and Burman and Zenkert [6] numerically and experimentally have investigated fatigue characteristics of foam. Noury et al. [7] studied fatigue crack growth in rigid PVC cellular foam under combined mode-I and mode-II loadings.

In sandwich structures the foam is typically the weakest part and is the first to fail under static or cyclic loading because it transfers the applied loads as shear stresses. Interface debond damages between the face and the core can originate either from the manufacturing process or during service. In sandwich structures interfacial defects have been studied by Triantafillou and Gibson [8], Carlsson et al. [9-11] and Zenkert et al. [12,13]. Berggreen [14] and Berggreen et al. [15] have studied the ultimate failure of debond damaged sandwich panels loaded with lateral pressure.

In this paper a core-skin debond a_1 parallel to the beam axis is considered (Fig. 1), in accordance with experimental data [16,17]. When subjected to flexural loading, this debond will propagate slowly along the top interface and eventually kinked into the core as a shear crack. Stress intensity factors are calculated using the Finite Element Method and assuming linear fracture mechanics and plane strain, plane stress conditions for the cracked sandwich beam. Results from the finite element analysis show the influence of the upper face sheet to the value of the stress intensity factors when the distance of the crack from the upper skin interface diminishes.

2 NATURE OF THE PROBLEM

The sandwich considered is depicted in Figure 1. It is composed from PVC-core, R-75 with properties given in Table 1. (Technical data from DIAB Inc.) and face sheets from 240F S2-glass fiber with epoxy resin. Face sheet was separated from the sandwich beam using cutting and polishing machine. The face sheet was loaded at different support spans and its tensile modulus was found $16300 MPa$ with Poisson's ratio 0.3 in the longitudinal direction [17]. The dimensions of the test specimen were $L = 228.6$ mm (support span) and $b = 63.5$ mm (width). The core thickness was $t_2 = 12.7$ mm and the face sheet thickness was $t_1 = 2.28$ mm. The overall thickness was 17.26 mm.

In the experimental investigation [16,17], the specimens were supported on two rollers with appropriate overhang. A crack initiated on the compression side just below the top face sheet/core interface. It was noticed that the crack always initiated at the sub-interface created by the resin soaked, and dry cells, below the actual top core-skin interface. This debonding crack was about 1-1.5mm below the interface. The crack runs parallel to the beam axis from the point of initiation towards the end support (Figure 1).

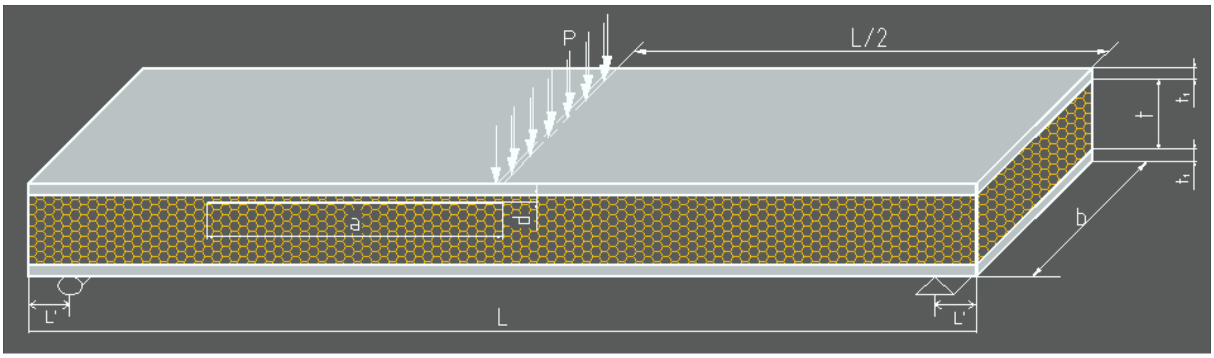

Figure 1 A cracked sandwich beam under flexural loading

3 NUMERICAL INVESTIGATION

The cracked sandwich beams are analyzed using the finite element method. Because of high stress gradients around the interface, different finite element meshes consisting of two dimensional plane strain and plane stress elements are used.

The finite element analysis is performed by the use of the general purpose finite element program ANSYS [18]. The 6 node two-dimensional plane strain triangular elements (PLANE 82) were used in order to model the beam. The frictionless contact area at the crack surfaces in the cracked sandwich beam, was modeled with 2-node linear contact elements (CONTACT 178) [18], in order to prevent one surface from entering into the other in the load transfer region. The contact friction is assumed zero since the friction properties on the crack surfaces can not be reliably measured and since the effect of friction on the closed part of crack surfaces is small [13,6,15,17]. Singular elements (mid-side nodes at ¼) were used at the two crack tips in order to simulate the singular stress behaviour.

In order to analyze the event-1 crack propagation, a small crack is considered at different distances d (Figure 1) below the interface immidiately under the central load introduction and parallel to the beam axis. This small crack is considered propagating under the interface. For the different crack lengths and for the applied load

$$P = rP_{ult} = 943.27N\,, \tag{1}$$

where $P_{ult}\left(=1347.52N\right)$ the average static failure load [16,17] of the sandwich beam and $r\left(=0.70\right)$ the lower stress level from the experimental ivestigation (the stress level r for a particular set of cycling loading defines the values of the maximum and minimum stresses).

The opening K_I and shear K_{II} mode stress intensity factors calculated from the nodal displacement on the crack lips, are [18]:

$$\begin{aligned} u &= \frac{K_I}{4G}\sqrt{\frac{r}{2\pi}}\left((2\kappa-1)\cos\frac{\theta}{2}-\cos\frac{3\theta}{2}\right)-\frac{K_{II}}{4G}\sqrt{\frac{r}{2\pi}}\left((2\kappa+3)\sin\frac{\theta}{2}+\sin\frac{3\theta}{2}\right),\\ \upsilon &= \frac{K_I}{4G}\sqrt{\frac{r}{2\pi}}\left((2\kappa-1)\sin\frac{\theta}{2}-\sin\frac{3\theta}{2}\right)-\frac{K_{II}}{4G}\sqrt{\frac{r}{2\pi}}\left((2\kappa+3)\cos\frac{\theta}{2}+\cos\frac{3\theta}{2}\right), \end{aligned} \tag{2}$$

where u and υ the sliding and opening displacements respectively, (r,θ) the polar-local coordinate system at the crack tip, G the shear modulus and $\kappa = 3-4\nu$ for plane strain, $\kappa = (3-\nu)(1+\nu)$ for generalized plane stress.

In case that there isn't any symmetry in the cracked model and $\theta = \pm 180^\circ$, we have:

$$K_I = \sqrt{2\pi}\,\frac{G}{(1+\kappa)}\frac{(\Delta\upsilon)}{\sqrt{r}}\,,\quad K_{II} = \sqrt{2\pi}\,\frac{G}{(1+\kappa)}\frac{(\Delta u)}{\sqrt{r}} \tag{3}$$

where Δu , $\Delta\upsilon$ the difference in displacements on the crack lips.

A very fine finite element mesh is considered in order to simulate the crack lengths. The finite element mesh consists of about 82000 elements PLANE 82 in the case that $d = 1.5mm$, 64000 elements in the case that $d = 1.0mm$ and 42000 elements in the case that $d = 0.5mm$. We have used different finite element meshes in the core as the distance of the crack from the upper skin interface changes but without changing the number of elements in the upper and lower skin laminate (about 4782 elements in the top laminate and 2290 elements in the bottom laminate). In order to build the finite element meshes in the core we have considered different parameters concerning the crack length, the "fine" mesh around the crack tip and the distances of the crack from the upper skin interface. Twelve singular elements have been used around the crack tips for every crack length. The number of contact elements changes according to the crack length and in the finite element program ANSYS a code in APDL [18], is created in order to insert the contact elements for every crack length.

4 NUMERICAL RESULTS

After the formation of a small crack, the cracked sandwich beam is studied. The crack is considered at different distances $d\,(= 1.5mm, 1.0mm, 0.5mm)$ from the upper skin interface and just below the concentrated force. The position of the right crack tip is considered constant, immediately under the concentrated from whereas the left crack tip moves to the left, as it was observed from the experimental investigation [16,17]. The results for the opening mode K_I and the shear mode K_{II} stress intensity factors based on relations (2) and (3) and for the plane strain and plane stress conditions, are given in Figures 2-7 for the left and the right crack tips.

From the numerical investigation it is seen that as the crack propagates, K_I and K_{II} values increase at the left crack tip (Figures 2,3). K_{II} increases very faster when comparing with K_I. It is observed that the value K_I-stress intensity factors are very lower comparing with the K_{II}-stress intensity factors. It is also observed that as the distance between the crack and the upper skin interface decreases the value of the K_I and most apparently of the K_{II} also decrease but the percentege differences between the values of K_{II} for $d = 1.5mm$ and $d = 1.0mm$ and for $d = 1.0mm$ and $d = 0.5mm$ are rather small. This is due for K_I to the fact that the stress field in the core, where the shear stresses are dominated, between the crack and the interface is rather complex because of the small distance from the interface to the crack. On the other hand for K_{II} the shear stresses in the core become higher as we move from the upper skin interface (see also [14,15]). In case that plane stress is considered instead of plane strain for $d = 1.0mm$, there are differences between the values of K_I and K_{II} (Figures 4,5). These differences increase as the crack lenght increases. At the right crack tip the K_{II} and K_I values (Figures 6,7) increase in a slow rate when comparing with the left crack tip. In particural the K_I values are very high for $d = 1.5mm$ comparing with the values of K_I for $d = 1.0mm, 0.5mm$, which are close to zero (Figure 6). This is due to the fact that the right crack tip is immediately under the load introduction and the stress field close to the interface is singular. On the other hand the K_{II} values for the different distances d (Figure 7) increase similarly but in a slow rate when comparing to the left crack tip. For the right crack tip it is observed that, the percentage differences between the plane stress and the plane strain cases, are rather small.

From the above analysis it results that a crack propagating into the core close to the upper skin interface, is subjected to mixed-mode loading conditions where Mode II is the dominating mode.

Density (kg/m^3)	75.2
Compressive strength (MPa)	1.1
Compressive modulus (MPa)	38.0
Tensile strength (MPa)	2.0
Tensile modulus (MPa)	62.0
Shear strength (MPa)	0.9
Shear modulus (MPa)	29.0

Table 1. Mechanical properties of R-75 [17]

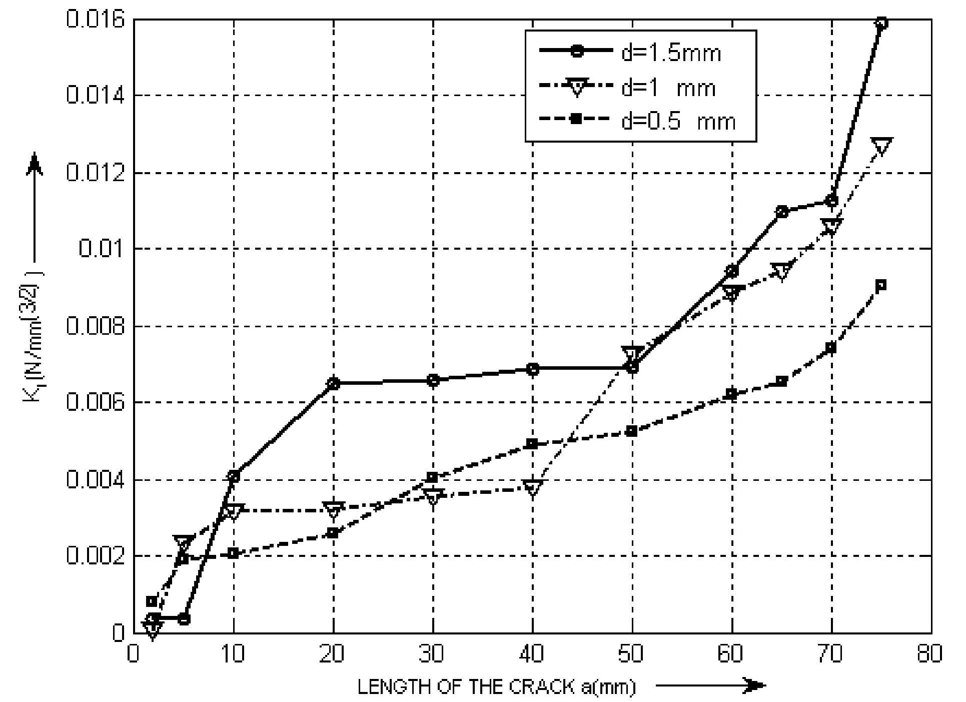

Figure 2 Values of the stress intensity factors K_I for the left crack tip and for different distances d from the upper skin interface.

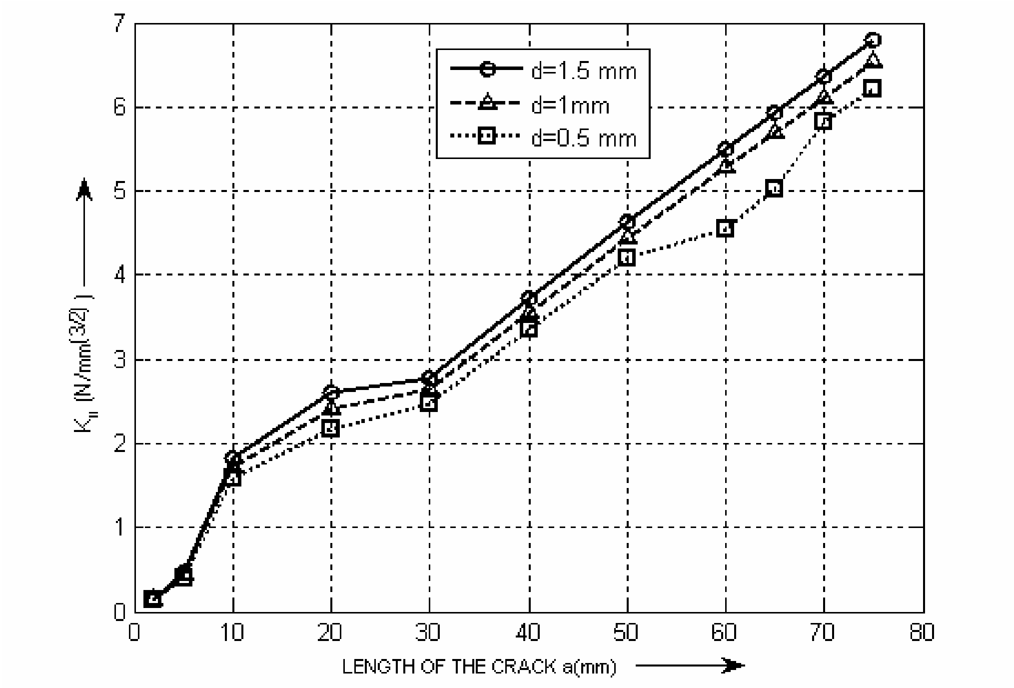

Figure 3: Values of the Stress Intensity Factors K_{II} for the left crack tip and for different distances d from the upper skin interface.

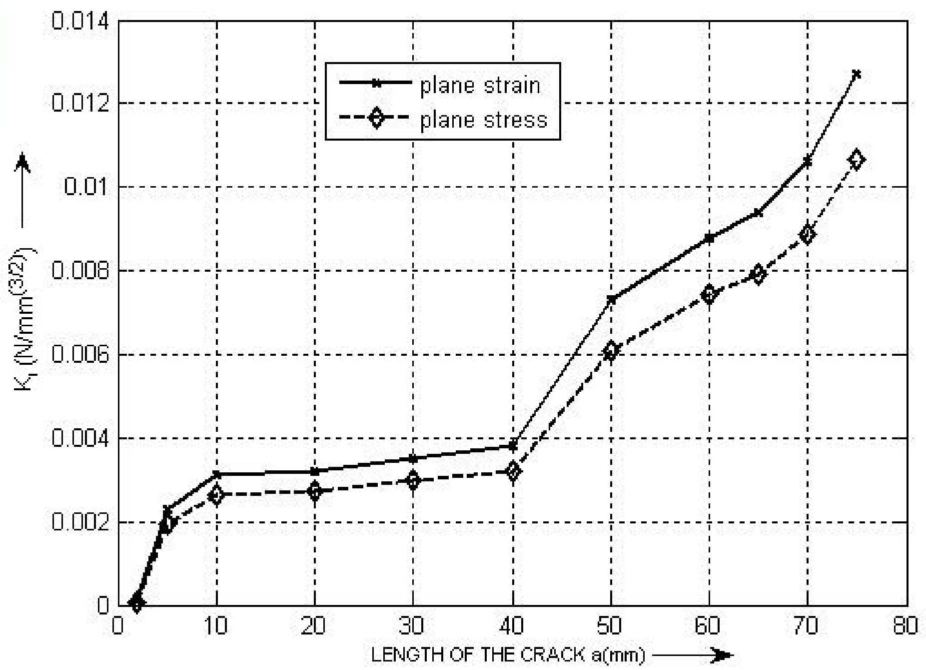

Figure 4:Differences between the plane strain and plane stress cases for the values of the left crack tip stress intensity factors K_I and for d=1mm.

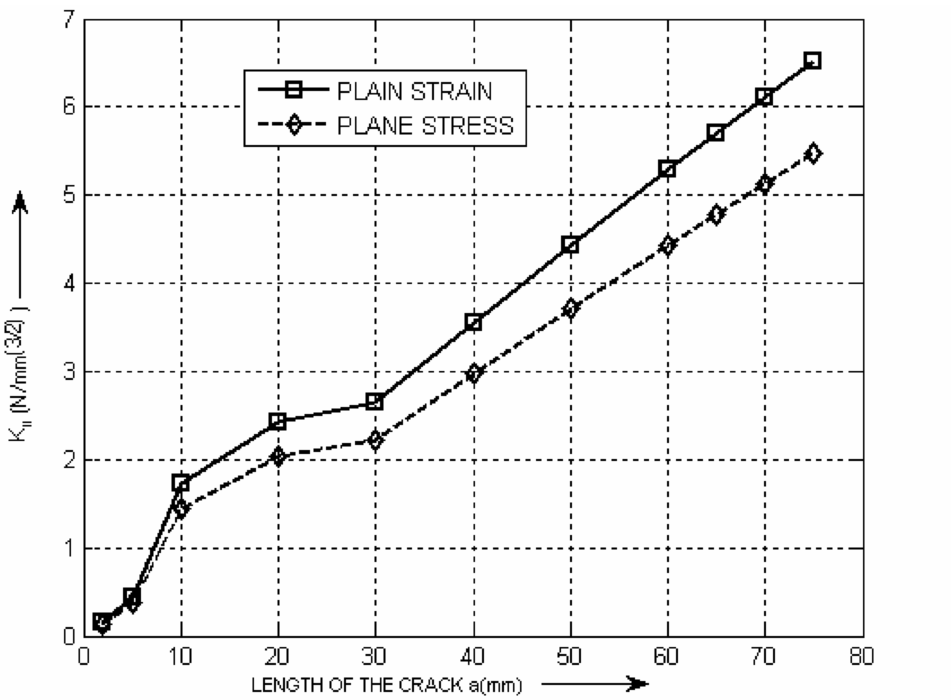

Figure 5:Differences between the plane strain and the plane stress cases for the values of the left crack tip stress intensity factors K_{II} and for d=1mm.

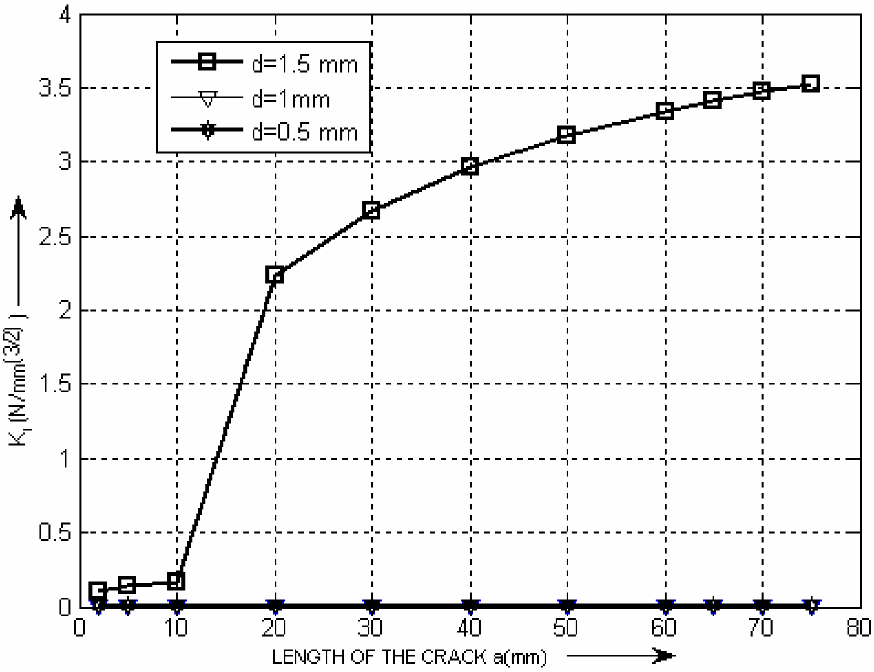

Figure 6: Values of the stress intensity factors K_I for the right crack tip and for different distances d from the upper skin interface.

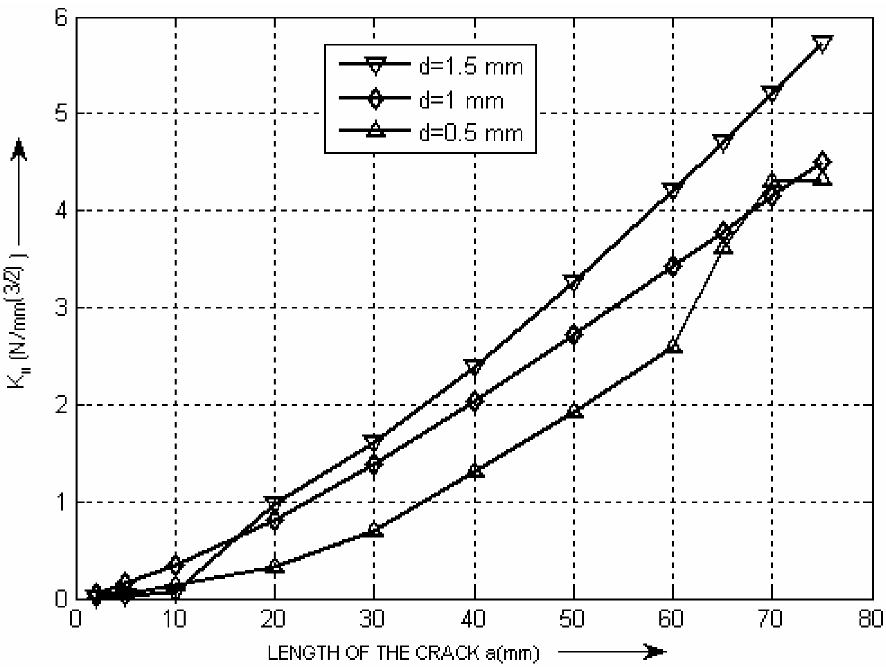

Figure 7: Values of the stress intensity factors K_{II} for the right crack tip and for different distances d from the upper skin interface.

5. CONCLUSIONS

The behavior of fractured sandwich composites loaded, in three-point flexure was examined numerically. An “extra fine” finite element mesh was used in this study better than those used in [19-21].

The crack propagation process was simulated numerically via the finite element method using different finite element meshes for the different crack lengths, in the core of a sandwich beam very close to the upper core-skin interface and parallel to the beam axis. The finite element analyses were static and non-linear elastic. The non-linearity concerns contact elements used at the crack surfaces. The results for the stress intensity factors have big deviations from those derived in [19] using a “coarse” finite elements mesh. The results for the left and right crack tips are comparable with those derived in [21] for $d = 1.5 mm$.

The stress intensity factors at the vicinity of the crack tips were calculated for the different crack lengths using the linear fracture mechanics approach. The crack lengths considered in the core were in accordance with the crack initiation and propagation in the core of the sandwich beam just below the top face in the sub-interface, observed in the experiments [16,17]. From the numerical investigation it follows that the core is mainly subjected to shear. The crack propagation on the compression side is generally mode II dominated. The differences in the K_I values at the right crack tip and for the different distances d from the upper skin interface, were due to the complex stress situation immediately down the concetrated load [22-25].

The above numerical investigation gives a first indication of the crack growth behaviour in sandwich beams under flexural loading. Although the percentage differences between the plane strain and plain stress cases in the value of stress intensity factors were rather small, a three dimentional finite element analysis is further needed in order to verify our results

REFERENCES

[1] L. H. Gibson, M. F. Ashby, “Cellular solid-structure and properties”, 2nd ed. Cambridge: Cambridge University Press; (1997).

[2] M. F. Ashby, L. J. Gibson, and S. K. Maiti, “Fracture Toughness of Brittle Cellular Solids”, *Scr. Metall.*, 18, 213-217 (1984).

[3] D. Zenkert, J. Backlund, “Poly(vinlchloride) Sandwich Core Materials: Fracture Behaviour under Mode II Loading and Mixed-mode Condition”, *Materials Science and Engineering* , A108, 233-240 (1989).

[4] A. M. Harte, N. A. Fleck, “The fatigue strength of sandwich beams with alloy foam core”, *International Journal of Fatigue*, 23, 499-507 (2001).

[5] C. Burchardt, “Bonded sandwich T-joint for maritime applications”, Ph. D. Dissertation, special Report No. 32, Institute of Mechanical Engineering, Aalborg University (1996).

[6] M. Burman, “Fatigue crack initiation and propagation in sandwich structures”, Doctoral thesis, Report 98-29, Department of Aeronautics, Royal Institute of Technology (1998).

[7] P.M.C. Noury, R. A. Shenoi, and I. Sinclair, "Fatigue crack growth in rigid PVC cellular foam under combined mode-I and mode-II loading", Proceedings of Fourth International Conference on Sandwich Construction, Editor Karl-Axel Olsson, EMAS Publishing, 2, 491-502, (1998).
[8] T.C. Triantafillou and L.J. Gibson, "Debonding in Foam Core Sandwich Panels", *Mater. Struct.,* 22, 64-89 (1989).
[9] L. A. Carlsson, L. S. Sendlein and S. L. Merry, "Characterization of Face Sheet/Core Shear Fracture of Composite Sandwich Beams", *Journal of Composite Materials*, 25, 101-116 (1989).
[10] L. A. Carlsson, "On the Design of the Cracked Sandwich Beam (CSB) Specimen", *Journal of Reinforced Plastics and Composites*, 10, 434-444 (1991).
[11] L. A. Carlsson, and S. Prasad, "Interfacial Fracture of Sandwich Beams", *Engineering Fracture Mechanics*, 44, 581-590 (1993).
[12] D. Zenkert, "Damage Tolerance of Foam Core Sandwich Constructions", Ph. D. thesis, *Report 90-8,* Department of Aeronautics, Royal Institute of Technology, Stockholm, Sweden (1990).
[13] D. Zenkert, "Damage of Sandwich Beams with Interfacial Debondings", *Composite Structures*, **17**, 331-350 (1991).
[14] C. Berggreen, "Damage tolerence of Debonded Sandwich Structures, Phd thesis. *Department of Mechanical Engineering, Technical University of Denmark* (2004).
[15] C. Berggreen, B.C. Simonsen and K.K. Borum, "Prediction of debond propagation in sandwich beams under FE-bared Fracture Mechanics and NDI Techniques", *Journal of Composite Materials*, 41, 493-520 (2007)
[16] N. Kulkarni, Fatigue response and life prediction of foam-core sandwich composites under flexural loading, Master thesis, Teskegee University, (2002).
[17] N. Kulkarni, H. Mahfuz, S. Jeelani, and L. A. Carlsson, "Fatigue crack growth and life prediction of foam core sandwich composites under flexural loading", *Composite Structures*, 59, 499-50 (2003).
[18] ANSYS Engineering Analysis System User's Manual, Swanson Analysis Systems, Inc., (1992).
[19] E.E. Theotokoglou, L.A. Carlsson, H. Mahfuz, "Numerical study of fractured sandwich composites under flexural loading" in Proceedings of the 7th International Conference on Sandwich Structures, Editors, Thomsen, O.T., Bozhevolnaya, E., Lyckegaard, A., Springer, 423-431 (2005).
[20] P.P.L. Matos, R.M. McMeeking, P.G. Charalambides and M.D. Drory, "A Method for Calculating Stress Intensities in Bimaterial Fracture", *Int. J. Fract.,* 40, 235-54 (1989).
[21] E.E. Theotokoglou, D. Hortis, L.A. Carlsson and H. Mahfuz, "Numerical study of fractured sandwich composites under flexural loading", *Journal of Sandwich Structures and Materials,* 10, 75-94 (2008).
[22] Y. Frostig, "On stress concentration in the bending of sandwich beams with transversely flexible core", *Composite Structures*, 5, 405-414 (1996).
[23] E.E. Theotokoglou, "Analytical determination of the ultimate strength of sandwich beams", *Applied Composite Materials,* 3, 345-353 (1996).

[24] J. Kim and S.R. Swanson, “Design of sandwich structures for concentrated loading”, *Composite Structures,* 52, 365-373 (2001).
[25] Y. Frostig and T.O. Thomsen, “Localized Effects in the Non-Linear Behavior of Sandwich Panels with a Transversely Flexible Core”, *Journal of Sandwich Structures and Materials,* 7, 53-75 (2005).

8th International Conference on Sandwich Structures
ICSS 8
A. J. M. Ferreira (Editor)

IN-PLANE TENSILE CORE DELAMINATION STRENGTH OF TUBULAR CELL POLYPROPYLENE HONEYCOMBS

Hamid Rahimi, Mir Hamid Reza Ghoreishy, Amir M. Rezadoust, Masoud Esfandeh, Vahid Khalili

Composites and Adhesives Department, Iran Polymer and Petrochemical Institute,
P.O. Box 14965-115, Tehran, Iran
E-mail: H.Rahimi@ippi.ac.ir, web page: http://www.ippi.ac.ir

Key words: Thermoplastic Honeycombs, In-plane properties, Surface Treatment, Modelling.

Summary

An investigation was conducted to study the in-plane tensile properties of adhesively bonded tubular polypropylene (PP) honeycombs. The adhesion level between the PP tubes was altered by varying the corona surface treatment time. In-plane tensile tests on the honeycomb cores were carried out to determine their mechanical properties and also to study the failure modes of samples. In addition, two-dimensional linear elastic finite element analyses (FEA) of representative models were undertaken using the ABAQUS software. The experimental results showed that the in-plane tensile properties of PP honeycombs increased with increasing surface energy of the PP substrates. The core delamination samples made with well-surface-treated tubes showed a relatively ductile behaviour whereas weakly-treated specimens failed in a brittle manner.

INTRODUCTION

Man-made honeycombs are being increasingly used in a variety of new commercial products due to their low density and high specific mechanical properties [1-2]. In the past few years, thermoplastic honeycombs have been introduced which are used in boat building and transport industries and are finding increasing applications in other engineering fields [3-4]. In general, thermoplastic honeycombs are intrinsically tough but their specific stiffness and strength properties are low in comparison with those of fibre-reinforced plastic honeycombs. However, the properties of these materials compare favourably with structural polymeric foams.

These honeycombs are manufactured by either heat fusing or adhesively bonding thermoplastic sheets or extruded profiles. A survey of published literature reveals that there are few publications dealing with the mechanical properties and processing of thermoplastic honeycombs [5-8]. Some researchers have used thermoplastic honeycombs as models to study the mechanical properties of cellular structures under compressive loading conditions [9-10]. Apart from a recent published paper on the in-plane tensile behaviour of Nomex honeycombs there is no cited publication addressing the in-plane tensile behaviour of thermoplastic honeycombs [11].

Accordingly, the main objective of this study was to determine experimentally the effect of adhesion level between PP tubes on the in-plane core delamination strength of honeycomb specimens. In addition finite element analyses were carried out to study the deformation characteristics of representative honeycomb models. In-plane tensile testing of honeycomb cores yields useful design data such as tensile modulus and strength, strain-to-failure and also valuable information about failure modes of these materials.

EXPERIMENTAL

The honeycomb core samples used in this study were made in-house by adhesively bonding extruded PP tubes using a two-part room temperature cure epoxy adhesive. The extruded PP tubes had an inside diameter of 6 mm and average wall thickness of 200 μm. The PP tubes prior to bonding procedure were surface treated using a Tantech corona discharge (CD) equipment.

Wettabilities of the substrates were evaluated as static contact angles using a Kruss G2/G40 contact angle measuring system. In order to determine the surface energy of the treated PP samples, water and di-iodomethane were used as probe liquids. Water being a highly polar and di-iodomethane representing a highly dispersive liquid.

Following the bonding procedure, the fabricated honeycomb core samples were sliced into required thicknesses using a hotwire technique. The core delamination tests were carried out using an MTS universal testing machine in accordance with ASTM C 363-94 standard. Rectangular honeycomb specimens, measuring approximately 254 by 127 mm, were subjected to in-plane tensile tests (figure 1). The thickness of honeycomb specimens was varied from 10 to 40mm. The tests were carried out at a cross-head speed of 5mm/min under ambient laboratory conditions (23 ± 3º C, 50 %rh).

NUMERICAL MODELLING

A typical two-dimensional FE model developed for the analysis of the honeycomb cores is shown in figure 1. The representative model was completely symmetrical about the y-axis and thus only half of the honeycomb was modelled and symmetry condition was imposed along the boundary. The tubes were modelled with the B21 beam elements. Each tube was modelled with 18 elements evenly distributed along the circumference of the cells. In total about 13000 elements were used to model the honeycomb core delamination sample. The bond between each tube was assumed to be perfect. The Young's modulus and Poisson ratio of the PP were taken to be 1250 MPa and 0.4 respectively.

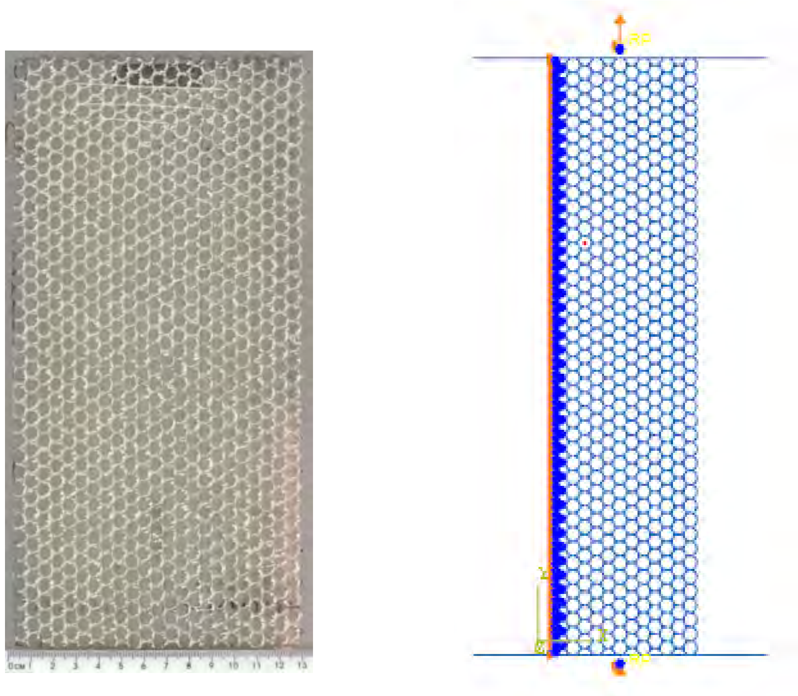

Figure 1 : Honeycomb core delamination sample and representative fe model

RESULTS AND DISCUSSION

A summary of the surface contact analysis study is shown in table 1. As expected, the contact angles decreased and the surface energy values increased with increasing corona surface treatment time.

Substrate	Contact angle (°)		(1) Owens surface energy parameters (mJ/m^2)		
	water	di-iodomethane	γ_s^P	γ_s^P	γ_s
As received PP	92.7	56	0.9	30.9	31.8
Lightly-surface treated PP	45.7	47	20.9	35.9	56.8
Well-surface treated PP	25.3	45	31.3	37	68.3

Notes: (1) Owens surface energy values [12]
(2) At least 5 specimens were tested for each test variable

Table 1 : Contact angle measurements and surface energy values of polypropylene substrates

Figure 2 shows the core delamination test results in which the performance of three different PP substrates is compared. The core delamination strength of these samples were 46, 58 and 104 kPa respectively. The tensile modulii of these samples were 1.2, 2.3 and 3 MPa for the weak, moderate and strongly treated tubes respectively. The strain-to-failure of samples increased with increasing surface treatment time and it reached a peak value of around 7% for the well-surface-treated sample. The difference in tensile properties is mainly attributed to the variation in adhesion level as a result of surface treatment. The non-linearty at the start of load-extension curves is due to various factors including the specimen settling down in the multi-pin grips. Table 2 also shows the energy-to-failure of these samples which were calculated from the area under the load-extension curves. The failure energy of well-surface-treated samples at 0.971 J was almost three times that of samples with no surface treatement.

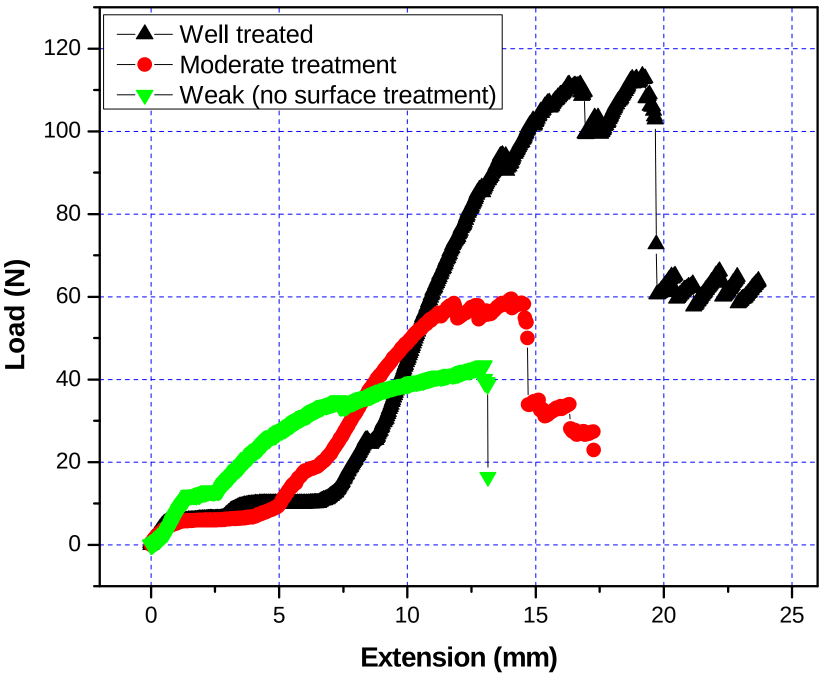

Figure 2 : Effect of polypropylene corona surface treatment on load-extension behaviour of honeycomb core samples

Parameter	Core adhesion		
	Weak	Moderate	Strong
Honeycomb core delamination strength (kPa)	45.55 (3.06)	58.29 (1.22)	103.59 (6.73)
In-plane tensile modulus of honeycomb core (MPa)	1.17	2.31	3
Strain-to-failure (%)	5	5.5	7.4
Energy to failure (J)	0.363	0.421	0.971

Notes: (1) At least five specimens were tested for each variable
(2) Numbers in parantheses represent standard deviations.

Table 2 : Summary of in-plane tensile properties of honeycomb cores

Figure 3 shows a core delamination sample under tensile load. Under load, the honeycomb core initially deformed elastically and with increasing load the PP tubes deformed into elliptical shapes. As the load increased, the adhesion between the PP tubes started to fail and in some cases rupture of tube walls occurred. It should also be noted that viscoelastic deformation of polypropylene is also likely to occur under loading. Experimental observations revealed that debonding between the tubes started at the edges and propagated across the width of the samples. This study also showed that it is vital to achieve optimum hexagonal packing condition otherwise misaligned nodes act as stress raisers and reduce core delamination strength.

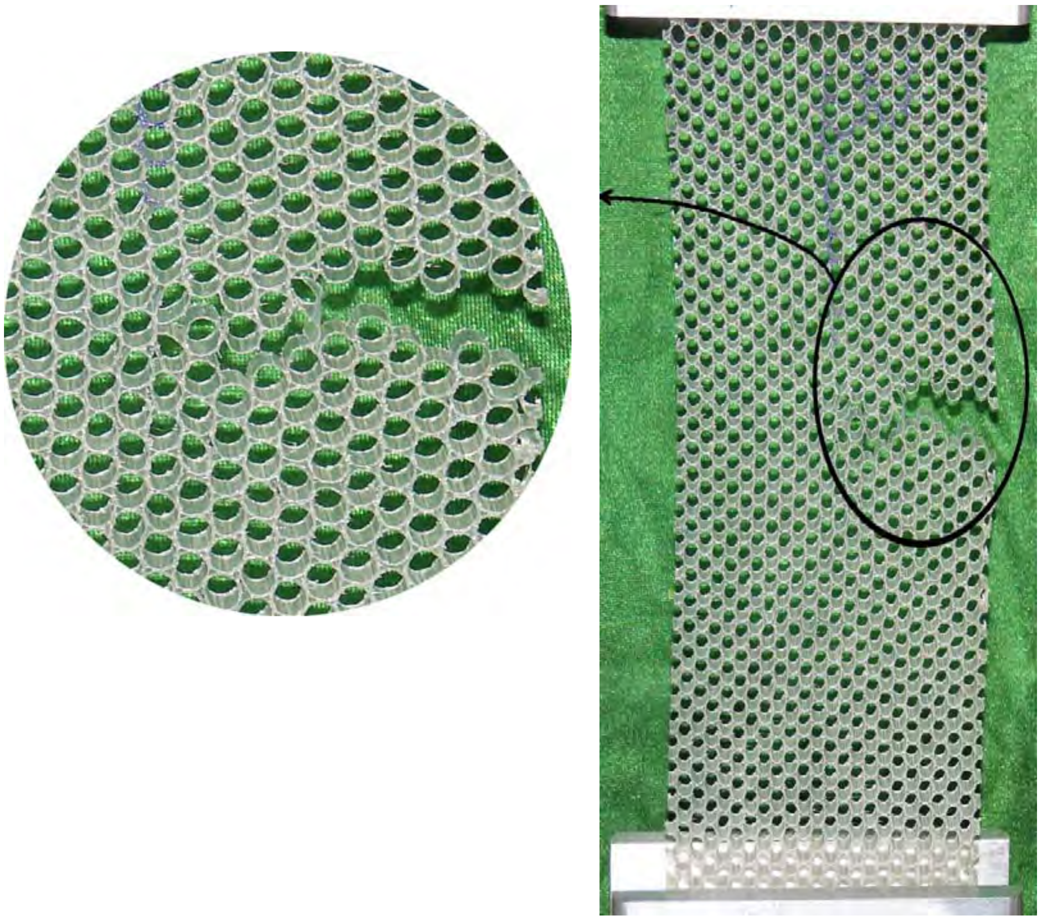

Figure 3 : Typical failure initiation pattern in tubular cell polypropylene honeycomb under tensile load

A representative finite element analysis result is shown in figure 4. The undeformed tubes (continuous lines) and the deformed tubes (dashed lines) are superimposed for clarity. The predicted load for an applied displacement value of 5 mm was 53 N compared to a value of 12 N for the experimental value of the well-treated sample. However, if we disregard the initial part of the load-extension curves (figure 2) until the slack is taken up, we observe a much better correlation between the fe and experimental result. It is important to note that the real joints are adhesively bonded and during loading condition the bonded tubes progressively undergo debonding process. The present fe models do not take into account the adhesion/debonding phenomena and are therefore inherently more rigid at higher loads. It should also be noted that the real honeycomb cells are not perfectly circular due to the processing conditions during extrusion and packing stage.

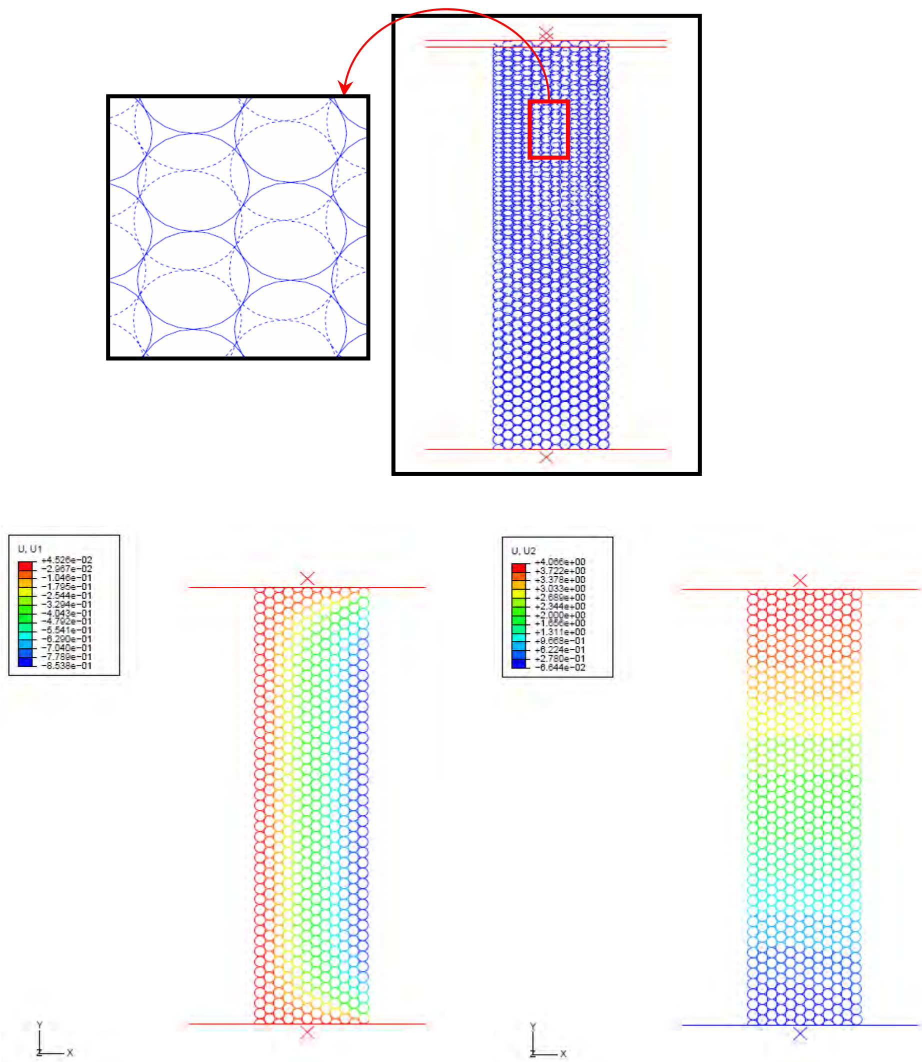

Figure 4 : FE results - deformed geometry and predicted displacements

CONCLUSIONS

Based on the particular programme of work undertaken involving in-plane tensile testing of polypropylene honeycombs, the following conclusions were reached:

- The tensile properties of PP honeycomb cores increased with increasing corona surface treatment time of tubes.
- The failure mode of honeycomb samples was dependent on the PP surface treatment level:- brittle failure for as-received samples (i.e. no surface treatment) and relatively ductile for well-surface-treated samples.
- In general, the present 2D finite element model seemed to perform reasonably well in predicting certain features of the honeycomb cores subjected to in-plane tensile load.

REFERENCES

[1] T. Bitzer, *Honeycomb Technology*, Chapman and Hall, (1997).

[2] L.J. Gibson and M.F. Ashby, *Cellular Solids*, Cambridge University Press, (1997).

[3] R. Filippi, "The structural sandwich with a polypropylene honeycomb core", *JEC Composites Magazine*, 7, 71-72, (2004).

[4] H. Ning, G.M. Janowski, U.K. Vaidya and G. Husman, "Thermoplastic sandwich structure design and manufacturing for the body panel of mass transit vehicle", *Composite Structures*, 80, 82–91, (2007).

[5] F. Meraghni, F. Desrumaux and M.L. Benzeggagh, "Mechanical behaviour of cellular core for structural sandwich panels", *Composites - Part A*, 30, 767-779, (1999).

[6] F. Meraghni, F. Desrumaux and M.L. Benzeggagh, "Damage analysis in sandwich beams with cellular core using micromechanics coupled to a statistical approach", *Journal of Sandwich Structures and Materials*, 6, 463-495, (2004).

[7] A. Passaro, P. Corvaglia, O. Manni and L. Barone, "Processing-properties relationship of sandwich panels with polypropylene-core and polypropylene-matrix composite skins", *Polymer Composites*, 25, 307-318, (2004).

[8] X. Fan, I. Verpoest and D. Vandepitte, "Finite element analysis of out-of-plane compressive properties of thermoplastic honeycomb", *Journal of Sandwich Structures and Materials*, 8, 437-458, (2006).

[9] S.D. Papka and S. Kyriakides, "In-plane crushing of a polycarbonate honeycomb", *International Journal of Solids and Structures*, 35, 239-267, (1998).

[10] J. Chung, A.M. Waas, "In-plane biaxial crush response of polycarbonate honeycombs", *ASCE Journal of Engineering Mechanics*, 127, 180–193, (2001).

[11] C.C. Foo, G.B. Chai and L.K. Seah, "Mechanical properties of Nomex honeycomb structure", Composite Structures, 80, 588-594, (2007).

[12] D.K. Owens and R.C. Wendth, **"**Estimation of the surface free energy of polymers", *Journal of Applied Polymer Science*, 13, 1741-1747, (1969).

8th International Conference on Sandwich Structures
ICSS 8
A. J. M. Ferreira (Editor)

ON THE BEHAVIOUR OF STRESS FIELDS AROUND A LAMINATE DROP

Jack Dyson[1,⋆], **Gianni Albertini**[1]

[1]Dip. di Fisica e Ingegneria dei Materiali e del Territorio (FiMET)
Universita Politecnica delle Marche
via Brecche Bianche, 60100 Ancona, Italy
⋆e-mail: jackdyson31@univpm.it

Key words: Sandwich structures, Modelling, Laminate drop, Multisegment integration

Summary. *The behaviour of materials where a sudden change in stiffness is forecast presents considerable analytical difficulty. Under such strange circumstances it becomes important to understand precisely the language of the model. The stress field elements are related through multiple differential coefficients and the presence of an anomaly in one component has serious consequences for the rest. Importantly for mission critical computations especially on a computer, the plausibility of the results must be confirmed and understood from a general point of view. The presence of finite discontinuity is an everyday occurance in engineering and in this paper we demonstrate how a seemingly unphysical stress relationship in a bonded laminate structure can theoretically still give continuous strains.*

1 INTRODUCTION

Discontinuity is common phenomenon, from shockwaves in gases to sharp changes of modulus in materials. Any analytical discussion is ultimately an idealisation of the reality. In so doing one can capture the most significant effect of a solution while carefully avoiding unneccessary complexity in what may be an already difficult problem. The physics of discontinuity in solid materials is one such case, where the responding internal stresses of a sample undergo steplike changes and the strains remain seemingly unaffected.

The continuity of matter demands cohesion under normal working conditions and this is what engineers' call the saftey zone of the material. Within the safety zone the material cannot break and therefore must remain whole under any working load. The size of the safety zone depends on the properties of the material at the microscopic level, but here it is expressly assumed that we remain within it (Hooke's Law).

We assume for this form of treatment the following to be true:

1. The only predominant quantities are the bending stress σ_{xx} and the bending strain ε_{xx} with all other stresses and strains being negligible in comparison to these.

2. The centroidal surface along the length of the beam is longitudinally unstressed and unstretched, and therefore it is called the neutral surface.

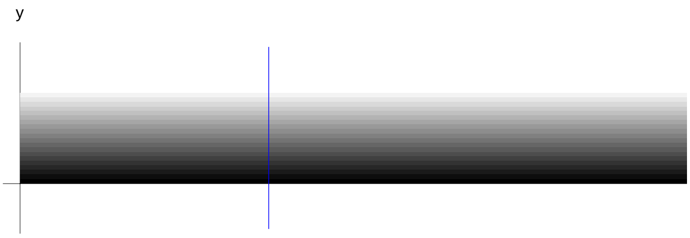

Figure 1: The Basic Cantilever Beam arrangement with a single plane of discontinuity (in blue).

3. All quantities are independent of the z coordinate.

which results in two important consequences in that of the 9 tensor components describing the problem only six now remain and of these remaining six two are directed in z and therefore are zero.

Hence the non-zero strain tensor components are (in the usual notation),

$$\frac{1}{2}\left(\partial_x u_x + \partial_x u_x\right) = \partial_x u_x \tag{1}$$

$$\frac{1}{2}\left(\partial_y u_x + \partial_x u_y\right) = \frac{1}{2}\left(\partial_x u_y + \partial_y u_x\right) \tag{2}$$

$$\frac{1}{2}\left(\partial_y u_y + \partial_y u_y\right) = \partial_y u_y \tag{3}$$

From the first assumption the last two equations are equate to zero and the second of these integrates partially,

$$\partial_y u_y = 0 \Rightarrow u_y = u_y\left(x\right) \tag{4}$$

and the first is therefore,

$$\partial_y u_x + d_x u_y = 0 \tag{5}$$

Integrating this,

$$u_x\left(x, y\right) = -y d_x u_y + c\left(x\right) \tag{6}$$

The function $c\left(x\right)$ vanishes identically because of the second assumption and hence the displacement problem is solved. Now using the Hooke's Law tensor equation with these strain components,

$$\varepsilon_{xx} = E^{-1}\left(\sigma_{xx} - \nu\left(\sigma_{yy} + \sigma_{zz}\right)\right) \approx E^{-1}\sigma_{xx} \tag{7}$$

$$\varepsilon_{xy} = G^{-1}\sigma_{xy} = 0 \tag{8}$$

So,

$$\partial_x u_x = -y d_x^2 u_y \Rightarrow \sigma_{xx} = -E y d_x^2 u_y \tag{9}$$

There is nothing else these equations can tell us. They are equations of in-beam local stresses and strains. There is nothing to help solve for the displacements locally in the form of Newton's equilibria. There are no specific macroscopic or boundary connection mechanisms. The fact that there are not, turns out to mean that there is a discrepancy in the problem formulation. We can't solve these equations as they stand and so have to impose upon them the equilibrium which we observe to hold. The axial moment inside the material generally exists and is about the z and the y axes. It must equal the total load moment at the point x. However since the $\sigma_{xx} = \sigma_{xx}(x, y)$ only, the integrated moment around the y-axis vanishes due to symmetry and we do not need to consider it further. The remaining contribution is a turning effect about the z-axis,

$$\int\int y\sigma_{xx} dz dy = -E d_x^2 u_y \int\int y^2 dz dy = M(x) \tag{10}$$

which is the celebrated Euler-Bernoulli equation,

$$-E I_z d_x^2 u_y = M(x) \tag{11}$$

2 LAMINATE AND BEAM-LIKE FINITE ELEMENT LOADING

If now the thin beam is divided up into finite elements which are themselves beamlike, then the internal moment is balanced by the following equilibrium involving shear load across the element,

$$d_x M = Q(x) + m(x) \tag{12}$$

Here $m(x)$ represents the externally applied moment distribution and we assume this to be continuous for non-composite solids. This equation is general and applies at a point without approximation. Since the material must not break and the beam elements are themselves thin, one can assume that the Euler-Bernoulli equation holds over every single element,

$$\int\int \sigma_{xx} dz dy = 0 \tag{13}$$

This assumption is only valid for macroscopic beam sections when the aspect ratio of each element does not allow variation of the stress field in the z-dimension and in particular all internal shearing can still be taken as negligible when compared to axial stresses. The results however will hold regardless of aspect ratio violation[1] because a more correct (but complex, i.e. the full multisegment method integration) treatment would divide the beam up not only in the x-axis but also in the y. The aspect ratio can be then fixed as we please while the element would shrink to a point (x, y) in the body of the beam and an analysis would would be presented with the need to integrate along the y-direction as well. This corresponds to an assumption of violation of the Bernoulli-Euler formula and is uneccessary in the present case.

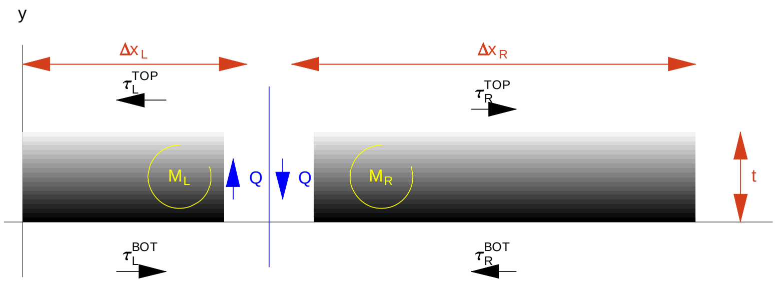

Figure 2: Two finite elements in equilibrium across a discontinuity divide in the material. The right hand element requires twice as much material volume to generate the same forces as the left hand one.

Suppose that at some arbitrary x_0 the material undergoes a sudden change in its material composition. The stiffness to the left is different to that on the right of the yz plane $\{(x_0, y)\,|0 \leq y \leq t\}$. The space just before this discontinuity plane we call the left approach (labelled L) and similarly the set of coordinates to its right is the right hand approach (labelled R). The beam can now be broken up into smaller finite elements each of which will exist in equilibrium with one another under generally applied external load distributions e.g. $m(x)$.

The change in stiffness generally means that the elements to the right need a different volume of material to resist loading than those to the left. However the material remains unbroken across the boundary and considering the two finite elements either side of the discontinuity plane we can apply the differential moment balance to obtain shear load equalization at the point x_0. This choice is of equilibrium is ensures that the beam does not accelerate vertically and thus break, so we have near this point of sudden stiffness change the following differential behavior,

$$\frac{\Delta x_R}{\Delta x_L}\frac{\Delta M_L}{\Delta x_R} + [m_R - m_L]|_{x_0} \approx \frac{\Delta M_R}{\Delta x_R} \tag{14}$$

where we may put (for non-composites),

$$[m_R - m_L]|_{x_0} = 0 \tag{15}$$

[1] when the beam finite elements are no longer "thin"

from continuity. Multiplying top and bottom by cross sectional area (yz-plane) obtains the same relationship in terms of element volume,

$$\frac{V_R}{V_L}\frac{\Delta M_L}{\Delta x_R} \approx \frac{\Delta M_R}{\Delta x_R} \tag{16}$$

The horizontal component of force is also subject to a similar constraint, and it will lead to the behavior of the x-displacement, which is not of concern here.

The last equation is a very strong statement; it shows that in a continuous material without any sudden changes the applied moment distribution to the left and the right must be equal because exactly the same volume of material is required to generate the load response $M(x)$, (i.e. $V_L = V_R$), but in the present case the element volume on the left is different from that on the right because the material has a different stiffness. The volume ratio is directly related to the ratio of the torsion constants on each side and for a Hooke's law material can be written,

$$\frac{V_R}{V_L} = \frac{\theta_R}{\theta_L} \tag{17}$$

so,

$$\frac{\theta_R}{\theta_L}\frac{\Delta M_L}{\Delta x_R} \approx \frac{\Delta M_R}{\Delta x_R} \tag{18}$$

Taking the limit $\Delta x_R \to 0$,

$$\frac{\theta_R}{\theta_L}\frac{dM_L}{dx} = \frac{dM_R}{dx} \tag{19}$$

or

$$M_R = \frac{\theta_R}{\theta_L} M_L + C_1 \tag{20}$$

near $x = x_0$ and C_1 is a constant of integration. This equation will cause the value of the left hand moment within the material to "jump" to the value of the right hand moment over the plane $x = x_0$ and therefore for a regular material discontinuity, the total shear load $Q(x)$ will undergo a sudden and linear change of gradient past the point of sudden stiffness change whereas a consequence of which the total load moment $M(x)$ suffers a step or piecewise discontinuity at the same point in the material.

3 BONDED LAMINATE MOMENT DISTRIBUTIONS

In composites, things get much worse because of $[m_R - m_L]|_{x_0}$. This factor can be shown not to vanish across the divide of a composite laminate since the distributed moment loading can here be written in terms of the actual stresses present on the element surfaces [1],

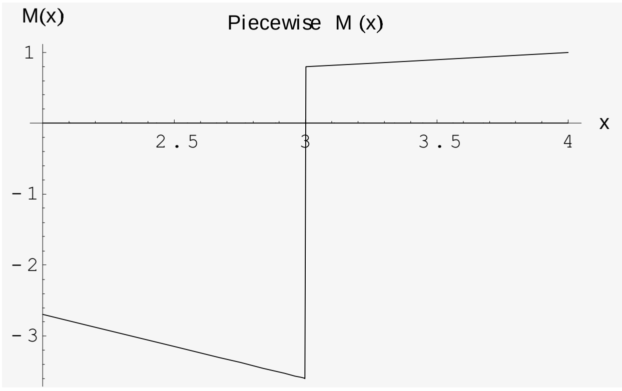

Figure 3: An example of a finite discontinuous "jump" in the total load moment function $M(x)$

$$[m_R - m_L]|_{x_0} \approx \frac{1}{2}\left(\tau_R^{TOP} + \tau_R^{BOT}\right)t - \frac{1}{2}\left(\tau_L^{TOP} + \tau_L^{BOT}\right)t \tag{21}$$

If one considers this thin beam to be part of a sandwich material then above and below it are adhesive layers with Young modulus E^a ($\sim$ GPa) and thickness t_a in which case the following is true,

$$[m_R - m_L]|_{x_0} \approx \left(\frac{E_R^a t}{t_a^R}\right) S_R - \left(\frac{E_L^a t}{t_a^L}\right) S_L \tag{22}$$

where the S quantity is very roughly the total relative displacement or slippage of the layers (beams) with respect to one another under load. Due to the high adhesive stiffness one expect slippage to be a very small quantity in general which will cancel out over a sudden discontinuity because the one expects more slippage for a weaker stiffness material. That would leave the material with a simple jump in the value of $M(x)$ across the divide as explored above. However, in a laminate things are not that straightforward, the parameter t_a is the adhesive thickness ($\sim 10^{-2}$ mm) and we see immediately that the effective value of t_a halves over x_0 by the dropping of a layer across a joint. This will have a profound effect on the discontinuity of $M(x)$ over the divide, as we now show: Normally E^a is by far the dominant *active* stiffness in a laminate and the ratio $\frac{\theta_L}{\theta_R} \sim \frac{E_L^a}{E_R^a}$ is found to be roughly 2 in the drop from 3 to 2 layer composites, and so we can approximate further,

$$S_L \sim \frac{E_R^a}{E_L^a} S_R \tag{23}$$

and therefore,

$$[m_R - m_L]|_{x_0} \approx \left(\frac{E_R^a t}{t_a^R}\right) S_R - \left(\frac{E_L^a t}{2t_a^R}\right) \frac{E_R^a}{E_L^a} S_R = \left(\frac{E_R^a t}{2t_a^R}\right) S_R \tag{24}$$

where in practice it is usual to have the sanwich to resin thickness ratio $t/t_a^R \sim 100$.The value of $M(x)$ is actually split severely by two effects: the first is a common feature of materials that undergo a "stiffness shock" effect in that the relative resistance per unit volume factor causes the total load moment to become finitely discontinuous or "piecewise" over $x = x_0$. However a second effect peculiar to laminates is also to be found manifesting itself within the net applied moment distribution $[m_R - m_L]|_{x_0}$ at the discontinuity: this fails to vanish and is generally very large. Hence as a conclusion, at the boundary we expect that the combination of these effects will split $M(x)$ by a very large but finite value at $x = x_0$. The principle motivator in this is the adhesive action missing on the right hand side of the divide in a layer-dropped composite. Mathematically, the function $M(x)$ transforms from a continuous one in the sample domain to one which is piecewise continuous, and as we will show below this has consequences in solution for the rest of the stress-field.

4 THE CASE OF FINITE DISCONTINUITY IN $M(x)$

The stiffness step in a material has been shown to imply discontinuities in the local stress field. Solving many finite element equations on a computer automates the mathematical treatment of the discontinuities such as explored above. When checking the validity of such computations, it is difficult to do so directly and an analytical approximation to the physical behaviour can give a qualitative understanding of the physical process within the material. The beam like elements derived above are very similar to the plate theory element used in 2.5 dimensional treatment by finite elements of a matrix composite and the presence of a discontinuity in stiffness always implies a jump in $M(x)$. We can therefore analyse a finite step in the moment function to obtain a qualitative variation of the stress field around a stiffness discontinuity point in laminate composites as well as simple beams.

The Bernoulli-Euler Theory can be stated in one other way, which relates the angular displacement β of an element to its vertical displacement,

$$-d_x u_y = \beta \tag{25}$$

From the Bernoulli-Euler equation we already know that,

$$-d_x^2 u_y = \frac{M(x)}{EI_z} \tag{26}$$

Writing the discussed variation of $M(x)$ as,

$$\frac{M(x)}{EI_z} = \varepsilon^{-1} [H_0(x - x_0) + 1] [H(x - x_0) + A] M_0(x) \tag{27}$$

where the H_0 is a standard Heaviside function, A is the offset below zero, and M_0 is the continuous total load moment of the beam where no stiffness changes occur. The factor

$\varepsilon = EI_z$, where it is assumed for this particular case that the stiffness halves suddenly for $x \geq x_0$ (for the general case $[H_0(x - x_0) + 1] \rightarrow \left(\frac{\theta_L}{\theta_R} - 1\right)[H_0(x - x_0) + 1]$).

Hence,

$$-d_x^2 u_y = \varepsilon^{-1}[H_0(x - x_0) + 1][H(x - x_0) + A] M_0(x) \tag{28}$$

or,

$$-u_y(x) = \varepsilon^{-1} \int^x \int^x [H_0(x - x_0) + 1][H(x - x_0) + A] M_0(x)\, dx dx \tag{29}$$

Simplifying,

$$[H_0(x - x_0) + 1][H(x - x_0) + A] \equiv (2 - A) H(x - x_0) - A \tag{30}$$

Now for an ordinary cantilevered beam the total bending moment does not vary, and so $M_0(x) \equiv M_0$. Using this and integrating the Heaviside function twice obtains,

$$-u_y(x) = \frac{1}{2} M_0 \varepsilon^{-1} \left[(2 - A) H(x - x_0)(x - x_0)^2 - Ax^2 + B_1 x + C_2\right] \tag{31}$$

where B_1 and C_2 are constants of integration. The initial displacement of a cantilever must vanish, i.e. $u_y(0) = 0 : C_2 = 0$. The constant B_1 can also be determined by requiring the displacement to vanish at some distance, say the length of the bar, $l > x_0$,

$$B_1(l) = Al - \frac{(2 - A)(l - x_0)^2}{l} \tag{32}$$

so that,

$$u_y(x) = -\frac{1}{2} M_0 \varepsilon^{-1} \left[(2 - A) H(x - x_0)(x - x_0)^2 - Ax^2 + B_1(l)\, x\right] \tag{33}$$

which solves the basic problem. This is a very useful equation indeed since it captures all the essential variation of the computer solution. Through it we can see exactly what is going on in the beam due to the sudden appearance of the stiffness drop. The Heaviside function is factored by $(x - x_0)^2$ and therefore the continuity of the displacement function is guaranteed across $x = x_0$. The appearance of the Heaviside term causes the development of a high gradient immediately after the point $x = x_0$ which continues until the beam can equalize it with a traditional type of term. What this shows is that the stiffness drop introduces a *shock* into the differential equation, which accelerates the subsequent solution until the beam can successfully absorb all the extra strain energy. Further, curiously, the Heaviside function comes into play after the stiffness drop. However the solution seems to be affected before the discontinuity too and one can demonstrate this by showing that the solution of the Euler-Bernoulli second order differential equation for a purely constant bending moment is,

$$u_y(x) \sim -\frac{1}{2} M_0 \varepsilon^{-1} \left[x \left(x - l \right) \right] \quad (34)$$

The reason is clear at once: the oscillatory behavior in the stiffness drop case is produced by forcing the solution to zero after the discontinuity. Both solutions are sketched below and give an idea of the different variations and mechanisms at work.

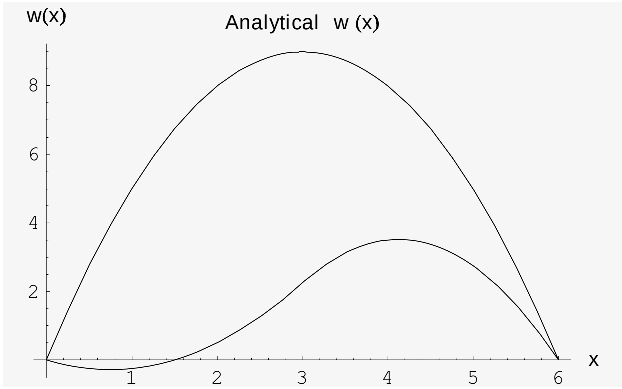

Figure 4: The vertical displacement solution for a cantilevered beam under compression in x with and without shock stiffness discontinuity. The umbrella parabola represents the variation for a simple cantilever while the more complex variation immediately below it is a result of the beam readjusting its equilibrium ($A = 0.5$) to absorb the discontinuities arising at the material interface at $x = 3$.

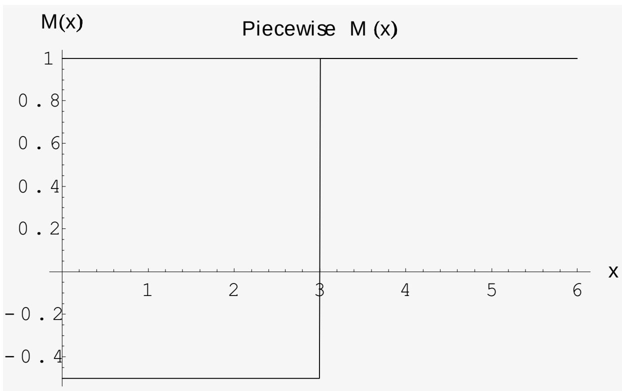

Figure 5: The bending moment $M(x)$ (step) in a cantilever beam with a finite stiffness shock discontinuity applied at $x = 3$. Also figured is the constant bending moment M_0 of a continuous material beam.

It is especially apparent that the Heaviside solution is extremely sensitive to the value of A more than any other parameter, and that is significant because A is the direct link between the bending moment $M(x)$ and the displacement function $u_y(x)$. The value of A controls whether there will be an oscillation in $u_y(x)$ and in that sense this negative amplitude of the bending moment actually damps the displacement wave, and in particular when,

$$A \sim \frac{\theta_L}{\theta_L - \theta_R} \tag{35}$$

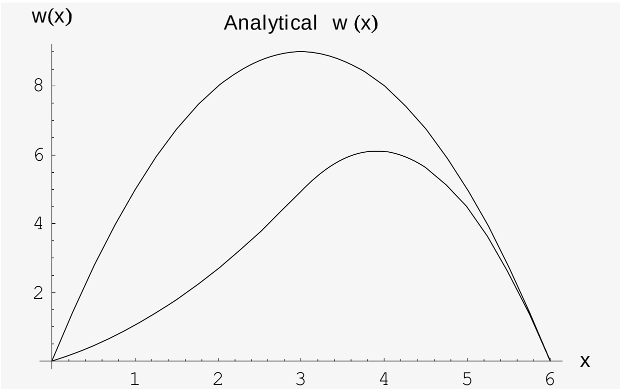

Figure 6: The vertical displacement solution for a cantilevered beam under compression in x with and without shock stiffness discontinuity. The umbrella parabola represents the variation for a simple cantilever while the more complex variation immediately below it is a result of the beam readjusting its equilibrium ($A = 0.3$) to absorb the discontinuities arising at the material interface at $x = 3$. Notice at such a low value of the A parameter the solution is severely damped and never comes near the abscissa.

the solution should vary like a simple cantilever beam but inverted. Such a high negative amplitude destroys completely the Heaviside term and restores an inverted form of the regular cantilever beam case. As $A \rightarrow 0.5$ the inverted cantilever solution gradually relents and $u_y(x)$ starts to become positive. Under these conditions the displacement solution will "vibrate" once, dying at the endpoints. In the case of the more sophisticated computer solution we can actually zero not only the displacements but also the in-plane rotations too. This shows up as a stationary point at either beam end in the plot of $u_y(x)$. Taking these as given then only a gradient significantly large at $x = x_0$ can induce the curve into oscillation. For a value of $A = 0.3$ we have figures 6 and 7 where the solutions have the undesirable quality of failing the ideal "abscissa-tangent" boundary conditions usually found in a working composite laminate. With such a rudimentary analytical model this is to be expected however. The computer has many more degrees of freedom and beam elements instead of just one, and the required solution is therefore compatible with what may seem at first to be stringent endpoint behavior. To demonstrate that even for a simple model some success is possible (at one end) we can set $A = 0.4$ and recompute to get a plausible result:

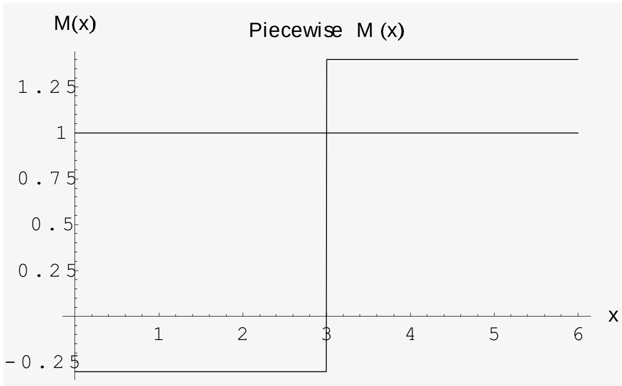

Figure 7: The bending moment $M(x)$ (step) in a cantilever beam with a finite stiffness shock discontinuity applied at $x = 3$. Also figured is the constant bending moment M_0 of a continuous material beam. The value of $A = 0.3$.

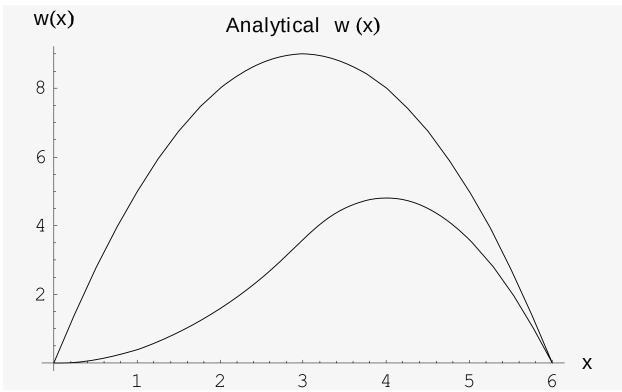

Figure 8: The vertical displacement solution for a cantilevered beam under compression in x with and without shock stiffness discontinuity. The umbrella parabola represents the variation for a simple cantilever while the more complex variation immediately below it is a result of the beam readjusting its equilibrium ($A = 0.4$) to absorb the discontinuities arising at the material interface at $x = 3$. The gradient is zeroed at the origin as well as the displacement and at the other end. This is all with a parabola solution which pushes the model to its limits.

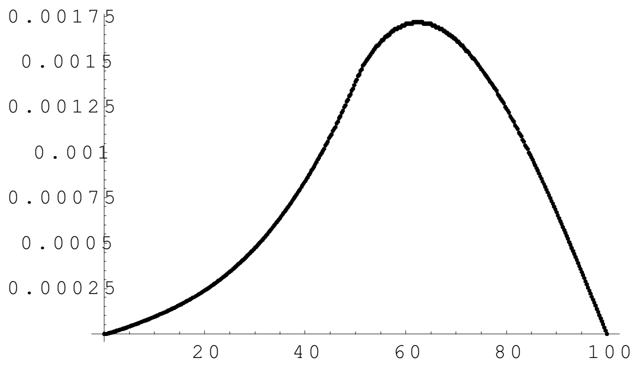

Figure 9: The output from commercial code ANSYS for the vertical displacement of a compressed composite laminate dropped at $x = 50$. This is a full FEA analysis for a thin beam with similar geometry to the case above and the results are qualitatively similar to the simpler model proposed above.

5 CONCLUSIONS

To summarise, the characteristics of a laminate bonded material can be qualitatively reproduced by applying a material stiffness shock to the Bernoulli Euler beam equation. This equation is also seen to hold in more exact numerical integration methodologies and in particular governs the finite-element formulation of the Multisegment integration method. As a result it is a fundamental constituent of any recipe predicting beam curvatures and we can use its simplicity to obtain a physical understanding of how and why the exact stress distributions behave as they do in both experiments and theory. The utility of such a simple approximation is in the qualitative diagnostics of interpreting computer simulations as well as providing rough theoretical estimates in closed form. Lastly the effective distributed load moment of the beam like finite-elements is seen to be non-zero in laminates across a drop region and is another source for discontinuity in $M(x)$.

REFERENCES

[1] O.T. Thomsen and F. Mortensen. *Interface Failure at Ply Drops in CFRP/Sandwich Panels*, Journal of COMPOSITE MATERIALS, Vol. 34, 1989, No. 02/2000.

DAMAGE

8th International Conference on Sandwich Structures
ICSS 8
A.J.M. Ferreira (Editor)

DAMAGE CHARACTERISTICS AND RESIDUAL IN-PLANE COMPRESSIVE STRENGTH OF HONEYCOMB SANDWICH PANELS

G. Zhou[*] and M.D. Hill[†]

[*] Department of Aeronautical and Automotive Engineering, Loughborough University, Loughborough, Leicestershire, LE11 3TU, UK. G.Zhou@Lboro.ac.uk

[†] Composites Research Centre, GKN Aerospace Engineering Services, Isle of Wight PO32 6LR, UK

Key words: sandwich panel, impact damage, residual compressive strength, damage tolerance.

Summary. *An experimental study of the in-plane compressive behaviour of both aluminium and nomex composite sandwich panels with 8 ply carbon/epoxy skins was conducted. All sandwich panels were impact-damaged at impact energy ranging from 2 J to 55 J. Dominant damage mechanisms were found to be core crushing, skin delamination and fracture with the former two absorbing most impact energy. While undamaged panels failed in region close to one loaded end, all impact-damaged nomex panels failed around the mid-section region. Two thirds of aluminium panels also failed in the mid-section region and one third failed in the loaded end region. The presence of the core played a unique role in in-plane compression and counteracted the deleterious effect of impact damage. The in-plane compressive behaviour has shown combined effects of impact damage and the core in a complex manner.*

1 INTRODUCTION

Composite sandwich constructions are widely used in aerospace structures due to their light weight, high strength-to-weight and stiffness-to-weight ratios, very good buckling resistance and good energy-absorbing capacity. A major concern with the mechanical performance of these sandwich structures is their susceptibility to localised manufacturing defect and/or impact damage; the latter could be caused by tool dropping, hail stones, or runway debris. As a result, a multitude of damage mechanisms such as skin-core debonding, core crushing and/or shear failure in addition to skin delamination and fibre fracture could occur. To maintain the aforementioned advantages in the case of any of these impact events, both mechanical properties from skins and core and geometric properties must be tailored in a design analysis such that the sandwich structures are damage tolerant. This requires a thorough understanding of how the damage mechanisms affect the reduction of the in-plane compressive strengths of the damaged sandwich structures.

A great deal of research has been carried out to investigate residual compressive or compression-after-impact (CAI) strength in damaged sandwich structures [1-2] involving very different approaches. Since the only standard related to the topic is ASTM C 364 [3] for the in-plane compressive strength of unsupported intact sandwich coupons and standard for sandwich panels is yet to be developed, most research works adopted wide column compression approach [4-5], in which the unloaded edges of sandwich specimens were left free. Very few [6-10] had the unloaded edges of sandwich specimens simply supported in in-plane compression. Although their compressive failure mechanisms might look similar, the respective contributions of skins and core to the reduction of compressive strengths could be very different. At present, there is little understanding of these differences, which is vitally important to the assessment of impact damage tolerance. The present work reports results of an investigation into the in-plane compressive behaviour of intact and impact-damaged composite sandwich panels using both aluminium and nomex honeycombs.

2 SANDWICH MATERIALS AND PANEL MANUFACTURE

Composite skins were made of unidirectional carbon/epoxy T700/LTM45 prepreg with a ply thickness of 0.128 mm. A symmetric cross-ply lay-up of $(0/90)_{2s}$ was selected due primarily to strength considerations. Although various skin thicknesses have been made, only the skins of 8 ply thick were used in fabricating in-plane compression panels. Two types of honeycomb cores used are 5052 aluminium with a density of 70 kg/m^3 (4.4-3/16-15) and nomex with a density of 64 kg/m^3 (HRH-3/16-4.0). The core depth of both aluminium and nomex honeycombs was 12.7 mm and a nominal panel thickness was 14.7 mm. The nomex honeycomb was dried in an oven overnight at 65°C before being bonded to the skins to remove any moisture absorbed from the atmosphere. Adhesive VTA260 was selected for interfacial bonding.

Skin laminates of 300 × 200 mm were laid up and cured first in an autoclave at 60°C under a pressure of 0.62 MPa (90 psi) for 18 hours. To aid adhesion, the skins were degreased before bonding. The 0° direction of the carbon fibres within the skins was aligned with the ribbon direction of the honeycomb core. For aluminium panels, each skin was separately bonded to the core in an oven at 80°C for 5 hours under a pressure of 0.1 MPa (15 psi). For nomex panels, skins were bonded to the core in an autoclave under the same conditions. Because of the condensation of nomex cells (a couple of cells around the panel edges), the pieces of nomex core used were slightly larger than that of the skins so that the condensed cells could be trimmed off. The sandwich panel was then cut into two nominal 200 mm × 150 mm specimens with the longer side aligned with the direction of compressive loading. Back-to-back strain gauges were bonded on the panel surfaces at selected locations in both the longitudinal and transverse directions (see in Fig. 2(a)) to monitor mean or membrane and panel bending strains. These strain data allowed both the local and global behaviour of the panels to be examined.

3 IMPACT AND IN-PLANE COMPRESSION EXPERIMENTAL PROCEDURES

Low-velocity impact tests were carried out on a purpose-built instrumented drop-weight impact rig in Fig. 1 by using a hemispherical (HS) impactor of 20 mm diameter with a 1.5 kg mass. Impact energies were regulated by selecting desired drop heights and ranged from 2 J to 55 J in this investigation. Each rectangular carbon/epoxy plate of 200 mm by 150 mm with a circular testing area of 100 mm in diameter was clamped by using a clamping device. Both impact and rebound velocities were measured respectively by two counters recording times over the distance fixed by a pair of photodiodes. This allows absorbed energies to be calculated directly. Both impact force and strain gauge responses could be recorded by a Microlink 4000 data acquisition system with a sampling rate of 50 μs. At each selected impact energy level, three impact tests were conducted with one being diametrically cut up for examination of damage mechanisms and the remaining two being reserved for in-plane compression test. Absorbed energy was also calculated via the closed area under load-displacement curves. All impact test results along with the extents of crushed core and skin delaminations are summarised in Table 1.

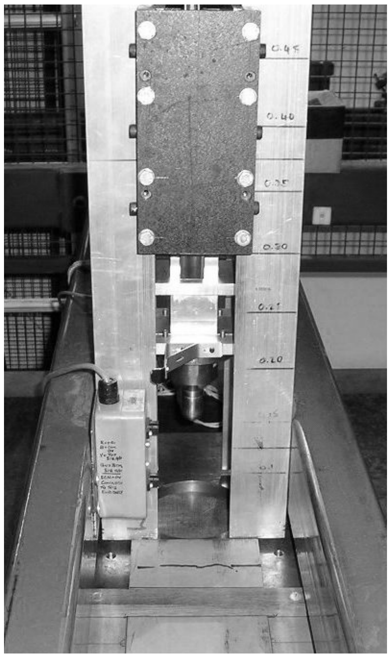

Figure 1 Drop-weight impact test rig

Table 1 Summary of impact and CAI tests

Panel ID	IKE J	Absorbed energy J	Percentage absorption %	Delamination extent mm	Core damage extent mm	CAI strength MPa	CAI retention factor %	Failure location -
Al control 1	0	0	0	0	0	270.6	0.93	Loaded end
Al control 2	0	0	0	0	0	322.0	1.10	Loaded end
Al 3.7J 1	2.60	1.75	0.67	-	-	207.0	0.71	Mid-section
Al 3.7J 2	3.66	2.44	0.67	30	32	190.7	0.65	Loaded end
Al 3.7J 3	3.62	2.39	0.65	30	32	219.0	0.75	Mid-section
Al 5J 1	5.20	3.49	0.67	42	39	221.8	0.76	Loaded end
Al 5J 2	5.40	3.55	0.66	42	39	195.3	0.67	Mid-section
Al 9.5J 1	9.54	6.11	0.64	-	-	243.9	0.83	Mid-section
Al 9.5J 2	9.51	6.60	0.69	-	-	190.3	0.65	Loaded end
Al 13J 1	13.68	9.19	0.67	53	57	203.8	0.70	Mid-section
Al 13J 2	13.76	9.22	0.67	53	57	215.2	0.74	Mid-section
Al 25J 1	24.34	24.24	1.00	66	74	187.6	0.64	Mid-section
Al 25J 2	25.54	24.15	0.95	66	74	150.4	0.51	Loaded end
Nom control 1	0	0	0	0	0	283.9	0.97	Loaded end
Nom control 2	0	0	0	0	0	293.1	1.00	Loaded end
Nom 5J	5.13	2.83	0.55	35	33	162. 4	0.56	Mid-section
Nom 9J	9.23	5.45	0.59	44	49	205.6	0.70	Mid-section
Nom 16J	16.29	10.03	0.62	59	64	187.0	0.64	Mid-section
Nom 28J	28.20	26.54	0.94	66	101	134.1	0.46	Mid-section

As part of the compression specimen preparation, the core at the panel ends intended for applying compressive load was removed to a depth of about 5 mm (slightly more than one cell size). Epoxy end pots were cast between the two skins to prevent an end-brooming failure and the two potted ends were machined to parallel. In each in-plane compression test (popularly known as compression-after-impact (CAI) test), a panel was placed in a purpose-built support jig, as illustrated in Fig. 2(b). The jig provides simple support along the unloaded edges, which were free to move in the width direction during loading. Quasi-static load was applied to the panel at the machined ends via either a universal testing machine at less than 1 mm/min. Although the loaded ends were not clamped, they were effectively close to the clamped condition but without clamping surface pressure. Load, strain and cross-head displacement in all tests were recorded through the same data acquisition system at a sampling rate of 0.5 Hz. All tested panels were cut up for study of damage mechanisms. All in-plane compression results for both intact and impact-damaged panels are summarised in Table 1.

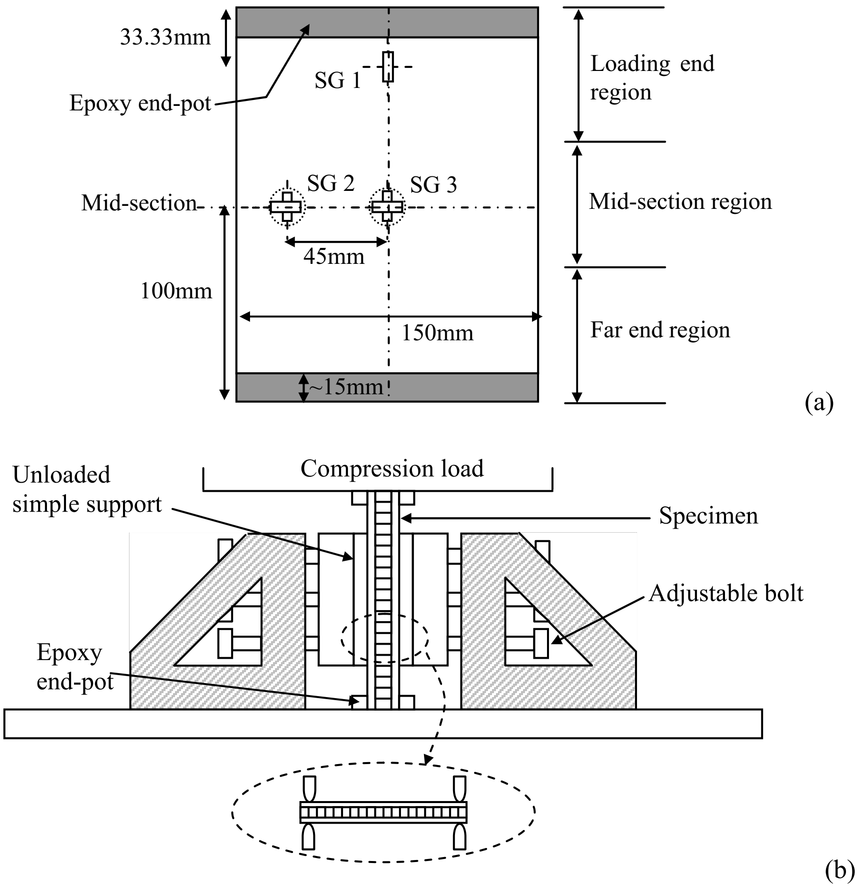

Figure 2 (a) Specimen dimensions and strain gauge locations and (b) experimental set-up for in-plane compression

4 CHARACTERISTICS OF DAMAGE MECHANISMS AND ENERGY ABSORPTION

As the assessment of the compressive strength reduction of impacted sandwich panels required quantitative information on a range of damage states with varying severity, the initiation and propagation of induced damage mechanisms must be characterised in terms of impact energy and damage extent. This effort was facilitated significantly when combined with much more cost-effective quasi-static bending and indentation tests companied by systematic microscopic inspections of cut cross sections in [11-12] on the assumption that the aluminium honeycomb was not considered rate-sensitive up to an impact velocity of 6 m/s.

For the aluminium sandwich panels, the initial damage threshold was exceeded at the lowest impact energy of 3 J and corresponded to a combination of core crushing and small delaminations in the shape of a cone towards the skin-core interface. At the apex of the contact area of the HS impactor the estimated contact pressure of about 11 MPa [13] exceeded the core stabilised compressive strength of 4.2 MPa, confirming the initiation of core crushing. As impact energy was increased, the damage mechanisms were characterised by continued core crushing and by propagation of top skin delaminations. A cross-sectional view of impact-damaged aluminium panel (Al 13J 2) is shown in Fig. 3. At about 25 J, top skin fracture occurred and the extent of damage in both the skin and core was very significant. In all tests, the extent of crushed core was generally greater than the extent of skin delamination. The gap between the two became greater for the given greater impact energy. The surface indent was also greater with the greater impact energy, as expected. There was no local skin-core debonding found before the ultimate load. The maximum depth of the crushed cells at impact energy of 25 J reached only about the middle of the cores and the bottom skin remained intact.

The damage characteristics of nomex panels were more or less the same as the aluminium ones, though the fractured nomex cells with a lesser degree of cells folding showed substantial spring-back upon unloading. A cross-sectional view of impact-damaged nomex panel (Nom 16J) is shown in Fig. 4. Furthermore, the flexural rigidity of undamaged nomex panels (within the elastic range) was significantly lower than that of the aluminium ones due to their relatively low shear strength and modulus. In addition, the local indentation in the nomex panels was found to be substantially more than the latter due to the slight lower compressive properties.

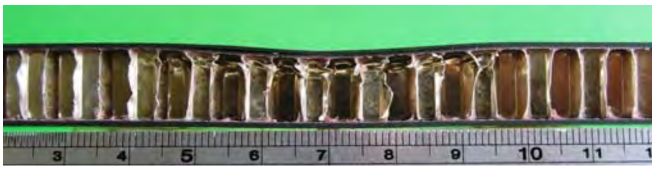
Figure 3 An aluminium sandwich panel impacted at 13 J


Figure 4 A nomex sandwich panel impacted at 16 J

The energy absorption characteristics were established over three regions in Figs 5 and 6 in terms of damage extent and absorbed energy. As can be seen in Fig. 5, the increase in both the skin delamination and crushed core extensions is nonlinear at the low end of energy range and is roughly the same in Region 1 and up to the middle of Region 2. From the middle of Region 2 that approximately corresponds to about 12 J, the respective extents of skin delamination and crushed core starts separating, with the former being substantially less than the latter. These trends more or less continue into Region 3 when fibre fracture in the impacted skin started occurring. It is interesting to note that the gap between the two extents is much wider for the nomex panels due likely to the relatively low flexural rigidity associated with low through-the-thickness shear properties of the nomex. In Fig. 6, the energy absorption characteristics of the damaged panels are seen to be steady and linear in Region 1 and 2, with a constant absorption of about 67%. These characteristics confirm that the continuation of core crushing was the major damage mechanism for absorbing impact energy. The increase in energy absorption went up to over 90% with still a constant rate, once fracture of the impacted skin occurred.

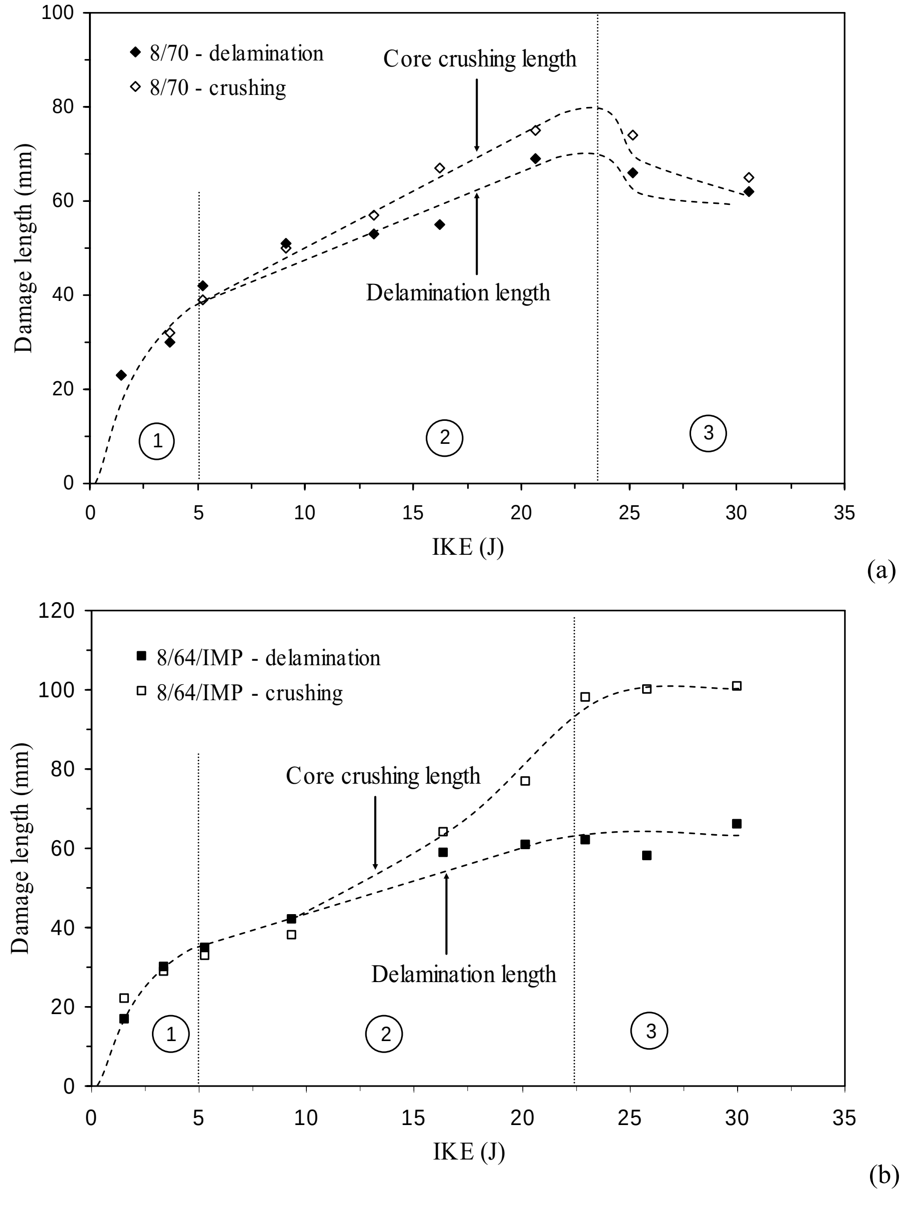

Figure 5 Extent of delamination and crushed core in (a) aluminium and (b) nomex honeycomb sandwich panels

5 RESIDUAL IN-PLANE COMPRESSIVE BEHAVIOUR

The in-plane compressive behaviour of the damaged sandwich panels was very complex due primarily to two factors in addition to the damage characteristics as discussed above. One is that sandwich construction itself was a complex structure on its own during in-plane compression because the two skins were stabilised and supported, to some degree, by the core in the through-the-thickness direction. Unless impact damage involving both the skin and core was very extensive with respect to panel width, the substantial damage alone within the impacted skin may not have been enough to degrade the compressive strength of the panel, if the shear rigidity of the core was relatively high with respect to the thickness and lay-up of the skins. As a result, interpretation of the in-plane compressive strength data became very difficult as the stabilising and supporting effect of the core could cancel out the effect of the impact damage with a substantial size. Thus, much of knowledge and understanding established from the compression of monolithic panels [14-15] could not necessarily apply to sandwich panels. The other is that the damaged region of the impacted panels lacked symmetry with respect to the compression loading and supporting conditions as the impacted skin was damaged with crushed core underneath with the distal skin remaining undamaged after impact. Therefore, the in-plane compressive strength reduction of damaged sandwich panels was attributed not only to impact damage and associated loss of symmetry but also to the relative magnitude of the shear rigidity of the panels.

The compressive responses of undamaged panels for the both longitudinal and transverse directions were examined in [17]. A tilting of one panel end was spotted at the early stage of loading via the bending strain response of the far-field strain gauges (SG1). As the local strain gauges (SG2) on the mid-section exhibited very small bending strain with large mean strain, these responses provided no indication of local buckling and thus the panel failed in the region close to the loaded end as shown in Fig. 7. The compressive response of undamaged nomex panels was very similar in terms of both strain response and failure characteristic.

Once impact damage was inflicted in panels, about two thirds of the aluminium panels failed around the mid-section region, as one example shows in Fig. 8, and all the impact damaged nomex panels failed in the same way. The remaining third of the impacted aluminium panels failed in a similar way to the control panels with the failure being close to one loaded end. Moreover, this result did not appear to be affected by the severity of the impact damage, as impact energies applied to those four panels spread from 3.7 J to 25 J. In the last case with the impact energy of 25 J, the respective extents of delamination in the impacted skin and crushed core were close to half the panel width. A further examination of the aluminium panels revealed that there was little difference in CAI strength between those with the mid-section failure and those with the end failure. However, the majority of the impact damaged nomex panels did show classic strain reversal, which immediately triggered catastrophic failure [17].

The presence of the core between the two skins provided a stabilising support to the skins in the through-the-thickness direction in terms of both transverse shear and normal compression. Hence the damage in the impacted skin could have been made difficult to propagate transversely, especially if the shear rigidity of the core was relatively high. In particular, the shear rigidity of the honeycomb cores in the width (or W) direction is even higher than that in the ribbon direction. On the one hand, the aluminium honeycomb had much greater transverse shear properties than the nomex. On the other hand, the tensile strength of adhesive of about 5.5 MPa was substantially greater than the stabilised compressive strength of 4.2 MPa for aluminium and 4.0 for nomex. As a result, the undamaged (distal) skin had to crush core first (see Fig. 8). The zone of crushed core in the aluminium panels was close to the distal skin, while the fractured cells in the nomex panels were close to the mid-plane of the panels.

Therefore, the likely reason for the inconsistent failure locations was due to a combination of the supporting effect and relatively high shear rigidity of the core. This seems to suggest that the denser core and/or core with greater transverse shear stiffness provides the sandwich panels with stronger compressive resistance, which is in agreement with some results in [16].

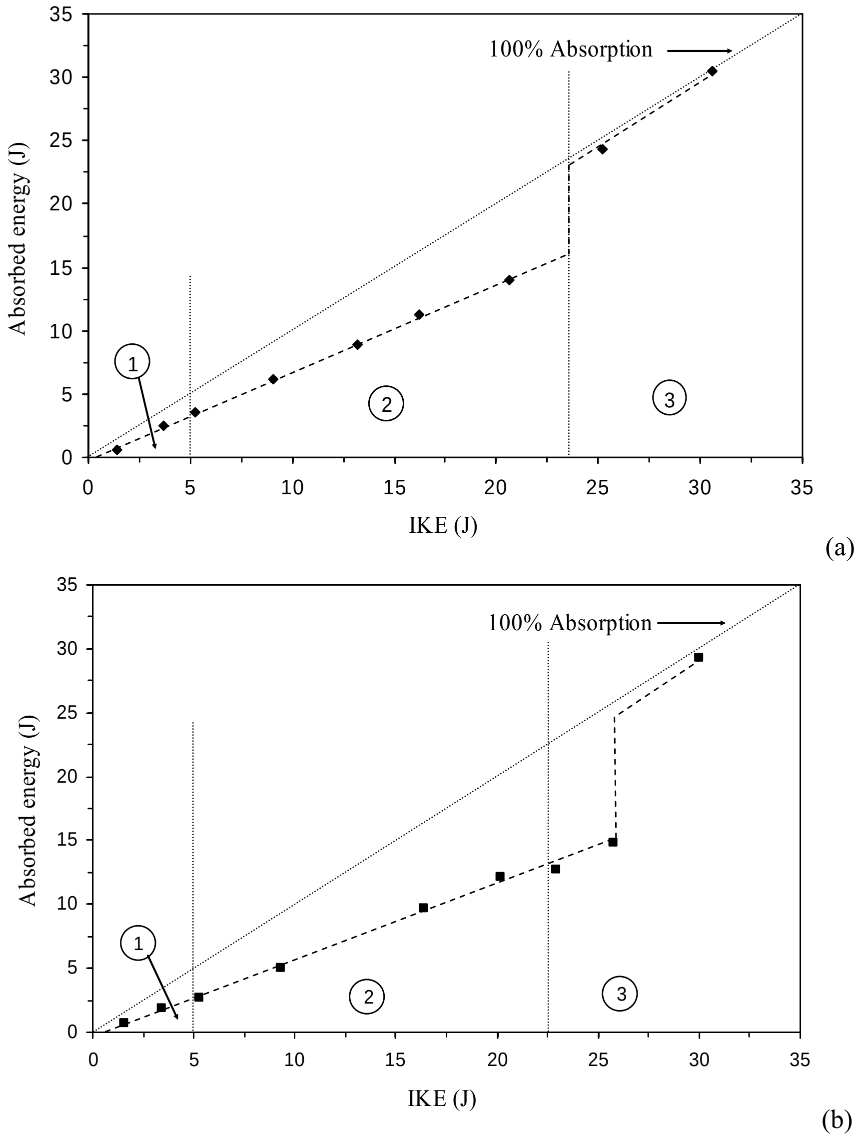

Figure 6 Absorbed energy of (a) aluminium and (b) nomex honeycomb sandwich panels

6 IMPACT DAMAGE TOLERANCE

A moderate reduction of CAI strength was immediate once the panels were impact-damaged in Fig. 9. From 3.7 J to 13 J, however, the variation of CAI strength was limited. Over this region, a state of damage in the panels was dominated by a steady growth of core crushing and skin delaminations. Although the corresponding increase of both the crushed core and delamination extents was about 75% over the impact energy range, it did not lead to the further reduction of CAI strength. This seems to suggest that the stabilising support of the core reduced the likelihood of local buckling development so that much of the effect of impact damage was cancelled out. Until impact energy level reached over 20 J, a further reduction of CAI strength became noticeable because of the fracture of the impacted skins. At the highest impact energy, the reduction of compressive strength was about 50% for the honeycomb sandwich panels. In addition, it is noted that the different failure locations among the CAI tested panels are not distinguished over the values of CAI strength. This suggests that the relative magnitude of the shear rigidity of the aluminium honeycomb was at the critical state such that a reduction of the shear properties could lead to the consistent mid-section failure, or vice versa.

Figure 7 Photographs of an undamaged aluminium sandwich panel after compression test

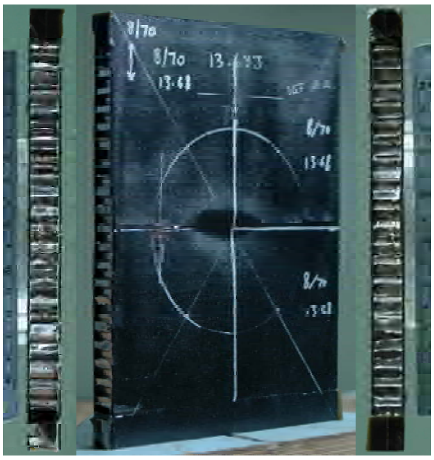

Figure 8 Photographs of an impact-damaged aluminium sandwich panel after CAI test

Tolerance of sandwich panels to impact damage is assessed through the retention of CAI strength as presented in Fig. 10 with the compressive strength retention factor (CSRF) plotted against damage extent (or impact energy in [17]). The damage tolerance of impact-damaged panels can also be assessed through residual mean compressive strains obtained from the far-field strain gauge locations as in [17].

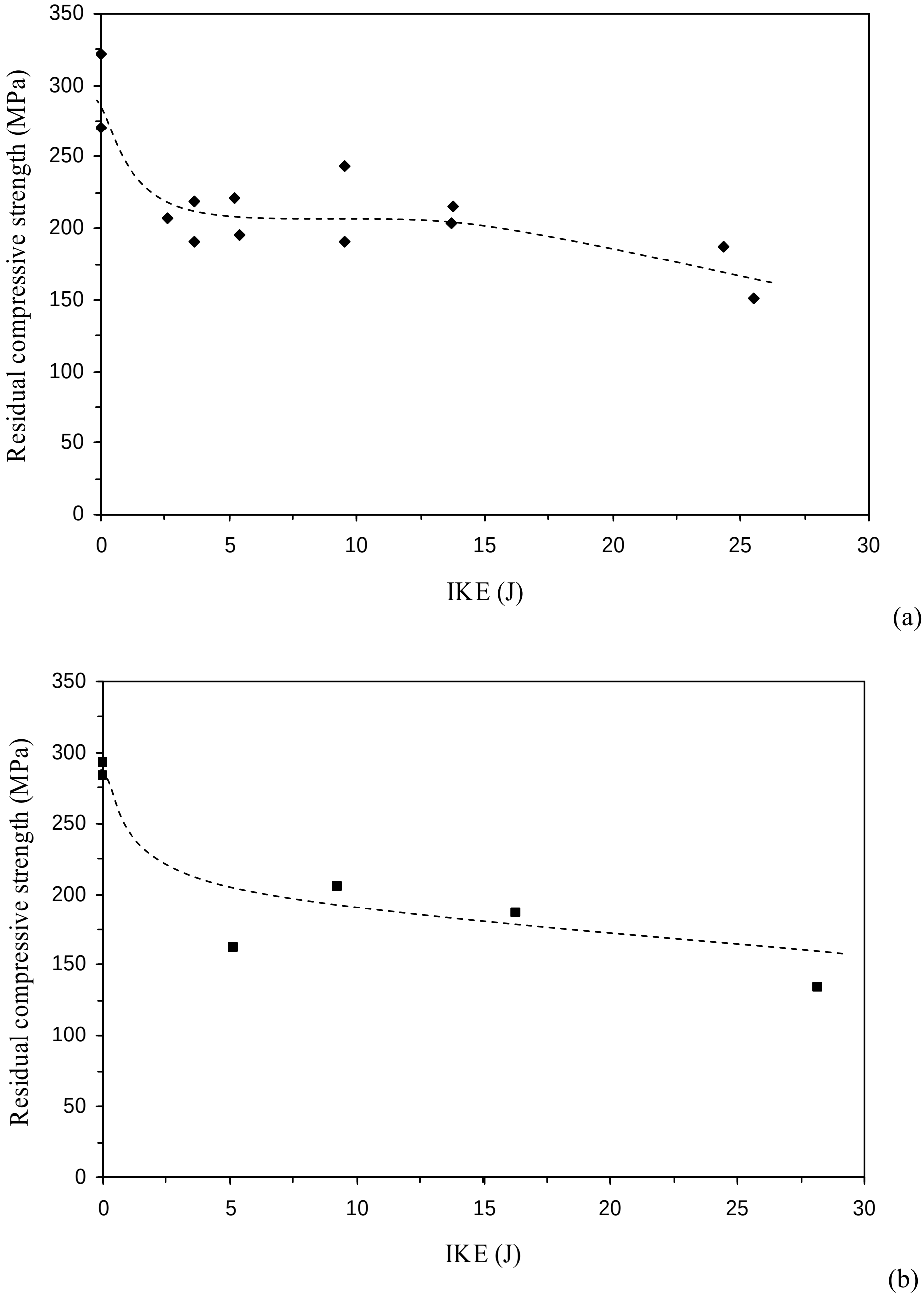

Figure 9 Variation of CAI strength with IKE for (a) aluminium and (b) nomex honeycomb sandwich panels

7 CONCLUSIONS

Both the aluminium and nomex composite sandwich panels were impact damaged with energy ranging from 2 J to 55 J. Dominant damage mechanisms were found to be core crushing, skin delamination and skin fracture with the former two absorbing most impact energy. As the initial damage occurred at relatively low load, energy absorption up to skin fracture was dominated by cell crushing. Different core materials with a similar density made little difference on either the damage or energy-absorbing characteristics.

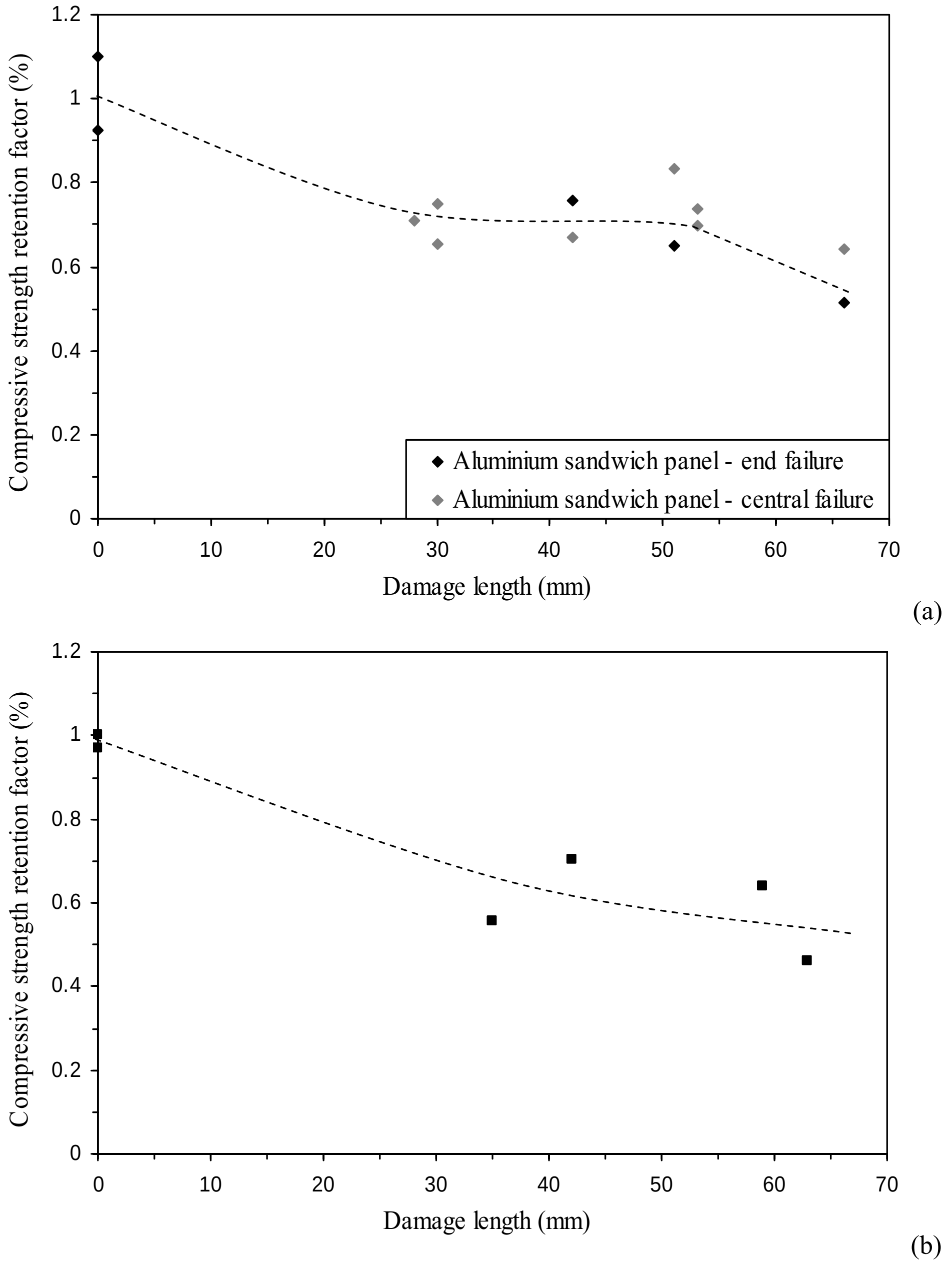

Figure 10 Compressive strength retention factor with damage length for (a) aluminium and (b) nomex honeycomb sandwich panels

Both intact and impact-damaged composite sandwich panels were in-plane compressed. While the undamaged panels failed in region close to one loaded end due to high flexural rigidity of the panels, all impact damaged nomex panels along with two thirds of aluminium panels failed around the mid-section region. However, one third of aluminium panels failed in the loaded end region. The presence of the core enhanced the shear rigidity and normal compression of the panels such that it seemed to counteract the deleterious effect of impact damage. As a result, these core properties played such a significant role in in-plane compression that they, along with the impact damage, affected the way in which the panels failed. Therefore, a further investigation over the role of the core in the in-plane compression of sandwich panels is essential to impact damage tolerance assessment.

REFERENCES

[1] S. Abrate, "Localized impact on sandwich structures with laminated facings", *Applied Mechanics Review*, 50, 69-82 (1997).

[2] J.S. Tomblin, T. Lacy, B.L. Smith, S. Hooper, A. Vizzini and S. Lee, "Review of damage tolerance for composite sandwich airframe structures", *DOT/FAA/AR-99/49*, 1-71 (1999).

[3] –, *Standard test method for edgewise compressive strength of sandwich constructions*, *ASTM-C 364 – 94*, 1994.

[4] M.K. Cviitkovich and W.C. Jackson, " Compressive failure mechanisms in composite sandwich structures", *J. of American Helicopter Society*, Oct. 260-268 (1999).

[5] P.A. Lagace and L. Mamorini, "Factors in the compressive strength of composite sandwich panels with thin facesheets", *J. of Sandwich Structures and Materials*, 2, 315-330 (2000).

[6] D.M. McGowan and D.R. Ambur, "Damage characteristics and residual strength of composite sandwich panels impacted with and without a compression loading", *AIAA-98-1783*, 713-723 (1998).

[7] J.S. Tomblin, K.S. Raju, J. Liew and B.L. Smith, "Impact damage characterization and damage tolerance of composite sandwich airframe structures", *DOT/FAA/AR-00/44*, 1-181 (2001).

[8] J.S. Tomblin, K.S. Raju, J. Liew and B.L. Smith, "Impact damage characterization and damage tolerance of composite sandwich airframe structures - Phase II", *DOT/FAA/AR-02/80*, 1-87 (2002).

[9] T.E. Lacy and Y. Hwang, "Numerical modeling of impact-damaged sandwich composites subjected to compression-after-impact loading", *Composite Structures*, 61, 115-128 (2003).

[10] J.S. Tomblin, K.S. Raju, and G. Arosteguy, "Damage resistance and tolerance of composite sandwich panels - scaling effects", *DOT/FAA/AR-03/75*, 1-70 (2004).

[11] G. Zhou, M.D. Hill and N. Hookham, "Damage characteristics of composite honeycomb sandwich panels in bending under quasi-static loading", *J. of Sandwich Structures and Materials*, 8, 55-90 (2006).

[12] G. Zhou, M.D. Hill and N. Hookham, "Investigation of parameters governing the damage and energy-absorbing characteristics of honeycomb sandwich panels", *J. of Sandwich Structures and Materials*, 9, 309-342 (2007).

[13] G. Zhou, "Static behaviour and damage of thick composite laminates", *Composite Structures*, 36, 13-22 (1996).

[14] G. Zhou and L. Rivera, "Investigation for the reduction of in-plane compressive strength in preconditioned thin composite panels", *J. of Composite Materials*, 39, 391-422 (2005).

[15] G. Zhou and L. Rivera, "Investigation for the reduction of in-plane compressive strength in preconditioned thick composite panels". *J. of Composite Materials*, 41, 1961-1994 (2007).

[16] A. Nokkentved, C. Lundsgaard-Larsen and C. Berggreen, "Non-uniform compressive strength of debonded sandwich panels - I. Experimental investigation", *J. of Sandwich Structures and Materials*, 7, 461-482 (2005).

[17] G. Zhou and M.D. Hill, "Impact damage and residual compressive strength of honeycomb sandwich panels", *Proc. ICCM*–16, Kyoto, July 2007.

8th International Conference on Sandwich Structures
ICSS 8
A. J. M. Ferreira (Editor)

DAMAGE AND FAILURE PROGRESSION OF CFRP FOAM-CORE SANDWICH STRUCTURES

Martin Rinker[*], Pierre C. Zahlen[†] and Ralf Schäuble[*]

[*] Fraunhofer Institut for Mechanics of Materials (IWM)
Walter-Hülse-Strasse 1, 06120 Halle, Germany
e-mail: martin.rinker@iwmh.fraunhofer.de, web page: http://www.iwmh.fhg.de

[†] Composite Technology Center GmbH
Airbus-Strasse 1, 21684 Stade, Germany
e-mail: pierre.zahlen@airbus.com, web page: http://www.ctc-gmbh.com

Key words: failure behaviour, load introduction, reinforcement elements, crack propagation.

Summary. *This paper deals with the mechanical investigation of 3-D reinforced CFRP foam-core sandwich structures. Whereas the not reinforced sandwich carries ideally in plane loads, out of plane loads are critical. Therefore reinforcement elements like CFRP hollow profiles, CFRP double T-beam and CFRP pins in thickness direction are integrated in the sandwich and have to be benchmarked for effectiveness. For analyzing the material behaviour of the reinforced sandwich it is necessary to know the material behaviour of the not reinforced sandwich. Therefore firstly bending tests were conducted and the deformation and failure behaviour were investigated. Several failure criteria were tested by finite element calculation to describe the foam-core failure. It was possible to show, that the consideration of residual stresses increases the accuracy of failure prediction. For the investigation of the effectiveness of the reinforcement elements, special tests were defined and adapted for reinforced sandwich respectively: out of plane compression test, out of plane shear test and 4-Point-bending test. The test results have shown, that both the stiffness and strength related to weight can be increased significantly with the reinforcement elements. Cracks in the sandwich are critical because they are not visible, if they are located in the foam or in the interface foam-skin. To decrease crack propagation crack stopper can be integrated in the sandwich. The potential of the load introduction (reinforcement) elements as crack stoppers needs to be analyzed. Therefore fracture mechanic tests like ENF and DCB were defined for the investigated sandwiches with and without reinforcement elements.*

1 INTRODUCTION

Sandwich structures offer a good ratio of bending stiffness and strength to weight. The application of carbon fibre reinforced polymers for the face sheets in combination with lightweight core materials provide potential for optimization. Using closed cell foams complex core preforms can be manufactured; therefore it is possible to produce high integral sandwich components. These can especially be used in structures which have a high ratio of strength and stiffness to weight and are at risk to fail by buckling. Hence those sandwich

structures qualify for application in planes for commercial aircrafts [1].
Compared to monolithic structures, the behaviour is more complex due to the combination of various materials and demands investigations of both, the single components and the whole composite. It has to be analyzed whether the use of failure criteria for the components is sufficient and which effects have to be investigated furthermore. Deformation and failure behaviour are for example influenced by thermal stresses.
Sandwich structures are ideally able to withstand in plane and bending loads but not out of plane loads due to the low stiffness and strength of the foam core. In real sandwich structures, out of plane loads mainly arise at load introduction points and joints to ribs or spars. To carry these loads from one face to the other, it is useful to integrate reinforcement concepts into the sandwich.

Remark: The investigations and results presented in this paper are complementary to the work presented during the ICSS 8 by Zahlen et al. in the paper "Advanced Manufacturing of Large, Complex Foam Core Sandwich Panels " [3].

2 STIFFNESS AND STRENGTH BEAHVIOUR OF CFRP FOAM SANDWICH

For Investigation of stiffness and strength behaviour of non reinforced CFRP sandwich structures the 4-Point-Bending test is used. With this test a complex stress condition can be induced to sandwich specimen. Firstly two theories have to be distinguished: shear weak and shear stiff bending. The shear stiff theory implies, that the base materials only have elastic properties in and infinite high stiffness out of plane direction. It is also assumed, that core and skin are tightly interconnected so no interlaminar deformation is allowed. These assumptions comply with the Classical Laminate Theory (CLT). Because of the very small foam shear modulus compared to the skin it may be expected, that too small bending will be calculated with this theory. The sandwich theory [2] is an amelioration of the CLT. This theory implies, that the skins only withstand in plane loads whereas the sandwich core carries out of plane shear loads from one skin to the other. In the bending test the displacement in thickness direction results from the bending and additionally from the shear deformation of the core. It should be clear, that the sandwich theory with rising different of material properties of core and skin becomes more exact.

Compared to 3-Point-Bending test the 4-Point-Bending test has an important benefit. The specimen carries between the two middle load introduction points only a constant bending moment without shear loads. This results in a constant compression load in the upper skin and in a constant tension load in the lower skin in this area. When laminar measurement systems like strain gauges are used to define skin tension or compression, it is important to have adequate great areas with homogenous stress conditions. Core shear deformation is measured between load introduction point and point of support just like 3-Point-Bending.

Knowing core shear strength, skin compression and tension strength, the sandwich failure scenario can systematic be varied. The distance between load introduction point and support point is the shear carrying length. Increasing the ratio of shear carrying length to the length between the two middle load introduction points while applying the same test load, results in a greater carried shear load, thus increasing tension and compression load of the skin. By adequate choice of shear carrying length the sandwich specimen will fail by core shear failure, skin compression- or tension failure ore by debonding of the skin. The ratio of skin tension and compression strength to core shear strength of the investigated sandwich is very high, so the core strength behavior was most of interest. By assumption of core shear failure, the most simple failure prediction is the calculation of the transverse force and comparing it with the shear strength of the core. This criterion is described in the test norm ASTM C 393. If the core not only carries shear loads but also normal loads (for example residual stresses), this criterion can not predict the failure exactly. This paper deals with the investigation of several foam failure criteria to find out, which of them describes the failure load most exactly.

2.1 Base materials and manufacturing

The sandwich core consists of the closed cell PMI (Polymethaacrylimid) foam Rohacell 51WF, with a density of 52 kg/m³ and a cell diameter of 0,5 - 0,7 mm. The face sheets are composed of six uni-directional CFRP layers, three of them are bindered to a dry triax lay-up for better handling. Each unidirectional layer consists of rovings with 12000 carbon filaments. The epoxy resin is used as both the matrix of the CFRP and as adhesive for the interface core-skin. Figure 1 shows the sandwich layup and the engineering constants of the base materials. The mechanical properties are provided by the manufacturer and are to be validated by the experiment.

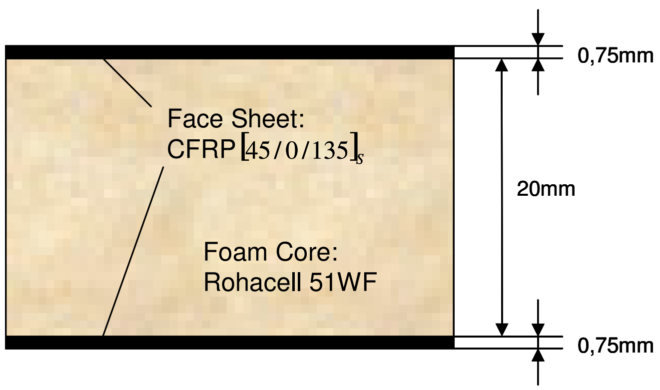

	CFRP		Foam
E_{11}	135 GPa	E^+	83,3 MPa
E_{22}	9,75 GPa	E^-	73,1 MPa
E_{33}	9,75 GPa	G	29,3 MPa
G_{12}	6 GPa	υ^+	0,32
G_{23}	2,99 GPa	υ^-	0,28
G_{13}	6 GPa		
υ_{12}	0,28		
υ_{23}	0,64		
υ_{13}	0,28		

Figure 1: Sandwich layup and engineering constants

The sandwich was manufactured by using open mould liquid composite molding (LCM) technology [3]. Therefore the dry fibres and the foam core were applied on an open mould and then evacuated by vacuum bagging. The resin infusion is only conducted by the vacuum in front of the flow front. With this infusion technology the CFRP skin and the bonding core-skin are manufactured in one step. It provides potential for saving production costs of CFRP and CFRP sandwich structures [1].

2.2 Experimental setup

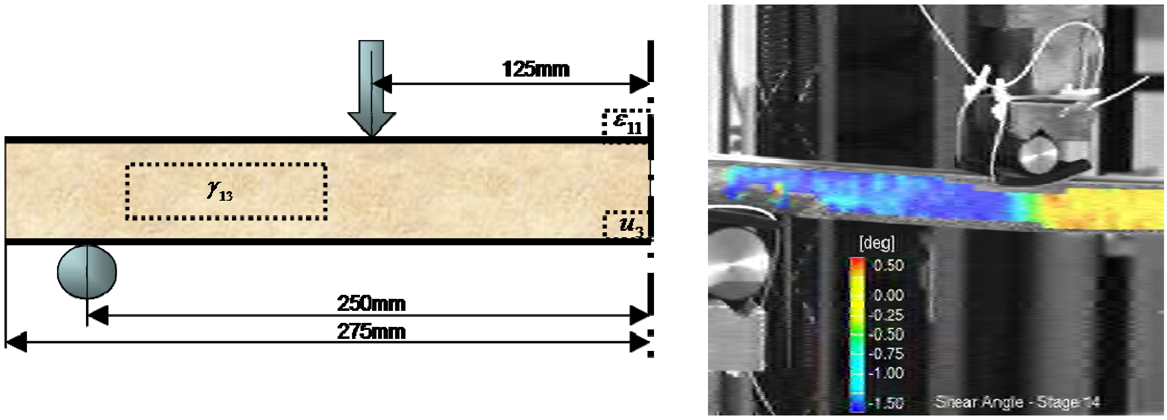

Figure 2: Experimental setup of 4-Point-Bending test with dimensions and measurement systems (left) and ARAMIS shear deformation exposure shortly before specimen failure (right)

Firstly eight specimens were sawn and tested non destructive by ultrasonic method. The specimen geometry was defined in consideration of ASTM C 393-00 for quarter point loading. The variation of the specimen measurement, especially of the sandwich thickness, was small, so the specimens can be assumed unique. Concomitantly to the experiment several measurement systems were used. The flexure of the specimen was measured by the testing machine, by an inductive displacement transducer and by the contactless deformation measurement system ARAMIS. Also the shear strain of the core as most important indicator and the strain of the skin were measured by ARAMIS (Figure 2).

2.3 Experimental results

The experimental measured deformation behavior was compared to the Classical Laminate Theory and the Sandwich Theory. It turned out that the measured bending is nearly 10% greater than calculated by the sandwich theory, what indicates that the sandwich bending stiffness is lower than assumed. The bending calculated by CLT is nearly 20% lower than the measured bending because of the unaccounted shear deformation of the foam core. The shear strain of the foam core shows a linear behavior until failure. The measured shear modulus conforms well to the value provided by the manufacturer. The measured results were also compared to Finite Element Analysis. Both, the bending of the sandwich and the core shear deformation are nearly unique for FEA calculation and sandwich theory. So the difference between measured bending and calculated bending by FEA and sandwich theory is founded in the skin stiffness. To validate this assumption, tensile tests with skin only were made. It turned out that the measured CFRP skin Young's Modulus in longitudinal direction is nearly 12% lower than calculated (CLT) with the provided engineering constants. Using the "new" skin Young's Modulus bending calculations were redone with the result, that the measured bending now conforms well to the calculated bending.

With increased loads the experiments were conducted until specimen failure, which occurred generally by core shear fracture. So the failure scenario corresponds to the assumption because of the high skin compression and tension strength compared to the core shear strength. The core shear strength provided by the manufacturer (0,81 MPa) was nearly exactly validated by the calculated transverse force with the measured fracture load (1358 N). During the inquest to assess the damage not only shear fracture (45° of thickness direction crack in the foam), but also a local compression damage (core crushing) under the load introduction point was found. Because of the abrupt shear failure and so the abrupt end of test, the local damage must have arisen before global specimen failure. These local damages can not be determined with the shear failure criterion but only with the following numerical calculations.

2.4 Comparison of foam failure criteria

For comparison of foam failure criteria several approaches were investigated: Rankine (Eq. 1), Tresca (Eq. 2), Beltrami (Eq. 3), Sandel (Eq. 4), Von Mises (Eq. 5) and ROHACELL®-Failure-Criterion (DKI/Röhm) (Eq. 6) [4,5]. All these equations calculate the comparison stress. To assess the efficiency ratio, the comparison stress has to be divided by a reference potential. For the criteria 2-6 this is the tension strength of the investigated material, only for the Rankine criterion two strengths have to be considered: If the maximum principal stress is a tension stress, it has to be divided by the tension strength, else by the compression strength of the investigated material. If the efficiency ratio reaches the value 1, the material will theoretically fail.

$$\sigma_V = \max\left(|\sigma_I|, |\sigma_{II}|, |\sigma_{III}|\right) \tag{1}$$

$$\sigma_V = \max\left(|\sigma_I - \sigma_{II}|, |\sigma_{II} - \sigma_{III}|, |\sigma_{III} - \sigma_I|\right) \tag{2}$$

$$\sigma_V = \sqrt{\sigma_I^2 + \sigma_{II}^2 + \sigma_{III}^2 - 2\upsilon\left(\sigma_I\sigma_{II} + \sigma_{II}\sigma_{III} + \sigma_{III}\sigma_I\right)} \tag{3}$$

$$\sigma_V = \sqrt{\sigma_I^2 + \sigma_{II}^2 + \sigma_{III}^2 - 2\upsilon\left(\frac{2-\upsilon}{1+2\upsilon^2}\right)\left(\sigma_I\sigma_{II} + \sigma_{II}\sigma_{III} + \sigma_{III}\sigma_I\right)} \tag{4}$$

$$\sigma_V = \frac{1}{\sqrt{2}}\sqrt{\left(\sigma_I - \sigma_{II}\right)^2 + \left(\sigma_{II} - \sigma_{III}\right)^2 + \left(\sigma_{III} - \sigma_{III}\right)^2} \tag{5}$$

$$\sigma_V = \frac{\sqrt{\left(12A_2 + 12A_1 + 12\right)I_{2D} + \left(4A_2^2 + \left(4A_1 + 4\right)A_2 + A_1^2\right)I_1^2} + A_1 I_1}{2A_1 + 2A_2 + 2} \tag{6}$$

To determine the efficiency ratio it becomes necessary to use the Finite Element Analysis method because of the stress condition they need as an input. Most of them are invariant based and all six stress components of the general stress condition are needed. To calculate these stresses, a three dimensional FEA model was built. Determining the efficiency ratio automatically is necessary for easy handling and usage in an industrial environment, like a company building commercial aircrafts. Therefore the criteria were implemented in the FEA Postprocessor MSC.Patran using the programming language PCL.

FEA calculations show, that in the area between load introduction point and support point the out of plane shear stress dominates in the foam core like the sandwich theory predicts. In the area under the load introduction point the normal stress in thickness direction dominates as compression load and also as compression load in longitudinal direction. The compression load in longitudinal direction results of the sandwich bending and is not negligible. So under the load introduction point a multiaxial stress condition occurs, which is not predicted by the Sandwich Theory or the Classical Laminate Theory.

Postprocessing with the experimentally determined middle fracture load (1358 N) shows no theoretical shear failure of the core (area between load introduction point and support point). All investigated criteria compute higher loads for failure in this area, so they are not conservative. Best results reach Tresca and ROHACELL®-Failure-Criterion (DKI/Röhm), which determine nearly 20% higher fracture loads for this area. Looking at the area dominated by compression loads (under the load introduction point), two failure criteria are conservative: Rankine and ROHACELL®-Failure-Criterion (DKI/Röhm) compute lower fracture loads than experimentally investigated. All other criteria calculate failure loads which are too high. The theoretical compression failure loads computed by Rankine (844 N) and ROHACELL®-Failure-Criterion (DKI/Röhm) (676 N) seem to be very small compared to the experimental determined failure load. So either the local damage arises at low level or both criteria are too conservative. This could result in a higher structure weight by dimensioning a component in consideration of the First Ply Failure Criterion. However the experiments have shown, that the global failure occurs abrupt with reaching the fracture load, supposable uninfluenced of the local compression damage. In consideration of all facts, the ROHACELL®-Failure-Criterion (DKI/Röhm) computes the best results.

2.5 Influence of residual stresses

Thermal stresses are caused by the different coefficients of thermal expansion of the sandwich components face sheet and foam core. The thermal expansion of a quasi-isotropic CFRP laminate is close to zero because of the transversal isotropic thermal expansion coefficient of the carbon fibre. It is negative in fibre direction and positive perpendicular to fibre direction. The ROHACELL foam core shows isotropic thermal behaviour with positive coefficient of thermal expansion. The sandwich curing temperature normally ranges from 160°C to 180°C. With cooling down to room temperature or to service temperature, the foam would contract while the CFRP face sheets show no thermal expansion. Because of the very high face stiffness compared to the foam stiffness, the core can not contract and residual stresses occur. Assuming that the curing temperature is 180°C and the material behaviour of the foam is linear elastic, residual stresses in the foam core rise up to 0,5 MPa by cooling down to room temperature (25°C). Considering foam strength (1,8 MPa) the thermal stress amounts to nearly 30%.

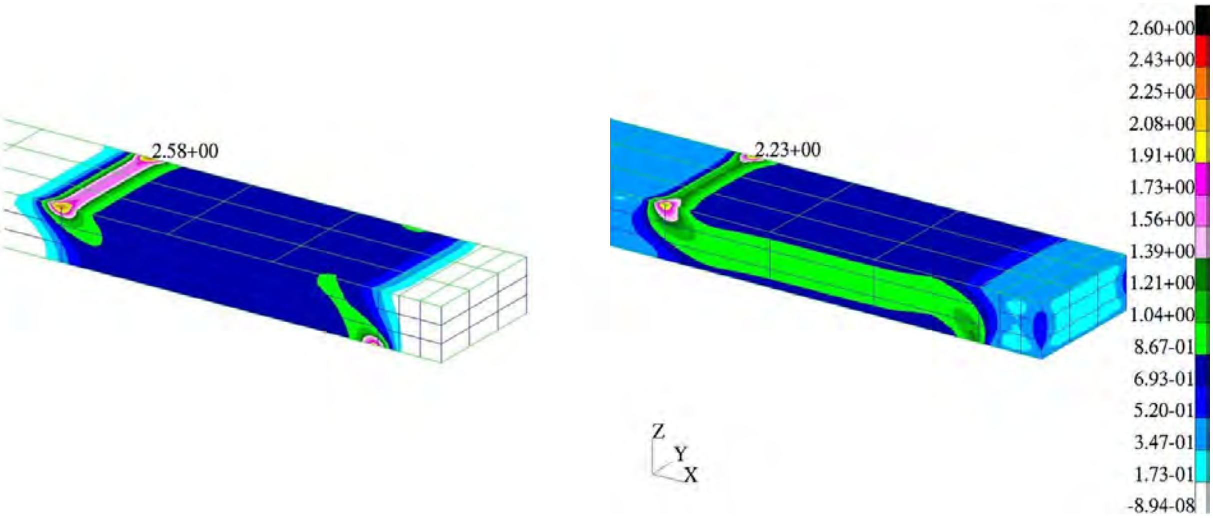

Figure 3: Efficiency ratio of the foam core determined by FEA with the ROHACELL®-Failure-Criteria (DKI/Röhm) without (left) and with (right) temperature load and experimental measured fracture load (1358 N) at 4-Point-Bending test. The CFRP skins are removed for plot.

Finite element calculations were done again for the ROHACELL®-Failure-Criterion (DKI/Röhm) with two loads: The bending load of 4-Point-Bending test (like before) and additionally a temperature load of cooling down from 180° to 25°. The influence of temperature load of the foam core is shown in Figure 3: The efficiency ratio now increases in the area of global shear fracture to a value nearly 1. So the theoretical failure load amounts to 98% of the one experimentally determined. It means both, a very good conformity of analysis and experiment and a conservative calculation. In the area under the load introduction point now higher failure loads are computed. This results from the temperature tension load, which is superposed to the compression loads in this area and decreases the efficiency ratio. Since the real fracture load of local damage under load introduction point is unknown, it can not conclude the efficiency ratio is right, but it seems more realistic. However the failure prediction was enhanced with consideration of thermal stress.

3 OUT OF PLANE LOAD INTRODUCTION IN SANDWICH STRUCTURES

Introducing loads into sandwich structures is generally complicated because of the great difference in the properties of the composed materials. For the investigated materials the tension stiffness and strength of the core are nearly 1000 times lower than the ones of the CFRP skin. So the skin can carry much higher loads compared to the core, which becomes in good dimensioned sandwich components only a spacer between the skins. In Figure 4 on the left a representative sandwich element is shown with the corresponding stress condition. The sandwich withstands ideally in plane loads which are carried almost entirely by the skin (blue

/ plus sign), while the out of plane normal and shear loads (red / minus sign) are carried by both, skins and weaker core. So the out of plane loads have to be kept low to prevent core failure. In real sandwich components these stresses can not be avoided, especially at load introduction points and lines like brackets, spars and ribs in aerospace structures. Also the local damages under the load introduction points measured in the prior 4-Point-Bending tests show the sensitivity of foam core to out of plane loads. To increase stiffness and strength in sandwich thickness direction, several load introduction elements are used. This can be punctiform, linear or laminar concepts. However this paper deals with the investigation of linear transmission of force into the assembly.

3.1 Investigated load introduction concepts

The range of integrated reinforcement elements in sandwich structures is wide. The demand on a high ratio of stiffness and strength to weight qualifies CFRP elements for usage in aerospace application. Also the use of the same material for sandwich skins and reinforcement elements provides potential for saving manufacturing steps and costs [3].

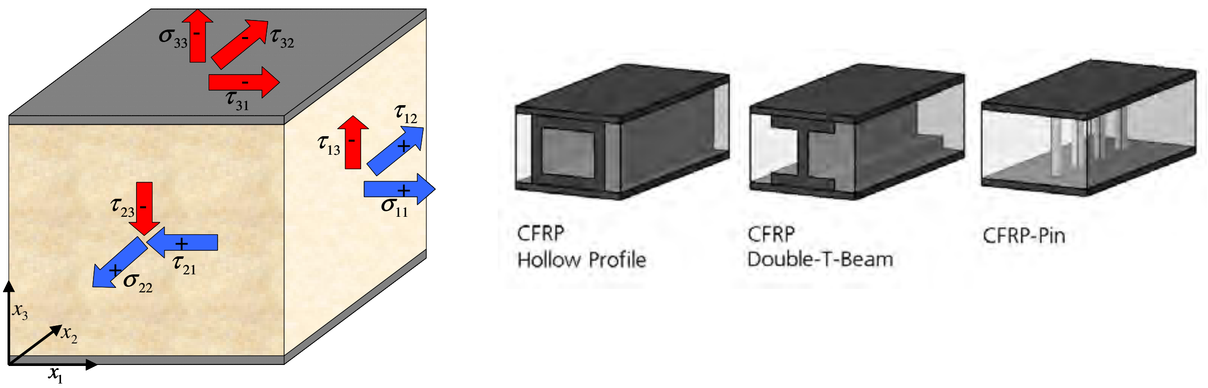

Figure 4: Good and unfavourable carried loads for sandwich without reinforcement (left) and investigated reinforcement elements to increase out of plane strength and stiffness (right)

Figure 4 (right) shows the three investigated load introduction elements. Their manufacturing is optimised for sandwich infusion process [3]: The hollow profiles are made of a dry carbon fibre tyre-tube, which is filled with a foam square profile and then placed in the sandwich. The infusion and curing of both, reinforcement elements and sandwich occur in one manufacturing step. The manufacturing of the double-T beam based on the same concept: Dry carbon fibre textiles are composed to a double-T beam and the infused together with the skin. The CFRP Pin was already cured before sandwich infusion, so they are only bonded to the skin and core.

3.2 Mechanical benchmark of load introduction effectiveness

Benchmark effectiveness of the sandwich load introduction elements the enhancement of out of plane stiffness and strength compared to not reinforced sandwich have to be investigated. In Figure 4 to the left the three stress components in thickness direction, which are critical for sandwich without reinforcement, are stated: σ_{33}, $\tau_{13} = \tau_{31}$ and $\tau_{23} = \tau_{32}$. For each component a separate test was defined. Reis [6] enforced out of plane shear and compression tests to investigate laminar GFRP pin reinforced sandwich structures. These tests are used in this investigation with some differences as well: Only linear load introduction elements are used and the tests are based on the German standard DIN 53291 for out of plane compression test (Figure 5 left upper) and DIN 53294 for out of plane shear test (Figure 5 on the right).

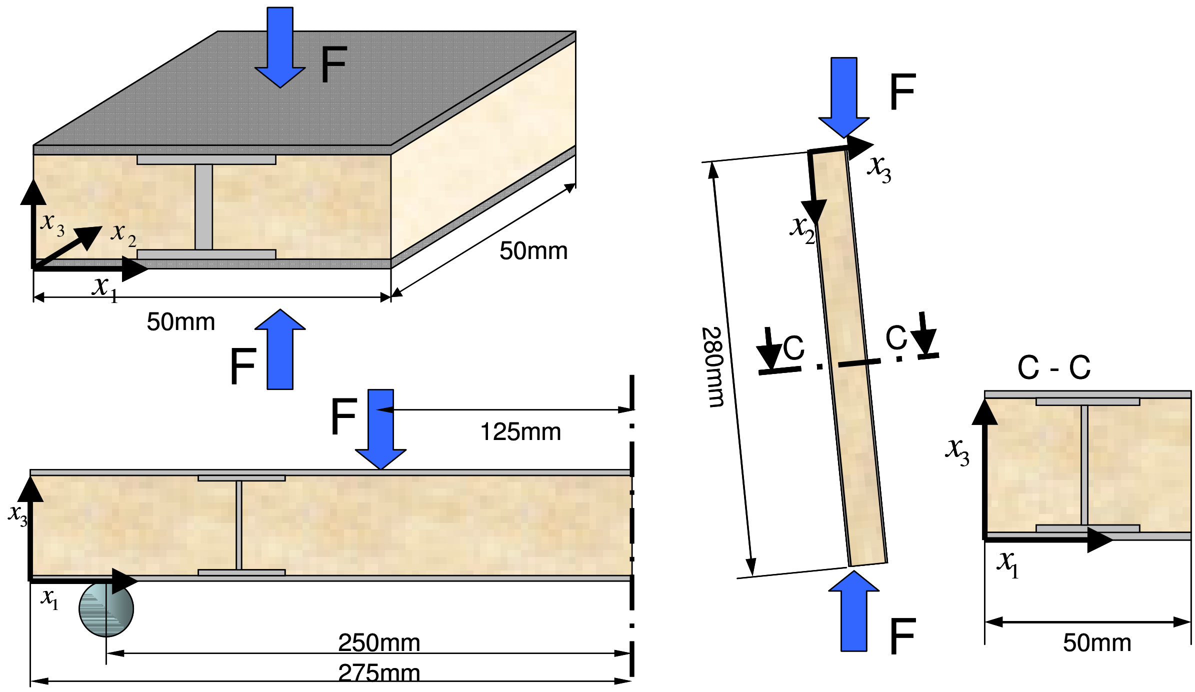

Figure 5: Mechanical Tests to benchmark effectiveness of sandwich reinforcement elements: out of plane compression test (left upper), 4-Point-Bending test (bottom left) and out of plane shear test (right)

With the out of plane shear test (Figure 5 to the right) the shear stiffness and strength in longitudinal direction of the reinforcement element was investigated, for the transverse direction the 4-Point-Bending test was used again. Figure 5 bottom left shows this test setup: The reinforcement element is placed between load introduction point and support point, the area were the transverse shear stress τ_{13} dominates. Hasebe [7] did 3-Point-Bending tests with reinforced sandwich beams, but like Reis with laminar reinforcement elements.

3.3 Effectiveness for out of plane compression load

Because of the limited amount of space, only some results of the benchmark of out of plane compression load introduction can be presented here. With every reinforcement concept, 6 tests were conducted and the mean with their standard deviations were calculated. In Figure 6 the experimental results of the compression tests are stated: the effective middle strength and stiffness. For determining the middle stress, the force of testing machine was divided by the specimen cross section. The strain was determined with the stroke of the testing machine. First of all, the tests measured repeatable results because of the small standard deviations, especially of the not reinforced sandwich. This means both, a good homogenous foam quality and a reliable manufacturing process [3]. The measured foam stiffness (197 MPa) and strength (4,3 MPa) are much greater than the values provided by the manufacturer (105 MPa and 1,7 MPa), but they are used for the comparison with the reinforcement concepts because this is conservative for benchmark of reinforcement effectiveness.

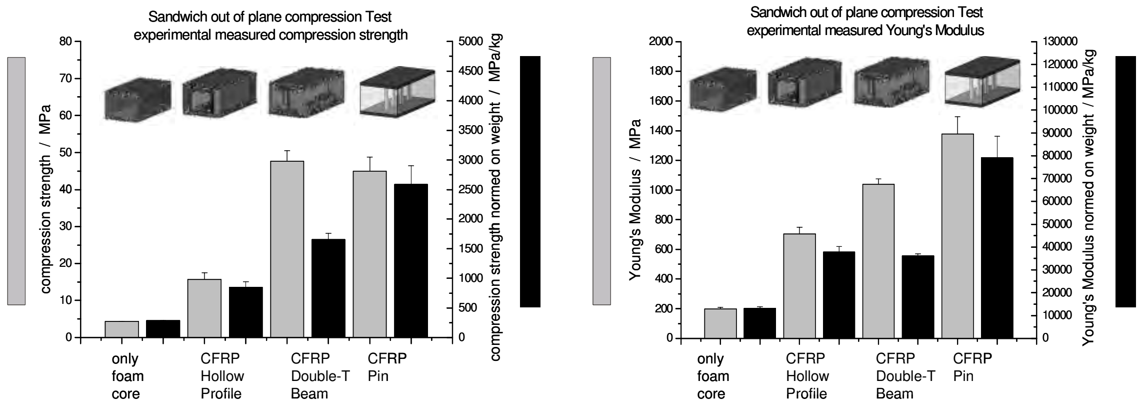

Figure 6: Experimental measured effective strength and stiffness of reinforced and not reinforced sandwich

The effective Young's Modulus increases with using the reinforcements CFRP hollow profile, CFRP double-T beam and CFRP Pin significant: factors 3,6 , 5,3 and 7,0. Comparing the stiffness related to their weight, the increase is a little bit lower. Also the sequence is different: The double T-Beam increases the stiffness more than the hollow profile, but the weight too. So the hollow profile seems more effective. The Pin reinforcement increases the stiffness related to weight with factor 6,0 and is compared to the hollow profile (2,9) and double-T beam (2,7) the most effective reinforcement concept (for out of plane compression stiffness).

The increase of the strength related to weight is much greater than the increase of stiffness. The factors compared to the weight related strength of not reinforced sandwich amount to 2,9 (hollow profile), 5,8 (double-T beam) and 9,0 (pin). Finally, the CFRP pin reinforcement results in the best increase of stiffness and strength related to their weight. It seems to be the best concept considering out of plane compression. Now these examinations have to be conducted with the 4-Point-Bending and out of plane shear test.

4 CRACK PROPAGATION IN CFRP FOAM SANDWICH STRUCTURES

Another failure scenario is the occurrence of cracks in the sandwich structure. Mostly cracks are located either in the foam core or in the interface between face sheet and core. These cracks are often caused by impact by tool drop or bird strike. In the last resort the impact damage is non visible and grows in service under cyclic loads [8]. To decrease crack growth or to restrict crack growth to a defined area, crack stopper elements can be integrated in the sandwich structure. The concept is using the load introduction elements as crack stoppers. Therefore the crack growth in fatigue loading with and without sandwich reinforcement has to be investigated.

4.1 Mechanical benchmark of crack stopper effectiveness

To investigate the effectiveness, methods based on fracture mechanics are used. A general overview about fatigue investigation methods of sandwich structures can be found in Sharma [10]. To determine crack growth under Mode I and Mode II loads, DCB (Double Cantilever Beam) and ENF (end Notched Flexure) Tests were carried out by Burman [9] with GFRP foam-core sandwich. He modified the Cracked Sandwich Beam test (CSB), which was firstly defined by Carlsson [11] but originally an ENF test is implemented with sandwich beams. However these tests were defined for the sandwich investigated in this research: with and without reinforcement elements.

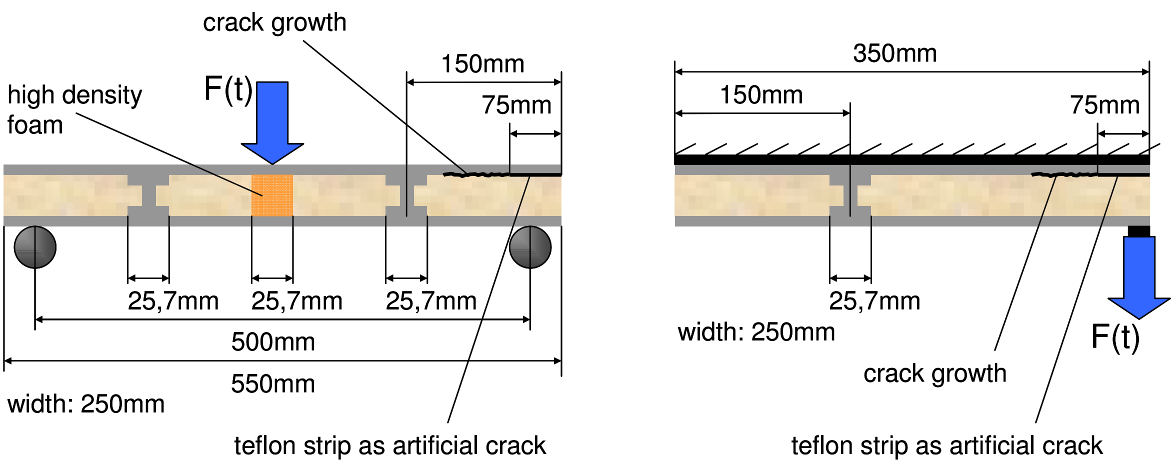

Figure 7: Adapted ENF (left) and DCB test (right) for sandwich with reinforcement

Figure 7 shows the defined fracture mechanic tests for this sandwich with reinforcement elements. The core has a thickness of 25,7mm, so the reinforcement elements all have a square area. The CFRP skin consists of the same base materials like the ones for the investigation of foam failure criteria but they are three times thicker: $3\times[45/0/135]_S$. The investigated foam core is Rohacell 71Rist, only for reinforcing the load introduction area a higher density foam is used (Rohacell 110Rist) because of its greater stiffness and strength.

4.2 Mode II crack propagation in sandwich without reinforcement elements

Firstly static ENF tests were enforced to determine the static fracture load. This amounts to 4202N with a standard deviation of 3,4%. Following cyclic tests were conducted with a load ratio $\left(R = \frac{\sigma_u}{\sigma_o} \right)$ of 0,1 , an upper load of 30, 50, 70% of the prior determined static fracture load and a test frequency of 2Hz. The test with the 30% upper load did not result in specimen failure and no crack propagation could be measured until $2{,}6 \times 10^6$ load cycles (when the test was aborted). The tests with 50 and 70% of upper load reached 1794782 and 150949 load cycles until fracture but no stable slow crack propagation could be determined. Indeed, there was a cyclic crack propagation for both 50% (73mm, shown in Figure 8 to the left) and 70% (12,5mm), but it was to fast to determine the crack prediction by the Paris law. So more tests with upper loads between 30 and 50% of fracture load should be conducted shortly. However, these test will be continued, but they already show the expected benefit of crack stoppers in sandwich structures: Preventing skin debonding of large areas in the sandwich in service.

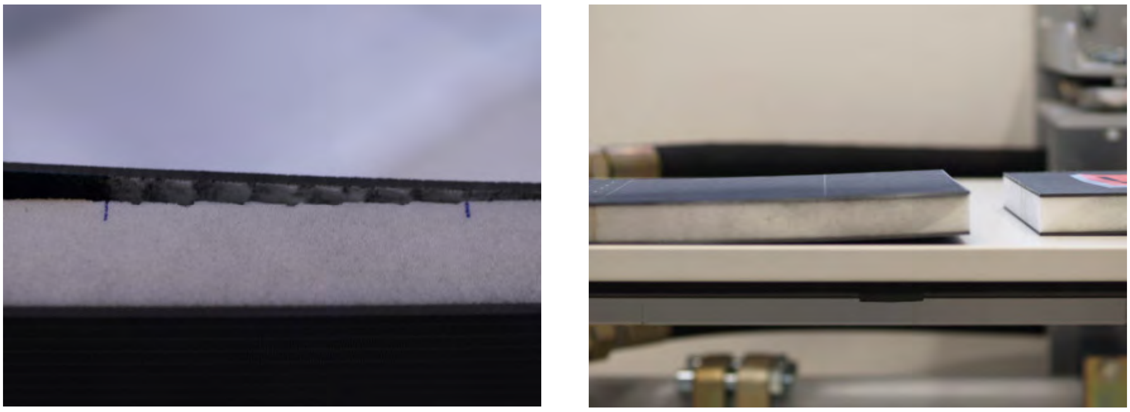

Figure 8: Mode II crack propagation under cyclic ENF test (left) and specimen curvature after debonding of the skin through specimen middle coming from residual stresses (right)

Another interesting result of the ENF test is the clearly visible curvature of the debonded sandwich plate. This confirms the assumption of prior calculations. The debonded sandwich now has an asymmetric laminate, where different thermal expansion coefficients result in curvature of the plate.

9 CONCLUSIONS

The bending deformation behaviour of the investigated CFRP foam-core sandwich can be well described with both the analytical sandwich theory and numerical calculations. The analytical solution agrees accurately with the numerical calculation. The classical assumption of the sandwich theory, that the skins have much greater stiffness and strength, applies well on this sandwich. The failure behaviour can become more complex, especially if out of plane loads occur. Such loads arise at load introduction points or lines like ribs ore hinges of airplane structures. In this case, analytical dimensioning with sandwich theory is not conservative, special foam failure criteria have to be used. Calculations have shown, that the ROHACELL®-Failure-Criterion (DKI/Röhm) determines the best results for this sandwich.

Residual stresses are caused by the different thermal expansion coefficients of the foam and the CFRP skin and by the difference of sandwich curing temperature and in service temperature. They are superposed to the service loads and affect the failure behavior positive and negative. The consideration in dimensioning calculations increases the accuracy of failure prediction.

To increase the out of plane strength and stiffness, integrated reinforcement elements were investigated: CFRP hollow profile, CFRP double T-beam and CFRP pin reinforcement. Therefore sandwich tests were adapted to investigate the effectiveness for all three out of plane stress components: out of plane compression, sandwich shear and 4-Point-Bending test Due to the restricted scale of paper, only results of out of plane compression test could be presented here. For this load case, the CFRP pin reinforcement results in the best ratios of out of plane compression stiffness and strength to weight.

Cracks in the foam-core or between skin and core can be critical if they grow through the whole structure, before they are visible. The reinforcement elements can be used as crack stoppers. For investigation of their crack stop effectiveness, fracture mechanic tests were conducted. ENF tests have shown, that the crack propagation is mostly fast after a long time with no crack growth. Therefore it is useful to have crack stop elements in large sandwich plates to decrease the crack propagation.

REFERENCES

[1] A. S. Herrmann, P. C. Zahlen and I. Zuardy, "Sandwich Structures Technology in Commercial Aviation", 7th International Conference on Sandwich Structures, Aalborg, Denmark, August 2005.

[2] J. R. Vinson, "The Behavior of Sandwich Structures of Isotropic and Composite Materials", Technomic Publishing Company, Lancaster (Pennsylvania), USA, 1999.

[3] P. C. Zahlen, M. Rinker and C. Heim, "Advanced Manufacturing of Large, Complex Foam Core Sandwich Panels", 8th International Conference on Sandwich Structures, Porto, Portugal, May 2008.

[4] W. Schneider and R. Bardenheiner, "Versagenskriterien für Kunststoffe", Journal of Materials Technology 6. Jahrgang / Nr. 8, 1975.

[5] A. Kraatz, "Anwendung der Invariantentheorie zur Berechnung des dreidimensionalen Versagens- und Kriechverhalten von geschlossenzelligen Schaumstoffen unter Einbeziehung der Mikrostruktur", Dissertation Universität Halle, Deutschland, 2007.

[6] E. M. Reis and S. H. Rizkalla, "Material Characteristics of 3-D FRP Sandwich Panels",

Third International Conference on Bridge Maintenance, Safety, and Management (IABMAS '06), Porto, Portugal, July 2006.

[7] R. S. Hasebe and C. T. Sun, "Performance of Sandwich Structures with Composite Reinforced Core", Journal of Sandwich Structures and Materials, 2000.

[8] C. Bergreen, "Damage Tolerance of Debonded Sandwich Structures", PhD thesis, Technical University of Denmark, 2004.

[9] M. Burman, "Fatigue Crack Initiation and Propagation in Sandwich Structures", PhD thesis, Royal Institute of Technology, Stockholm, Sweden, 1998.

[10] N. Sharma, R. F. Gibson, E. O. Ayorinde, "Fatigue of Foam and Honeycomb Core Composite Sandwich Structures: A Tutorial", Journal of Sandwich Structures and Materials, 2006.

[11] L. A. Carlsson, "On the Design of the Cracked Sandwich Beam (CSB) Specimen", Journal of Reinforced Plastics and Composites, Vol. 10, No. 4, 434-444, 1991.

8th International Conference on Sandwich Structures
ICSS 8
A. J. M. Ferreira (Editor)

STRESS AND FAILURE ANALYSIS OF REPAIRED SANDWICH COMPOSITE BEAMS USING A COHESIVE DAMAGE MODEL

Dimitra A. Ramantani*, Raul D.S.G. Campilho*, Marcelo F.S.F de Moura*, Antonio T. Marques*

* Faculdade de Engenharia da Universidade do Porto (FEUP)
Universidade do Porto
Rua Dr. Roberto Frias, 4200-465 Porto, Portugal
e-mail: dimitraramantani@hotmail.com, web page: http://www.fe.up.pt

Keywords: Sandwich structures, Adhesive joints, Fracture, Mixed-mode damage model, Finite element analysis

Summary: *The behaviour of a repaired sandwich beam subjected to four point bending is investigated numerically using the ABAQUS® software and special developed interface elements including a cohesive mixed-mode damage model based on the indirect use of Fracture Mechanics. The two major repair configurations for sandwich structures namely overlap and scarf repair, are studied. The interface elements placed at the middle of the adhesive, parent laminate/adhesive and adhesive/patch interfaces allow to obtain stress distributions at these locations as well as to simulate damage onset and growth. The influence of several geometrical parameters, such as overlap length and patch thickness, in the case of overlap repair, and scarf angle, in the case of scarf repair, is evaluated in terms of stress analysis and strength predictions. Conclusions were drawn about design guidelines of the sandwich composite repair.*

1. INTRODUCTION

Sandwich structures are widely used nowadays in transportation industry such as aerospace, aeronautical, railway, automotive and marine industry where special properties such as high flexural stiffness, high impact strength, high corrosion resistance, fatigue resistance and low thermal and acoustics conductivity are necessary and recommended [1]. The most frequent case of in-service damage for sandwich structures is delamination caused by low velocity impact. Delamination can occur within one of the skins of the sandwich material or at the interface between one skin and the core. This phenomenon can highly reduce the ability of the material to withstand structural loading. Under special in-plane loading conditions (a well-known example is the in-plane compression) the crack may become unstable and propagate considerably even under very low stress levels [2, 3]. Moreover, the high replacement cost of composite materials along with current ecological requirements makes repair a beneficial option towards enhancement of composite products life. The repair of sandwich structures suffering delamination can be executed with an application of a composite patch since no replacement of the core is taking place. Adhesive bonding of the patch is one of most common repair techniques carried out, either in the condition of temporary repair or permanent repair. Adhesive bonding is preferable than mechanical fastening because of the well known advantages of the technique such as less sources of stress concentrations, more uniform distribution of load, and better fatigue properties. Considering the repair techniques used in the case of composite laminates, in sandwiches, there are two major options available to bond the patch, namely overlap and scarf joining. In the overlap joining, a circular patch is applied external over the damaged zone, while in scarf joining, a tapered circular patch is inserted in the damaged area and adhesively bonded. The later repair technique proved to be more structurally efficient for composite laminates but is more expensive and time consuming. In all of the types of repair the main concerns are the prediction of the residual strength of the initially damaged composite and the durability of the repaired one.

The work in this paper is dedicated to the study of overlap and scarf repairs of sandwich structures loaded under four point bending using the commercial software ABAQUS®. The objective of the simulations is to obtain stress distributions at critical regions and to evaluate the residual strength of the repaired beams using a cohesive mixed-mode damage model. This model is incorporated in the ABAQUS® software via interface elements. The interface elements are placed along all the bondlines (Fig. 4) and specifically at the middle of the adhesive, parent laminate/adhesive, adhesive/patch and also adhesive/core interfaces allowing to simulate damage initiation and propagation. The main geometrical parameters concerning the good performance of the repair which are the overlap length and patch thickness, in the case of overlap repair, and the scarf angle, in the case of scarf repair, are studied in terms of stress analysis and strength predictions.

2. COHESIVE DAMAGE MODEL

A cohesive mixed-mode damage model based on interface finite elements was considered to simulate damage onset and growth. A linear constitutive relationship between stresses ($\boldsymbol{\sigma}$) and relative displacements ($\boldsymbol{\delta}$) is established (Fig 1). The model requires the knowledge of the local strengths ($\sigma_{u,i}$, i=I, II) and of the critical strain energy release rates (G_{ic}). Damage onset is predicted using the following quadratic stress criterion

$$\begin{aligned} &\left(\frac{\sigma_{\mathrm{I}}}{\sigma_{\mathrm{u,I}}}\right)^2+\left(\frac{\sigma_{\mathrm{II}}}{\sigma_{\mathrm{u,II}}}\right)^2=1 \quad \text{if} \quad \sigma_{\mathrm{I}}\geq 0 \\ &\sigma_{\mathrm{II}}=\sigma_{\mathrm{u,II}} \qquad\qquad\qquad \text{if} \quad \sigma_{\mathrm{I}}\leq 0 \end{aligned} \tag{1}$$

where σ_i, (i=I, II) represent the stresses at a given integration point of the interface finite element in each mode. Mode I represents the local opening mode and mode II the shear one at the interface. Crack propagation was simulated by the linear energetic criterion

$$\frac{G_{\mathrm{I}}}{G_{\mathrm{Ic}}}+\frac{G_{\mathrm{II}}}{G_{\mathrm{IIc}}}=1\,. \tag{2}$$

The area under the minor triangle of Figure 1 represents the energy released in each mode, while the bigger triangle area corresponds to the respective critical fracture energy. When equation (2) is satisfied damage propagation occurs and stresses are completely released, with the exception of normal compressive ones. The subscripts “o” and “u” refer to onset and ultimate relative displacement, respectively, and the subscript “m” denotes mixed-mode case. A detailed description of the model used is presented in [4].

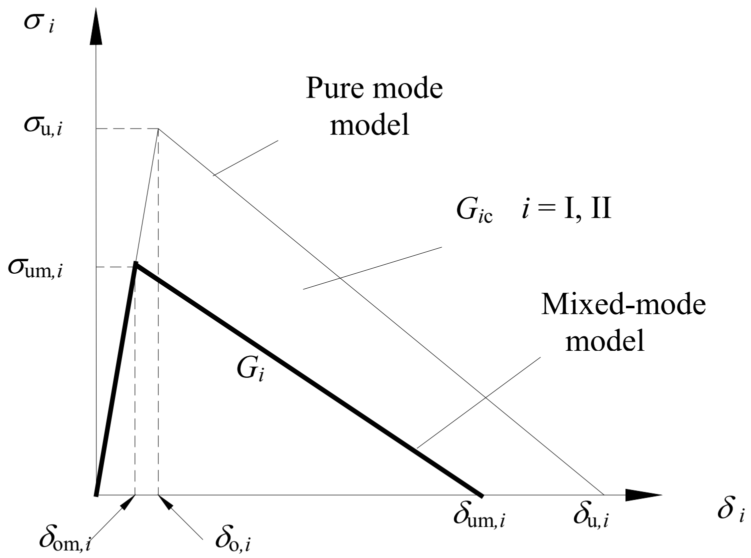

Figure. 1: The linear softening law for pure and mixed-mode cohesive damage model.

σ_i, stress in mode i; $\sigma_{u,i}$, local strength in mode i; $\sigma_{um,i}$, stress component (i) leading to damage initiation in mixed mode; δ_i, relative displacement in mode i; $\delta_{o,i}$, damage onset relative displacement in pure mode i; $\delta_{u,i}$, ultimate relative displacement in pure mode i; $\delta_{om,i}$, damage onset relative displacement (i) in mixed mode; $\delta_{um,i}$, ultimate relative displacement (i) in mixed mode; G_i, strain energy release rate in mode i; G_{ic}, critical strain energy release rate in mode i.

3. ANALYSIS

The presented work consists of a two-dimensional nonlinear material and geometrical analysis of a repaired sandwich beam subjected to four point bending. Plane stress conditions and rectangular 8-node and triangular 6-node solid finite elements available in the ABAQUS® library were considered. Overlap and scarf repair configurations were simulated (Fig. 2). The skins and the patches of the repaired sandwich beams are unidirectional carbon-epoxy laminates with 0° orientation, the core in the form of foam and the adhesive a high resistant resin. Their properties are presented in Table 1 [4, 5]. Geometrical details for both repair configurations are given in Figure 2. Symmetry conditions were used in the middle of the joint (line A-A in Fig. 2). Details of the mesh at the overlap and scarf region are shown in Figure 3.

Faces and patches (carbon-epoxy)			Core (Divinicell H100, PVC Foam)	Adhesive (epoxy resin)		
				Elastic property	Plastic property	Fracture properties
E_1=1.09E+05 MPa	υ_{12}=0.342	G_{12}=4315 MPa	E=111 MPa	σ_e=36MPa	σ_s=40MPa	G_{IC}=0.3 N/mm
E_2=8819 MPa	υ_{13}=0.342	G_{13}=4315 MPa	ν=0.1	E=2000MPa	ε_s=0.1	G_{IIC}=0.6 N/mm
E_3=8819 MPa	υ_{23}=0.380	G_{23}=3200 MPa		ν=0.35		

Table 1: Mechanical and Fracture properties of the materials used.

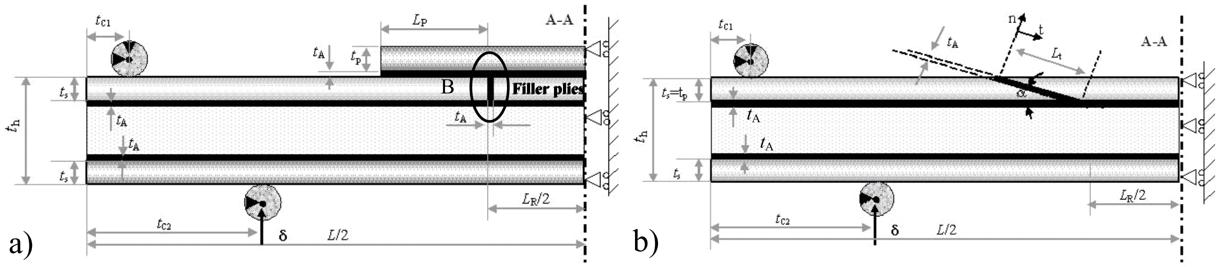

Figure 2: a) Overlap and b) scarf repair geometry.

t_h(thickness of the beam)=17.2mm; ts(thickness of the skins)=0.6mm; t_A(thickness of the adhesive)=0.2mm; t_p(thickness of the patch)=0.3-1.2mm, L(length of the sandwich beam =700mm; L_R(length of damage)=60mm; L_p(overlap length)=5-30mm, L_t(bond length along the scarf tangential direction); α(scarf angle)=3^0-45^0; t_{c1}= 35mm; t_{c2}= 225mm;
A–A(symmetry line); δ(applied displacement); B(vertical adhesive bondline connecting the upper skin and the filler plies); t–n(local coordinate system).
* L_e(ply thickness)=0.15mm, w(width)=25mm.

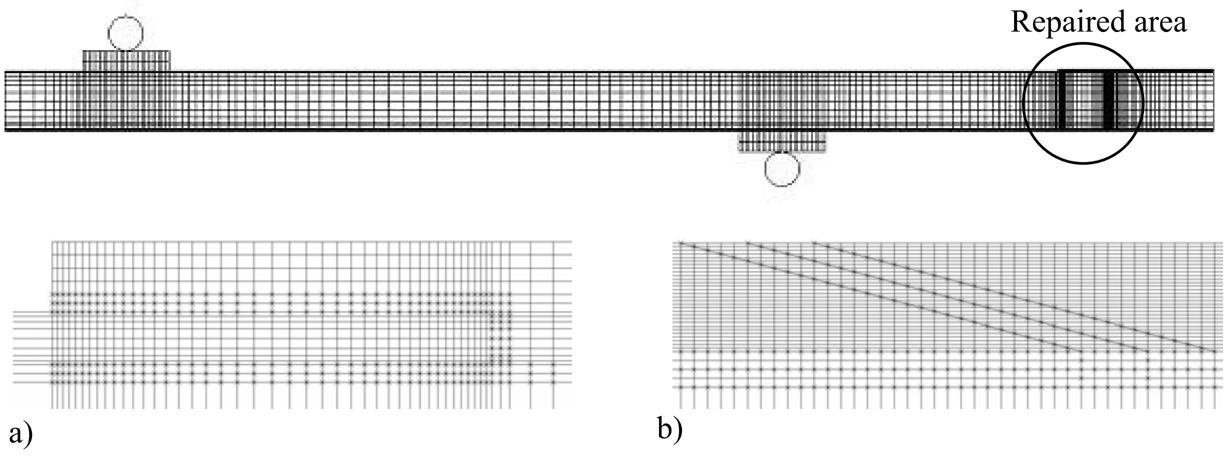

Figure 3: Finite element model of the repaired sandwich beam and details of the mesh for a) an overlap and b) a scarf repair.

The location of the interface finite elements is shown in Figure 4. These elements were places along all the adhesive bond lines and specifically at the interface between the composite (skin and patch) and the adhesive, at the interface between the core and the adhesive and also atthe middle of the adhesive. Interlaminar failure was not considered in the analysis. The objective of the simulations is to define the influence on the repair efficiency of the main geometrical parameters concerning the good performance of the repair which are the overlap length and patch thickness for the overlap repair and the scarf angle for the scarf repair.

a) 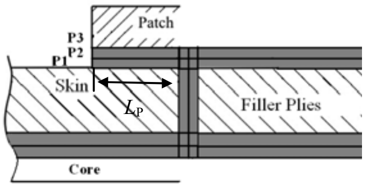

b) 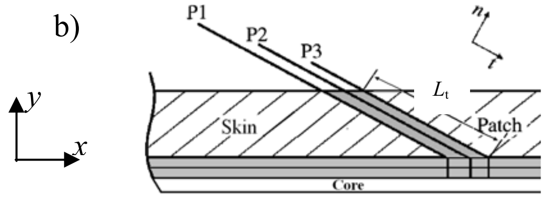

Figure 4: Location of the interface finite elements in the numerical a) overlap and b) scarf model.

P1, interface between the parent laminate (skin) and the adhesive; P2, middle of the adhesive; P3, interface between the adhesive and the patch along the L_p and L_t bond lines

3. 1. Overlap repair

Stress analysis was performed initially for an overlap repair of 15 mm using a 0.6 mm thick patch, equal to the thickness of the skins of the sandwich beam. Figures 5 and 6 present the shear- and peel-stress distribution profiles at three specific locations in the joint, the skin/adhesive interface, P1, the middle of the adhesive, P2, and the adhesive/patch interface, P3, (Fig. 4). They are normalized by τ_{avg}, the average shear stress at the middle of the adhesive. Both stress profiles correspond to the typical ones obtained for this kind of joints [4, 6, 7]. The shear stresses present two high pronounced peaks at the extremities of the overlap at the skin/adhesive interface, P1. Negligible stress concentrations are observed at the ends of the P2 and P3 interfaces. The inner region of the adhesive is almost unloaded.

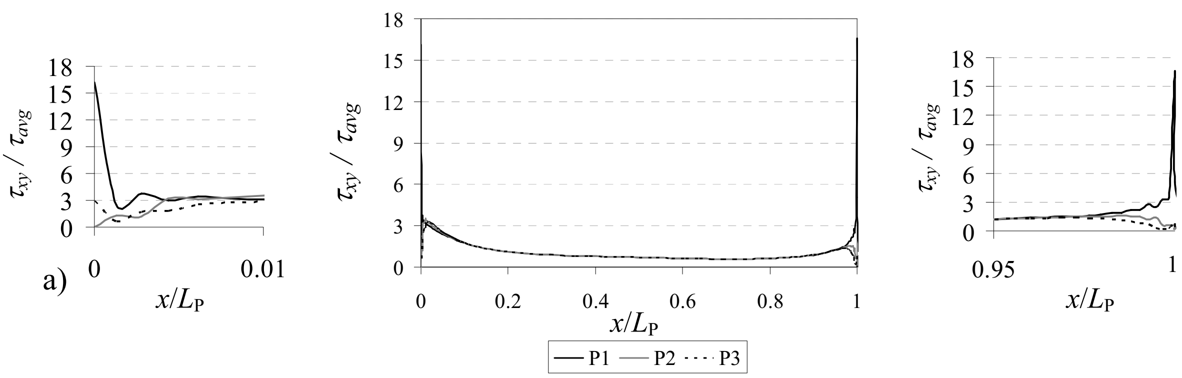

Figure 5: Normalized shear-stress distributions at locations P1, P2 and P3 (Fig. 4).

The peel stress distributions exhibit also peak stresses at the ends of the overlap. A high positive value is present at the beginning of the overlap and at the skin/adhesive interface, P1. At the end of the overlap, the values of peek stresses are much lower and negligible compared to the one at the opposite side. It is evident that failure will occur at the beginning of the overlap and at the skin/adhesive interface, P1. It must be noted that the high values of peel-stresses at the beginning of the P1 interface could also induce delamination between adjacent layers of the laminates.

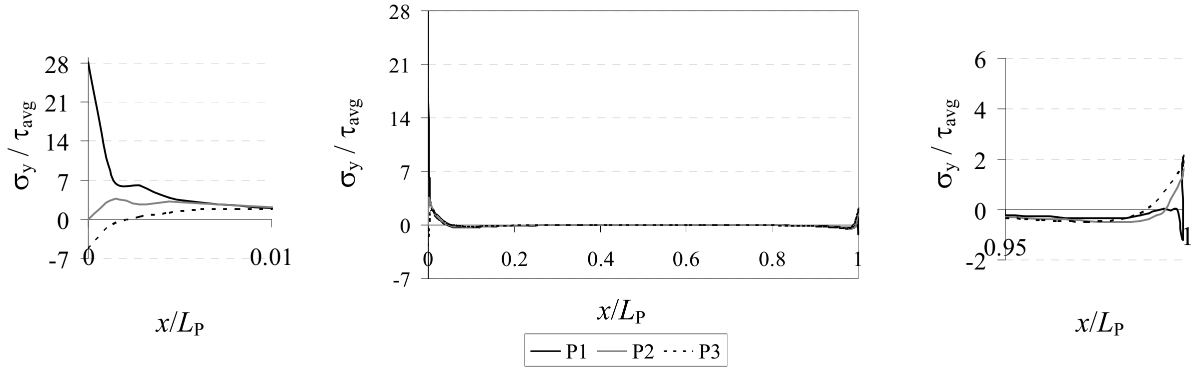

Figure 6: Normalized peel-stress distributions at locations P1, P2 and P3 (Fig. 4).

Overlap length

The first parameter to be studied in the case of an overlap repair in order to define its influence on the joint's residual strength was the overlap length. Four different overlap lengths were considered in the analysis: 5, 10, 15 and 20mm. In Figure 7 the failure load (P_f) and the efficiency of the repair (η) as a function of the overlap length L_P are presented. P_f represents the load leading to the debonding onset at the critical regions of the repair while η is considered to be the ratio between P_f of the repaired specimen and the failure load of an equivalent undamaged one.

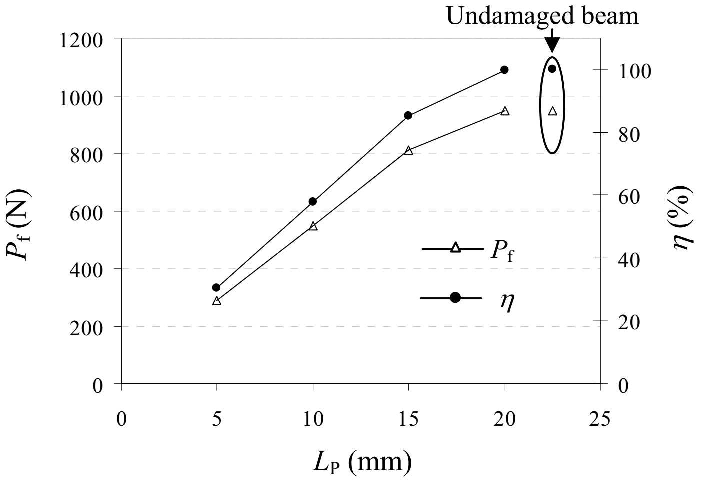

Figure 7: Failure load, P_f, and repair efficiency, η, for different values of overlap length.

It is observed that the increase of the failure load and subsequently of the efficiency of the repair is higher for the smaller overlap lengths, decreasing for overlaps higher than 15mm. This phenomenon can be explained by the shear stress distribution at the adhesive presented in Figure 8 since, as the overlap length increases, the inner region of the adhesive becomes almost unloaded.

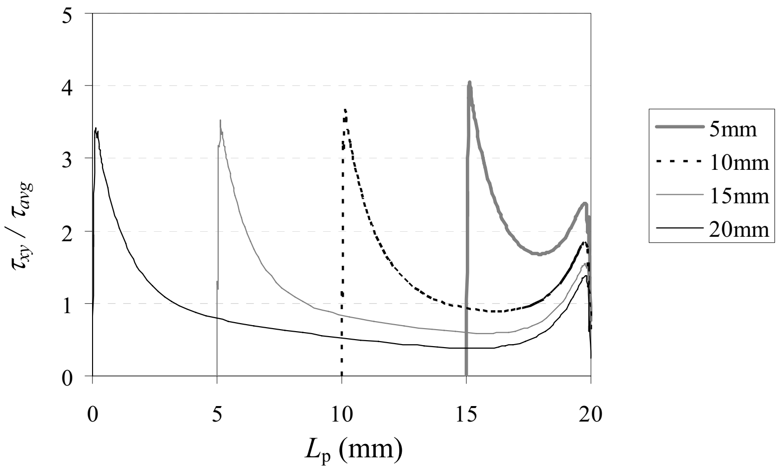

Figure 8: Normalized shear stress distributions at the adhesive for different values of overlap length.

Patch thickness

The patch thickness does not seem to have any influence on the repair efficiency (Fig. 9). This phenomenon can be explained by observing the failure mechanism of the joint while moving from a thin (e.g. 0.3mm/2-plies) to a relatively thick (e.g. 1.2mm/8-plies) patch. It is obvious that when the patch thickness decreases, the deformability of the joint increases and failure occurs prematurely in the vertical adhesive region B (Fig. 2) due to elevated normal stresses. On the other hand, it was observed in the analysis and also verified by previous studies [4] that as the patch thickness increases, the peel- peak stresses at the beginning of the overlap increase as well. Although failure always initiates at the vertical adhesive region B, (Fig. 2), high values of peel stresses lead to prior disbond of the patch. Very high values of peel stresses in the beginning of the overlap could also induce delamination between adjacent layers of the patch before failure of the adhesive takes place, which could limit even more the repair strength [4].

Damage growth

The damage onset was identified by simply observing the occurrence of softening onset at the nodes of the interface elements located at the region of the repair joint. In the overlap repair, it was observed that failure initiates in the vertical adhesive bonding region connecting the skin with the filler plies (region B, Fig. 2) and specifically at the interface between the skin and the adhesive due to high pronounced normal stresses. The crack grows along the interface and towards the patch and the core. Another crack also starts at the left bond edge of the overlap at the skin/adhesive interface, P1, and grows along the overlap. This kind of failure was observed for all the overlap repairs studied. It could be noted that in real case the crack, after the failure of the B region, would probably continue propagating into the core. Indication of this are extensively distorted elements of the core in the basis of the B region.

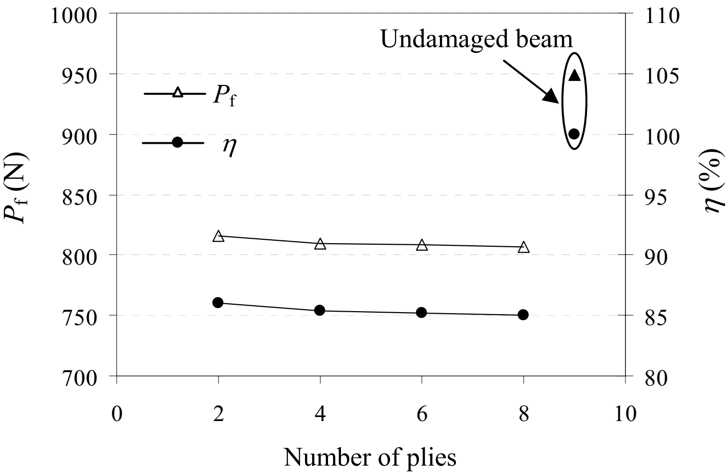

Figure 9: Influence of the patch thickness on the repair efficiency, η, and failure load, P_f.

3. 2. Scarf repair

Stress analysis was performed using a 3° scarf angle. Figure 10 presents the shear-stress distributions at locations P1, P2 and P3 (Fig. 2) normalized by the average shear stress in the middle of the adhesive thickness (t_{avg}). These stresses are almost constant and very similar along the bond length for the three locations considered. In the middle of the adhesive, P2, slight stress concentrations exist near the ends, with the ends being practically unloaded. At the P1 and P3 interfaces, two highly pronounced stress peaks in the lower and the upper bond edge respectively are present, while along the rest of the bond line the stresses follow the same trend as in the middle of the adhesive. It was observed that in the middle of the adhesive, the stress concentrations near the upper and lower bong edge, are located respectively under and above the ends of the P3 and P1 interfaces where the pronounced shear peaks are present. The normalized peel-stress distributions (Fig. 11) at the three aforementioned locations in the scarf joint are also nearly constant between both ends with peaks present at specific locations. At the skin/adhesive interface, P1, a highly pronounced peel peak is observed at the upper bond edge, reaching 80% of the average shear stress within the adhesive. This peak is located under the beginning of the P3 interface. In the middle of the adhesive, P2, peel-stress peeks are observed at both edges of the bond length. A pronounced peak is located right under the beginning of the P3 interface and a lower peak right above the end of the P1 interface. At the adhesive/patch interface, P3, a peel-stress peak is located exactly at the opposite side relatively to the one observed at the P1 interface. The magnitude of the peaks at the end of the scarf are much lower compared to the ones observed in the beginning of the scarf signifying a potential region of damage initiation. Comparing with shear- and peel-stresses in the case of overlap repair, it can be noted that in overlap joints stress concentrations are markedly higher. Both shear- and peel-stress distributions show an agreement with numerical results obtained in Ref [8].

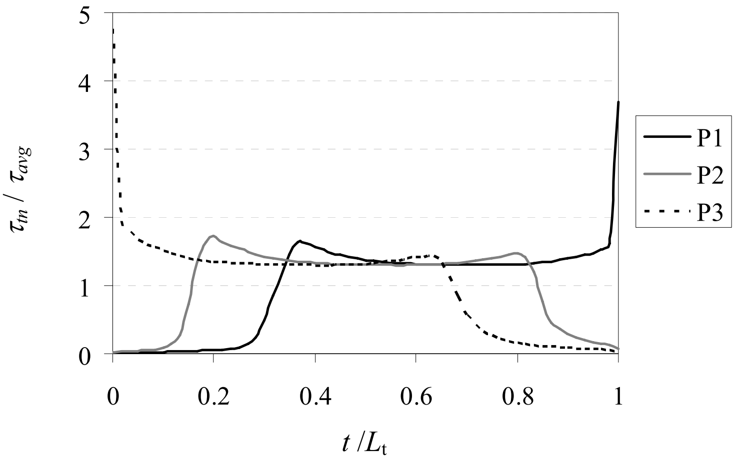

Figure 10: Normalized shear-stress distributions at locations P1, P2 and P3 (Fig. 4) along the normalized bond length.

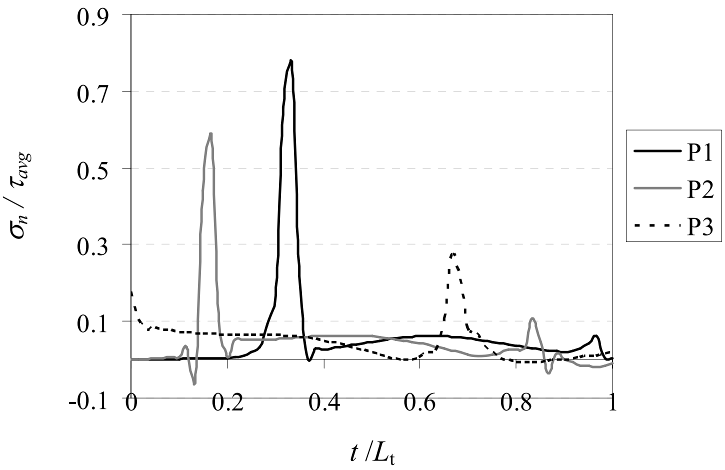

Figure 11: Normalized peel-stress distributions at locations P1, P2 and P3 (Fig. 4) along the normalized bond length.

Scarf angle

A stress analysis was performed for scarf angles of 3, 6, 9, 15, 25 and 45º. Normalized shear- and peel- stress distributions at the middle of the adhesive, P2, are presented in Figures 12 and 13 for the six values of scarf angles considered. It is observed that peel-stresses are much lower than shear-stresses for smaller scarf angles, and increase up to a scarf angle of

45°, at which both stress components present approximately the same magnitude. These results are in agreement with the analytical results presented by Objois *et al* [11]. Both shear- and peel- stress profiles are influenced by the change of the scarf angle. As the scarf angle increases, the stress peaks observed at both edges of the bond length have a tendency to become flatter. In fact, for a 45° scarf angle, it was observed that specifically the shear stresses become almost constant. The low stresses at the edges of the bond length also tend to disappear with the increase of the scarf angle.

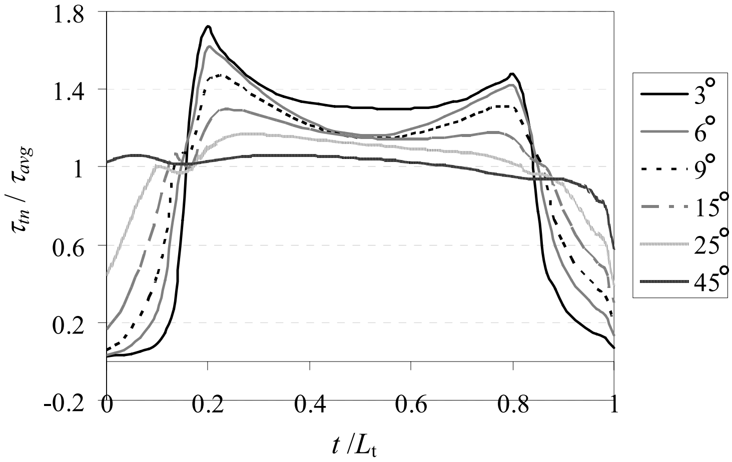

Figure 12: Normalized shear-stress distributions for different scarf angles at location P2 along the normalized scarf length.

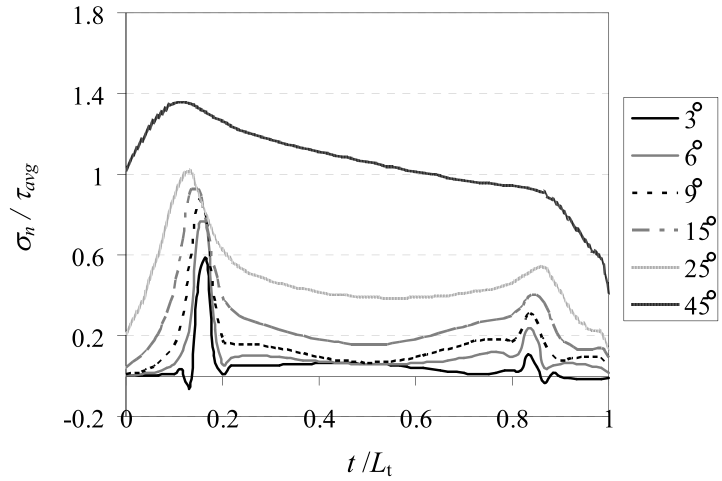

Figure 13: Normalized peel-stress distributions for different scarf angles at location P2 along the normalized scarf length.

Figure 14 presents the failure load (P_f) and the efficiency of the repair (η) as a function of the scarf angle. For scarf angles between 15 to 45º, only a small difference is observed in terms of P_f and η. For scarf angles below 15º, these two parameters increase exponentially with scarf angle reduction. This fact is related to the increase of the bond length and the reduction of peel-stresses (Fig. 13), as the scarf angle is reduced. 50% efficiency is recorded for a 3° scarf angle, corresponding to a failure strength of 391 MPa. The trend observed in Figure 14 is consistent with that found in Refs [8-10] where experimental, numerical or both results are presented for scarf repaired laminates.

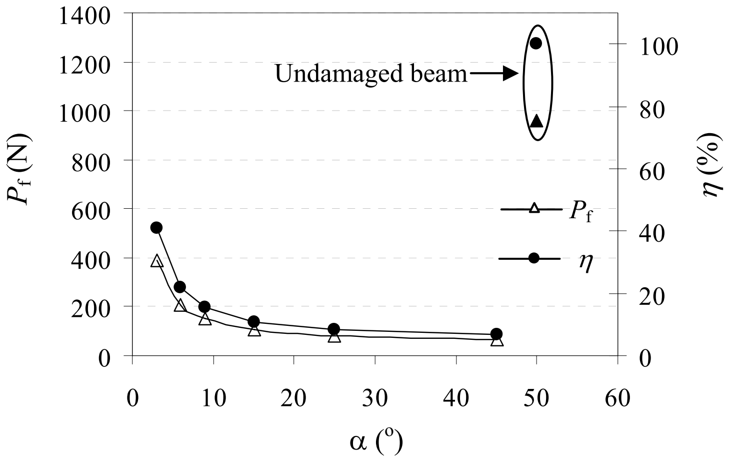

Figure 14: Failure load, P_f, and efficiency, η, for the different scarf angles considered.

<u>Damage growth</u>

In scarf repairs damage initiates at the upper bond edge of the scarf and specifically at the adhesive/patch interface, P3, where high pronounced shear stresses are present (Fig. 10), and grows towards the lower scarf bond edge. A crack also starts at the bottom of the scarf , as it is a strong singularity point, and propagates towards the core. It should be noted that in real case the crack would probably continue propagating inside the foam core and not at the interface between adhesive and foam as it was observed in the analysis.

4. CONCLUSIONS

In this work, overlap and scarf repairs on composite sandwich materials were studied. A cohesive mixed-mode damage model was implemented in the model via interface elements placed along the adhesive bond lines and at three locations; the interface between the composite plates (skin and patch) and the adhesive, the interface between the core and the adhesive and also the middle of the adhesive (Fig. 2.). These interface elements allow obtaining stress distributions at critical locations and performing strength predictions. The objective of this work was to analyze numerically the effect of main geometric parameters for overlap and scarf repairs.

One of the main findings of this work was related to the influence of the overlap length on the failure load of the repair joint. It was verified that above a certain value of overlap length, there is no strength advantage, since from a certain overlap length the central region of the repair joint becomes unloaded. It was also verified that the thickness of the patch does not have an influence on the repair efficiency, a fact closely related to the failure mechanism of the joint. For thin patches failure occurs prematurely in the vertical adhesive B region (Fig. 2) connecting the skin to the filler plies. High values of normal strains are induced in this region due to the higher deformability of the joint. For patches with high stiffness, although failure initiates at the B region, elevated values of peel stresses at the beginning of the overlap lead to prior detachment of the patch. These elevated values could also induce delamination between adjacent layers in the composite reducing even more the repair efficiency of the joint. The strength of the undamaged beam was recovered for a patch having the thickness of the skins of the sandwich beam and an overlap length of 20mm.

In the case of scarf repairs the strength increases with lower scarf angles because of the respective increase of the bond length, leading to an enhancement of the joint strength. For lower scarf angles, failure of the adhesive is dominated by shear. Peel-stresses increase with the scarf angle. The strength of the undamaged beam was not obtained for any scarf angle. Finally a combination of the aforementioned repair geometries was evaluated.

5. REFERENCES

1. D. Zenkert, "The Handbook of Sandwich Construction", EMAS, 1997
2. C. Berggreen, "Non-uniform Compressive Strength of Debonded Sandwich Panels – II. Fracture Mechanics Investigation", *J. Sandwich. Struct. Mater*, 7, 483-517 (2005)
3. M.F.S.F. de Moura, J.P.M Goncalves, A.T. Marques, P.M.S.T. de Castro, "Prediction of Compressive strength of carbon-epoxy laminates containing delamination by using a mixed mode damage model", *Composite structures*, 50, 151-157 (2000).
4. R.D.S.G. Campilho, M.F.S.F. de Moura and J.J.M.S. Domingues, "Modelling single and double-lap repairs on composite materials", *Compos. Sc. Technol.*, 65, 1948-1958 (2005).
5. K.N. Shivakumar, H. Chen, A. Bargava, "Effect of geometric constraint on fracture toughness of PVC foam core sandwich beams", *Sandwich structures 7: Advancing with Sandwich Structures and Materials*, DOI: 10.1007/1-4020-3848-8-13, 131-142 (2006).
6. J.Y. Cognard, P. Davies, L. Sohier, R. Créac'hcadec, "A study of the non-linear behaviour of adhesively-bonded composite assemblies", *Compos. Struct.*, 76, 34-46 (2006).
7. A.G. Magalhaes, M.F.S.F. de Moura, J.P.M Goncalves, "Evaluation of stress concentration effects in single-lap bonded joints of laminate composite materials", *Int. J. Adh. & Adhesives*, 25, 313-319. (2005)
8. R.D.S.G. Campilho, M.F.S.F. de Moura, J.J.M.S. Domingues, "Stress and failure analyses of scarf repaired CFRP laminates using a cohesive damage model", *J. Adhesion Sci. Technol*., 21, 855–870 (2007).
9. R.A. Odi, C.M. Friend, "An improved 2D model for bonded composite joints", *Int. J. Adh. & Adhesives*, 24, 389-405 (2004).
10. D.W. Adkins, R.B. Pipes, *Proceedings of the Fourth Japan–US Conference on Composite Materials*, pp. 845–854 (1988).

11. Objois A., Assih J., Troalen, J.P., “Theoretical Method to Predict the First Microcracks in a Scarf Joint”, J. Adhesion, 81, 893–909 (2005).

8th International Conference on Sandwich Structures
ICSS 8
A. J. M. Ferreira (Editor)

EXPERIMENTAL AND NUMERICAL ANALYSIS ON MECHANICAL BEHAVIOR OF COMPOSITE SANDWICH STRUCTURES

F. E. Sezgin[a], M. Tanoglu[a*], S. B. Bozkurt[a], O. O. Egilmez[b]

[a] Mechanical Engineering Department
[b] Civil Engineering Department
İzmir Institute of Technology
Gülbahçe Campus, 35437 Urla, İzmir, Turkey
E-mail: metintanoglu@iyte.edu.tr, fatmasezgin@iyte.edu.tr,
baharbozkurt@iyte.edu.tr, ozguregilmez@iyte.edu.tr
Web page: http://www.iyte.edu.tr/mechweb, http://www.iyte.edu.tr/civil

Key words: Composites, sandwich structures, modeling, mechanical properties

Summary: *The aim of this study is to manufacture polypropylene based honeycomb cored composite sandwich structures with prescribed core thicknesses and to evaluate mechanical properties. The experimental results will be correlated with the finite element analysis results.*

1 INTRODUCTION

Sandwich composite structures have been applied in aerospace applications and civil infrastructures due to their low weight, high flexural stiffness, high transverse shear stiffness and corrosion resistance [1-2]. In addition, these materials have high structural crashworthiness because in a sudden crash they are capable of absorbing large amounts of energy. In general, two thin stiff facesheets and a thick lightweight core bonded between them are the components of the sandwich structures. The mechanical properties of the sandwich structure and their components have great importance in terms of industrial applications. According to the design needs, optimum material types can be employed [3-5]. Various combinations of core and faceplate materials are utilized by researchers worldwide in order to achieve improved crashworthiness [6].

In a sandwich structure, strong and stiff facesheets carry the bending loads where the low density core material carries the shear loads [3-6]. The core material has a purpose to keep the facesheets separated in order to maintain a high moment of inertia, also it has relatively low

* Corresponding autor: Dr. Tanoglu, Tel: 90 232 7507806

density (e.g., honeycomb or foam), which results in high specific mechanical properties of the panel under loadings. Therefore, sandwich panels are efficient in carrying bending loads. Additionally, they provide increased buckling resistance to shear panels and compression members [6]. When the structure is subjected to bending, the laminates act together, resisting the external bending moment so that one laminate is loaded in compression and the other in tension. The core resists transverse forces, at the same time, supports the laminates and stabilizes them against buckling and local buckling [3].

Composites are more difficult to model than an isotropic material such as iron or steel because each layer may have different orthotropic material properties, therefore while defining the properties and orientations of the various layers, great attention must be paid and element type, layer configuration, failure criterion must be defined properly for the purpose of accurate modeling [7-8]. Composite sandwich structures have also the problem intrinsic anisotropy and non-homogeneity that complicate their correct modeling [2].

In this work the main objective is to improve the understanding of the failure mechanisms of the composite sandwich structures. Therefore, glass fiber reinforced/PP based honeycomb cored composite sandwich structures were developed by hand lay-up lamination technique and in order to understand the mechanical and energy absorption behavior of the sandwich structures as a function of core thickness, flatwise compression (FC), edgewise compression (EC) and three point bending (3PB) tests and the PP based core material flatwise compression tests were conducted on the corresponding specimens for various core thicknesses,.

The modeling of these sandwich structures are being carried out with three dimensional finite element (FE) models. Commercial ANSYS 11 finite element analysis software is being used for utilizing the test data in order to predict the mechanical behaviors of the sandwich structures. In the finite element analysis, the test results of each constituent are being evaluated as the input data for ANSYS and the linear elastic material properties are being used. The experimental data are being compared with numerical results.

2 EXPERIMENTAL

2.1 Materials

E-glass non-crimp fabrics, epoxy thermosetting resin and polypropylene based honeycomb core materials were used to fabricate composite sandwich panels (Fig.1). As the reinforcement constituent of composite facesheets, E-glass 0°/90° non-crimp fabrics were provided by Telateks Inc., İstanbul, Turkey. Resoltech™ epoxy resin with an amine hardener was used as the matrix polymer. PP based core material with hexagonal cell configuration and five different core thicknesses (5, 10, 15, 20 and 40 mm) were used in the fabrication of the sandwich panels.

2.2 Composite fabrication

The sandwich structures were laminated by hand lay-up technique in which, glass fabrics were wetted by epoxy resin and the core material was laminated with the upper facesheet of the sandwich structure in a mold, coated with a mold release agent. After the lamination procedure, composites were cured at room temperature under the pressure of 50 kPa. A post curing for 2 hours at 100°C was applied in an oven after curing.

Figure 1: Core material and sandwich structure samples fabricated in this study.

2.3 Mechanical property characterization

To determine the mechanical properties of the fabricated sandwich structure, Schimadzu™ AGI universal test machine was used according to the ASTM specifications and for each testing at least five specimens were tested. Test techniques, ASTM numbers and measured properties can be seen in Table 1.

Test	Standard	Testing Speed	Measured Properties
Flatwise compression test	ASTM C365-00	0.5 mm/min	Compression strength Compression modulus Energy absorption characteristics
Edgewise compression test	ASTM C364-99	0.5 mm/min	Energy absorption characteristics Collapse modes Facing compressive stress
Three point bending test	ASTM C393-00	3 mm/min	Core shear stress Facesheet bending stress Panel bending stiffness

Table 1: Test methods that were used in order to determine the mechanical properties of the sandwich structure

2.3 Finite element analysis

Numerical simulations are being conducted by using ANSYS (2007) finite element software. An 8-node finite strain element (SHELL 281) is being used for the purpose of modeling the constituents and the whole sandwich structure. The finite element parameters (number of nodes, elements) vary according to the thicknesses of the core material. In order to obtain reliable data, the aspect ratio of the elements stayed within 1:3.

Experimental results were used as material data and composite modeling was done for the non-crimp E-glass fibers. The post-elastic analysis is neglected in order to achieve a numerical solution rather simple and applicable to characterize the composite sandwich structure by a numerical procedure in the elastic region.

The numerical analysis are being carried out to compare the theoretical model with the experimental results, therefore the structural behavior of the sandwich structure with different core thicknesses can be predicted before application.

3 RESULTS AND DISCUSSION

3.1 Behavior of sandwich structure

The mechanical behavior of the sandwich structures was tested. Flatwise compression test was applied to the sandwich structures and the typical mechanical behavior of the composites is exhibited in Figure 2. As seen in the load-deformation curve, elastic deformation is observed in the first linear region, after this region a drop of the load occurred due to the buckling deformation of the cell walls. In Fig 2-a, at the initial linear region, bending was not observed at the cell walls. After the first drop, the load increased slightly with a low slope and densification occurred at the folded cell walls. In Fig 2-b, specific crash energy absorption (Es,a) is also illustrated. When collapse occurs in the sandwich structure, energy absorption rate changes, slope of the Es,a curve decreases. After the densification region, load starts to increase linearly. This increase is due to the densification of the sandwich structure and it increases the energy absorption.

In Fig. 3, the flatwise compression modulus values are given as a function of core thickness. As seen from the figure, the compression modulus values are increased with the core thickness increment. This is because the FWC properties of the sandwich structures are dependent on the core material behavior [2]. The increase of the modulus with the increase of cell wall thickness is given in Fig 4 and Table 2.

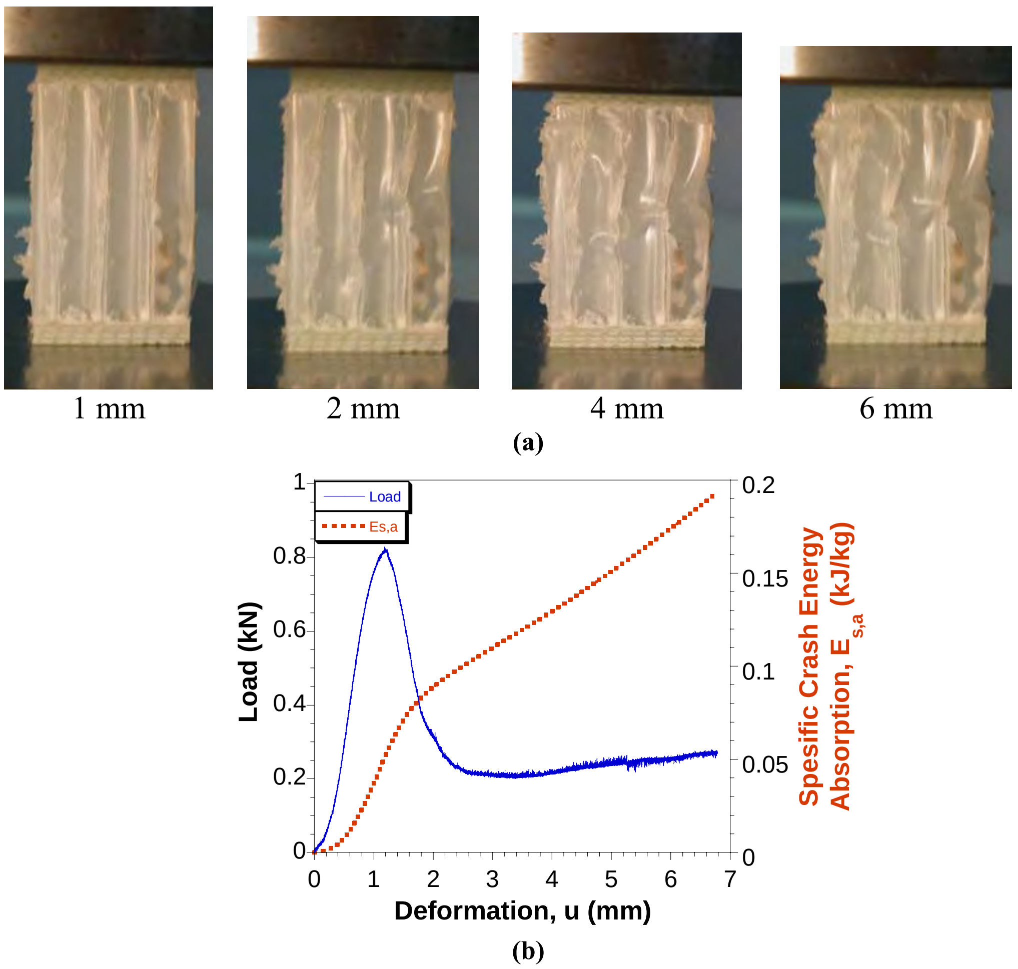

Figure 2: Behaviour of composite sandwich structures with honeycomb core material and glassfiber/epoxy facesheets under flatwise loading: (a) collapse sequence images and (b) load-deformation graph of the test specimen and the specific crash energy absorption, Es,a graph during the test.

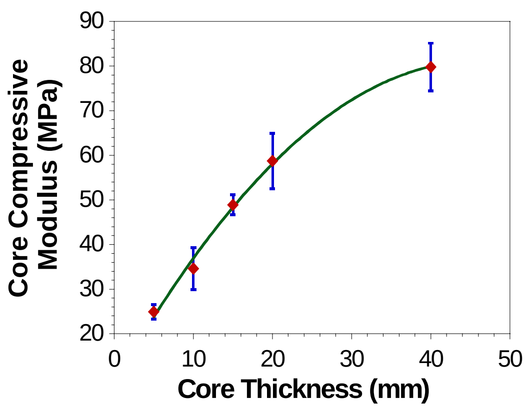

Figure 3: Flatwise compession modulus change as a function of core thickness of honeycomb cored, E-glassfiber/epoxy composite sandwich structures under flatwise compression loads

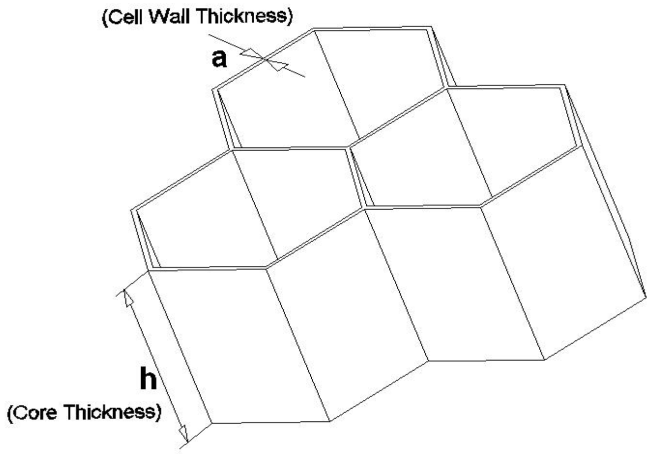

Figure 4: Polypropylene based honeycomb core representation

Core Thickness (h) (mm)	Cell Wall Thickness (a) (micrometer)
5	209.90 (±15.39)
10	220.83 (±18.96)
15	233.3 (±17.25)
20	262.44 (±13.67)
40	260.00 (±18.74)

Table 2: Honeycomb core cell wall thickness values for various thicknesses.

Edgewise compression test was applied for the sandwich structures and their mechanical behavior was evaluated for varying core thicknesses. Typical load-deformation graph, specific absorbed crash energy variation and collapse sequence images of the sandwich structure with 20 mm core material is given in Fig. 5. Absorbed crash energy was calculated from the area under the load-deformation curve. Specific crash energy absorption (absorbed energy/weight of the composite) determines the influence of core thickness for the energy absorption capacity. Under the edgewise compression loading, facesheets are the load carrying members and the core material does not have significant contribution on the strength. Under this loading configuration, the first linear part of the load-deformation curve indicates the elastic deformation of the sandwich structure. Sandwich panel buckling initiated with the de-bonding of the core and facesheets at the edge of the panels. The shear failure occurred at the interface between the core and the stiffer facesheet laminate. Failure occurred in the compressed side of the core, the opposite side, remained perfectly bonded to the facesheet. The deflection of the panel increased as the compression continues and this causes high frictional resistance. At the large deformation ratios, facesheets fractured. The fracture of the facesheets started from the tensioned face and continued through the thickness. This mode of collapse is called "sandwich panel column buckling" as also reported in the literature [3]. In this stage, bending resistance of the sandwich structure decreases, therefore, crash energy absorption decreases.

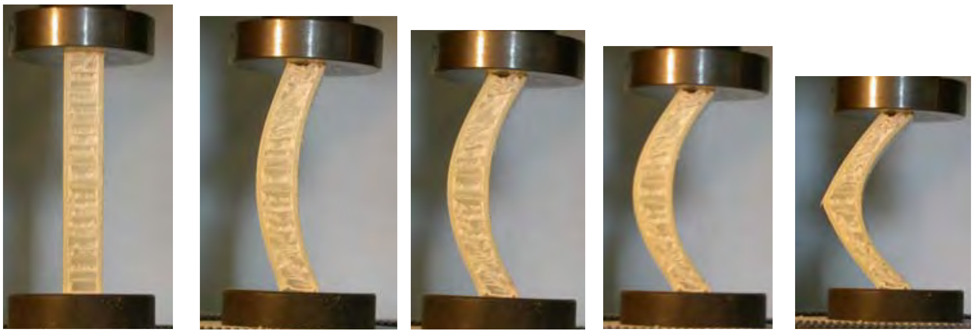

1mm 5mm 10mm 15mm 25mm

(a)

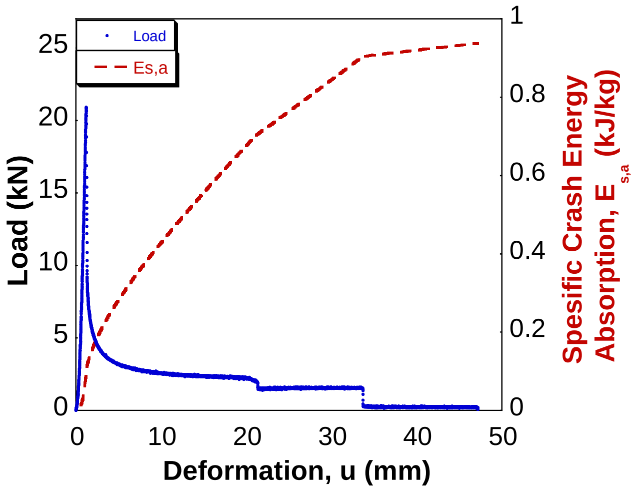

(b)

Figure 5: Behaviour of composite sandwich structures with honeycomb core material and glass fiber/epoxy facesheets under edgewise loading: (a) collapse sequence images of the specimen and (b) load-deformation graph of the test specimen and the specific crash energy absorption, Es,a during the test.

Three point bending test was applied to the sandwich structures and core shear stress and facesheet bending stress variation in accordance with the core thickness increment was evaluated. As it can be seen from Figure 6 (a) and (b), these values decreased with the core thickness increment. This results show that, core shear stress decreases while the core thickness is increased. As it can be observed from Figure 7, panel bending stiffness increased with the core thickness increment.

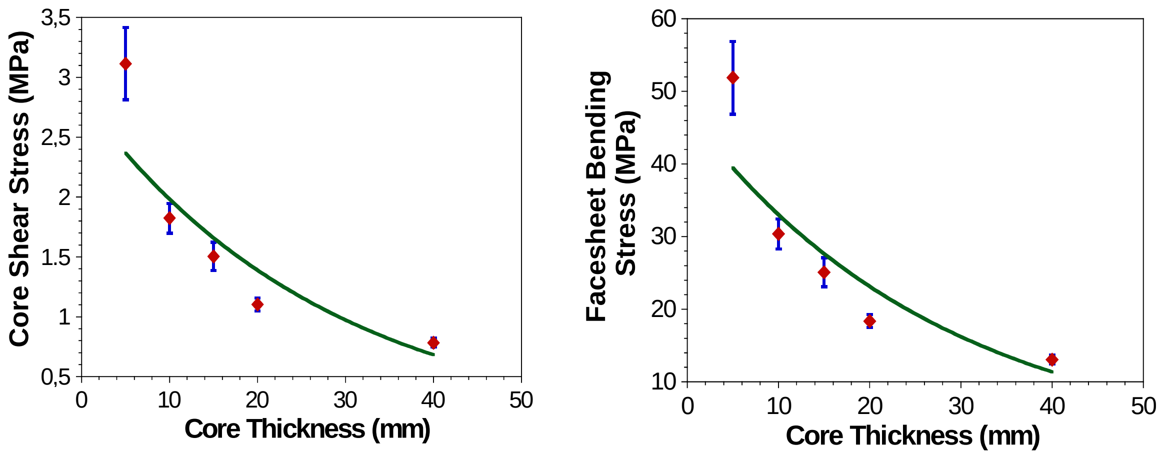

(a) **(b)**

Figure 6: Behaviour of composite sandwich structures with honeycomb core material and glassfber/epoxy facesheets under three point bending loading (a)core shear stress, (b)facesheet bending stress variation with the core thickness increment

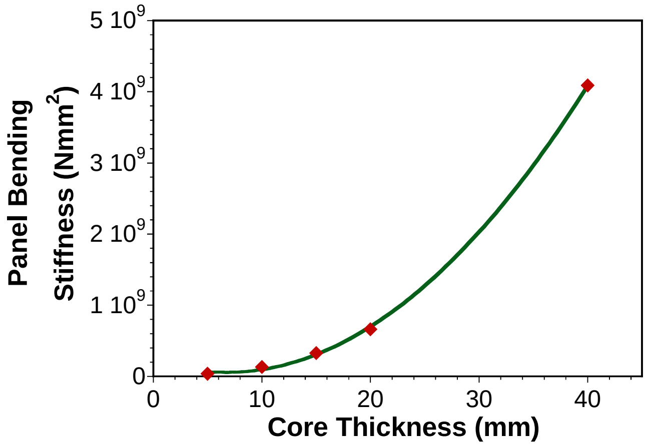

Figure 7: Variation of the panel bending stiffness of composite sandwich structures with honeycomb core material and glassfber/epoxy facesheets under three point bending loading in accordance with core thickness increment

3.3 Finite element analysis

In order to analyze composite sandwich structures by finite element analysis technique, polypropylene based honeycomb core was analyzed for the compression test first. For this analysis, the cell walls of the 5 mm honeycomb core (Fig. 4) were considered as one element and the material properties of the bulk material were taken from literature. For the second step, each cell wall was considered as composed of 4, 9 and 16 elements. Each model was analyzed under the same load and the deformation values were evaluated. As a result, the optimum element number for the honeycomb core material was obtained as 9 elements for each cell wall (Fig. 8).

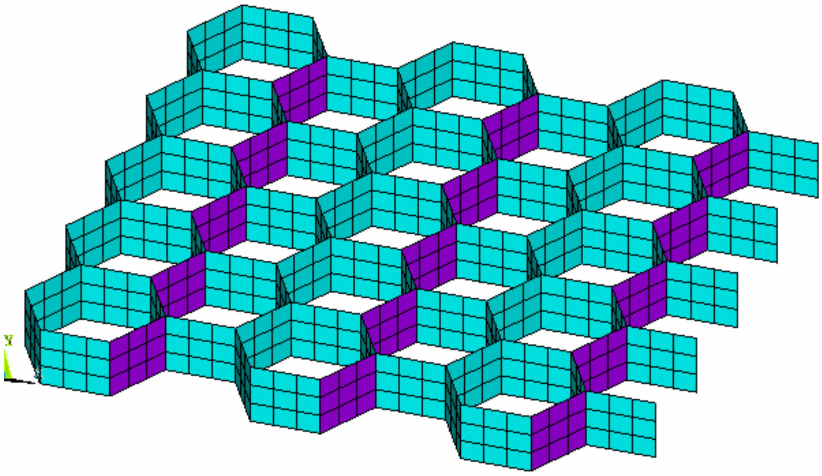

Figure 8: Flatwise compression test sample of a PP based honeycomb core modeled with optimum element number

Additional finite element analysis is being carried out for the purpose of comparison between experimental and numerical data as well as to provide an improved model of the composite sandwich structures. The obtained results will be presented within the study.

9 CONCLUSIONS

In this study, the mechanical properties of composite sandwich structures fabricated with E-glass fiber/epoxy facesheet and polypropylene (PP) based honeycomb core were evaluated.

Application of the flatwise compression test to the sandwich structure showed that, compression strength and modulus increased with the core thickness as a result of honeycomb cell wall thickness increase. During the test, honeycomb core cell walls buckled and densificated. This caused a continuous increase of the load following the sudden decrease of the maximum load level. In addition, it was observed that only the core material influences the flatwise compressive properties of sandwich panel.

Under the edgewise compression loading of sandwich structures, facesheets bended and failure occurred at large deformation values. In the edgewise compression test, mostly "sandwich panel column buckling" collapse mode was observed.

Three point bending test results showed that core shear stress and facesheet bending stress decreased while the panel bending stiffness increased with the core thickness increment.

REFERENCES

[1] K. Shivakumar, H. Chen and S. A. Smith "An evaluation of data reduction methods for opening mode I fracture toughness of sandwich panels", *Journal of Sandwich Structures and Materials*, 7, 77-90 (2005).

[2] C. Borsellino, L. Calabrese, A. Valenza, "Experimental and numerical evaluation of sandwich composite structures", *Composite Science and Technology*, 64, 1709-1715 (2004).

[3] W. J. Cantwell, R. Scudamore, J. Ratcliffe, P. Davies, "Interfacial fracture in sandwich laminates", *Composite Science and Technology*, 59, 2079-2085 (1999).

[4] A. W. van Vuure, J. Pflug, J. A. Ivens, I. Verpoest, "Modelling the core properties of composite panels based on woven sandwich-fabric preforms", *Composite Science and Technology*, 60, 1263-1276 (2000).

[5] A. Ural, A. T. Zehnder, A. R. Ingraffea, "Fracture mechanics approach to facesheet delamination in honeycomb: measurement of energy release rate of the adhesive bond", *Engineering Fracture Mechanics*, 70, 93-103 (2003).

[6] A. G. Mamalis, D. E. Manolakos, M. B. Ioannidis, P. D. Papapostolou, "On the crushing response of composite sandwich panels subjected to edgewise compression: experimental", *Composite Structures*, 71, 246–257 (2005).

[7] Release 11.0 Documentation for ANSYS

[8] R. R. Tanov, *A Contribution to the Finite Element Formulation for the Analysis of Composite Sandwich Shells*, PhD Thesis, University of Cincinnati, 2006

8th International Conference on Sandwich Structures
ICSS 8
A. J. M. Ferreira (Editor)

EFFECT OF THE FORMING PROCESS OF THE FOAM CORE ON THE MECHANICAL PROPERTIES OF A CURVED SANDWICH BEAM

Pascal Casari, Frédéric Jacquemin and Annick Perronnet
Institut de Recherche en Génie Civil et Mécanique (GeM)
Université de Nantes
2 rue de la Houssinière, 44300 Nantes, France
e-mail: Pascal.Casari@univ-nantes.fr, Frederic.jacquemin@univ-nantes.fr,
web page: http://www.univ-nantes.fr

Key words: Sandwich structure, curved beam, bending, PVC foam, gradient, manufacturing.

Summary. *The focus of this work is put on the thermoforming process applied on a foam core in order to manufacture a curved sandwich structure. This step induces a density gradient across the width, and consequently an effect on the mechanical behavior of the sandwich structure.*

1 INTRODUCTION

Actual publications model the behavior of a sandwich structure considering a core material without any gradient across the width, or just a pre-existing gradient. It has been shown in [1] that the core was affected by a density gradient across the width. All this was not considering curved structures and especially the thermoforming process of the core. In fact, this manufacturing step induces a density gradient followed by an evolution of the mechanical properties. Moreover, some residual stresses are created and may affect the geometrical stability of the structure [2]. These components have been assessed in order to provide both a highlight on the manufacturing process of PVC foam cores and a set of experimental results to be included in thermo mechanical modeling of sandwich structures.

2 MATERIALS AND METHODS

The experiments are conducted on a sandwich curved beam (Figure 1). A foam core flat panel (a) (Airex C70 – 200 kg/m3, 50 mm thick) is curved under vacuum (b) in a climatic chamber at 130°C. The skins are manufactured by wet layup (c) of 8 E-glass fabrics comprised of balanced woven roving (350g/m²) and chopped roving (300g/m²) stitch-bonded together with an epoxy resin. The skins of the sandwich part are joined at the ends as monolithic laminates and clamped to the testing machine (d) by means of eye-shaped heads ensuring free rotations.

a)

b)

c)

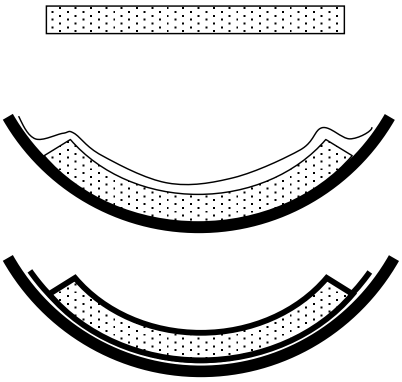

Beam dimensions and mechanical properties:

- Internal radius: 380 mm
- External radius: 442 mm
- Width of the beam: 110 mm
- Skin thickness: 6 mm
- Foam thickness: 50 mm
    - Distance from the loading axis to the internal skin: 150 mm.
- Elastic modulus of the foam: 200 MPa

d)

Figure 1. Foam core process and curved beam under tensile test

2.1 Initial foam core properties

The foam density profile has been measured by means of a procedure explained in [1]. Density across the width is obtained by matter removal. Some coarse parallelepipedic foam samples are cut from a raw foam panel and the shape of the remaining piece is corrected by means of a polishing operation. Then, the samples are weighed before and after the removal of thin layers of approximately 2 mm by a mechanical polishing. Specific care is brought in order to keep the surfaces plane and parallel. The density is then estimated by measuring the weight and the dimensions of the body as shown in Figure 2.

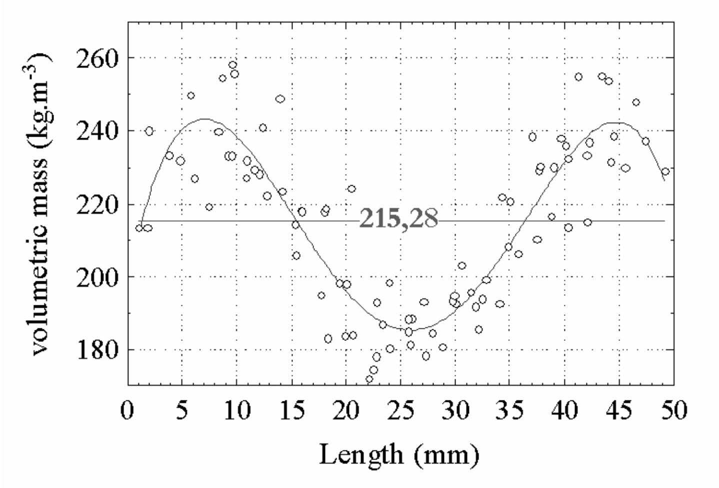

Figure 2. Architecture of the microstructure of the PVC foam core.

The next step is the thermoforming of the foam core before laminating the skins. The specimen is marked on both sides, heated up to 130°C and bended into a female mould with an internal radius of 430 mm. Some marks have been previously put on the faces of the foam panel in order to estimate the strains of the expanded and the shrunk sides. An overview of the result and the corresponding elastic Young's modulus is given in Figure 3. The evolution of this modulus is assumed to be fully correlated to the density across the width, with an average of 200 MPa.

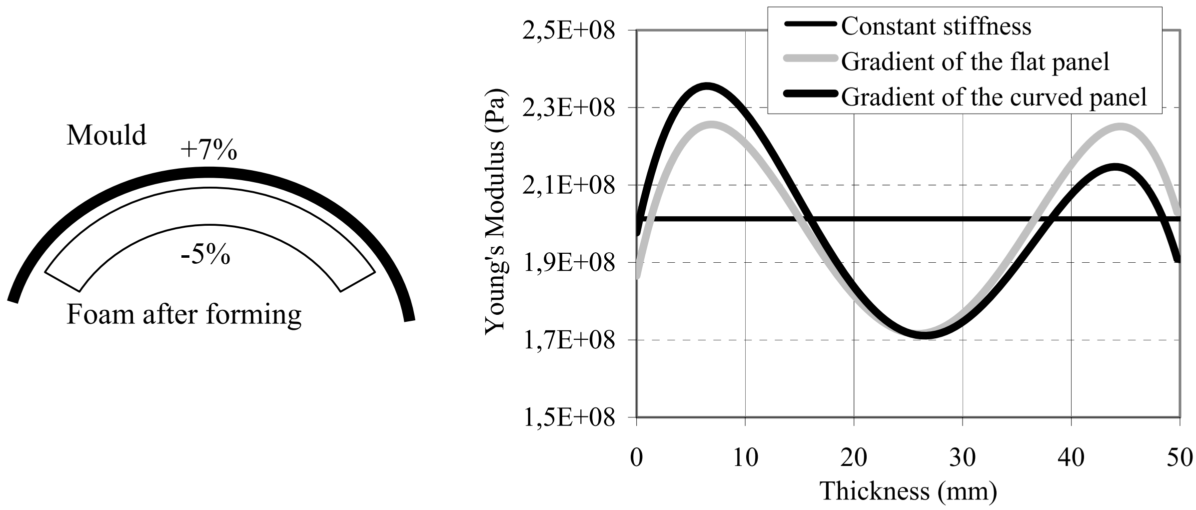

Figure 3. Strains due to the thermoforming step under vacuum against a mould and corresponding stiffness.

This result suggests that the density profile should be updated in order to take both the gradient of density and the thermoforming step into account. The density increases in the inside of the curve and decreases in the outside.

2.2 Microstructure

A set of pictures is taken in order to highlight a difference in the microstructure across the width (Figure 4).

The first picture (a) is located on the top of the sample and reveals the effect of the expansion of 7% associated to a density above the average.

The second picture (b) shows quite big cells provided by the initial foaming process.

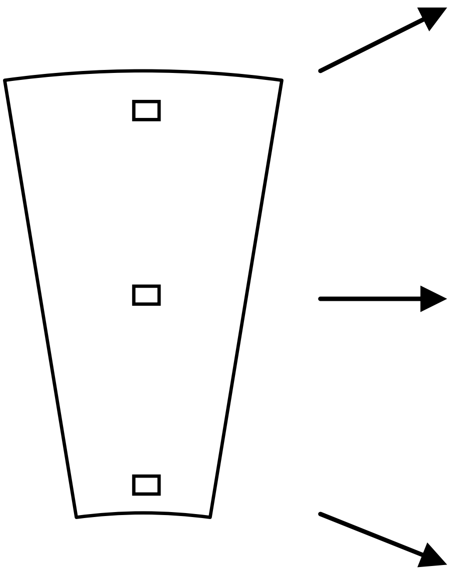

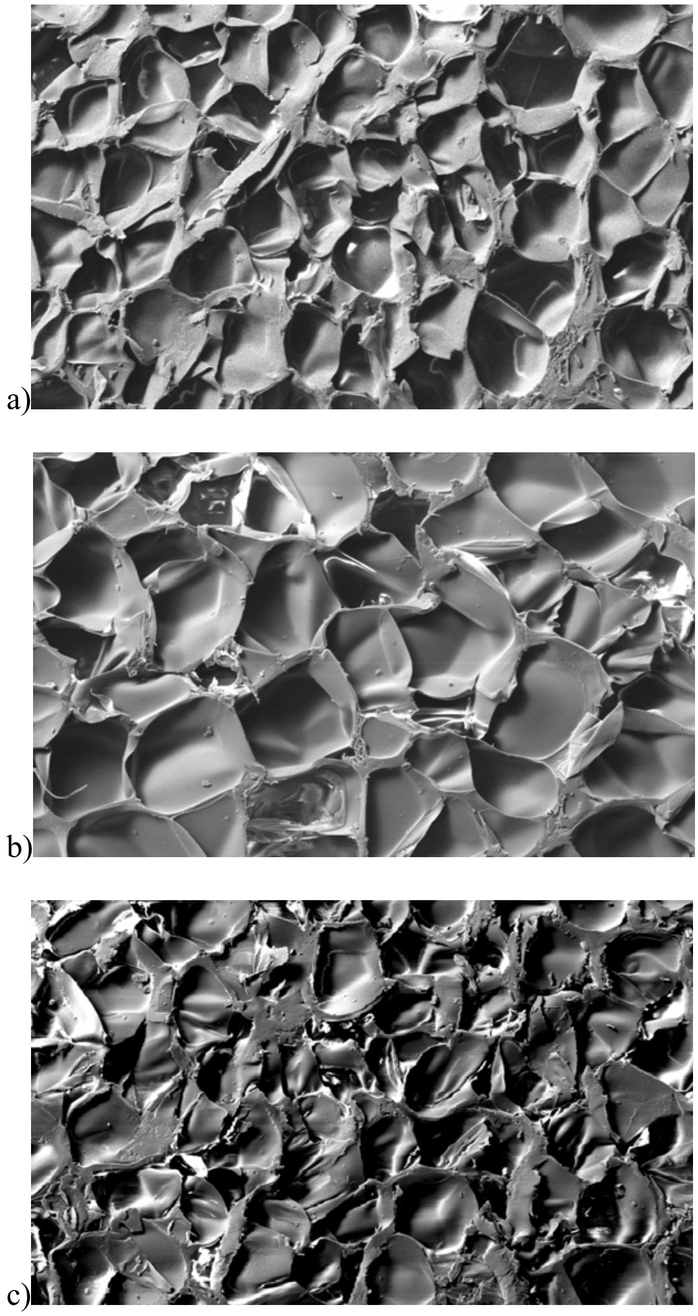

The third picture (c) gives a set of cells shortened in the horizontal direction. The cell walls look creased.

The pictures width represent 2.2 mm of the foam core

Figure 4. Microstructure of the PVC foam core.

Foam core manufacturers often provide manuals in order to adopt the right parameters for PVC foam core thermoforming. It consists in applying a temperature in combination to weights or vacuum. Here, the foam core is thermoformed at 125°C under vacuum. The key point of the process consists in maintaining the foam specimen at high temperature; otherwise the surfaces of the panel cool down rapidly, which leads to crack and failure.

3 MECHANICAL TESTING

A tensile test is conducted on the curved sandwich beam (Figure 1) in order to apply a bending load in combination to shear and transverse deformations. Here the effect of the supports is not significant compared to the one of bending tests [3]. Indeed, the load is applied at the ends of the specimen.

Strains are measured by means of pictures taken from the side of the beam; a reference picture before loading and a deformed picture once load is applied. Then they are analyzed by means of a Digital Image Correlation technique [4]. This kind of investigation is now well known, and provides a full displacement field which can be derived in order to get the strains of the observed surface. The size of a pixel is approximately 0.05 mm. The natural roughness of the core provides a satisfactory random pattern is size and in gray level. A typical strain field is given in Figure 5. The peaks are produced mostly by a random noise and the absence of smoothing of the results.

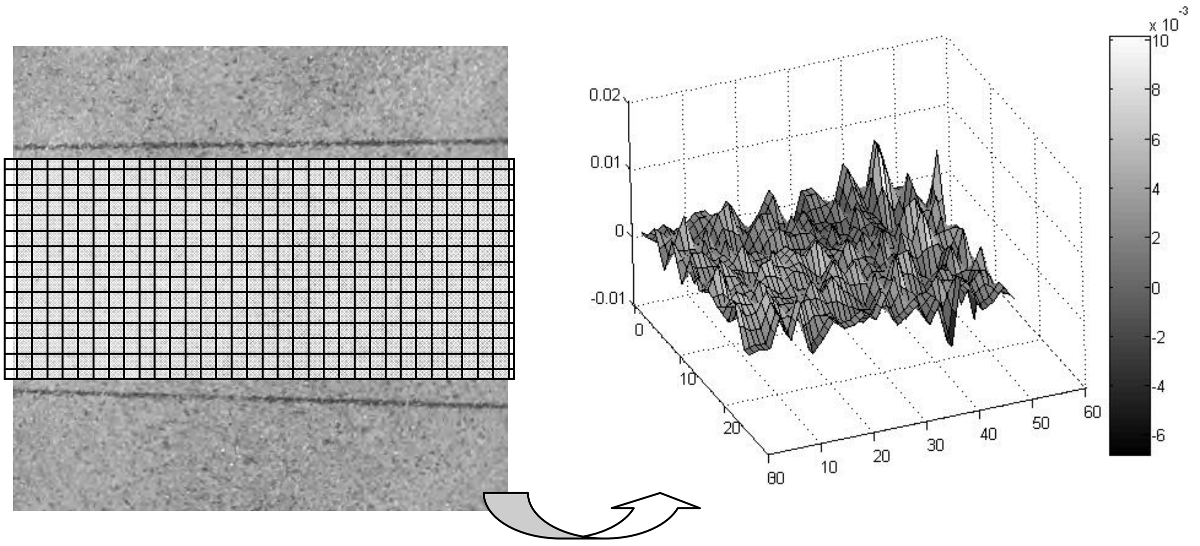

Figure 5. Strain field from Digital Image Correlation

The method is applied to the specimen (Figure 6). Two areas (a) or (c) have been selected in order to quantify strains by deriving displacements. A mesh is defined across the width of the foam core (b) or (d) and each square is statistically analyzed on the deformed picture in order to find the displacement of its center which provides the best correlation with a square from the reference picture, and displacements can be drawn over the analyzed surface. Finally, strains are given across the width and reveal scatter which is mostly due to some defects in the random pattern of the picture.

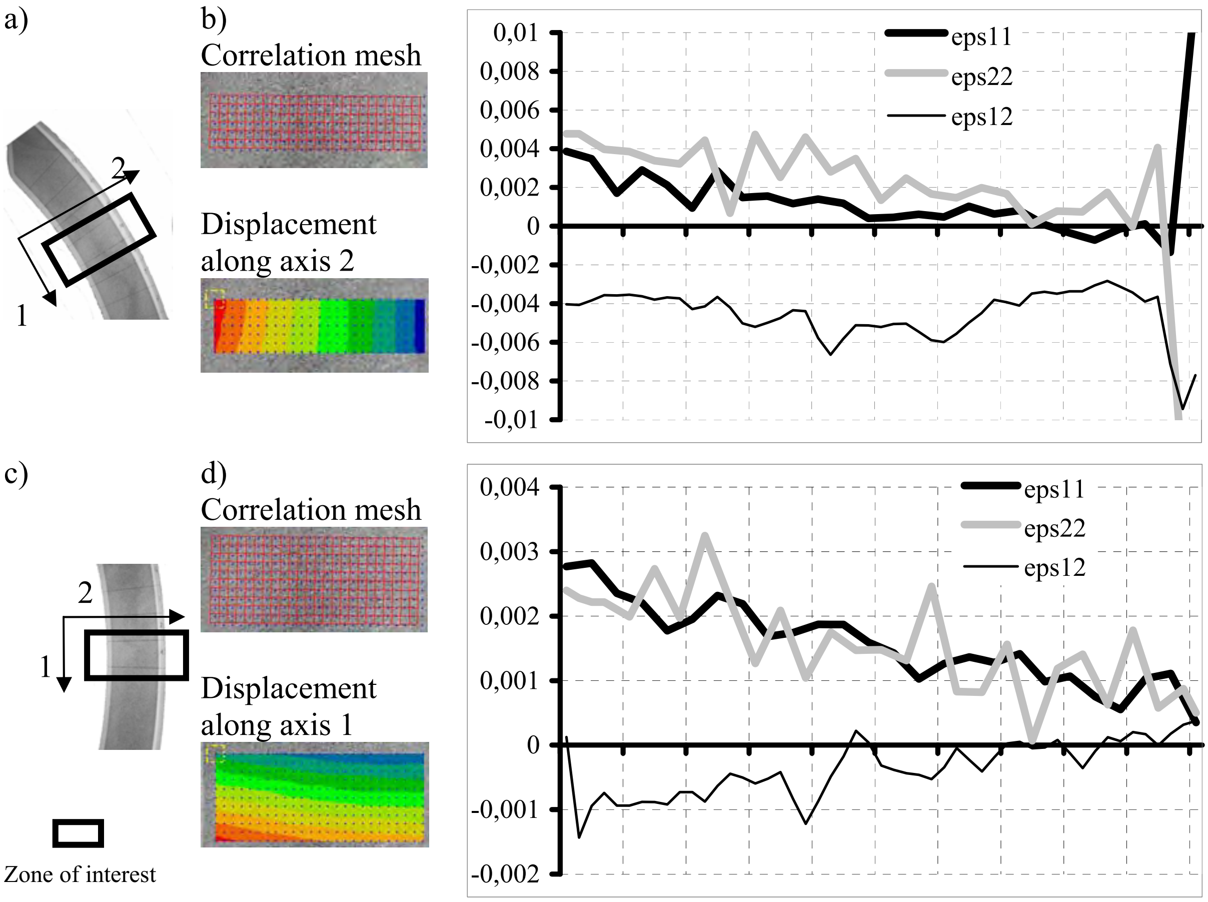

Figure 6. Digital Image Correlation overview and strains across the width.

4 MECHANICAL MODELING

The beam is modeled with Finite Elements under plane strain state and two hypotheses are assessed: the first one with constant elastic stiffness for the core, and the second one with a variable elastic stiffness across the width. Here the focus is put on the effect of a gradient of mechanical properties in the core on the mechanical response of the sandwich structure, even if some studies provided efficient tools for the calculation of the mechanical response of sandwich curved structures [5, 6]. The evolution of the variable Young's modulus was drawn in Figure 3 and the strain profiles are drawn in Figure 7.

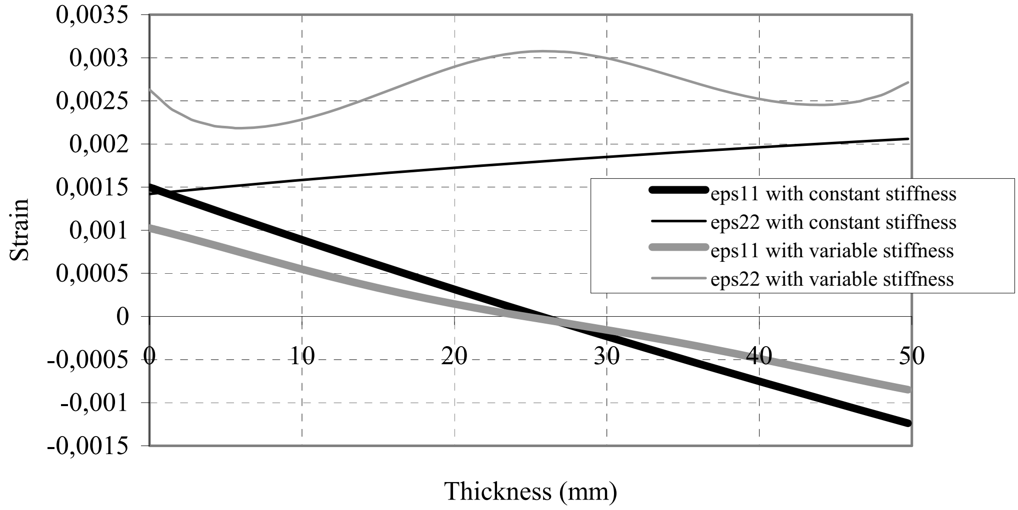

Figure 7. Strain profiles across the width with or without stiffness gradient in the core.

The strains estimated by the model (Figure 7) are far from the ones measured during the tests (Figure 6). This mismatch could be due to an edge effect which leads to invalidate the hypothesis of plane strains or to a symmetry defect.

5 CONCLUSION

The application of sandwich structures under curved shapes leads to a specific analysis because of the foam core thermoforming process. It has been shown that the core undergoes a significant variation in morphology, and therefore in density and stiffness across the width. Firstly, this effect has been shown by means of a micro structural observation. The cell size of the core looks bigger outside the curved shape and smaller inside the curve.

Secondly, the thermoforming step shows a variation of maximal and minimal strains with an increase of 7% of elongation on the extended side, and 5% of shrinkage on the compressed side of the foam panel. This significant variation has been chosen to define a linear stiffness variation across the width, which is added to the one from the initial foam core process. Then the impact of such density variation is assessed by means of a test on a curved sandwich beam. A tensile test is conducted and a corresponding mechanical model is defined in order to evaluate the strain profiles. There is a mismatch between the model and the test results which could be assessed by improving the representation of the structure through a 3D effect.

Aknowledgments: The authors are grateful to Alcan Composites Company for providing the foam core samples. They would like to thank Michel Roche and Jean-Michel Lebrun, from the University of Nantes, for managing the manufacture of the sandwich beams the fixtures.

REFERENCES

[1] C. Ferreira, F. Jacquemin, P. Casari. "Measurement of the Non-uniform Thermal Expansion Coefficient of a PVC Foam Core by Speckle Interferometry - Influence on the Mechanical Behavior of Sandwich Structures". *Journal of Cellular Plastics; vol. 42: pp. 393 - 404, 9 2006.*

[2] P. Casari & L. Gornet. "Characterization of residual stresses in a composite curved sandwich beam". Composites Part A: Applied Science and Manufacturing, Volume 37, Issue 4, April 2006, Pages 672-678.

[3] A. M. Layne, L. A. Carlsson. "Test method for measuring strength of a curved sandwich beam". *Experimental Mechanics, Volume 42, Number 2 / June, 2002*

[4] S. Bergonnier, F. Hild, S. ROUX. "Digital image correlation used for mechanical tests on crimped glass wool simples". Journal of Strain Analysis for Engineering Design. Vol 40. Num 2. Pages 185-198. 2005

[5] E. Bozhevolnaya & Y. Frostig. "Non-linear closed-form high-order analysis of curved sandwich panels", Composite Structures, Vol. 38, No. 1-4, 1997, pp. 383-394, ISSN 0263-8223.

[6] A. Lyckegaard and O. T. Thomsen. "Nonlinear analysis of a curved sandwich beam joined with a straight sandwich beam". Composites Part B: Engineering. Volume 37, Issues 2-3, April 2005-March 2006, Pages 101-107.

[7] Zenkert, D. (1995). "An Introduction to Sandwich Construction". Chameleon Press Ltd., London.

NEW MATERIALS

8th International Conference on Sandwich Structures
ICSS 8
A. J. M. Ferreira (Editor)

LATEST DEVELOPMENTS ON HIGH PERFORMANCE SANDWICH FOAM CORES BASED ON PMI

Hermann F. Seibert*

* Evonik, Röhm GmbH
Kirschenallee, 64293 Darmstadt, Germany
e-mail: hermann.seibert@evonik.com, web page: http://www.rohacell.com

Key words: Sandwich Structures, Mechanical Properties, Foam, ROHACELL®

Summary. *This article introduces the development on a new high performance sandwich foam core based on Polymethacrylimide (PMI). The new PMI Grade shows significant improvements regarding ductility, specific mechanical properties and specific resistance to compressive creep. The new Grade thus leads towards additional weight saving potential and better impact resistance.*

1 INTRODUCTION

Due to high strength- and stiffness-to-weight ratio compared to monolithic structures, sandwich constructions are widely used in aerospace, marine and other transport applications Sandwich structures consist of an upper and a lower face sheet bonded to a low density lightweight core material. The stiff and strong face sheets carry the in-plane stresses while the core carries the shear stresses produced by transverse loads. Sandwich structures are particularly suitable for bending and in-plane compression load cases.

ROHACELL® is a family of closed-cell **P**oly**M**ethacryl**I**mide (PMI) foams that are ideally suited for strong and lightweight sandwich construction. PMI structural sandwich foam cores offer the highest level of specific stiffness and strength, good fatigue properties, high temperature resistance (up to 230°C) and unsurpassed resistance to compressive creep. Over the years, 9 different Grades have been developed to meet specific demands in specific fields of applications, ranging from sports applications to aerospace applications.

Driven by the constant demand for improvement, a new generation of even more advanced and higher performance PMI foam, has been successfully developed. This new PMI foam is called ROHACELL® HP.

The paper will summarize the property profile of the already existing product range and will introduce this new Grade. It will be shown that significant improvements regarding specific resistance to compressive creep could be achieved, leading towards significant part weight savings.

Furthermore it will be shown that the new Grade is more ductile, compared to the already existing Grades, but still offers unsurpassed specific material properties.

Sandwich technology contributes significantly to solving weight problems in many fields of application, in particular in transportation. If we focus on the manufacture of aircraft components, mostly NOMEX® and aluminium honeycombs are used as core materials. They offer excellent strength-to-weight and modulus-to-weight ratios.
On the other hand, the non-isotropic and open-cell character of honeycombs causes some problems during core shaping and curing of sandwich components. Honeycombs do not withstand lateral forces/pressures and tend to collapse during core shaping and sandwich cure. They do not fully support prepreg layers during cocuring operations, which results in surface imperfections, zones of poor laminate consolidation and fibre disorientations, leading towards the necessity to introduce knock-down factors into the design calculation. [1, 2, 3]. Fig. 1

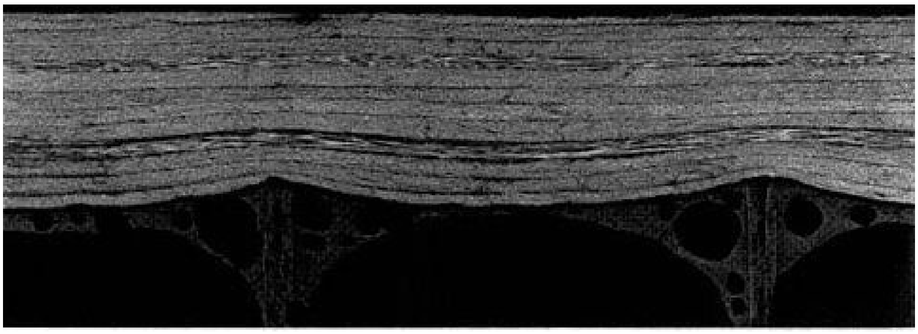

Figure 1: dimpling and laminate imperfections of HC sandwich skins

Another major problem is extensive moisture absorption and corrosion, which limits the performance of the component and causes increased expenditure for repair and higher service life costs [4].

2 HISTORY OF PMI FOAMS – ACTUAL PRODUCT PORTFOLIO

In 1967 the first generation of PMI sandwich foam cores was introduced at the K-Exhibition in Düsseldorf. Already in 1971 the material was successfully introduced as structural sandwich core for helicopter fuselage panels. Today PMI foams are called out in more than 190 specifications worldwide, 96% being aerospace specifications.

Beside a range of products for industrial applications such as sporting goods, wind turbine blades, medical equipment, railcar structures, ship, antennae, electromagnetic and automotive applications, a range of different PMI Grades suitable for aerospace applications have been developed over the years.

These can be subdivided as follows:

- PMI for autoclave cure

- ROHACELL ® A suitable for autoclave cure up to 125°C at 0,3 MPa pressure
- ROHACELL ® WF suitable for autoclave cure up to 180°C at 0,7 MPa pressure
- ROHACELL ® XT suitable for autoclave cure up to 190°C at 0,7 MPa pressure post cure temperature up to 230°C

- PMI for RI (Resin Infusion) and RTM (Resin Transfer Molding)

- ROHACELL ® IG-F suitable for RI, VARI – processing up to 125°C
- ROHACELL ® RIST suitable for RI (Resin Infusion) and RTM (Resin Transfer Molding) - processing up to 180°C curing
- ROHACELL ® RIMA suitable for RI (Resin Infusion) and RTM (Resin Transfer Molding) - processing up to 180°C curing, minimized surface resin absorption

Over the years the development of mew PMI Grades has always been prompted by new or increasing demands from the market. The development of the XT (e**X**tended **T**emperature) Grade marked a mile stone as resistance to creep compression in comparison to the already existing A and WF Grade could be significantly improved. The material is also suitable for BMI prepreg cure cycles and can take post curing temperatures of up to 230°C. The engine cowling of the Tiger helicopter is a good example for such a PMI/BMI sandwich application. Fig 2

Figure 2: engine cowling of Tiger helicopter

3 TAILORING THE CELL SIZE OF PMI FOAMS

As a result of a comprehensive R&D project Evonik Röhm developed a method to tailor the cell size of PMI foams. Again, demands from the markets respectively the spread out of resin infusion and RTM processes initiated the research. The goal was to develop structural foams having the same level of strength-to-weight ratio and resistance to creep compression as the A, WF and XT grade but a much smaller cell size. Smaller cell size means lower surface resin absorption. As PMI foams are the only 100% closed cell foams minimizing surface resin absorption was key to weight saving. Surface resin absorption is simply a function of the cell diameter. Fig. 3

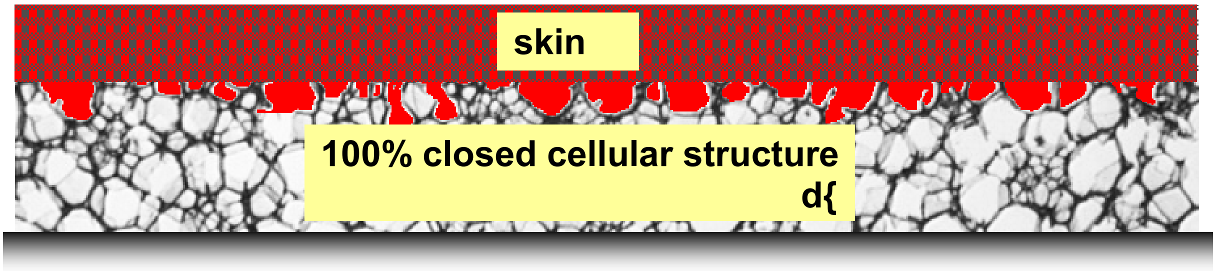

Figure 3: surface resin uptake = f(d/2)

Fig. 4 shows the difference in cell size of the WF Grade, RIST and RIMA Grade at the same magnification.

Figure 4: tailoring the cell size for RI and RTM processing

The cell size of WF Grade is suitable for prepreg type resin viscosity. Even resins with a poor flow can penetrate the cut open cells at the surface and thus realize a good skin-to-core adhesion. Based on a procedure developed and approved by the German RIM Committee (Fig 5) it could be shown that RIST Grade realizes a 50% reduction in cell size and RIMA offers another 50% reduction in cell size.

Although the cells of the 2 RI Grades are significantly smaller, good adhesion characteristics could be maintained at minimal surface resin absorption. Fig 6.

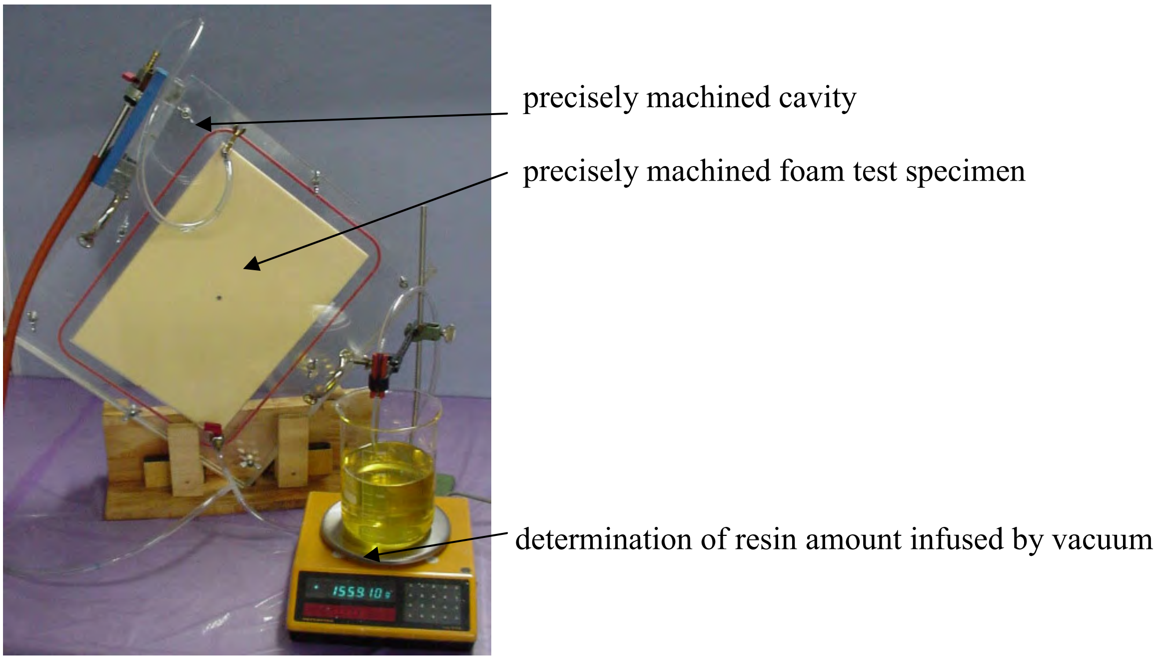

Figure 5: test equipment to determine surface resin absorption

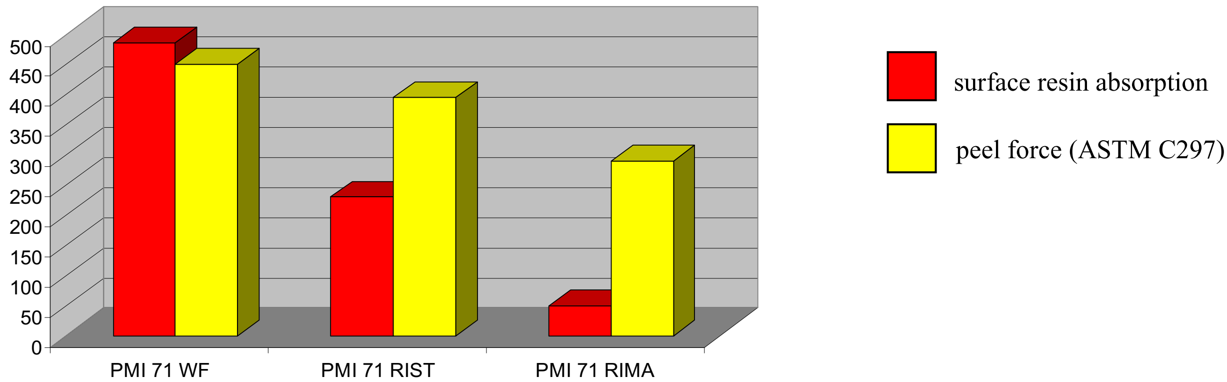

Figure 6: surface absorption vs. peel force, comparison of WF, RIST and RIMA

The 100% closed cellular structure of PMI foams makes them the ideal sandwich core material for any kind of Resin Infusion (RI) or RTM (Resin Transfer Molding) processing. Excellent results could also be obtained in the so called SLI (Single Line Injection) process, developed by DLR (German Aerospace Research Institute) [5], [6], [7]

4 EFFECTS OF SMALLER CELL SIZE ON PROPERTIES

It is already known, that the stability of polymer-based cellular structures in general is increasing if the cell size is decreasing. This is valid for PMI foams in particular, as they represent the only commercially available 100% closed cell foams. This increasing stability of the structure results in improvement of mechanical properties and also in a more ductile behavior of the foam, meaning e.g. higher elongation at break. Fig. 7, Fig. 8, Fig. 9

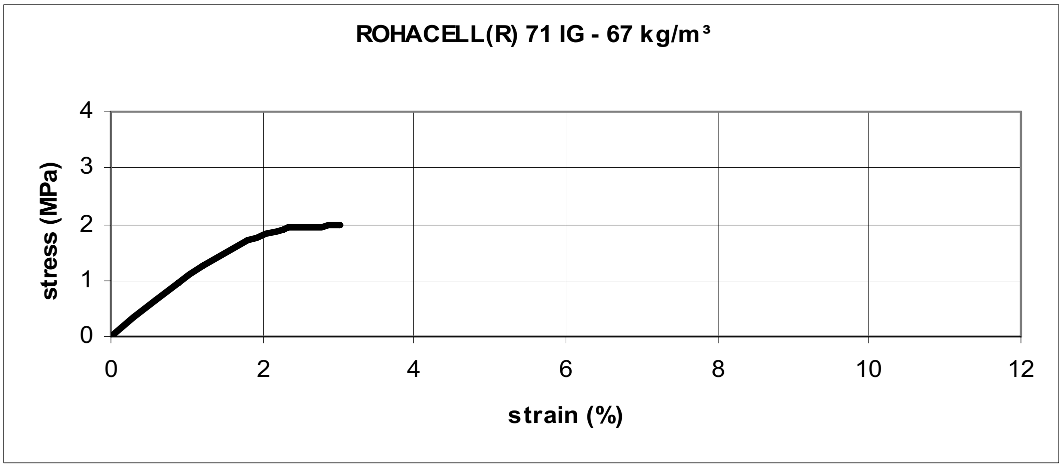

Figure 7: stress / strain diagram for IG Grade

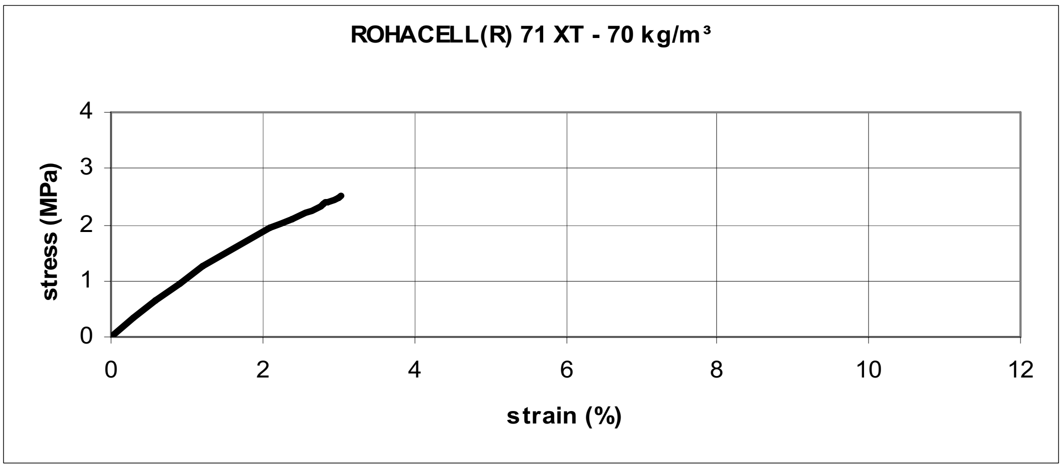

Figure 8: stress / strain diagram for XT Grade

Both PMI Grades show a similar stress / strain behavior with about 3 % elongation at break, while XT shows higher tensile strength and young´s modulus.

Fig 9 shows the stress / strain diagram for the RIMA grade having a significantly smaller cell size. Elongation at break is about 10%, while the young´s modulus is only 8% below the value for the XT grade.

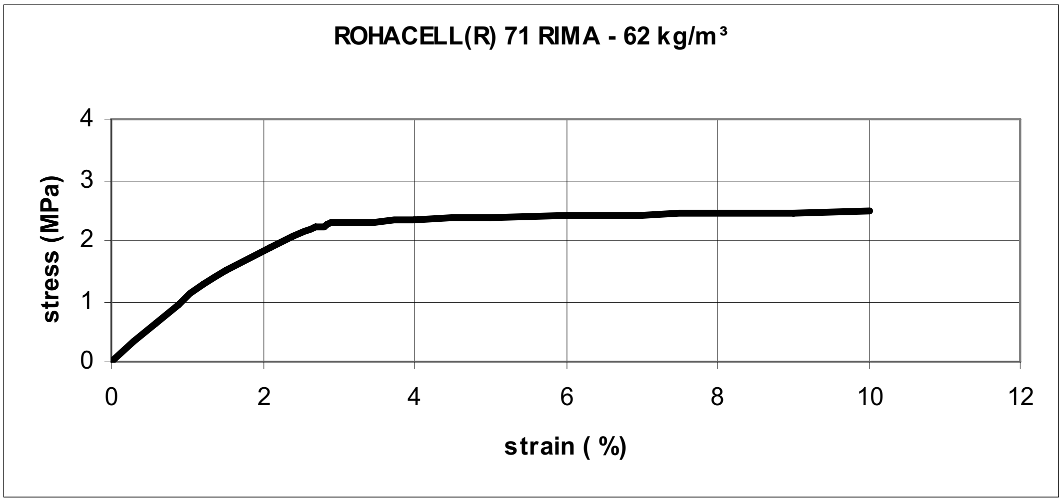

Figure 9: stress / strain diagram for RIMA Grade

5 DEVELOPMENT OF NEW PMI GRADE ROHACELL® HP

The goal of the project was to realize a new PMI Grade integrating the following properties:

1. maintain level of young´s modulus of the XT Grade
2. maintain excellent resistance to compressive creep of the XT Grade
3. significantly improved ductility

Presentation of results:

- Tensile properties

Fig. 10 shows the stress / strain diagram of the newly developed PMI Grade. Elongation at break is 7% while weight specific tensile strength and young´s modulus are exceeding those of the XT Grade.

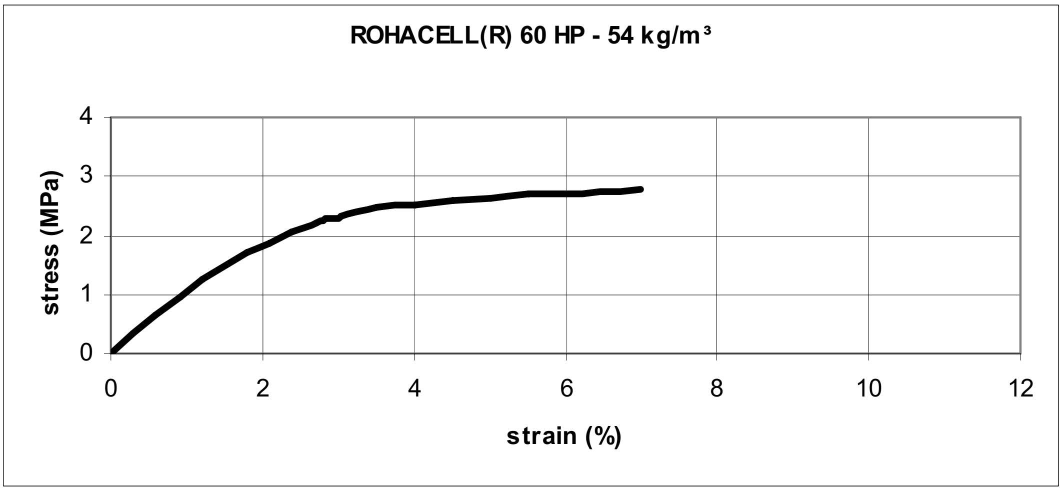

Figure 10: Stress / strain diagram of new HP Grade

- Resistance to creep compression

Fig. 11 compares creep compression results of XT Grade and new HP Grade after testing at different autoclave pressures at a temperature of 180°C, duration of cure cycle 2 hrs.

PMI foams need to be dried and or heat treated (HT) to ensure the appropriate resistance to creep compression under the given curing conditions during part manufacturing. HT means enhanced drying and does not mean any kind of additional post expansion chemical reaction.

In service, PMI-cored sandwiches show significantly less moisture absorption compared to honeycomb-cored (HC) sandwich components. It is well known, that significant amounts of water can occur in HC-cored components. This water leads towards freeze-thaw problems, respectively to skin-to-core delamination. [4]

The following graph refers to creep compression testing of the –HT version of the XT and the new HP grade.

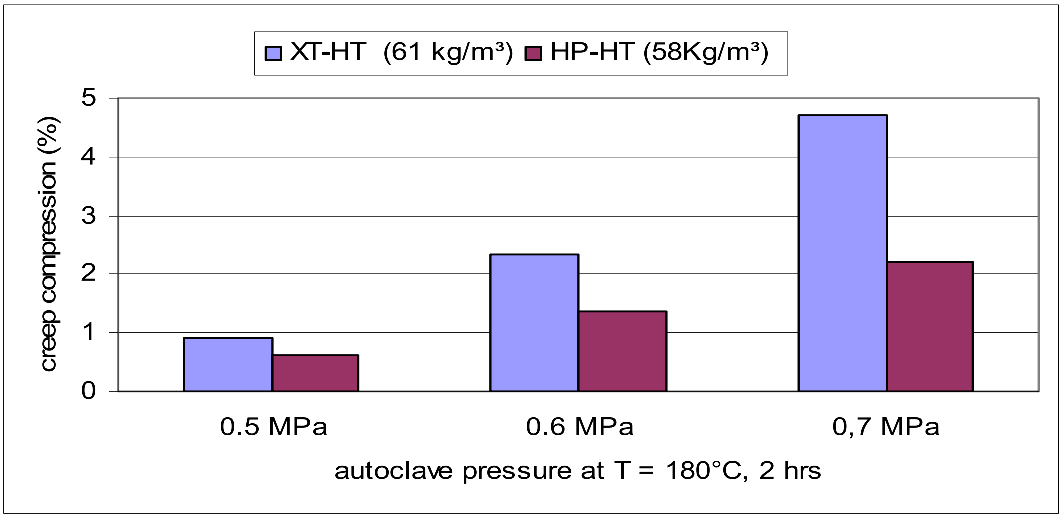

Figure 11: creep compression – comparison of XT-HT to HP-HT

It becomes obvious, that the new PMI Grade HP even exceeds the excellent resistance to creep compression of the XT grade. Fig. 12 concludes the improvement obtained regarding creep compression and density/weight reduction compared to other high-temperature capable PMI

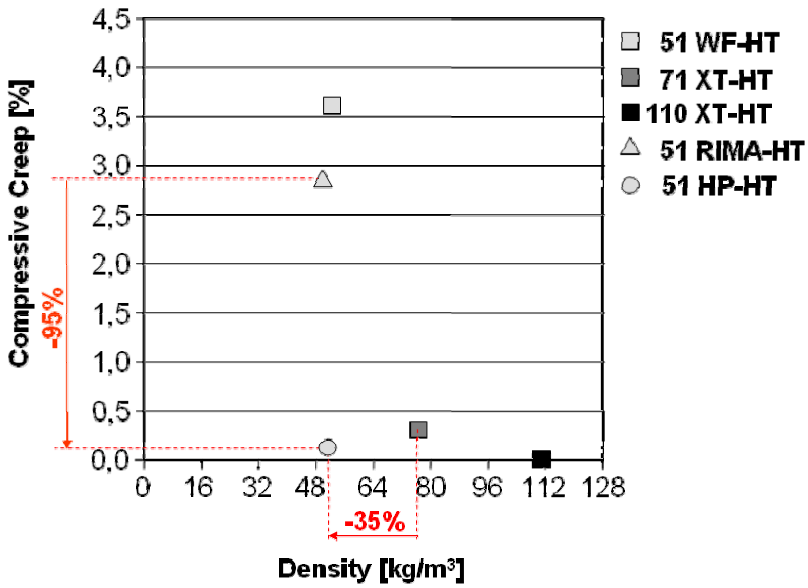

Figure 12: comparison of weight specific creep compression

6 CONCLUSION

The new PMI Grade ROHACELL® HP is setting new standards regarding weight specific mechanical properties and resistance to creep compression.
The improvements compared to the XT Grade are summarized in Fig. 13.

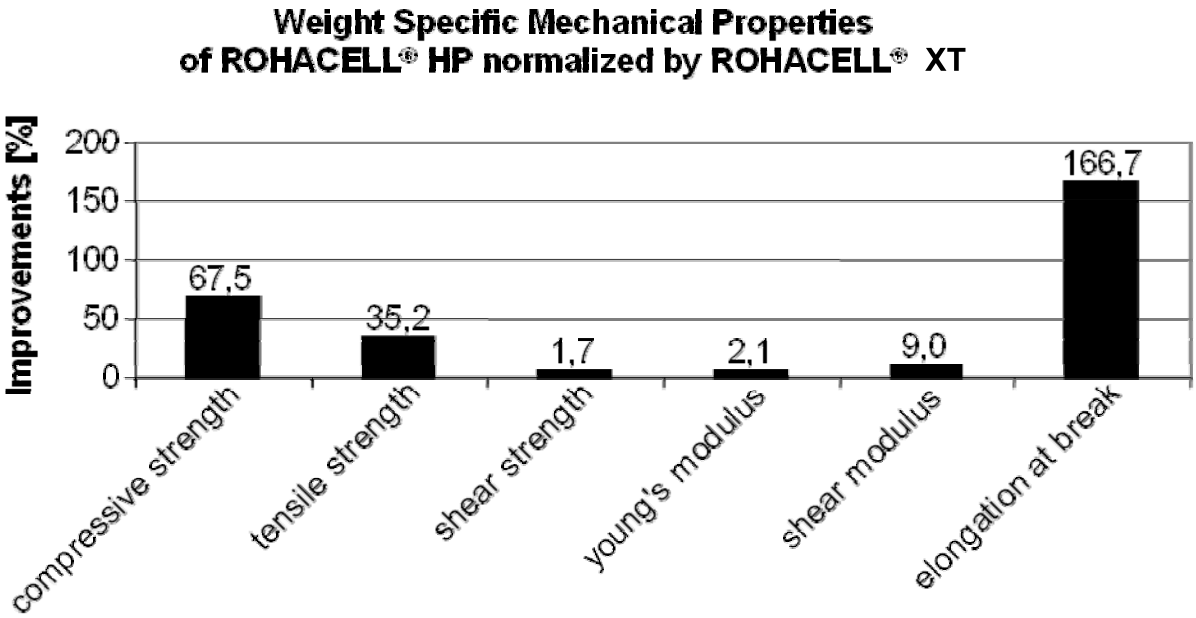

Figure 13: summary of improvements HP Grade versus XT Grade

A new, even more advanced PMI Grade has been successfully developed. It´s outstanding specific mechanical properties and resistance to creep compression are leading towards realization of further weight savings.
Recently run autoclave trials prove that the HP grade in a density of 95 kg/m³ can withstand 10 bar of pressure at T = 180°C, 2hrs with just only 2% of creep compression.
The new Grade also shows improved moisture absorption properties.
The particularly tailored cellular structure / cell size are leading towards significant improvements regarding NDT inspection.

6 REFERENCES

[1] N.N.,"Composites for a Widebody", Aerospace Composites & Materials (1992)

[2]Allen J. Klein, "Cocuring Composites", Advanced Composites (1988)

[3] N.N., Sikorsky Aircraft, "Cocured, Foam Filled Structural Component Design Considerations" (1985)

[4] Ron Banuk, Northrop Corporation B-2 Division, "Design Considerations for Foam and Honeycomb Core Structure"

[5] Markus Kleineberg(1), Lars Herbeck(1), Carsten Schöppinger(2), (1) DLR German Aerospace Center, Lilienthalplatz 7, Braunschweig. (2) Invent GmbH, Christion Pommer Str. 34, 38112 Braunschweig, "Advanced Liquid Resin Infusion-A New Perspective For Space Structures “

[6] Dr.-Ing. L. Herbeck, Markus Kleineberg, C. Schöppinger, German Aerospace Center, Lilienthalplatz 7, 38108 Braunschweig, “Foam Cores In RTM Structures: Manufacturing Aid Or High-Performance Sandwich?”

[7] V. Altstädt, F. Diedrichs, T. Lenz, Polymer And Composite Section, Technical University Hamburg, H. Bardenhagen, D. Jarnot, Airbus Stade Facility, Germany, ”Polymer Foams As Core Materials In Sandwich Laminates (Comparison With Honeycomb)”

8th International Conference on Sandwich Structures
ICSS 8
A. J. M. Ferreira (Editor)

A NEW SANDWICH STRUCTURED COMPOSITE WITH ENTANGLED CARBON FIBERS AS CORE MATERIAL. PROCESSING AND MECHANICAL PROPERTIES

Laurent Mezeix [*†], Christophe Bouvet[†], Bruno Castanié [†] and Dominique Poquillon[*]

[*] CIRIMAT
Université de Toulouse
ENSIACET, 118 route de Narbonne, 31077 Toulouse, France
E-mail: laurent.mezeix@ensiacet.fr

[†] LGMT, IGM
Université de Toulouse
LGMT, bât 3PN, 118 route de Narbonne, 31062, Toulouse, France

Key words: Sandwich structures, Manufacturing, Experimental mechanics.

Summary: *Ventilated core materials are elaborated from entangled carbon fibers. They are studied in this paper for an application as core material for sandwich structure. Core material is elaborated from carbon yarn with hand carding, and removing carbon fibers epoxy coating. Carbon/epoxy prepreg is used for sandwich skins. To increase stiffness, fibers need to be cross-linked and epoxy resin is chosen and applied by vaporization. The purpose of this paper is to compare the compressive response of entangled carbon fibers at different compression rate. Results are compared with polymethacrylimide foam and Nomex honeycomb. Energy absorption per unit mass is also compared with these materials.*

1 INTRODUCTION

Many different sandwich panels are used for aeronautical applications. Open and closed cell structured foam, balsa wood or composite honeycomb are often used as core materials. When the core material contains closed cells, water accumulation into the cell has to be taken into account. This phenomenon occurs when in service conditions lead to operate in humidity atmosphere. Then, water vapor from air naturally condenses on cold surfaces when the sandwich panel temperature decreases. This water accumulation might increase significantly the weight of the core material. Core with a ventilated structure helps to prevent this phenomenon. Periodic cellular metal (PCM) has been motivated by potential multifunctional applications that exploit their open architecture as well as their apparent superior strength and stiffness: pyramidal [1, 2], lattice [3 - 8], kagome truss [9 - 14] or woven [15 - 17]. One of the drawbacks of these materials is the expensive cost of the manufacturing. In the present study, ventilated core materials are elaborated from entangled carbon fibers. This type of materials has been studied previously [18] and promising crash absorption properties have been evidenced. The simplicity of elaboration is one of the main advantages of this material. Mixing different sorts of fibers, by example adding fibers with good electrical conduction properties is also possible.

Sandwich panels with entangled cross-linked carbon fibers as core material are elaborated using carbon/epoxy skins. So, epoxy resin was used for cross-linking core fibers. Elaboration of core materials and sandwich sampled will be first detailed. Then compression tests in quasi-static conditions and for 4 m.s^{-1} speed impact tests will be described.

2 MATERIALS AND METHODS

2.1 Raw materials used

The commercial carbon fibers (12K) consist of a yarn of stranded carbon filaments. Filaments diameter is 7 µm and epoxy coating represents 1 wt%. Fibers were provided by the company ATG Composite, France. Skins were provided by Hexcel, reference G803 /42%/ 914. Skins consist of prepreg of carbon epoxy satin stitch. The initial prepreg thickness equals 0.28 mm. Table 1 shows prepreg and carbon yarns properties.

	Carbon yarns	Carbon prepreg
Density	1760 kg/m^3	1290 kg/m^3
Tensile strength	4300 MPa	420 MPa
Tensile modulus	238 GPa	52 GPa
Compression strength		400 MPa
Poisson's ratio		0.03
Shear modulus		3.86 GPa

Table 1. Carbon prepreg and carbon yarns properties

To increase stiffness of the entangled materials core of the sandwich panel, carbon fibers are cross-linked using epoxy resin provided by the company SICOMIN, France. Table 2 shows batch (hardening agent + resin) properties.

Density	≈ 1100 kg/m^3
Viscosity (25 °C)	285 mPa.s
Polymerization at 80 °C	10'

Table 2. Epoxy properties

Results concerning sandwich panels elaborated with core made of entangled carbon fibers will be compared with those obtained with polymethacrylimide foam (Rohacell 110 RIMA) and honeycomb (Hexcel, HRH-78) as core material. Table 3 shows polymethacrylimide foam and Nomex honeycomb properties.

	polymethacrylimide foam	Nomex honeycomb
Density	110 kg/m^3	50 kg/m^3
Compressive strength	3.6 MPa	2.2 MPa
Tensile strength	3.7 MPa	
Flexural strength	5.2 MPa	
Shear strength	2.4 MPa	0.85 MPa *
Elastic modulus	180 MPa	125 MPa *
Shear modulus	70 MPa	31.7 MPa *

Table 3. Properties of polymethacrylimide foam and Nomex honeycomb, *out of plane test

2.2 Characterizations, devices used

Carbon fibers were observed using a Scanning Electron Microscope (LECO435VP) operating at 15 kV. To remove initial epoxy coating, yarns are treated in a solution of dichloromethane for 24 hours, then cleaned 2 hours in methanol. For all the tests carried out during this work the specimens are carefully weighed using SARTORIUS balance (±10µg) and their volume are measured. A paint spray gun (Fiac UK air compressors) is used to vaporize epoxy. Resin is heated up to 35 °C to decrease viscosity and thus allows a better vaporization.

2.3 Core elaboration

The core thickness was kept constant on the samples. The value of 20 mm was chosen and this value was also the carbon fibers length. Different materials architectures have been tested. The simplest architecture is obtained by entangling the raw yarn (12 K + 1 wt% epoxy coating) shown on Fig. 1a. It was chosen to decrease yarn size by hand carding. Indeed used smaller yarns sizes allow to decrease relative density [18]. As shown on Fig. 1b, fibers separation is not homogeneous due to the effect of epoxy coating. To obtain smaller yarns, epoxy coating need to be removed as described in paragraph 2.2. Fig. 1c shows that the fibers separation is better. A previous work on carbon fibers entanglement for an application as core material shows that the stiffness obtained is too low when carbon fibers are not cross-linked [19]. In this study epoxy cross-link was successfully realized using paint spray gun during the entanglement of carbon fibers. Fig. 2 shows SEM observations on fibers coated by spray gun. Fibers separation is good, epoxy cross-links are numerous but some epoxy drops remain on carbon fibers.

(a) (b) (c)

Fig 1. (a) Carbon yarn as received; (b) hand carding from raw carbon fibers, (c) hand carding fibers after chemical uncoated

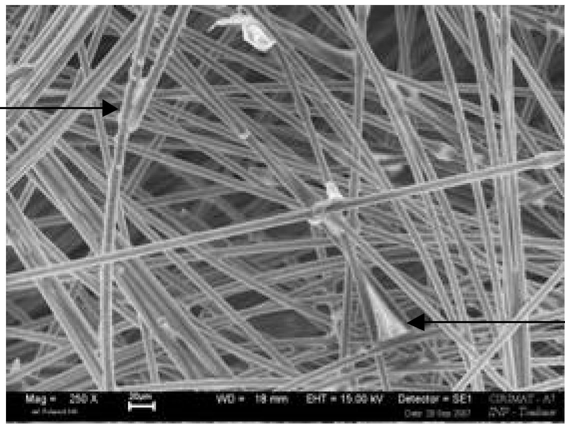

Fig 2. SEM observation of uncoated then cross-linked fibers by epoxy spraying

2.4 Sandwich samples elaboration

The chosen materials for core realization of the sandwich samples were the one illustrated on Fig. 2. It was obtained from entanglement of uncoated yarns which were hand carded. Then, epoxy was sprayed to cross-link fibers. Samples are manufactured in specific mould. To obtain enough homogeneous and stiffness core material, carbon fibers are compressed. The density obtained before epoxy spaying is about 400 kg/m^3. Many tests were performed on entangled samples with smaller core density. But, in this cases, the core homogeneity was not enough correct between the lower and the upper skin of the sample. The sandwich skin face sheets consisted in carbon/epoxy $[0]_2$ prepreg. To improve interface between the core and the skin, epoxy resin is sprayed on skins. Sandwich structures are polymerized at 180°C for

4 hours in a furnace under laboratory air. For the compression and dynamic crushing tests, samples are cylindrical(Fig 3b). The diameter is 30 mm for a height of 20 mm. Fig. 3a shows a typical sandwich beam obtained

(a)

(b)

Fig 3. (a) sandwich beam (b) cylinder sample

2.5 Experimental methods

- *Compression tests*

The quasi-static compressive response of the entangled carbon fibers sandwich core were measured in a screw-driven test machine MTS with a 5kN load cell. The applied velocity $v_0 = 0.02$ mm.s^{-1} corresponding to a nominal strain rate of $\dot{\varepsilon} = 10^{-3}$ s^{-1}. The unloading is at the same strain rate. The sample is introduced between the lower and the upper part of the device. A compressive preloading of 2N is applied because the uncertainty of measurement ± 1 N. Tests were performed on sandwich samples and on core materials (Fig 5).

- *Dynamic crushing tests*

The dynamic compressive responses of the entangled carbon fibers sandwich and core material were measured in an impact test system. System consists of a drop weight system. Fig 4 shows the features:

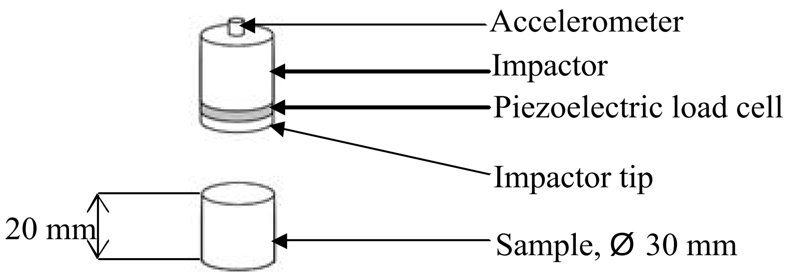

Fig 4. Impact apparatus

- A 2 kg free failling mass
- A piezoelectric load cell mounted under the mass to measure the force between the mass and the sample.
- An accelerometer mounted over the mass to measure the acceleration.
- A flat striker of 30 mm diameter.

- An optical sensor to measure the velocity just before impact.
- An analogical data acquisition system (YOKOGAWA)

The impact force F_{impact} between the impactor and the specimen is determineed due to the measured force, $F_{measure}$, taken by the load cell:

$$F_{impact} = \frac{m_{impactor}}{m_{impactor} - m_{tip}} F_{measured} \quad (1)$$

Where $m_{impactor}$ and m_{tip} are respectively the mass of the impactor (2 kg) and the impactor tip (0.23 kg). The impact velocity is about 4 m.s^{-1}. Tests were performed on sandwich samples and on core materials. Strain s and true strain e are determined by equations (2) and (3):

$$\sigma = \frac{F_{impact}}{S_0} \quad (2)$$

$$\varepsilon = \ln(1 - \frac{\Delta h}{h_0}) \quad (3)$$

Where F_{impact} is obtained by the equation (2) and S_0 is the sample area (700 mm^2). ?$_h$ is the variation of thickness and h_0 the initial thickness (20 mm). The purpose is to compare the quasi-static responses with those obtained at low speed impact.

3 RESULTS AND DISCUTION

3.1 Quasi-static compression tests

Figure 5 shows results about compression tests and impact tests on sandwich and core entangled samples. Firstly, we can observe for quasi static compression that the deformation of sandwich structure is lower than the one core material. Linear behavior exists during the beginning of the quasi static compression. Young modulus corresponding at this part is respectively 22 MPa and 11 MPa for sandwich and core samples. This linear behavior is due to the strength of vertical fibers. Stiffness is bigger with the presence of skin because fibers are less free to bend. A remanent strain is observed for all samples, due to the fibers rearrangement during the compression. Table 4 shows Young Modulus for the quasi static tests on the different materials used. Young Modulus is determined in the linear part before the peak stress in the case of foam and honeycomb. Young Modulus determined during these experiments are very low compared to supplier data. But compressive strength obtained during these tests are closed to awaited values. Experiments need to be done again to check Young modulus values. The difference of Young modulus between entangled carbon fibers and others core materials tests is larger. Figure 6 shows results about quasi-static compression and impact tests on Nomex honeycomb and polymethacrylimide foam. No significantly difference is observed between core and sandwich samples.

Work is still necessary to increase stiffness of entangled carbon fibers samples and in the same time to decrease density.

	Young modulus [MPa] on core sample	Young modulus [MPa] on sandwich sample
Honeycomb	70 (50 kg/m^3)	70 (90 kg/m^3)
Polymethacrylimide foam	50 (110 kg/m^3)	60 (190 kg/m^3)
Entangled carbon fibers	11 (400 kg/m^3)	22 (500 kg/m^3)

Table 4. Young Modulus in quasi static compression. Density is given into brackets

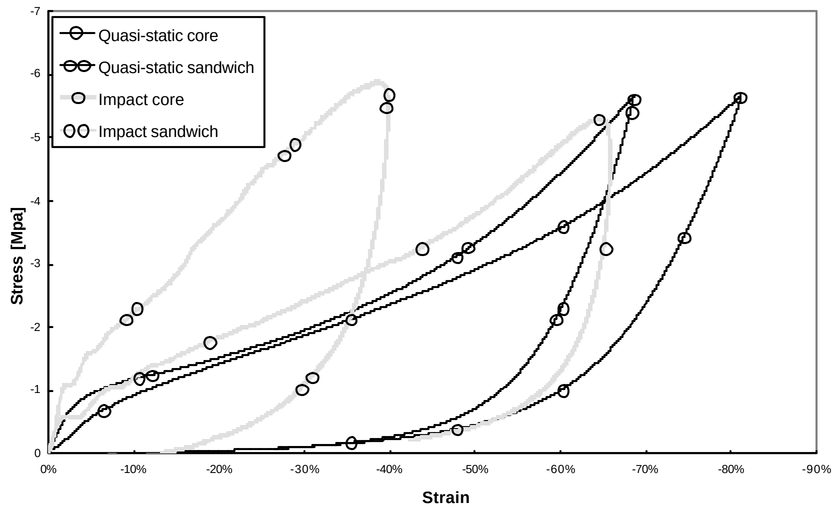

Fig 5. Stress-Strain curve for quasi static compression and impact tests on samples

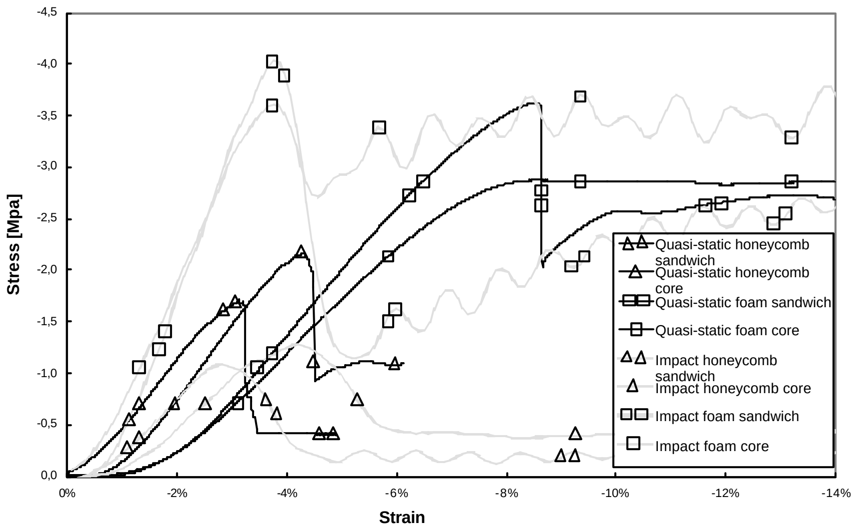

Fig 6. Stress-Strain curve for quasi static compression and impact test on Nomex honeycomb and polymethacrylimide foam samples

3.2 Dynamic crushing

In the current study, samples were tested at energy level of 15 J. We can observe on the Figure 5 that the difference between quasi static and impact is not very important for the core samples, while for the sandwich, the difference is more noticeable. More experiments are needed to explain this behavior. Moreover, like in quasi static, stiffness on sandwich sample is superior to core sample under impact.

It is important to notice that during impact tests, strain rate is not constant. Indeed strain rate is about 20 s^{-1} for an impactor speed of v = 4 $m.s^{-1}$ in the beginning of impact and decrease to 0 s^{-1} when strain is maximum.

3.3 Energy absorption

The energy absorption per unit mass, Wm, can be used to compare different cellular structures. This specific energy is defined from the area under the nominal stress nominal strain curve as

$$W_m = \frac{1}{\rho}\int_0^{\varepsilon} \sigma(\varepsilon) d\varepsilon \qquad (4)$$

Where s is the stress of the structure and e is the strain and ? is the density. The Figure 8 shows the energy absorption per unit mass for entangled carbon fibers, for quasi static tests and low velocity impact tests at energy level of 15 J. Firslty, energy absorption per unit mass of entangled core is more important than for sandwich. This point is explained by higher strain obtained (for the same stress level) for core material than for sandwich structure. The presence of skins on which many fibers are glued by epoxy decreases fibers motion and friction which participate in energy absorption. Secondly, there is no significant difference between quasi-static compression tests and dynamic compression tests at low speed impact. Under the same stress, energy absorption per unit mass is almost the same between quasi static and impact tests.

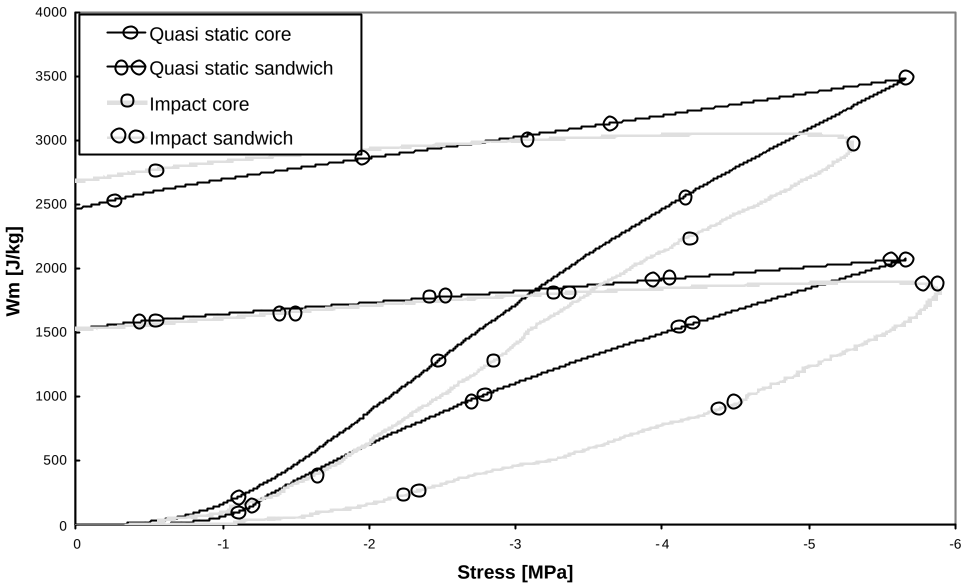

Fig 8. Energy absorption per unit mass versus stress, this for core and sandwich samples.

Figures 9a. and 9b. show respectively the energy absorption per unit mass versus pressure under quasi static tests and impact tests. Firstly, in both cases, we can observe that under 1 MPa, energy absorption of entangled carbon fibers (core and sandwich samples) is very low (less than 100 J/kg). For higher stresses, energy absorption per unit mass increases linearly. Indeed entangled carbon fibers do not present a plateau behavior although Nomex honeycomb and polymethacrylimide foam present it after a peak stress. The plateau behavior is interesting because without increasing stress, energy absorption increase. But the level of this plateau is the level of the maximum stress allowed. As shows on Fig. 9b, entangled carbon fibers compression tests do not reveal any plateau of energy absorption but an increasing energy absorption capacity when stress increases.

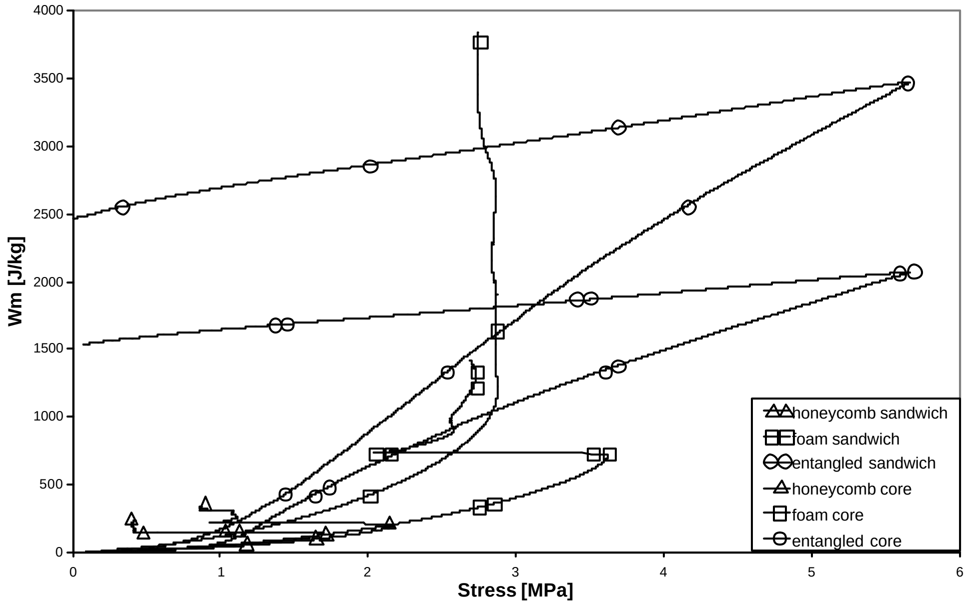

(a)

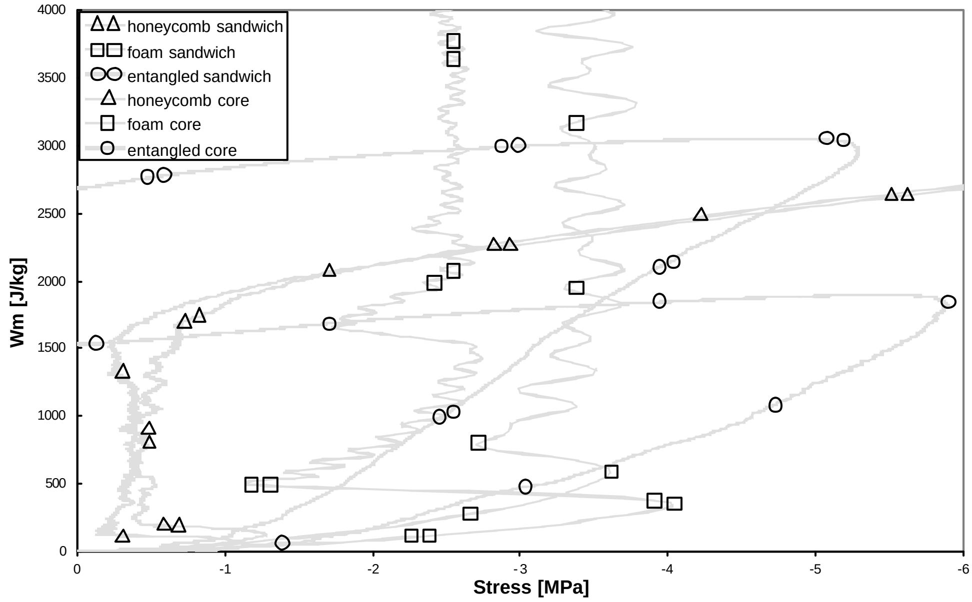

(b)

Fig 9. Energy absorption per unit mass versus stress (a), during quasi static tests (b) during impact tests. Absorption per unit mass is given by equation 4

4 CONCLUSIONS

Compression behavior and energy absorption have studied under both quasi-static compression tests and low velocity impact conditions. Comparison has made between entangled carbon fibers, Nomex honeycomb and polymethacrylimide foam. Comparison has also been carried out between core materials alone and sandwich samples. The conclusive remarks can be summarized as follows:

1. Delete epoxy resin coating of carbon fibers allows reducing significantly the size of yarn, but yarns size obtained is not homogeneous. The density of cross-linked entangled carbon fibers, about 500 kg/m^3, is high for an application as core material.
2. The stiffness of entangled fibers carbon is less than other core material tested.
3. Under quasi-static compression tests and low velocity impact conditions cross-link entangled carbon fibers do not present a plateau behavior. But an increasing absorption energy capacity.

Entangled fibers have several advantages like easy manufacturing and possibility to mix different sorts of fibers. Application like core material present also advantages: possibility to reeve cables on the core, add fibers with good electrical conduction, capacity to have curve sandwich panel and variation of core thickness. However, materials elaborated during that study have still a too high density. Solutions are in progress to increase stiffness and to decrease significantly density in same time for new entangled core materials.

REFERENCES

[1] Douglas T. Queheillalt, Haydn N.G. Wadley, *Pyramidal lattice truss structures with hollow trusses*, Materials Science and Engineering A 397, pp 132 – 137, 2005.
[2] Douglas T. Queheillalt, Yellapu Murty and Haydn N.G. Wadley, *Mechanical properties of an extruded pyramidal lattice truss sandwich structure*, Scripta Materiala 58, pp 76 – 79, 2008.
[3] T. Liu, Z.C. Deng, T.J. Lu, *Design optimization of truss-cored sandwiches, with homogenization*, International Journal of Solids and Structures 43, pp 7891-7918, 2006.
[4] H.L Fang, W Yang, B. Wang, et al. *Design and manufacture of a composite lattice structure reinforced by continuous carbon fibers*, Tsinghua Sci Tech 2006, Volume 11, Number 5, pp 515-522, 2006.
[5] Gregory W. Kooistra, Douglas T. Queheillalt, Haydn N.G. Wadley, *Shear behavior of aluminum lattice truss sandwich panel structures*, Materials Science and Engineering, 2007.
[6] J.C. Wallach, L.J. Gibson, *Mechanical behavior of a three-dimensional truss material*, International Journal of Solids and Structures 38, pp 7181 – 7196, 2001.
[7] F. Coté, V.S. Deshpande, N.A. Fleck, A.G. Evans, *The compressive and shear responses of corrugated and diamond lattice materials*, International Journal of Solids and Structures 43, pp 6220 - 6242, 2006.
[8] L. Valdevit, J.W. Hutchinson, A.G. Evans,, *Structurally optimized sandwich panels with prismatic cores*, International Journal of Solids and Structures 41, pp 5105 - 5124, 2004.

[9] Wang, A.G. Evans, K. Dharmasena, H.N.G. Waldley, *On the performance of truss panels with Kagome cores*, International Journal of Solids and Structures 40, pp 6981-6988, 2003.
[10] S. Hyun, A.M. Karlsson, S. Torquato, A.G. Evans, *Simulated properties of Kagomé truss core panes*, International Journal of Solids and Structures 40, pp 6989-998, 2003.
[11] Ji-Hyun Lim, Ki-Ju Kang, *Mechanical behavior of sandwich panels with tetragonal and Kagome truss cores fabricated from wires*, International Journal of Solids and Structures Volume 43, issu 17, pp 5228 - 5246, 2006.
[12] Lee Y.-H et al., *Wire-woven bulk Kagome truss cores*, Acta Materiala 55, Issue 18, October 2007, pp 6084 - 6094, 2007.
[13] H.L. Fan et al., *Sandwich panels with Kagome lattice cores reinforced by carbon fibers*, Composites Structures 81, issu 4, pp 533 - 539, 2006
[14] H.L. Fan, F.H. Meng, W. Yang, *Mechanical behavior and bending effects of carbon fiber reinforced lattice materials*, Arch Appl Mech 75, pp 635 - 647, 2006.
[15] J. Brandt, K. Drechsler and F.J. Arendts, *Mechanical performance of composites based on various three-dimensional woven -fibre preforms*, Composites Science and Technology 56, pp 381-386, 1996.
[16] M.K. Bannister, R. Braemar, P.J. Crothers, *The mechanical performance of 3D woven sandwich composites*, Composite Structures 47, pp 687 - 690, 1999.
[17] H. Judawisastra, J. Ivens, I. Verpoest, *The fatigue behaviour and damage development of 3D woven sandwich composites*, Composite Structures 43, pp 35 - 45, 1998.
[18] D. Poquillon, B. Viguier, E. Andrieu, *Experimental data about mechanical behavior during compression tests for various matted fib res*, Journal of Materials Science, Volume 40, Issue 22, pp 5963 - 5970, 2005.
[19] Laurent Mezeix, *Fibres de carbone utilisées comme matériaux d'âme pour structure sandwich,* Master Thesis report, Material Science Master's degree, University of Toulouse, Jun 2007.

8th International Conference on Sandwich Structures
ICSS 8
A. J. M. Ferreira (Editor)

CORE METAL ALLOY
- A NEW SANDWICH MATERIAL WITH NATURAL STONE -

Krabatsch T. [*] **and Wellnitz J.** [*, †]

[*]PRIVAT-INSTITUT für Technik und Design e.V.
Marie-Curie-Straße 6, 85055 Ingolstadt, Germany
e-mail: krabatsch@itd-in.de, web page: www.itd-in.de

† Fachhochschule Ingolstadt
University of Applied Sciences
Esplanade 10, 85049 Ingolstadt, Germany
e-mail: info@fh-ingolstadt.de, web page: www.fh-ingolstadt.de

Key words: stone, metal, competitive price, construction, security, design

Summary: *CMA (Core Metal Alloy) is a new sandwich material combining the favorable properties of natural stone and metal. Using two widely available and low priced components, the laminate will reach a competitive price level. The fields of application include construction, security and design.*

1 INTRODUCTION

Light construction is the philosophy of gaining maximum reduction in weight. Especially in times of raising ecological damage, R&D are on their way to find lighter constructions. On one hand the way leads through constructive weight optimisation, on the other hand through developing totally new materials. Variable sandwich- and laminate-structures combine different materials in order to create optimised material behaviour. In this regard availability and price of material play the major role and therefore realising some possibilities isn't always that easy.

Strengthening plastics using carbon fibre herein surely was one of the most interesting ideas in former times. The developed combinations turned out to be suitable for usage and are certainly very good at their field of application. Also combinations with plastics and glass fibre are well known, and GLARE® was a further development in using aluminium.

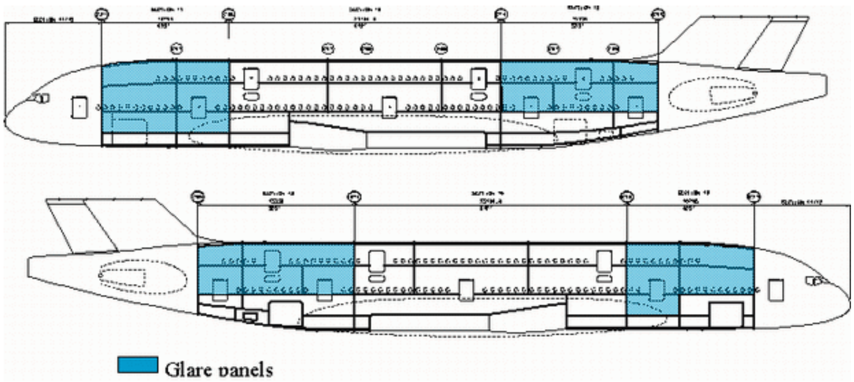

Figure 1: GLARE® application (courtesy Airbus)

Although GLARE® has proven the enormous potential of new materials it nevertheless turned out to implicate some serious problems.

2 APPROACH

To consider availability and price being the major focus in developing a new material a new idea needs to be found.
In the field of metallic materials a lot of realisable variants have been created and are still in use. Especially in modern Airplanes aluminium is often used as a light and stable metal in a lot of fields. The problem of difficulties in availability is negligible and one can count on the experiences in using aluminium as it creates reliable and save constructions. To minimize damage in cases of debris containment a combination with an impact resistant material is very interesting and surely opens interesting fields of application.

Again using availability and price as the keywords makes natural stone being a very interesting construction element. Our earth is a terrestrial planet, meaning that it is a rocky body, … It is the largest of the four solar terrestrial planets, both in terms of size and total mass.

Figure 2: Earth

The “Private Institute for Techniques and Design e.V” (ITD) and the “University of Applied Sciences Ingolstadt” in a while are therefore intensively working on developing a brand new composite. A thin foil of stone is brought to a metal carrier which is the source for creating a laminate of several coatings. The result is called “Core Metal Alloy” (CMA) and combines advantages of both of the different elements.

Figure 3: CMA

By changing the properties of the three constituents - metal, stone and the way of bonding the behaviour of the laminate can be adjusted to the user's requirements. There is no need for temperature treatment on the material and no difficulties of machining. By using high temperature resistant adhesives it even could be used in hot environments
(up to 500°C and higher). A density of 2,7 kg/dm³ with simultaneously very good bending behaviour and impact resistance, the CMA reaches different fields of the market. Even while applying for the protection of utility patent on the material and all the work on, it got set to a state secret which immediately leaded to a stop of further procedure.

3 RESEARCH AND DEVELOPMENT

In the running development phase the ITD decided to cooperate with a competent partner in the fields of natural stone from Italy. The goal of this cooperation is to get a material that is a marketable product for series production in production lines.
Especially the cases of debris containment in combination with very interesting camouflage effects show lots of application possibilities in aerospace. The composites visual appearance and deformation characteristics will also be interesting aspects in near future. Stone creates an atmosphere of luxury. Furthermore the different types, colours and treatments of the natural stone offer nearly unlimited design possibilities.
Further fields of application in aviation include but are not restricted to:

- Through the composition of the surface and by using adequate colour selections CMA has a great potential for an attractive, light and stable material.
- Stone inlays, similar to those made of exotic woods used in car interior design, could provide interesting design options.
- CMA provides an attractive appearance combined with superior abrasion characteristics and a stability which could substitute the entire floor substructure and thus help to reduce the aircraft's weight. With a defined surface roughness the composite is a safe, non slippery and non flammable floor covering.
- Fairings especially built for debris containment (e.g. cross engine debris), belly fairings, C ducts, cowling doors,…

The current research mainly is working on the optimisation by running several tests. Finding different values for Tensile strength, Young's Modulus Bending- and impact behaviour are just a short overview of our work. Within a first phase the CMA
in a combination of aluminium and granite could pas a B3 shelling test with completely stopping the projectile of a .357 Magnum.

Figure 4: CMA with 4 Layers of stone after shelling with .357 Magnum

Beside very good laboratory work, the work on running numerical methods is continuously extending the market potential.
Market studies show a high amount of a possible use and a great capability of this idea. Beside aviation, examples could be transport, automobile industry and engineering - just to mention some. Availability is not a problem any more and the interesting price of the stone gives CMA the attractiveness it needs to survive in its market.

4 PRODUCTION

The production of preproduction models is laboratory work. Layers of an "AB" combination - consisting of metal and stone - are produced in different types depending on their needs. By bringing several layers together symmetrical and asymmetrical plates can be created and formed.

Figure 5: schematic of CMA

Figure 5 shows the first “ABA” Layer of a symmetrical “ABABA” assembly. The used material is a combination of Bianco Sardo and aluminium using an adhesive. Research work also is working on possibilities of bonding (Ceramic, Ultrasonic,…) and optimisation of serial production.

5 EXPERIMENTAL AND NUMERICAL INVESTIGATIONS AND VALIDATION

For a better understanding of the materials behaviour several experimental and numerical testing is planed for within the projected research. One of the steps is the comparison of a mathematical model with laboratory work which is done in cooperation with the University of Applied Sciences in Ingolstadt. Within a three-point-bending test a probe gets bent while data of force and elongation are collected.

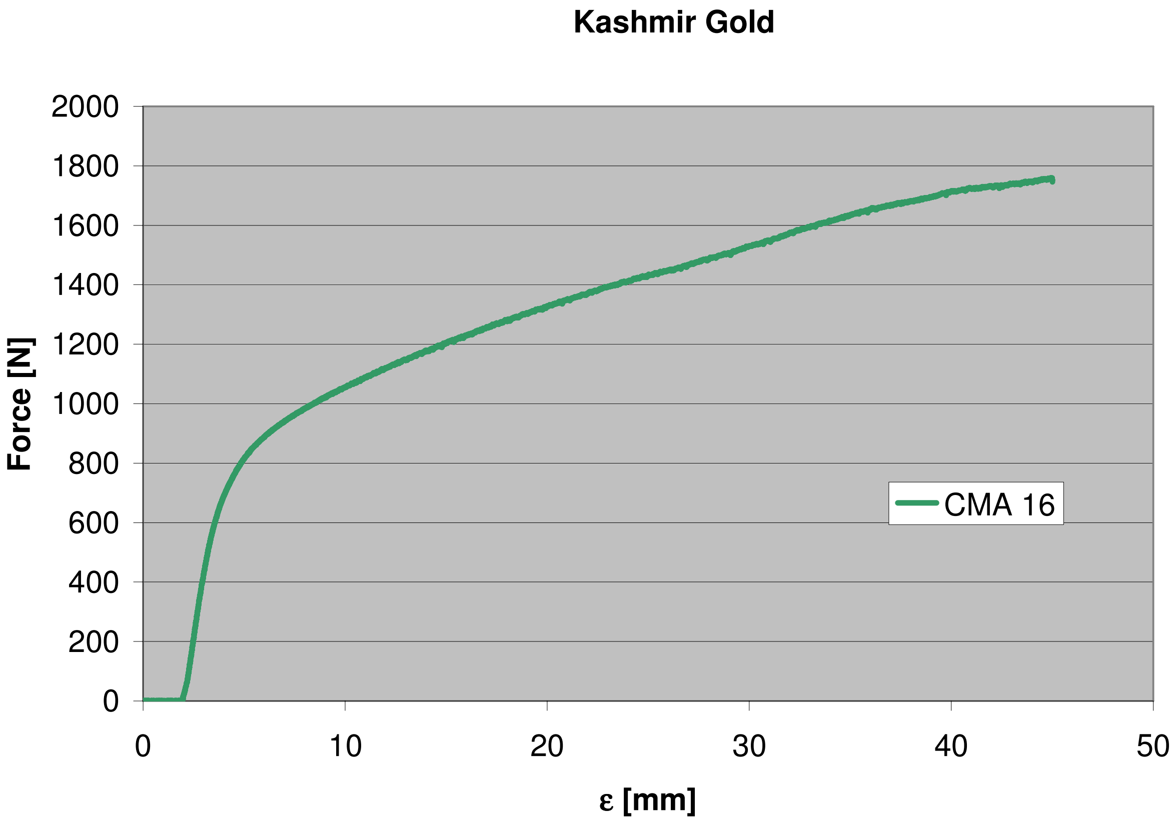

Figure 6: Force over elongation after a 3-Point-Bending test with a 5 Layer CMA using Kashmir Gold

Although stone is very brittle, the fact that it is used in thin foils and set between aluminium provides it with a very good bending behaviour. That even allows a certain amount of bending the stone, without loosing the function of the composite.

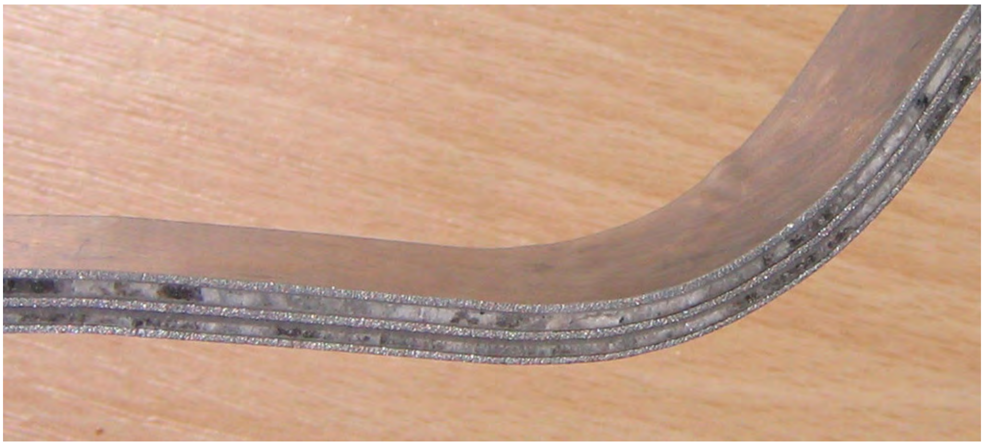

Fig. 3.2.2: 5 Layer CMA using Bianco Sardo after bending

By calculating a Young´s Modulus of the entire laminate a model can be built for FE methods to integrate the CMA in engineering construction methods.

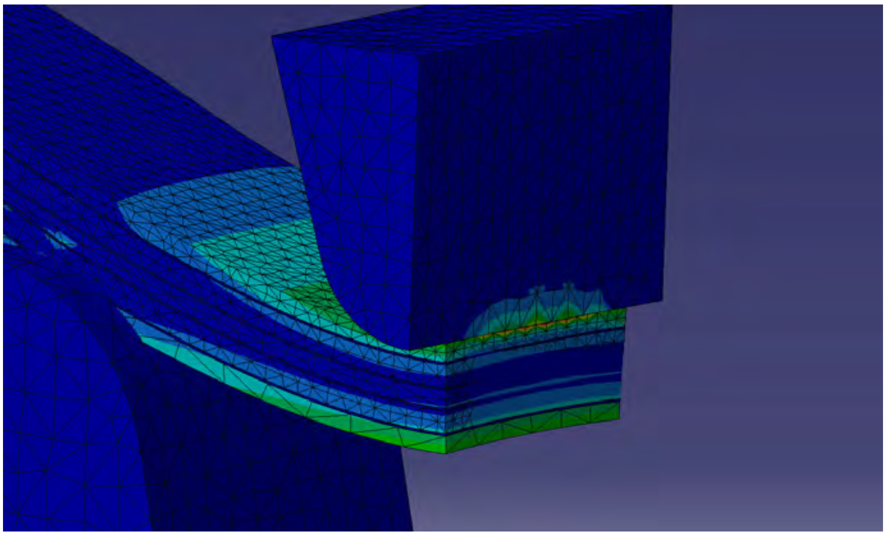

Fig. 3.2.3: FE simulation of a 5 Layer CMA

For supporting the theory several laminate theories have been applied to composite laminates. The classical laminate theory is an extension of the Love – Kirchhoff assumption for isotopic plates and can be applied if the laminate is thin because transverse shear stresses are not considered [7]. As the problem of shear stress can not be neglected, there is a need for a higher order shear deformation theory. In this case the third order theory of Reddy [1] will be used to describe the inner activities.

6 OUTLOOK

Next steps are to continue the evaluation of CMA. Therefore the ITD is intensively working together with the University of Applied Sciences in Ingolstadt which allows the use of very modern laboratories. The ITD has built up a slow speed impact testing system for penetrating materials with different projectiles like ice, stone, chips, etc.…

Fig. 4.1: impact testing system

Possibilities of the system are:

- maximum of projectile size 300x300
- projectile: ice 50 g, stone 10 g
- distance of acceleration 5 m
- work pressure 8 bar
- maximum of velocity 250 m/s

Several tests on carbon material have already been made and shall be processed with CMA in the next future.

REFERENCES

[1] J.N. Reddy, *Mechanics of Laminated Composite Plates*, CRC Press, USA, 1997.

[2] H. Altenbach, J. Altenbach, R. Rikards, *Einführung in die Mechanik der Laminat- und Sandwichtragwerke*, Deutscher Verlag für Grundstoffindustrie Stuttgart, Erlangen, 1996.

[3] H. Mang, G. Hofstetter, *Festigkeitslehre*, Springer, Wien, 2000.

[4] T. Krabatsch, CMA *Forschungsbericht 2007,* Ingolstadt, 2008.

[5] U. Burger, Ein neues Konzept für Projektil- und Splitterschutz durch Leichtbaukonstruktionen mit modernem Ringgeflecht, *3. Landshuter Leichtbau-Colloquium Tagungsband*, S.55-64, Fachhochschule Landshut, 2007.

[6] http://cgi.tu-harburg.de/~kvwww/cgi-bin/cgi1/kvsh/kvsh_Forschung.html, Stand 2007.

[7] http://de.wikipedia.org/wiki/Hauptseite, Stand 2007.

[8] A.J.M. Ferreira, C.M.C. Roque, P.A.L.S. Martins, *Analysis of composite plates using higher-order shear deformation theory and a finite point formulation based on the multiquadric radial basis function method*, Composites, Part B 34 627-636, 2003.

8th International Conference on Sandwich Structures
ICSS 8
A. J. M. Ferreira (Editor)
©FEUP, Porto, 2008

CHARACTERISATION OF MAGNETORHEOLOGICAL ELASTOMER MATERIALS FOR THE CORE OF SMART SANDWICH STRUCTURES

W.J. Choi, Y.P. Xiong, R.A. Shenoi

School of Engineering Sciences, Ship Science
University of Southampton
Highfield, Southampton SO17 1BJ, UK
e-mail: wjc@soton.ac.uk

Key words: Smart sandwich structure, MRE core, shear modulus, adjustable stiffness.

Summary. *This paper presents results from tests carried out on the effect of magnetorheological elasotmer (MRE) material make-up, processing features and cure under the magnetic field with respect to the volume of iron particles on shear properties. As core material of smart sandwich structure, performance characterization of the smart function in terms of curing time, air bubble effect and the volume of iron particles of MRE is explored. The purpose of this paper is to find out storage shear modulus and loss factor of MRE specimens and to explore the ideal volume fraction of iron particles, curing time under magnetic field and air bubble effect to maximize shear modulus changes. Since shear properties of MRE changes dominantly in small strain ranges, MRE is shown as being a core material of a sandwich beam which achieves adjustable stiffness.*

1 INTRODUCTION

Magnetorheological (MR) material consists of micron sized magnetically permeable particles suspended in a non-magnetic medium. The properties of such materials can be controlled by magnetic field strength. Research in the field of MR material was started in the late the 1940s. In recent years their potential capability has been increasingly recognised as a semi active control device for car suspensions, buildings and bridges. MR Elastomer (MRE) is composed of natural or synthetic rubber and iron particles. MRE is a durable material while MR Fluid has disadvantages of deposition, environmental contamination and sealing problems. MRE can be operated in severe temperatures (-50°C to 150°C) with low voltage supplies. Their variable properties enable its use vibration minimization of adaptive structures.

Jolly *et al.* [1] showed that the maximum percentage of change in modulus is being observed in the vicinity of 1-2% strain. They calculated the percentage change in natural frequency of a simple second order system in terms of the percentage change in the modulus of the controllable elastomer in response to an applied field. Davis [2] predicted the optimal particle volume fraction for the largest fractional change of about 27% by numerical means and proved with experiment. Lokander and Stenberg [3] tested the shear property of MRE by using two different types of iron particles in order to find out substantial effects of MRE. They showed that MRE with large irregular particles have a large MR effect although the particles are not aligned within the material and that the rheological properties of the matrix material do not influence the MR effect. Blom and Kari [4] showed that cyclic loading conditions with different strain amplitudes manifest a dependence of the viscoelastic storage modulus with the maximum stiffness change being up to 115% in the audible frequency range. Varga *et al.* [5] reported that the most significant effect was found if the applied field is parallel to the particle alignment and the mechanical stress. Stepanov *et al.* [6] investigated viscoelastic behaviour of highly elastic magnetic elastomers by three different experimental techniques, namely elongation, static and dynamic shears. They observed an increase in modulus of up to 100 fold at small 1-4% deformations.

MRE has been used in applications where stiffness or resonance changes are needed. The MRE tuned vibration absorber (TVA) device can modify a mechanical systems response to external disturbances through energizing an internal electromagnet so that unexpected vibrational loads can be dissipated through activation of the MRE material via a closed loop control system [7]. The MRE TVA system is fail-safe because the system will continue to manage the device as a passive isolator in the event of an power system failure. Deng *et al.* [8] applied MREs to an adaptive tuned vibration absorber (ATVA). They showed that the MRE TVA achieves a relative frequency change is up to 147% with 60dB absorption of frequency response. Ginder *et al.* [9] showed an MRE application for automotive bushing.

MRE can be adapted as a core material in sandwich beams. Yalcintas and Dai [10] analysed free vibration to observe the theoretically predicted vibration responses in real time and vibration suppression capabilities of three layered MR adaptive sandwich beams. The vibration amplitudes decreased by as much as 20 dB and the natural frequency shifts were as high as 30%. The ability to incorporate MRE materials in critical parts of a large sandwich structure, with a potential to modify modulus, could permit better structural response in ships structure, large offshore structures and buildings in earthquake prone areas.

In this paper, a number of different MRE compositions, achieved by blending varying proportions of iron powder and elastomers, are manufactured. Shear properties of the MRE in relation to the volume of iron particles, curing time and air bubble effect are studied experimentally. The feasibility of incorporating these MRE materials into the core of a composite beam structure are explored to incorporate MRE materials into a number of test beams with different configurations to measure its response under different field and loading conditions both for the MRE material samples and the composite beam structure.

2 THEORETICAL STUDY

For the equation of MRE elastomers [11], the overall magnetic energy density (energy per unit volume) is expressed as follows

$$U_{MRE} = U_{host} + U_M \tag{1}$$

U_{host} is energy density of the host elastomer from the Ogden strain potential [2] as follows,

$$U_{host} = \sum_{i=1}^{3} \frac{2\mu_i}{\alpha_i^2}(\lambda_1^{\alpha_i} + \lambda_2^{\alpha_i} + \lambda_3^{\alpha_i} - 3) \tag{2}$$

where λ_i is the principal extension ratio, μ_i and α_i are fits to uniaxial stress-strain data. For incompressible materials the principal stretches are $\lambda_1\lambda_2\lambda_3 = 1$. U_M is the magnetically induced energy density of elastomer as follows [11],

$$U_M = \mu_0 M(H) \cdot H \tag{3}$$

where $M(H)$ denotes the magnetization curve, μ_0 denotes the magnetic permeability of the vacuum and is equal to $4\pi \times 10^{-7}$ H/m and H stands for the magnetic field strength. The nominal stress of elastomer can be defined as follows,

$$\sigma_{host} = \left(\frac{\partial U_{host}}{\partial \lambda_x}\right) \tag{4}$$

and the stress-strain relationship of an ideal polymer can be described by neo-Hookean stress-strain relation

$$\sigma_{host} = G(\lambda_x - \lambda_x^{-2}). \tag{5}$$

The total shear modulus of MRE (G) can be described as follows,

$$G = G_{host} + G_M^E \tag{6}$$

where G_{host} is the shear modulus of host elastomer by the following alternative expression

$$G_{host} = \frac{1}{3}\lim_{\lambda_x \to 1}\left(\frac{\partial^2 U_{host}}{\partial \lambda_x^2}\right) \tag{7}$$

where G_M^E is the magnetically induced modulus which can be defined as follows,

$$G_M^E = \frac{1}{3}\lim_{\lambda_x \to 1}\left(\frac{\partial^2 U_M}{\partial \lambda_x^2}\right). \tag{8}$$

For iron particles, Rosensweig [12] introduced the interaction energy of these two point dipoles as follows,

$$E_{12} = \frac{1}{4\pi\mu_0\mu_1}\left[\frac{\mathbf{m_1}\cdot\mathbf{m_2}}{r^3} - \frac{3}{r^5}(\mathbf{m_1}\cdot\mathbf{r})(\mathbf{m_2}\cdot\mathbf{r})\right] \tag{9}$$

where μ_1 is the relative permeability of MRE and $\mathbf{r}$ is the distance between each particle. For a dipole *i*, the dipole moment of each particle $\mathbf{m_i}$ is given by [2]

$$\mathbf{m_i} = \frac{4\pi}{3}{R_i}^3 J_p \mathbf{e_z} \tag{10}$$

where R_i is the radius of each particle, J_p is the average particle polarization and $\mathbf{e_z}$ is a unit vector in z direction. The total energy density is thus derived; then the stress induced by the application of a magnetic field can be evaluated by taking the derivative of the inter-particle energy density in terms of the shear strain. The preyield modulus G of the particle is as follows [1],

$$G \cong \frac{\phi J_p^2}{2\mu_1 \mu_0 h^3}, \qquad \epsilon < 0.1 \tag{11}$$

where h is defined as r_0/d, which is the gap between particles in a chain, r_0 is the distance between the particles and d is diameter of each particle. It can be seen that h is determined by volume of iron particles and also curing time under the magnetic fields. When the iron particles are aligned and locked into the nonmagnetic medium during the cross-linking period, the distance between the particles become smaller in terms of curing time.

3 MATERIAL SPECIFICATIONS AND TEST PROCEDURE

The specimens are made using room temperature vulcanizing (RTV) silicone (Elastosil M4644, Wacker Co.) including catalyst, and 3-5 micron sized iron powder particles (CIP CC, BASF). The volume fraction of each specimen is measured by the weight of the materials. Iron powders are mixed for 10 minutes to achieve even dispersion. Air bubbles are pulled out in a vacuum chamber in order to increase the stability of the material. After pouring the mixture into aluminum moulds, the curing process is conducted between two permanent magnetic poles in order to get different properties at different curing times.

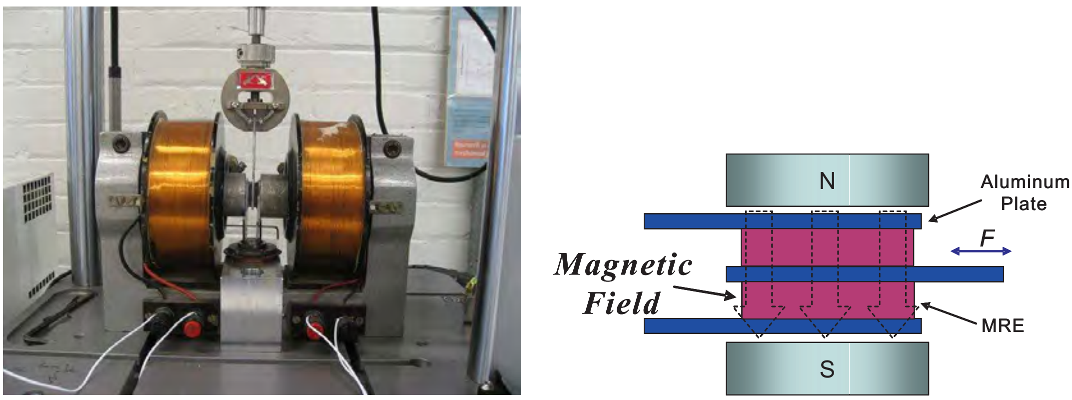

(a) (b)

Figure 1: (a) Electrodyanmic test setup with electromagnet (b) Mechanism

In order to measure shear properties of MREs under small shear strain ranges, an electrodynamic test instrument (Instron E1000) is used as shown in Fig. 1a. The test specimen is fitted within a closed-loop electromagnet which is connected with a current supply and which produces up to 0.32T of magnetic field strength. When a sinusoidal oscillating displacement is applied, the magnetic field strength travels from one pole to the other as shown in Fig. 1b. Then the load cell measures transferred force from the specimen. The shear modulus (G′) can be calculated by the amplitude of sinusoidal displacement (ΔL) and transferred load (ΔF) while the loss factor ($tan\delta$) is measured by the phase difference between dynamic loads and displacement curves as follows [13],

$$G' = \frac{\Delta F}{\Delta L}\frac{h}{4ab} \tag{12}$$

where a, b and h are length, thickness and width of specimen respectively. Four specimens in terms of different curing time (i.e. 1hr, 2hr, 4hr and 24hr) under the magnetic field with different volume of iron particles are prepared. In order to find out effect of shear strain, tests are carried out with different shear strain ranges from 0.3% to 10%.

4 TEST RESULTS AND DISCUSSIONS

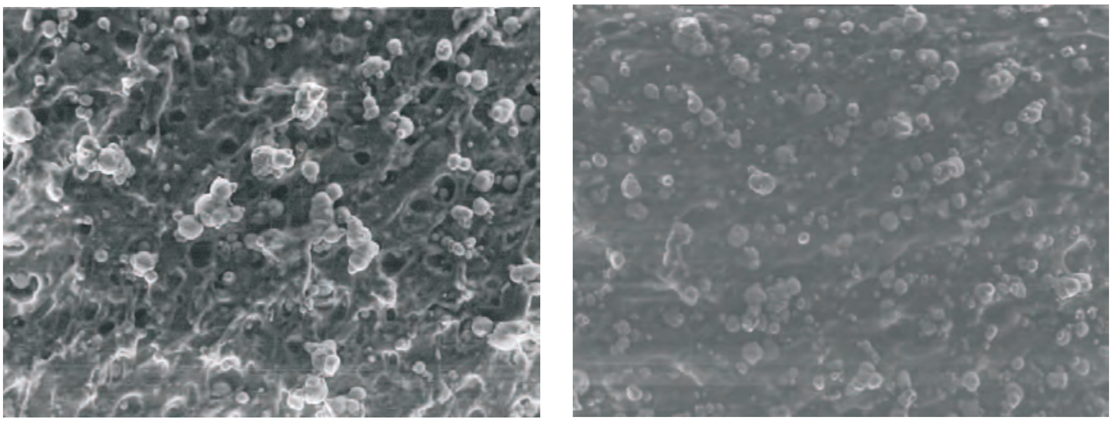

(a) (b)

Figure 2: SEM images of MRE (a) with air bubbles and (b) no air bubbles cured under without magnetic field. The width of the each image is 80 μm.

Fig. 2 shows the SEM images of the MRE with iron particles which are evenly distributed in both specimens. Fig. 2a shows the existence of air bubbles in the silicone medium when cured without deploying vacuum while Fig. 2b shows the effect when the silicone medium is subjected to a vacuum in order to draw out the air. It is noticeable that the latter results in virtually no air bubbles being present.

Fig. 3 shows the shear modulus change in terms of curing time under a magnetic field. In the case of 24hr cured MRE is higher than that of other specimens as shown in Fig. 3a. The results also show that most of shear modulus change are in proportion to curing time. This implies that the average polarization of iron particles (J_p) increases as curing time increases as described in Eq. 11. This indicates that the curing time under the magnetic field in terms of the volume of iron particles may affect MRE performance. The trend in shear property changes in terms of curing time is linear. Fig. 3b. shows the relative shear property changes. The highest shear property change is up to 57% for 20 vol% of MRE.

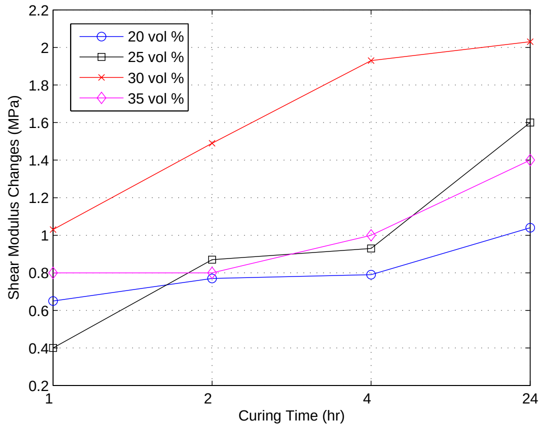

(a) Absolute change

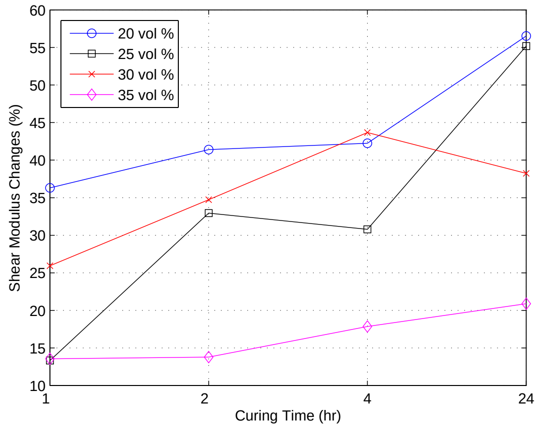

(b) Relative change

Figure 3: Shear modulus change of MRE in terms of curing time under magnetic field (a) absolute change, (b) relative change. This data corresponds to the 0.3% strain at 10Hz and 0.32T

The shear modulus change in terms of different volume percent of iron particles (i.e. 20, 25, 30, 35 and 40vol%) is shown in Fig. 4. The result indicates the absolute shear modulus change with 30 vol% MRE is about 1.8 MPa as shown in Fig. 4a this is higher than that of any other volume fraction of iron particles. The relative shear modulus change with 27 vol% MRE is about 55% as shown in Fig. 4b., which is similar to the value of Davis [2].

Fig. 5 shows the shear modulus change considering the effect of air bubbles. The MRE specimens contain air bubbles when the material is cured without vacuum degassing. The shear modulus change with 30 vol% MRE with air bubbles is about 49% at 50 Hz while that of the MRE specimens without air bubbles is about 40%. This indicates that air bubbles allows iron particles to have more dipole moment ($\mathbf{m_i}$) as shown in Eq.10.

Fig. 6 shows that the shear modulus change is likely to be high as the applied strain becomes small. It is worth noting that the change in loss factor is also dependent on the strain ranges. The yielding is significant by a pronounced drop off in the rheological effect (Fig. 6a) and an increase in field dependent energy dissipation (tanδ) (Fig. 6b). The loss modulus shows a maximum value in the region about 10% strain where the storage modulus decreases. Since shear properties of MRE change dominantly in small strain ranges, MRE is shown as being a

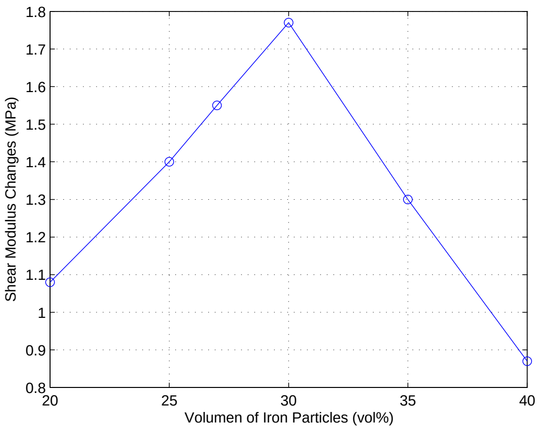

(a) Absolute change

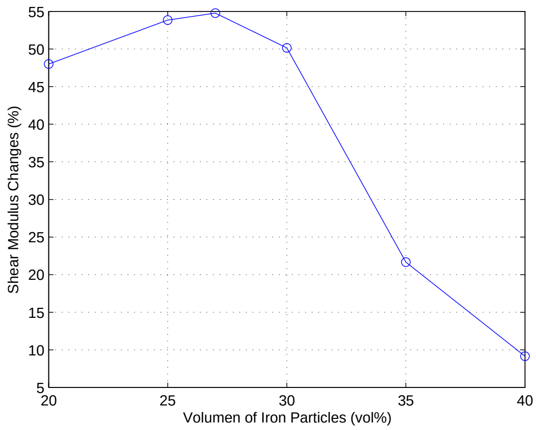

(b) Relative change

Figure 4: Shear modulus change in terms of volume change (a) absolute change, (b) relative change. This data corresponds to the 0.3% strain at 1Hz and 0.32T

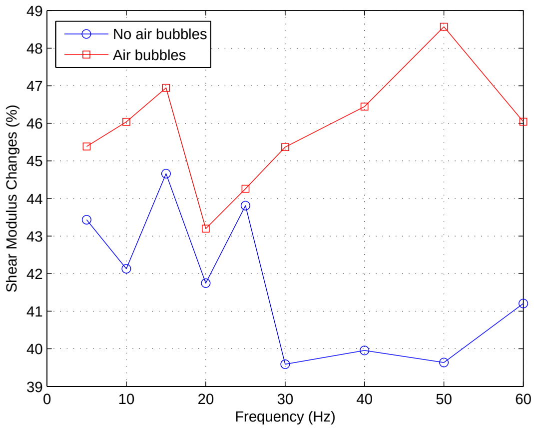

Figure 5: Shear modulus change of MRE in terms of air bubbles effect. This data corresponds to the 0.3% strain at 0.32T with 24hr cured MRE

core material in sandwich beam to achieve adjustable stiffness. This leads to the conclusion that an MRE core can be made adaptive to design a sandwich configured tunable noise and vibration isolation for applications.

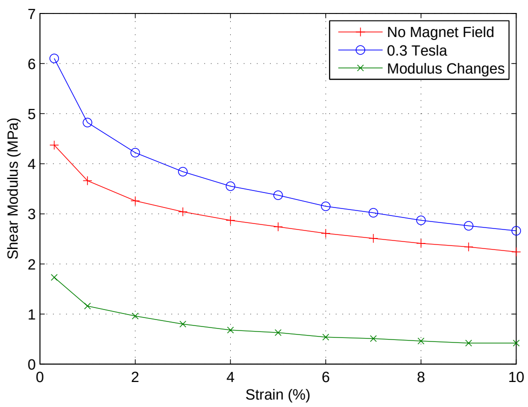

(a) Shear modulus

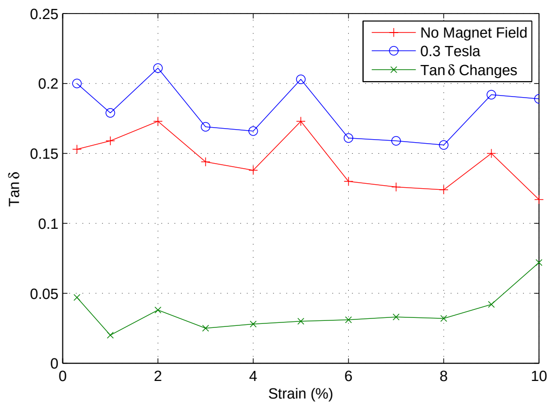

(b) Loss factor

Figure 6: Property changes in terms of different strain ranges (a) shear modulus (b) loss factor. This data corresponds to the 24hr cured MRE at 30Hz

5 CONCLUSIONS

This article has reported the shear property tests on the effect of MRE materials. The performance characterization of the smart function in terms of curing time, air bubble effect and the volume of iron particles of MRE is explored. From these tests, we conclude the following.

The relative shear modulus change with 27 vol% MRE, which is optimum volume fraction of iron particles, is about 55%. The results also show that most of shear modulus change are in proportion to curing time. The shear modulus change of MRE with air bubbles is bigger than that of the MRE specimens without air bubbles. The change in storage shear modulus and loss factor are also dependent on the strain ranges and the yielding is significant by a pronounced drop off in the rheological effect. This implies that an MRE core can be made adaptive to design a sandwich configured tunable noise and vibration isolation system.

References

[1] M.R. Jolly, J.D. Carlson, and B.C. Munoz. A model of the behavior of magnetorheological materials. *Smart Mater. Struct*, 5:607–614, 1996.

[2] LC Davis. Model of magnetorheological elastomers. *Journal of Applied Physics*, 85(6):3348–3351, 1998.

[3] M. Lokander and B. Stenberg. Performance of isotropic magnetorheological rubber materials. *Polymer Testing*, 22(3):245–251, May 2003.

[4] P. Blom and L. Kari. Amplitude and frequency dependence of magneto-sensitive rubber in a wide frequency range. *Polymer Testing*, 24(5):656–662, August 2005.

[5] Z. Varga, G. Filipcsei, and M. Zrínyi. Magnetic field sensitive functional elastomers with tuneable elastic modulus. *Polymer*, 47:227–233, 2006.

[6] G.V. Stepanov, S.S. Abramchuk, D.A. Grishin, L.V. Nikitin, E.Yu. Kramarenko, and A.R. Khokhlov. Effect of a homogeneous magnetic field on the viscoelastic behavior of magnetic elastomers. *Polymer*, 48(2):488–495, January 2007.

[7] Faramarz Gordaninejad. *Tunable Shock and Vibration Isolation System*. US Navy Proposal Submission, NAVSEA, 2006.

[8] H. Deng, X. Gong, and L. Wang. Development of an adaptive tuned vibration absorber with magnetorheological elastomer. *Smart Materials and Structures*, 15(5):N111–N116, 2006.

[9] J.M. Ginder, M.E. Nichols, L.D. Elie, and S.M. Clark. Controllable stiffness components based on magnetorheological elastomers. In *Wereley, N.M.(ed. Smart and Materials 2000: Smart Structures and Integrated Systems, Proceedings of SPIE 3985)*, pages 418–425, 2000.

[10] M. Yalcintas and H. Dai. Vibration suppression capabilities of magnetorheological materials based adaptive structures. *Smart Materials and Structures*, 13:1–11, 2004.

[11] S. Abramchuk, E. Kramarenko, G. Stepanov, L. V. Nikitin, G. Filipcsei, A. R. Khokhlov, and M. Zrnyi4. Novel highly elastic magnetic materials for dampers and seals: Part i. preparation and characterization of the elastic materials. *POLYMERS FOR ADVANCED TECHNOLOGIES*, 2007.

[12] R.E. Rosensweig. *Ferrohydrodynamics*. Cambridge University Press, 1985.

[13] Mario Baccaredda, Enzo Butta, Vittorio Frosini, and Silvano de Petris. Mechanical secondary relaxation effects in polysulfone. *Journal of Polymer Science Part A-2: Polymer Physics*, 5(6):1296–1299, 1967.

8th International Conference on Sandwich Structures
ICSS 8
A. J. M. Ferreira (Editor)

DESIGN OF A NEW TRUSS CORE FABRICATED OF WIRES

Heonsoo Kim, Byung-Chul Lee and *Ki-Ju Kang

*Department of Mechanical Engineering
Chonnam National University
300 Youngbong-dong, Buk-gu, Gwangju, 500-757, South Korea
e-mail: kjkang@chonnam.ac.kr, web page: http://altair.chonnam.ac.kr/~kjkang/

Key words: PCM(Periodic Cellular Metal), Sandwich Panel, Truss Core, Pyramidal Truss

Summary. *Core with a high load bearing capacity can be advantageous in improving overall performance of a sandwich panel. For PCM (Periodic Cellular Metal) cores in a shape of octet, pyramid, or Kagome truss, the high load capacity could be achieved by increasing relative density of the core. Namely, short and thick truss struts composing the truss PCMs gives the high load capacity. But the limit inherent in the topology or fabrication process of truss cores has been an obstacle to designing a high strength sandwich panel with the single-layered truss PCM cores. In this work, a truss PCM core with new topology which could be considered as a variation of conventional pyramidal truss is introduced. With the new type of core structure, it is possible to increase relative density of core more easily and consequently to achieve the high load capacity of the core without any limits. Analytic solutions for its normal and shear strength are derived and compared with those for pyramidal core. Results of experiments are presented to show the structural performance of the new core structure under out-of-plane compression and in-plane shear loading. The design flexibility of sandwich panels with this new core is demonstrated and its potential applications are discussed.*

1. INTRODUCTION

Various types of truss PCMs (Periodic Cellular Metals) have been introduced, since a sandwich panel having them as a core was proved as good as that with a honeycomb core [1]. The examples are pyramidal [2,3], octet [4], Kagome truss [5] as shown in Fig. 1. And these truss cores are fabricated by various methods such as investment casting [4], stacking-up of wire meshes [6], bending of expanded metal [3,7,8], and weaving of wires [9,10].

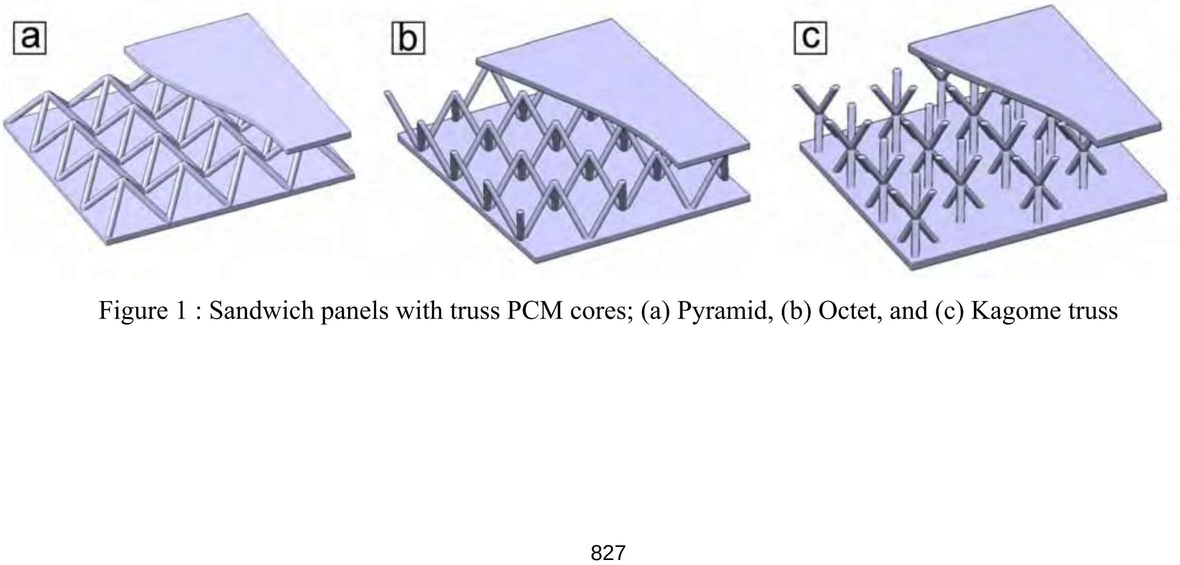

Figure 1 : Sandwich panels with truss PCM cores; (a) Pyramid, (b) Octet, and (c) Kagome truss

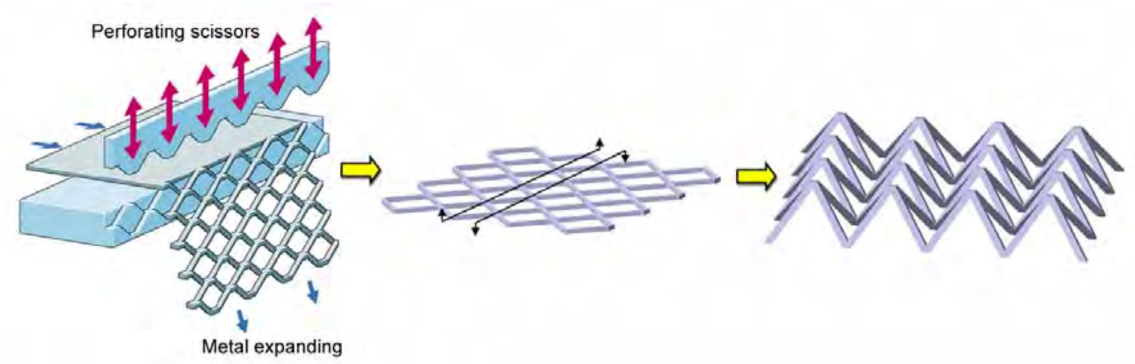

Figure 2 : Pyramidal core fabricated by expanding and bending [3]

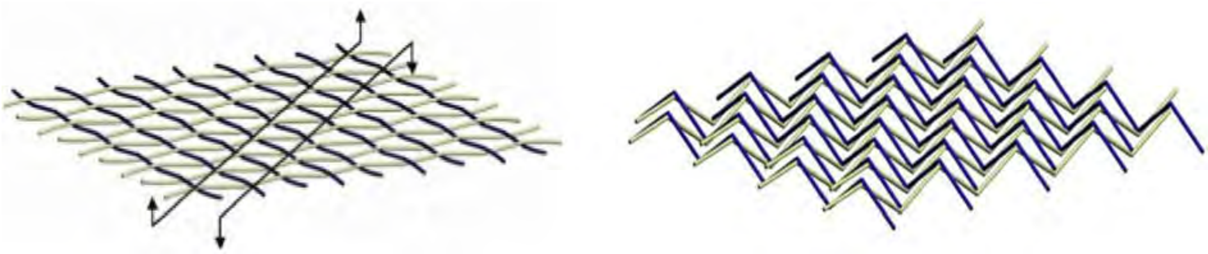

Figure 3 : Pyramidal truss core fabricated by weaving and bending of wires

General criteria for marketability of any type of sandwich cores are the morphology, fabrication cost and raw materials. The criterion of morphology is that the core should consist of one of the three truss PCMs for the highest strength. To reduce manufacturing cost, simple, continuous and well-developed processes are required. Conventional well-established metal forming processes such as press working and expanding seem promising. But the strength and manufacturing cost strongly depend on the third criterion, that is, raw materials. Wrought and high strength alloys are desirable.

For a single-layered truss core, a fabrication process based on the expanded metal process (Fig. 2) would be attractive in terms of fabrication cost and raw material. With this process, pattern cutting and expanding into a diamond mesh are simultaneously carried out in a single stroke of press working without any material loss and then the mesh is bent into a triangular wave pattern to form a pyramidal truss core [3]. However, for a high strength and/or thick metal sheet, it may be not easy to obtain geometrically precise and good quality truss cores.

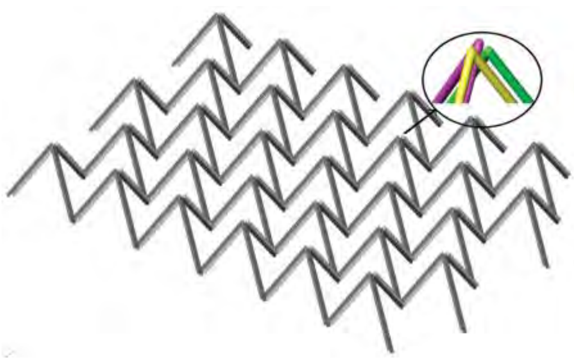

Fig. 4 : Octet truss fabricated of wires

As the alternative, idea of using wires as a raw material has been suggested. For example, wires are woven into a plain metal mesh and bent into a pyramidal truss shape (Fig. 3) [2].

Or wires are bent into a triangular wave pattern and assembled into an octet truss shape

(Fig. 4) [9]. Wires as raw materials seem very attractive, because high strength, good quality wires such as a piano wire can be made at low cost. However, if one tries to fabricate one of the above truss PCMs by using thick wires for the higher strength, the interference among wires would be a technical challenge, which may cause the deflections of struts composing the truss structure [10].

For truss PCM (Periodic Cellular Metal) cores, the high load capacity could be achieved by increasing relative density of the core. Namely, short and thick truss struts composing the truss PCMs give the high load capacity. But, the limit inherent in the topology or previous fabrication process of truss cores has been an obstacle to designing a high strength sandwich panel with a single-layered truss PCM cores.

In this work, a new topology for a truss PCM, which is named 'zigzag truss', is introduced. This truss PCM is fabricated by simply bending wires and has no interference among wires and the least limit in designing strength of a sandwich panel. The latter means that this truss core has high flexibility in designing its relative density. In the followings, the basic idea and the topology are described in details, first. Analytic solutions for its normal and shear strength are derived and compared with those for pyramidal core. Results of experiments and finite element analysis are presented to show the structural performance of the new core structure under out-of-plane compression and in-plane shear loading. The design flexibility of sandwich panels with this new core is demonstrated through finite element analysis and its potential applications are discussed.

2. ZIGZAG TRUSS

Zigzag truss can be considered as a variation of the pyramidal truss. Fig. 5(a) illustrates a typical pyramidal truss and Figs. 5(b) and 5(c) show two different evolutions from the pyramidal truss to the zigzag truss in their top views. When employed as a core of a sandwich panel, the vertices of the pyramidal truss not only connect the struts, but also join with solid face sheets. As long as the joining with the face sheets are maintained and the face sheets are undeformed, all either ends of the four struts composing each unit truss are not necessary to join only at a single point, i.e., the vertex. Instead, the joining point can be separated into two parts. The middle of Fig. 5(b) shows an example. The vertices joining

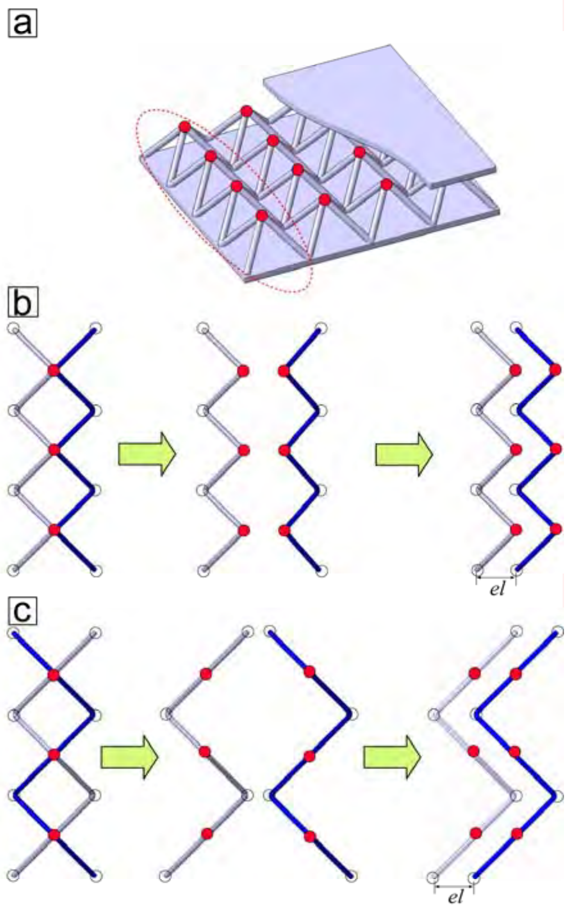

Figure 5 : (a) Pyramidal truss cored sandwich, (b) Evolution to zigzag core (intermediate), and (c) Evolution to zigzag core (final)

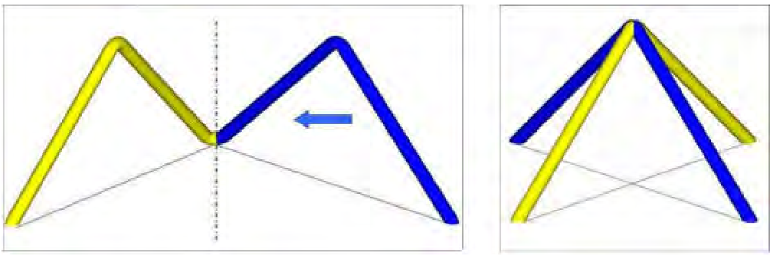

Figure 6 : Transformation of zigzag core to pyramidal core

with the top face sheet, which are marked by blind circles, are separated and consequently the single row of trusses shown in the left of Fig. 5(b) are separated into two parts, while they keep being connected with the face sheet. It is expected that there is any deterioration in the strength due to the separation under compression or shear loading. In order to reduce the area occupied by the truss core, one of the two rows may reverse its orientation, as shown at the right of Fig. 5(b), simply by turning-over or shifting. The biggest benefits of this new topology are that each row can be fabricated by bending wires into a triangular wave pattern and that there is no interference among wires. However, if assembling with face sheets is considered, the new topology has a shortcoming. Namely, the wires in a triangular wave pattern cannot hold themselves between two face sheets, and they must be supported by some extra structures until joining with the face sheets is completed.

As the alternative, the 'zigzag truss' was invented [11]. Fig. 5(c) illustrates its evolution. The single row of trusses shown in the left of Fig. 5(c) is separated into two parts in a way different from Fig. 5(b). See the middle of Fig. 5(c). And then one of the two rows reverses its orientation, as shown at the right of Fig. 5(c). Each row can be simply fabricated by two-way bending. In addition to the benefits of the other topology shown in Fig. 5(b), this topology has one more benefit in its assembling process. Namely, the wires formed in this topology can stand by themselves, without any extra structures, even before joining with the face sheets is completed. Fig. 6 shows the similarity and difference between the two unit trusses, i.e., pyramidal and zigzag trusses. If a half of the zigzag truss is translated into the other half so that the two vertices meet, as shown in Fig. 6(a), it becomes the pyramidal truss. Fig. 7(a) illustrates the configurations of a sandwich panel with a zigzag truss core. To highlight the core, the top face sheet is uncovered. Fig. 7(b) shows its top and front views.

To control the relative density of the zigzag truss core, the gap between zigzag-formed wires, eL, can be adjusted, as shown in Fig. 5(c). Fig. 8 illustrates the examples with three different gaps.

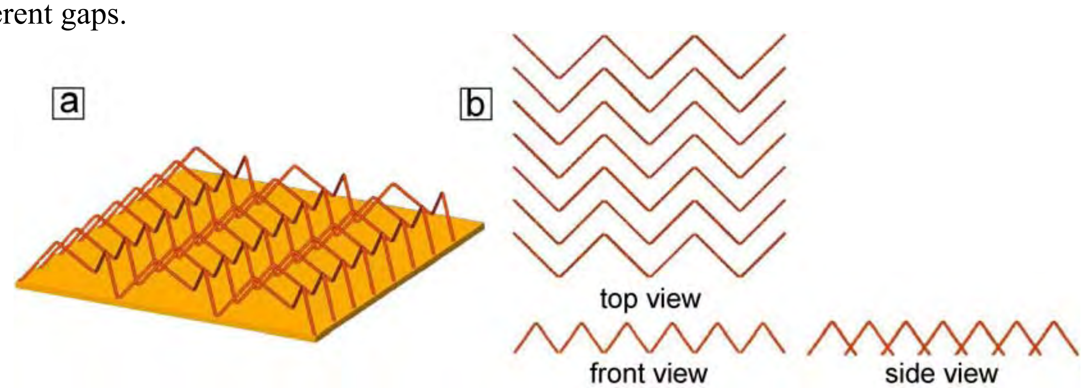

Figure 7 : (a) Zigzag truss core, (b) its projection chart